REPORT DOCUMENTATION PAGE

Form Approved
OMB No. 0704-0188

1. AGENCY USE ONLY *(Leave blank)*	2. REPORT DATE	3. REPORT TYPE AND DATES COVERED
	1996	

4. TITLE AND SUBTITLE
A Model To Estimate A Worker's Exposure To Spray Paint Mists

5. FUNDING NUMBERS

6. AUTHOR(S)
Gary Nicholas Carlton

7. PERFORMING ORGANIZATION NAME(S) AND ADDRESS(ES)
University of North Carolina

8. PERFORMING ORGANIZATION REPORT NUMBER
96-029D

9. SPONSORING / MONITORING AGENCY NAME(S) AND ADDRESS(ES)
DEPARTMENT OF THE AIR FORCE
AFIT/CI
2950 P STEET, BLDG 125
WRIGHT-PATTERSON AFB OH 45433-7765

10. SPONSORING / MONITORING AGENCY REPORT NUMBER

11. SUPPLEMENTARY NOTES

12a. DISTRIBUTION / AVAILABILITY STATEMENT
Unlimited

DISTRIBUTION STATEMENT A
Approved for public release
Distribution Unlimited

12b. DISTRIBUTION CODE

13. ABSTRACT *(Maximum 200 words)*

19960809 049

14. SUBJECT TERMS	15. NUMBER OF PAGES 185
	16. PRICE CODE

17. SECURITY CLASSIFICATION OF REPORT	18. SECURITY CLASSIFICATION OF THIS PAGE	19. SECURITY CLASSIFICATION OF ABSTRACT	20. LIMITATION OF ABSTRACT

GENERAL INSTRUCTIONS FOR COMPLETING SF 298

The Report Documentation Page (RDP) is used in announcing and cataloging reports. It is important that this information be consistent with the rest of the report, particularly the cover and title page. Instructions for filling in each block of the form follow. It is important to ***stay within the lines*** to meet ***optical scanning requirements***.

Block 1. Agency Use Only *(Leave blank)*.

Block 2. Report Date. Full publication date including day, month, and year, if available (e.g. 1 Jan 88). Must cite at least the year.

Block 3. Type of Report and Dates Covered. State whether report is interim, final, etc. If applicable, enter inclusive report dates (e.g. 10 Jun 87 - 30 Jun 88).

Block 4. Title and Subtitle. A title is taken from the part of the report that provides the most meaningful and complete information. When a report is prepared in more than one volume, repeat the primary title, add volume number, and include subtitle for the specific volume. On classified documents enter the title classification in parentheses.

Block 5. Funding Numbers. To include contract and grant numbers; may include program element number(s), project number(s), task number(s), and work unit number(s). Use the following labels:

C	- Contract	**PR**	- Project
G	- Grant	**TA**	- Task
PE	- Program Element	**WU**	- Work Unit Accession No.

Block 6. Author(s). Name(s) of person(s) responsible for writing the report, performing the research, or credited with the content of the report. If editor or compiler, this should follow the name(s).

Block 7. Performing Organization Name(s) and Address(es). Self-explanatory.

Block 8. Performing Organization Report Number. Enter the unique alphanumeric report number(s) assigned by the organization performing the report.

Block 9. Sponsoring/Monitoring Agency Name(s) and Address(es). Self-explanatory.

Block 10. Sponsoring/Monitoring Agency Report Number. *(If known)*

Block 11. Supplementary Notes. Enter information not included elsewhere such as: Prepared in cooperation with...; Trans. of...; To be published in.... When a report is revised, include a statement whether the new report supersedes or supplements the older report.

Block 12a. Distribution/Availability Statement. Denotes public availability or limitations. Cite any availability to the public. Enter additional limitations or special markings in all capitals (e.g. NOFORN, REL, ITAR).

- **DOD** - See DoDD 5230.24, "Distribution Statements on Technical Documents."
- **DOE** - See authorities.
- **NASA** - See Handbook NHB 2200.2.
- **NTIS** - Leave blank.

Block 12b. Distribution Code.

- **DOD** - Leave blank.
- **DOE** - Enter DOE distribution categories from the Standard Distribution for Unclassified Scientific and Technical Reports.
- **NASA** - Leave blank.
- **NTIS** - Leave blank.

Block 13. Abstract. Include a brief *(Maximum 200 words)* factual summary of the most significant information contained in the report.

Block 14. Subject Terms. Keywords or phrases identifying major subjects in the report.

Block 15. Number of Pages. Enter the total number of pages.

Block 16. Price Code. Enter appropriate price code *(NTIS only)*.

Blocks 17. - 19. Security Classifications. Self-explanatory. Enter U.S. Security Classification in accordance with U.S. Security Regulations (i.e., UNCLASSIFIED). If form contains classified information, stamp classification on the top and bottom of the page.

Block 20. Limitation of Abstract. This block must be completed to assign a limitation to the abstract. Enter either UL (unlimited) or SAR (same as report). An entry in this block is necessary if the abstract is to be limited. If blank, the abstract is assumed to be unlimited.

A MODEL TO ESTIMATE A WORKER'S EXPOSURE TO SPRAY PAINT MISTS

by

Gary Nicholas Carlton

A dissertation submitted to the faculty of the University of North Carolina at Chapel Hill in partial fulfillment of the requirements for the degree of Doctor of Philosophy in the Department of Environmental Sciences and Engineering, School of Public Health.

Chapel Hill

1996

Approved by:

Michael R Flynn
Advisor

David Leith
Reader

Donald L. Fox
Reader

Stephen M Rappaport
Reader

M. D. Symons
Reader

ABSTRACT

GARY NICHOLAS CARLTON. A Model to Estimate a Worker's Exposure to Spray Paint Mists (Under the direction of Michael R. Flynn)

Although local exhaust ventilation reduces exposure to airborne contaminants, current design methodology is limited because the relationship between exposure and ventilation is seldom known for a specific industrial operation. This research addressed this deficiency by introducing the notion of an empirical-conceptual model. These models relate exposure to ventilation through various process parameters responsible for the generation and transport of contaminants. To illustrate the modeling technique, an empirical-conceptual model of a spray painting task was developed. A conceptual model described three processes that determine the exposure: droplet formation, droplet transfer, and droplet transport. Each process was examined and important factors which characterize the processes identified. These factors were then grouped into four dimensionless variables using dimensional analysis. A laboratory set-up used a mannequin, flat plate and spray nozzle in a wind tunnel to find the functional relationship among these variables. The model indicates worker orientation to the freestream has a significant influence on breathing zone concentrations. The magnitude of the dimensionless quantity consisting of nozzle pressure, worker height, liquid viscosity, and freestream velocity determined in which orientation the concentration was higher.

The influence of process parameters on the breathing zone droplet size distributions was then investigated. Droplets were collected on treated polycarbonate membrane filters and sized with a light microscope. The results indicate worker

orientation strongly influences the breathing zone size distributions, with larger sizes resulting when the worker stands so the freestream flows to the worker's side than to the back. This difference is attributed to overspray transport mechanisms that depend on the interaction of the spray gun air jet with the freestream.

The empirical model was then evaluated in the field. Eight workers in a paint shop were sampled over five weeks. Forty percent of the measured task exposures are within the estimated experimental error of the model prediction and 71% are within a factor of three of the prediction. Four of the eight worker mean exposures are within one standard error of the model prediction. These results indicate the prospect for empirical-conceptual models to predict exposure and to aid in the design and economic optimization of engineering controls.

ACKNOWLEDGMENTS

I would like to thank my advisor, Dr. Michael Flynn, and my committee members, Dr. Donald Fox, Dr. David Leith, Dr. Stephen Rappaport, Dr. Parker Reist, and Dr. Michael Symons, for their support and encouragement during the course of my studies.

Thank you to the men and women of the Robins Air Force Base Component Repair Paint Shop, whose help was invaluable in the completion of the field studies, especially Lee James, shop supervisor, Ron Fowler and Joanne Fluellan. I would also like to acknowledge Henry Petronious and Lee Langley of the Robins AFB Bioenvironmental Engineering office for technical support during the field studies, and the US Air Force Armstrong Laboratory Analytical Division, Brooks AFB, for analysis of the charcoal tube samples.

I am grateful to Dr. Russell Wiener and Fu-lin Chin of the EPA Air Research Laboratory for the use of and assistance in operating the VOAG, and Tom Peters of Research Triangle Institute for help in properly calibrating the VOAG. Many thanks to Dr. Robert Bagnell and Vicki Madden of the UNC Pathology Microscopy Laboratory for showing me how to use the image processing system. Their many useful suggestions and sense of humor kept me going when I thought I could never count another particle again in my life.

Special thanks to Maryanne Boundy, Kwangseog Ahn, Premkumar Muthedath, Jordan Kovitz, and Pete Raynor of the Baity Laboratory. I would also like to recognize Randall Goodman and Cliff Burgess of the Instrument Shop, who modified their spray booth for my use, and did so many other things for me I cannot remember them all. Without their help I would not have been able to complete this research. Finally, thank you to Neil McKenney of Medical Illustrations for drawing the figures.

This dissertation is dedicated to my daughter, Kathelyn. Thank you for believing in me. I love you dearly.

TABLE OF CONTENTS

Chapter **Page**

Chapter **Page**

LIST OF TABLES

LIST OF FIGURES

Chapter 1: Introduction

1.1. Statement of Problem

Local exhaust ventilation captures airborne contaminants and reduces worker breathing zone concentrations. Implicit in this statement is a relationship between exposure and ventilation. Because the form of this relationship is seldom known for a specific industrial operation, an industrial hygienist cannot predict the effectiveness of a ventilation design prior to installation.

Exposure models attempt to describe this relationship between exposure and ventilation. These models are generally referred to as either "theoretical" or "empirical". Theoretical models apply computational fluid dynamics to solve the governing equations that determine the distribution of contaminants in air (Flynn *et al.*, 1995; Flynn *et al.*, 1996). Analytical solutions to these equations, however, are difficult, while numerical simulations are restricted by current computer capabilities. As a result, theoretical models are limited to relatively simple situations which do not reflect the complexity of industrial operations.

The observation that exposures are variable (Rappaport *et al.*, 1993; Kromhout *et al.*, 1993) complicates development of an exposure model. The underlying assumption of an empirical model is that exposure variability results from process parameters that vary among tasks and workers. Associating measured exposures to these parameters statistically results in an "empirical-statistical" model (Dement *et al.*, 1983; Kromhout *et al.*, 1994; Woskie *et al.*, 1994). Statistical analysis, however, can obscure the functional relationship among exposure, ventilation, and the process parameters, making it difficult to apply these models toward the design of a local exhaust ventilation system.

A different type of empirical model relates exposure to ventilation and the variable process parameters through a conceptual model. This is the so-called "empirical-

conceptual" model. First, a conceptual model of the industrial operation is developed, outlining contaminant generation and transport processes that lead to the exposure. Each of these processes is examined and important factors that characterize them are identified. These factors are then grouped into nondimensional ratios using the technique of dimensional analysis. Finally, experiments are performed to determine the functional relationship among the ratios. An industrial hygienist potentially can generalize an empirical-conceptual model to a new situation (Taylor, 1974). These models raise the prospect for exposure prediction and the economic optimization of local exhaust ventilation design.

This research developed an empirical-conceptual model for a compressed air spray painting task. Spraying paint is widespread throughout industry, but can result in exposure to paint mists. These tasks are amenable to modeling because limited numbers of identifiable factors determine the exposure. Although this research concentrates on a specific industrial operation, the modeling concepts developed here should be applicable to other operations of interest to the industrial hygienist.

1.2. Research Strategy

This research consisted of three phases. The first phase developed the empirical-conceptual exposure model. The second phase investigated the particle-size nature of the exposure. The third phase was a field evaluation of the model.

1.2.1. Model Development

The goal of this phase was to develop an exposure model that could be field tested. In this regard it was important to describe the processes inherent in spray painting operations that lead to worker exposure. The following conceptual model was the basis for identifying important process parameters.

(1) *Droplet formation.* This initial process produces paint droplets that coat the workpiece. These droplets have a characteristic size distribution which influences

subsequent processes and the eventual worker exposure. The size distribution primarily depends on: spray gun nozzle pressure (p_n); paint viscosity (μ_l); and the ratio of air-to-liquid mass flows fed to the spray gun (m_a/m_l) (Kim and Marshall, 1971; Lefebvre, 1989; Kwok, 1991).

(2) *Droplet transfer*. This process creates the paint mist or overspray (m_o) which is the source of the exposure. The efficiency of droplet transfer to the workpiece is a function of both droplet momentum and spray gun-to-workpiece distance. Because this distance is relatively constant, droplet momentum dominates the transfer process. The velocity of the air jet leaving the spray gun imparts momentum to the droplets. This velocity results from the gun nozzle pressure.

(3) *Droplet transport*. In the final process, the overspray moves into the worker's breathing zone and produces the exposure. Transport depends on freestream velocity (U) if painting occurs in a spray booth. Other important factors are the worker's dimensions (height H and breadth D) and worker orientation to the freestream (90° orientation, freestream to the worker's side; 180° orientation, freestream to the worker's back) (Flynn and George, 1991; Flynn and Shelton, 1990).

The conceptualization of exposure therefore is based on the initial droplet size, the transfer efficiency of the task, and the overspray transport mechanism. Although development of an empirical-conceptual model does not require a complete understanding of these processes, it is important for the conceptual model to include all processes that determine the exposure. A faulty conceptual model will result in an exposure model that in all likelihood will fail its field evaluation. In addition, improvements in the exposure model are ultimately related to a better understanding of the processes that lead to the exposure. For spray painting tasks, the more known about droplet size distributions, spray transfer efficiencies, and overspray transport mechanisms, the better the model will reflect reality.

Dimensional analysis results in the following dimensionless relationship between the worker's average breathing zone concentration (C) and the process parameters identified in the conceptual model:

$$\frac{CUHD}{m_o} = \Phi\left(\frac{m_a}{m_l}, \frac{p_n H}{\mu_l U}, \text{orientation}\right) \quad (1)$$

To find the functional relationship among these quantities, experiments were done using a laboratory mock-up of a spray painting task. It is important for the same processes dominating actual spraying operations be recreated in the laboratory, namely that the droplet size distributions be similar; transfer efficiencies be measurable; and transport mechanisms be comparable. To this end, a Spraying Systems 1/4J nozzle represented the spray gun. This nozzle operates on the same principle as actual spray guns, uses similar nozzle pressures and air-to-liquid flow ratios, and produces comparable droplet size distributions. Corn oil, having a viscosity similar to enamels, was used to simulate paint. A flat plate represented the workpiece, producing uniform air jet rebound and reproducible transfer efficiencies. Overspray generation rates were measured by a mass balance on liquid sprayed and transferred to the flat plate. Spraying took place in a calibrated wind tunnel. The average freestream velocities in the tunnel varied from 75 to 200 fpm, typical of field spray booths. A mannequin 41 inches in height and 8 inches in breadth represented the worker. Although the laboratory set-up was reduced in scale compared to actual field operations, varying worker orientation to the freestream recreated the transport mechanisms extant in actual field spraying tasks.

The three independent dimensionless groups m_a/m_l, p_nH/μ_lU, and worker orientation were varied over values typical of field spraying tasks. Mannequin breathing zone concentrations were measured for total aerosol mass. The collected data were analyzed to determine the functional relationship among the independent variables and the dependent dimensionless concentration group, $CUHD/m_o$. An important part of this analysis is to understand why such a functional relationship exists.

1.2.2. Particle Sizing

The goal of the second phase was to obtain a better understanding of the size characteristics of spray paint mists and the transport mechanisms that lead to exposure. Previous investigators who measured paint overspray found significant, but unexplained variability in size distributions. One source of this variability could be the sampling method used, which may have biased the measured mass median diameters (MMD).

To reduce this bias, a new method for sampling volatile aerosols was developed. Droplets were collected on polycarbonate membrane filters and sized with an optical microscope and image processing system. To prevent the droplets from collapsing on the filter surface when collected, the filters were coated with a spread retardant.

The sampling method required calibration to relate the droplet size observed on the filter to the true diameter prior to collection. To measure this spread factor, monodisperse droplets were generated with a Vibrating Orifice Aerosol Generator (VOAG). Corn oil droplets from 2.9 to 16.7 μm were collected on treated filters and sized with an optical microscope. The results show a spread factor of 1.34. A goniometer indicates the spread factor increases slightly for droplets larger than the VOAG could generate, but not enough to affect the droplets of interest in spraying operations.

Paint mist size distributions were measured in the same laboratory set-up used in phase one of the research. Nozzle pressures, air-to-liquid mass flow ratios, and worker orientation to the freestream were varied across values typical of spraying tasks. Samples were collected in the breathing zone of the mannequin using the new sampling method. Breathing zone geometric mean diameters (GMD) and spray MMDs were computed for each experimental run. In addition, the count data were converted into mass frequency distributions.

Sampling continued in an actual spray booth. The booth measured 46.5 square feet in cross-sectional area and 13.6 feet deep. The author, 5 feet 11 inches in height, painted a flat plate 3 feet wide and 6 feet tall with a high-solids enamel thinned to a viscosity of 45 centipoise. Paint was applied to the flat plate with spray guns using the fan spray pattern and back-and-forth motion common in actual spraying tasks. Both

conventional and "high-volume low-pressure" (HVLP) spray guns were used. Nozzle pressure and worker orientation were varied. Measured breathing zone size distributions were compared to those found in the laboratory.

1.2.3. Field Evaluation

The final phase was a field evaluation of the empirical-conceptual model developed in phase one. The field evaluation consisted of 55 spray painting tasks sampled on eight workers in a paint shop at Robins Air Force Base, Georgia. Tasks were selected such that a flat plate was a reasonable representation of the workpiece with air jet rebound similar to that seen in the laboratory. Worker breathing zone concentrations were measured with 5-μm PVC filters backed-up with two large charcoal tubes in parallel. The charcoal tubes collected solvent that evaporated from the collected droplets during sampling. Spray gun nozzle pressure, paint viscosity, mass of paint sprayed, worker height and breadth, and spray booth average freestream velocity were measured for each spraying task. Overspray generation rates were estimated from the measured transfer efficiency at the spray gun nozzle pressure used. All tasks were video taped to determine the task time, spray time, and time spent spraying in the 90° and 180° orientations.

The task exposures were calculated from the collected solids and solvent masses and the task time. The exposures predicted by the model were found from the measured task parameters, calculated overspray generation rates, and the functional relationship between $CUHD/m_o$, p_nH/μ_lU, and worker orientation. The measured and predicted exposures were then compared to determine the goodness-of-fit to the empirical-conceptual model.

1.3. Summary of Findings

1.3.1 Model Development

(1) Experimental data indicate the dimensionless concentration group, $CUHD/m_o$, is a strong function of the quantity p_nH/μ_lU and worker orientation to the freestream. A significant interaction occurs between p_nH/μ_lU and worker orientation. $CUHD/m_o$ is higher in the 90° orientation when p_nH/μ_lU exceeds 5.0×10^6 but higher in the 180° orientation if p_nH/μ_lU is less than 5.0×10^6. $CUHD/m_o$ reaches an asymptotic value of 0.134 in the 90° orientation and 0.006 in the 180° orientation for values of p_nH/μ_lU greater than 1.5×10^7.

(2) In the 180° orientation for a fixed nozzle pressure, mannequin breathing zone concentrations increased as the freestream velocity increased. In the 90° orientation, however, increased ventilation reduced measured breathing zone concentrations. This difference between the orientations suggests different overspray transport mechanisms dominate the two worker orientations and lead to the different orientation curves found.

(3) The quantity p_nH/μ_lU is a ratio of two time scales. One is related to the residence time of the overspray droplets in the vicinity of the painting task (H/U), and the other is related to the transfer efficiency of the painting task (μ_l/p_n). Therefore, p_nH/μ_lU incorporates the relative contributions of the droplet transfer and transport processes in producing an exposure.

(4) Air-to-liquid mass flow ratio was not a significant factor in predicting breathing zone concentrations in either orientation. The quantity m_a/m_l is an important factor in the transfer efficiency of the task, but fails to enter the model because transfer efficiency was not directly used to develop the model. Using overspray generation rate to normalize the quantity $CUHD/m_o$ allows application of the model to conventional spraying tasks which exhibit transfer efficiencies different than those found in the laboratory.

1.3.2. Particle Sizing

(1) Laboratory results indicate a strong orientation effect, with overall average GMDs of 13.5 μm in the 90° orientation and 10.9 μm in the 180° orientation. The same effect was observed in the field, although the measured GMDs were smaller than those found in the laboratory. The difference between the two orientations is attributed to different transport mechanisms. In the 90° orientation the transport mechanism results from the interaction of the spray air jet with the booth freestream. The air jet propels the overspray toward the booth inlet, where it mixes with the incoming freestream and passes through the worker's breathing zone. The transport mechanism in the 180° orientation is unclear. The presence of the orientation effect both in the laboratory and in the field, however, indicates the transport mechanisms present in actual spraying operations were recreated in the laboratory set-up.

(2) Neither air-to-liquid mass flow ratio nor spray MMD influenced the resulting breathing zone size distributions. This result suggests factors that influence the spray MMD, but not the transport of overspray to the worker, probably have minimal bearing on the resulting breathing zone size distribution. One such factor is paint viscosity. These results also suggest that droplet transport is the most important process in determining the particle size-nature of exposure to paint mists.

(3) Nozzle pressure did not significantly influence particle size in the field and was a factor only in the 180° orientation in the laboratory. In this latter case mean breathing zone GMDs decreased as nozzle pressure increased. Since air mass flow is proportional to spray gun nozzle pressure, these results again suggest that interaction of the air jet with the spray booth freestream, and the transport mechanism that results from this interaction, is the most important process affecting breathing zone droplet sizes.

1.3.3. Field Evaluation

(1) Forty percent of the measured worker task exposures are within the estimated experimental error of the model prediction. Seventy-one percent are within a factor of

three of the prediction. If tasks are excluded that either did not fit the model assumptions well or where a sampling or analysis error likely occurred, then the percentage within a factor of three increases to 84%. Statistical analysis on the revised data set indicates the model is an unbiased estimator of exposure.

(2) Four worker mean exposures are within one standard error of the model prediction. These four workers were among the five on whom the most samples were taken. These results indicate that an empirical-conceptual model can predict a worker's mean exposure within a standard error.

(3) Overspray generation rates were probably higher than estimated due to movement of the workers and their spray guns, the tendency for the spray pattern to miss the edge of a workpiece, and varying spray gun-to-workpiece distances. In addition, objects oriented at an angle to the worker's body diverted overspray away from the worker, resulting in overspray motions different than those observed in the laboratory. The worker may also have received additional solvent exposure from mixing and cleaning during the spraying tasks. All these factors influence the predictive ability of the model.

1.4. Future Research

Improvements in the empirical-conceptual model developed in this research ultimately depend on insight into the droplet formation, transfer, and transport processes that result in the exposure. Because droplet formation depends on the spray gun used and the adjustment of spray parameters that an industrial hygienist has limited control over, the emphasis should be on better estimates of transfer efficiencies and knowledge of overspray transport mechanisms.

Transfer efficiencies should be measured for actual spray guns in motion. These measurements should be done not only for typical field nozzle pressures but also for a range of liquid viscosities to better understand the importance of the time scale μ_l/p_n to transfer efficiency. Workpiece shape and angle to the worker's body, and spray gun-to-workpiece distance all influence transfer efficiency and require study.

The transport mechanism that leads to exposure in the 180° orientation should be identified. Adding a fluorescent dye to the liquid sprayed in the laboratory set-up will allow flow visualizations and better understanding of droplet transport in both 90° and 180° orientations. Computational modeling can assist by simulating the interaction of the spray air jet with the freestream. The influence of freestream velocity on both exposure and breathing zone size distributions requires a more systematic study.

The model orientation curves should be verified for an actual spray gun over a range of p_nH/μ_lU values. Of special interest is the behavior of the model for an HVLP spray gun, which has p_nH/μ_lU values to the left of the cross-over point for the orientation curves. If an HVLP gun produces higher exposures in the 180° orientation than in the 90° orientation, this could impact the positioning of worker and workpiece to reduce exposure. The model suggests that an HVLP gun, even though promising lower overspray generation rates, could produce higher exposures than a conventional gun depending on worker orientation. A field study to test this hypothesis could influence the recent recommendation by NIOSH to switch to HVLP spraying.

The model should better address the orientations a worker stands in when spray painting. The model as currently evolved limits orientation to the generic definitions of "90°" and 180°" but in actuality orientations other than these are possible. A model developed for a mannequin that rotates among many worker orientations, similar to the work done to develop inhalable mass samplers (Mark and Vincent, 1986), could produce non-orientation specific models. These models may have increased applicability and usefulness to the industrial hygienist. A model specific for down-draft spray booths would also be of benefit.

Finally, and most importantly, the modeling concepts developed here should be applied to other operations of interest. Exposures open to empirical-conceptual modeling include mineral oil mist generated during metal-working operations, particulates produced during abrasive blasting, and powders released during milling operations. Wider use and acceptability of the modeling technique will lead to improved control methods and reduced worker exposures.

Chapter 2: Development of the Model[1]

2.1. Abstract

Exposure models traditionally have emphasized the statistical association between process parameters and measured exposures. These "empirical-statistical" models can illuminate factors important to controlling exposure, but are difficult to generalize for various reasons. A different modeling technique may have wider applicability. Known as "empirical-conceptual" models, they are based on a conceptual model that identifies contaminant generation and transport processes leading to the exposure. Dimensional analysis is used to group important process parameters into nondimensional ratios, then the relationship among these ratios is found from experiments. To illustrate the method, this research developed an empirical-conceptual model of a spray painting task. Dimensional analysis identified four dimensionless quantities important to these tasks. A laboratory set-up of a mannequin, flat plate, and spray nozzle in a wind tunnel found the relationship among these quantities. The model successfully explained the variability in the average breathing zone concentration of the mannequin within the measurement uncertainty of the experimental set-up. Mannequin orientation to the freestream had a significant effect on breathing zone concentrations. In addition, the magnitude of a dimensionless quantity consisting of spray nozzle pressure, mannequin height, liquid viscosity and average freestream velocity predicted in which orientation the breathing zone concentration was higher. Differences between the experimental set-up and actual spraying tasks could limit the model. This research, however, indicates the prospect for empirical models based on dimensional analysis to predict breathing zone concentrations. This could lead to better control methods and reduced exposures.

[1]Submitted to *Applied Occupational and Environmental Hygiene* under the title "A Model to Estimate Worker Exposure to Spray Paint Mists".

2.2 Introduction

A primary goal of industrial hygiene is to control worker exposure to hazardous materials and prevent occupational disease. If inhalation is the route of exposure, hygienists typically base judgments for appropriate control measures on breathing zone sampling. In some cases, references are available that outline effective controls for specific hazards, e.g., the American Conference of Governmental Industrial Hygienists (ACGIH) Ventilation Manual.[1] Another less frequently used method for evaluating control options is exposure modeling.

There are two types of exposure models, theoretical and empirical. Theoretical models use computational fluid dynamics to solve the basic governing equations determining the distribution of contaminants in air. These equations, however, are intricate and analytical solutions are impossible. Current capabilities limit numerical results to relatively simple situations, which do not reflect the complexity of most industrial operations.

Empirical models address this complexity by relating the exposure to various process parameters. Kromhout *et al.*[2] sampled the rubber manufacturing industry in The Netherlands and correlated exposures to tasks performed, ventilation characteristics, and production variables. Woskie *et al.*[3] looked at exposures to metal-working fluids in automotive component manufacturing and developed a model based on several factors, including the fluid type, the presence or absence of local exhaust ventilation, and the atmospheric conditions. Kromhout called this modeling technique the "empirical-statistical" approach because the model relates exposure to the parameters by multiple linear regression. It is difficult to apply these models to new situations, however, since additional factors, not considered in developing the model, may be important. Also, the assumption of linearity between exposure and factors can leave a lot of variability in exposure unexplained since there is no guarantee the dependence is linear. In addition, factors which do not vary much during sampling will not show up in the model, even though they may be important in controlling the exposure.

A different type of empirical model relates the exposure to the process parameters not by their statistical association but through a conceptual model. This "empirical-conceptual" approach is appropriate if a limited number of identifiable factors determine the exposure. A conceptual model of the industrial operation is developed, outlining contaminant generation and transport processes leading to the exposure. Each process is examined and factors that characterize the process identified. Once these factors are known, an empirical model results from dimensional analysis, a process of grouping the factors into nondimensional ratios and performing experiments to determine the relationship among these ratios. Besides improving physical insight into the problem, this method has the potential to generalize the model to new situations.[4] The model does not require an assumption of linearity. Furthermore, as long as a sound conceptual understanding of the problem exists, the model should include all factors important to controlling the exposure.

Spray painting tasks are well-suited to test whether an empirical-conceptual model can predict worker exposures. Spraying paint gives workers good control over the quality of finish, but results in exposure to paint mists. Even though generation of this mist and its interaction with the flow field in a paint spray booth is complex, a limited number of factors determine the exposure. Spray painting tasks lend themselves to modeling since these factors are identifiable.

This research develops an empirical-conceptual model to predict breathing zone concentrations of paint mist during spray painting tasks. If validated in the field, this model will allow the industrial hygienist to identify work practice changes and improve the efficiency of engineering controls. Although spray painting is the process of interest, the modeling concepts developed here should have applicability to other industrial operations as well, e.g., mineral oil mist generated during metal-working operations and particulates produced during abrasive blasting.

2.3. Conceptual Model

The spray application process of most concern from an exposure viewpoint is compressed air atomization. Also known as pneumatic or twin-fluid atomization, this is the most widely used spray application process in industry.[5] It is popular because it can atomize viscous liquids like paint and adjust the atomization quality by varying air and liquid flows to the atomizer. Compressed air atomization is classified as either conventional or high-volume low-pressure (HVLP) spraying. Conventional spraying operates at air pressures greater than 20 psig while HVLP spraying involves lower pressures, usually 10 psig or less.

Compressed air atomization produces a paint mist that can enter a worker's breathing zone and lead to an exposure. This exposure results from three sequential processes common to all spraying tasks, shown conceptually in Figure 2.1.

The *droplet formation* process produces the droplets that coat the workpiece. A spray gun causes compressed air to interact with the paint and form droplets. Paint atomizers are universally external-mixing, meaning the paint and air interact outside of the atomizer. They are also generally parallel flow, characterized by the atomizing air and liquid flowing in the same direction when they contact. The spray gun discharges the liquid through a fluid nozzle as a liquid stream. A hollow column of air emitted from the spray gun's air nozzle surrounds this stream. Shear forces develop along the surface of contact between the two fluids causing the liquid to disintegrate into droplets.[6] This interaction is complex, and empirical observations are the primary basis for knowledge of the resulting droplet size distributions.[7] The most important factors that affect these distributions are: air pressure at the nozzle (p_n); liquid paint viscosity (μ_l); and ratio of air-to-liquid mass flows (m_a/m_l).[7-9]

The *droplet transfer* process creates the paint mist or overspray. The air jet leaving the spray gun imparts a forward velocity to the droplets. This jet produces an air flow pattern around the workpiece. Larger droplets deviate from the air flow streamlines and deposit on the object. Smaller droplets with insufficient momentum to deposit follow the streamlines and become entrained in the air flow around the object to form the

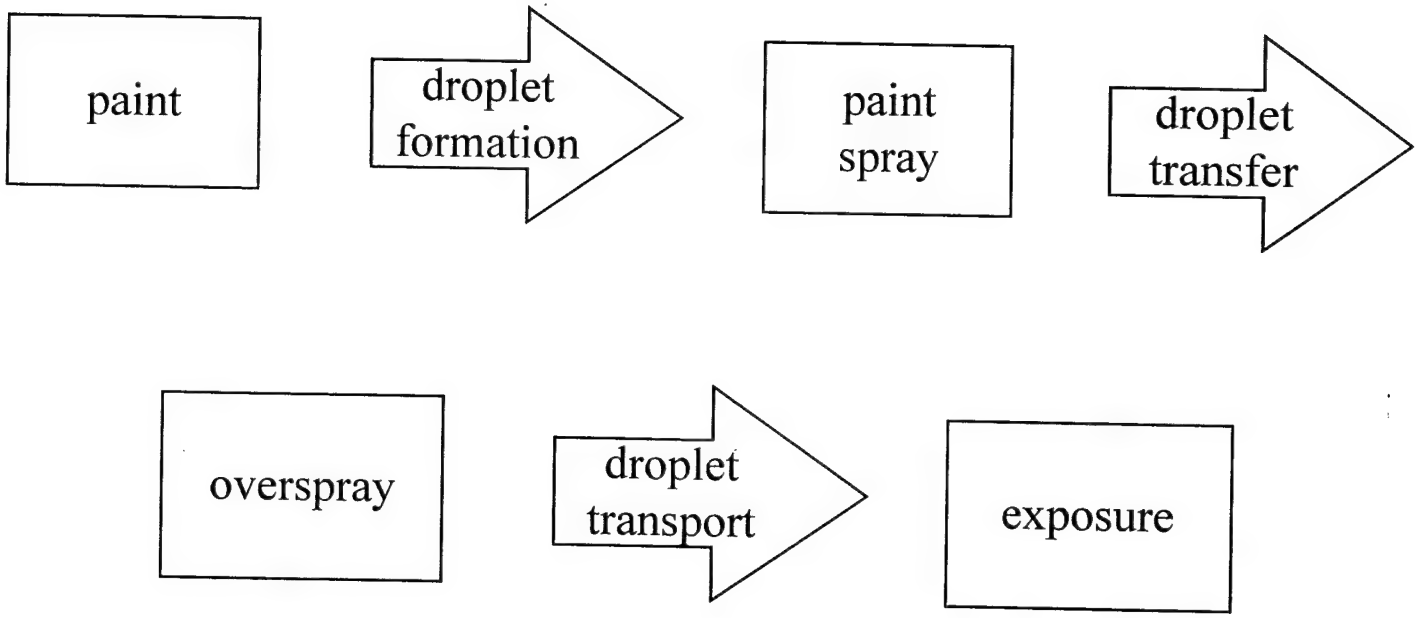

Figure 2.1: Conceptual model of a spray painting task

overspray (m_o). The transfer efficiency of the spray, or the fraction of droplets that impact on the workpiece, depends primarily on droplet momentum and the spray gun-to-workpiece distance.[9-10] Droplets receive their momentum from the velocity of the air jet, which for compressed air atomizers results from the nozzle air pressure (p_n). Spray gun-to-workpiece distances do not vary much among compressed air painting tasks; recommended guidelines are to keep the gun within six to eight inches of the object.[5]

In the final process, *droplet transport*, the overspray may enter the worker's breathing zone. This is typically the stage where intervention takes place to control the exposure. This intervention is usually local exhaust ventilation if painting occurs in a spray booth. ACGIH recommends ventilation rates as average freestream velocities (U).[1] Small booths encompass the workpiece and capture the overspray like an enclosing hood. Larger booths allow the worker to stand in the freestream while painting. The freestream propels the overspray toward one end of the booth where an air-cleaning device, usually a dry filter bed or water curtain, removes the droplets. The worker generally orients the workpiece so the freestream flows either to the worker's side (90° orientation) or to the worker's back (180° orientation); see Figure 2.2. The uniform freestream can cause a boundary layer to form around the worker and a reverse flow region to develop downstream of the worker.[11] Contaminants generated in this wake can move into the breathing zone when the worker is in the 180° orientation.[12] Investigators document a difference in breathing zone concentration (C) when a mannequin is positioned in these two orientations and holds a passive contaminant source.[13,14] In this instance mannequin height (H) and breadth (D) influence breathing zone concentrations. This research emphasizes these larger spray booths where this orientation effect may be important.

Droplet evaporation proceeds concurrently with droplet transport. Overspray droplets decrease in size as the solvent fraction volatilizes. This change in size distribution affects the movement of the overspray and results in worker exposure to solvent vapors, though vapor concentrations are generally low during spraying tasks if ventilation is available.[15-19] The overspray, consisting of paint solids and unevaporated solvent, contributes most of the worker's total mass exposure. This research develops an empirical model based on dimensional analysis for this overspray contribution to the exposure.

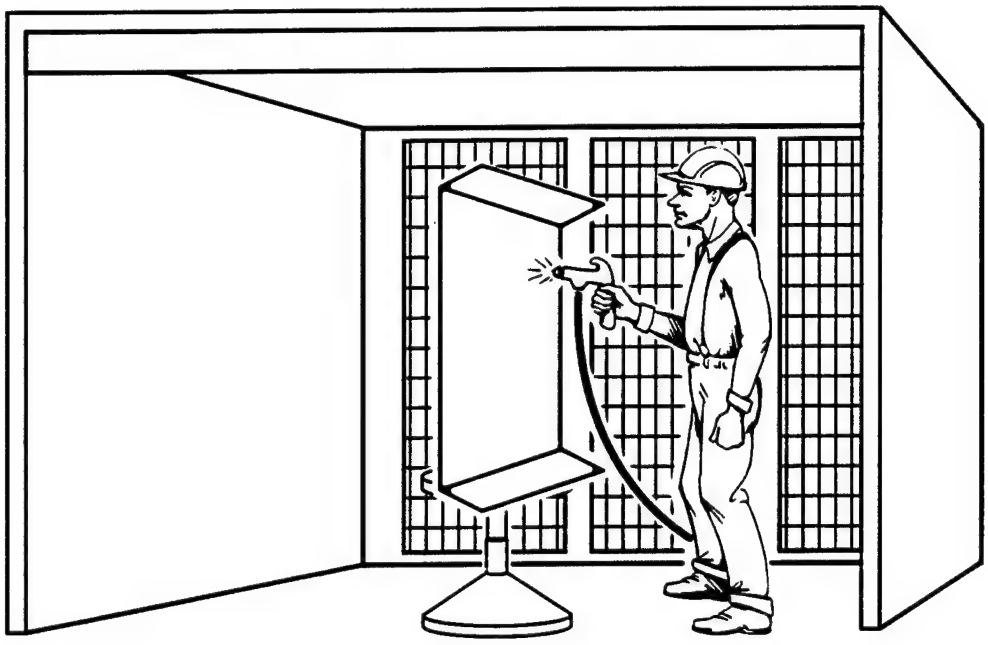

90° ORIENTATION

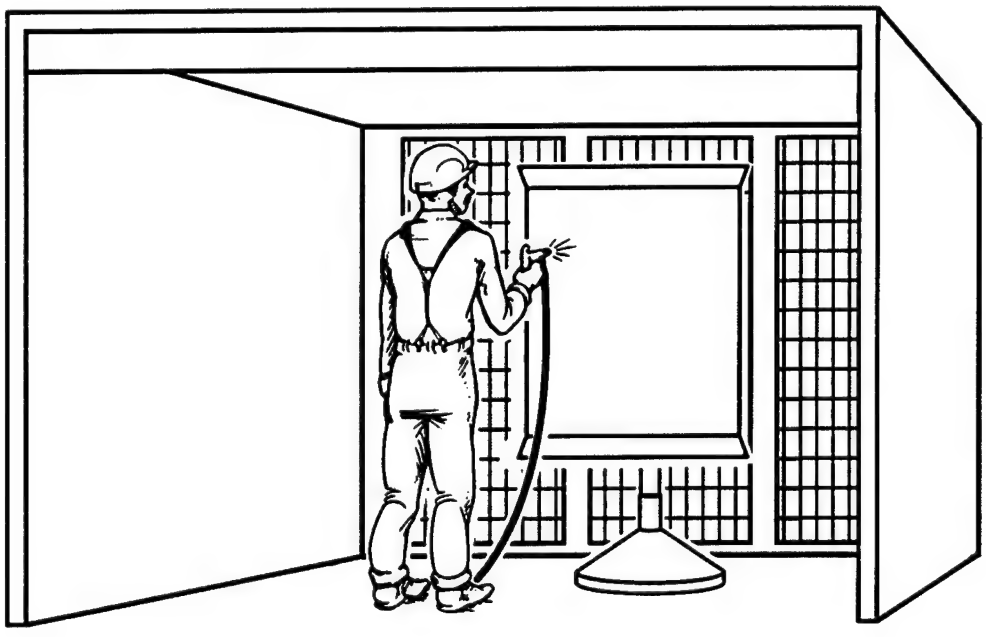

180° ORIENTATION

Figure 2.2: Worker orientation to the freestream. In the 90° orientation the freestream flows to the worker's side; in the 180° orientation, to the worker's back.

2.4. Empirical Model Development

The overspray leads directly to the worker's exposure. Controlling this overspray will result in lower breathing zone concentrations and reduced exposures, all other factors being equal. A successful model based on the overspray generation rate should lead to better control measures and allow application to a wide variety of spraying tasks.

The primary hypothesis is that the worker's average breathing zone concentration during a spraying task (C) is a mathematical function (ϕ) of the factors defining the conceptual model shown in Figure 2.1. These factors are: overspray mass generation rate; spray nozzle pressure; paint viscosity; ratio of air-to-liquid mass flows; freestream velocity; dimensions of the worker; and worker orientation to the freestream. Representing the functional dependence among these nine variables as an equation,

$$C = \phi\left(m_o, p_n, \mu_l, \frac{m_a}{m_l}, U, H, D, \text{orientation}\right) \qquad (1)$$

Since Newton's second law is not relevant to this problem, the FMLT measuring system reveals the nondimensional form of this relationship. This system designates four primary quantities (force, mass, length and time). The Buckingham Pi Theorem states the number of dimensionless groups equals the difference between the number of initial variables and the number of primary quantities.[4] Therefore, five nondimensional variables describe the functional relationship among the nine variables pertinent to a spray painting task. A dimensional analysis after selecting m_o, μ_l, U and H as the four repeating variables which do not by themselves form a dimensionless group provides the following nondimensional representation of the problem:

$$\frac{CUH^2}{m_o} = \Phi\left(\frac{m_a}{m_l}, \frac{p_n H}{\mu_l U}, \frac{H}{D}, \text{orientation}\right) \qquad (2)$$

Assuming the ratio of body height to breadth is fairly constant among workers[20] reduces the number of dimensionless groups by one and results in the final model:

$$\frac{CUHD}{m_o} = \Phi\left(\frac{m_a}{m_l}, \frac{p_n H}{\mu_l U}, \text{orientation}\right) \qquad (3)$$

The dimensional analysis indicates the concentration group $CUHD/m_o$ is a function of worker orientation to the freestream and two other nondimensional groups. The previously identified group, m_a/m_l, influences droplet size distributions from pneumatic nozzles.[7,8] The second group, p_nH/μ_lU, is new. This dimensionless quantity incorporates four important elements of the task: the spray gun (p_n), the paint (μ_l), the spray booth (U), and the worker (H).

2.5. Methods

2.5.1. Laboratory Set-up

A laboratory model of a spray painting task was used to determine the relationship among the nondimensional groups. Spraying took place in a wind tunnel which simulated a paint spray booth. The tunnel has a cross-sectional area of 25 square feet, is eight feet deep, and has uniform velocity profiles due to a flared entrance flange and a pegboard rear wall. Average freestream velocities (U) from 75-350 fpm with longitudinal component of freestream turbulence intensities of 6-11% are possible in the tunnel.

The laboratory model used a Spraying Systems 1/4J spray nozzle fitted with a 60100 fluid cap and 120 air cap (Spraying Systems Co., Wheaton, Illinois). This pneumatic, external-mixing spray nozzle operates at nozzle pressures and air-to-liquid mass flow ratios similar to a compressed air spray gun and produces comparable droplet size distributions, characterized by Kim and Marshall.[9] The nozzle operates in both gravity feed and siphon configurations. Changing the gravity feed or siphon height of a liquid container varied the liquid mass flow (m_l) to the nozzle, measured by weighing the

container before and after spraying. A compressed air source provided air for the nozzle. A pressure regulator adjusted the nozzle pressure (p_n) and air mass flow (m_a). Fixing the nozzle pressure and adjusting the liquid container height set the air-to-liquid mass flow ratio (m_a/m_l).

A mannequin 41 inches in height (H) and eight inches in breadth (D) simulated the worker. A flat plate the same height as the mannequin represented the workpiece. A flat plate produces a uniform air jet rebound and forms a reproducible overspray generation rate. Flat plates can model many common objects such as jet engines, wing flaps, refrigerators and vehicles because the air rebound from the surface facing the worker is similar to a flat plate. A flat plate also presented a small cross-sectional area to the air flow with the mannequin in the 90° orientation, preventing unnecessary blockage of the air flow and unwanted fluid dynamic effects not present in many real spray booths. The spray nozzle was at the position of the right hand of the mannequin (upstream in the 90° orientation), eight inches from the flat plate.

Corn oil simulated the paint. Corn oil is nonvolatile and combines safety, low cost and good simulation of paint properties. Because it is a natural product, a single manufacturer provided the corn oil to reduce variations in physical properties. The liquid viscosity (μ_l) varied from 39.8 to 55.2 centipoise due to liquid temperature changes, typical values for an enamel paint.

2.5.2. Overspray Generation Rate

Corn oil that impacted the flat plate during spraying drained into a trough located beneath it. The difference in trough weight before and after spraying determined the mass of corn oil transferred to the plate. The overspray generation rate (m_o) was the difference between the liquid mass flow (m_l) and the rate of corn oil transfer to the plate.

2.5.3. Breathing Zone Concentration

NIOSH Method 0500 for total aerosol mass (37-mm polyvinyl chloride membrane filters with 5-μm pore size, sampled at 2.0 lpm)[21] was the sampling method for measuring mannequin breathing zone concentrations (C), although the concentration recorded by this method may differ from the unsampled aerosol due to sampling error.[22] Among the important errors are the inlet sampling efficiency of the cassette affected by the aerosol size distribution, ambient air velocity, and sampler orientation[23-27]; transport loss from deposition on the cassette walls[24,28-29]; the filter collection efficiency[30]; and evaporative loss from the filter during sampling.[31] The inhalable dust sampler developed at the Institute of Occupational Medicine addresses the transport loss problem by weighing the filter and cassette as a single unit, but the high tare weight of the cassette makes it unsuitable for monitoring short-term tasks where the collected mass is less than about 0.5 mg.[28] In addition, snce orientation was a primary factor in the model, the NIOSH sampling method was preferred because sampling efficiencies in the 90° and 180° orientations are known[26], allowing inferences on the effect of sampling error on the results. Because previous sampling conducted during industrial paint spraying operations showed "closed-face" sampling potentially underestimates the overall worker exposure[32], all sampling was in the "open-face" mode. The collection efficiency of 5-μm pore size filters for droplets that contribute to the mass exposure (greater than 1 μm diameter) is essentially complete.[30] The use of nonvolatile corn oil reduced evaporative loss from the filter during sampling. A Cahn model 27 electrobalance with 0.001 mg sensitivity determined filter weights. Spraying lasted long enough to ensure adequate mass collection using the NIOSH recommended range of 0.1 to 2.0 mg as a guide, usually 5 to 10 minutes.

2.5.4. Experimental Design

The three independent dimensionless groups, m_a/m_l, p_nH/μ_lU, and orientation, were varied to determine their functional relationship with the dependent nondimensional concentration group, $CUHD/m_o$. The air-to-liquid mass flow ratios were 0.70, 0.90 and 1.30. There were two worker orientations, either 90° or 180° to the freestream. The nozzle pressure and wind tunnel velocity varied from 20-50 psig and 75-200 fpm respectively, providing p_nH/μ_lU values from 2.56×10^6 to 2.34×10^7. The quantity p_nH/μ_lU varied over ten experimental values for each value of m_a/m_l and orientation, giving a total of 60 experimental trials. Each trial had three replicates for a sum of 180 experimental runs.

2.6. Results

The functional relationship of p_nH/μ_lU to the concentration group $CUHD/m_o$ for the two worker orientations to the freestream is shown in Figure 2.3. Statistical analysis indicates m_a/m_l is not a significantly factor ($p = 0.72$). Therefore, the points shown are averages of the nine runs (three replicates of three m_a/m_l values) for each p_nH/μ_lU value. Error bars represent one standard deviation. The orientation curves cross when p_nH/μ_lU equals 5.0×10^6. $CUHD/m_o$ is higher in the 90° orientation if p_nH/μ_lU exceeds 5.0×10^6, but if p_nH/μ_lU is less than 5.0×10^6 $CUHD/m_o$ is higher in the 180° orientation.

A regression analysis found the following best-fit curves, graphed in Figure 2.3.

90° orientation:

$$\frac{CUHD}{m_o} = \frac{1}{\left\{7.44 + 1.08 \times 10^3 \exp\left[-5.64 \times 10^{-7} \frac{p_n H}{\mu_l U}\right]\right\}}, \; r^2 = 0.98 \qquad (4)$$

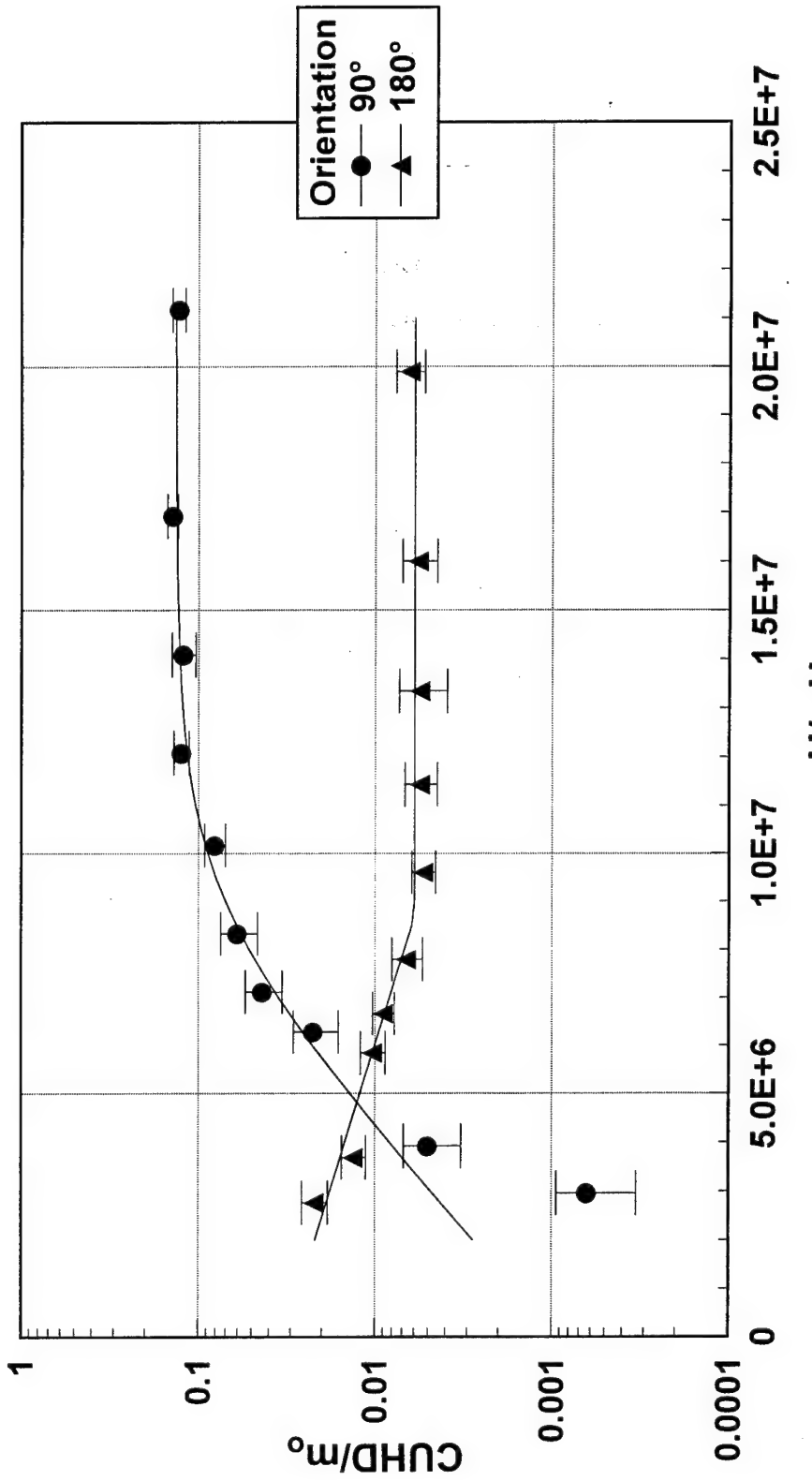

Figure 2.3: Functional relationship between the dimensionless groups identified by dimensional analysis as important to a spraying task

180° orientation:

$$\frac{CUHD}{m_o} = 3.23 \times 10^{-2} \exp\left[-1.94 \times 10^{-7} \frac{p_n H}{\mu_l U}\right], \; p_n H/\mu_l U < 9.0 \times 10^6, \; r^2 = 0.95 \quad (5)$$

$$= 0.006, \; p_n H/\mu_l U > 9.0 \times 10^6 \quad (6)$$

A measurement uncertainty analysis estimated the bias (fixed) and precision (random) experimental error in the nondimensional groups.[33] Bias is the systematic error constant for the duration of the experiment. Precision is the closeness of agreement among repeated measurements of the same quantity. Bias and precision are combined into an uncertainty, the limits within which the true value of the dimensionless group is expected to be. These estimates are listed in Table 2.1.[2] The relatively large uncertainty in $CUHD/m_o$ is due to inaccuracy in the NIOSH sampling method (±11.04%).[21]

Table 2.1: Estimated Measurement Error and Uncertainty in Nondimensional Groups (percent)

Nondimensional Group	Bias Error	Precision Error	Uncertainty (95%)
$CUHD/m_o$	4.5	6.1	13.0
p_nH/μ_lU	6.8	3.6	9.9
m_a/m_l	2.4	0.9	3.0

[2]See Appendix A for a more complete discussion of experimental error and measurement uncertainty.

2.7. Discussion

The results shown in Figure 2.3 provide an empirical exposure model. Worker orientation and the nondimensional group p_nH/μ_lU explain the variability in the average value of the concentration group $CUHD/m_o$ within the measurement uncertainty of the experimental set-up. Why m_a/m_l is not a significant factor is addressed in Chapter 4.

As mentioned earlier, the measured breathing zone concentration is less than the actual concentration due to sampling error. As a result, the actual values of $CUHD/m_o$ are higher than indicated in Figure 2.3, meaning the orientation curves are "shifted down" from their true values. This sampling error, however, is generally greater in the 90° orientation than the 180° orientation at the freestream velocities used in this experiment.[26] This difference means the measured values of $CUHD/m_o$ are reduced more in the 90° orientation than in the 180° orientation. Therefore, the 90° orientation curve in Figure 2.3 is "shifted down" more than the 180° orientation curve. Even with this greater sampling error in the 90° orientation the two orientation curves do not overlap within experimental error except at their crossover point, leading to the conclusion that the orientation curves are different.

The most striking result apparent from Figure 2.3 is the importance of worker orientation to the freestream. George *et al.*[11] identified this orientation effect for a passive contaminant source (tracer gas) released near a mannequin in a wind tunnel. They found higher breathing zone concentrations in the 180° orientation for all wind tunnel velocities (49-265 fpm). The situation for an aerosol injected with significant momentum into a flow field is more complex. For a given nozzle pressure, liquid viscosity, and average freestream velocity, the mannequin's breathing zone concentration is higher in the 90° orientation if p_nH/μ_lU exceeds 5.0×10^6, but higher in the 180° orientation when p_nH/μ_lU is less than this value. These results are counter to common industrial hygiene recommendations to place contaminant sources between the worker and exhaust to lower exposures. At least in the laboratory, this rule is invalid for low values of p_nH/μ_lU.

Observation of the spraying task provides an explanation for the crossover effect. At high nozzle pressures (corresponding to larger values of p_nH/μ_lU) and the mannequin in the 90° orientation, the air jet propelled some of the overspray droplets toward the wind tunnel entrance (see Figure 2.4). The freestream eventually captured these droplets, reversing them back into the wind tunnel and through the breathing zone of the mannequin. In the 180° orientation the air jet appeared to overwhelm any reverse flow effect and prevented droplets from entering the wake of the mannequin; the freestream captured the droplets before they could enter the breathing zone. The result was higher breathing zone concentrations in the 90° orientation when nozzle pressures were high. On the other hand, when nozzle pressures were low (corresponding to smaller values of p_nH/μ_lU), the freestream captured the droplets quickly and few entered the breathing zone in the 90° orientation. In the 180° orientation, however, separation downstream from the mannequin possibly became important. The low momentum of the droplets allowed them to enter the wake and resulted in increased breathing zone concentrations. The end result was higher breathing zone concentrations in the 180° orientation at lower nozzle pressures.

Although the influence of freestream velocity on breathing zone concentrations was not the primary purpose of this experiment, an interesting trend was observed in the 180° orientation. For a fixed nozzle pressure, the concentration increased as the velocity increased. This trend was apparent at all nozzle pressures but was most pronounced at the lowest nozzle pressure of 20 psig. These findings agree with those of Kim and Flynn[34] that increases in freestream velocity may lead to higher breathing zone concentrations in the 180° orientation. This trend was not apparent in the 90° orientation; in all cases, increased ventilation reduced mannequin breathing zone concentrations. Although additional testing is necessary, these trends again indicate the importance of worker orientation.

Several limitations restrict the applicability of the model to field spraying tasks. The laboratory set-up was static and spraying was continuous. In actual spraying tasks, the worker and spray gun move and spraying is intermittent. The spray gun-to-workpiece

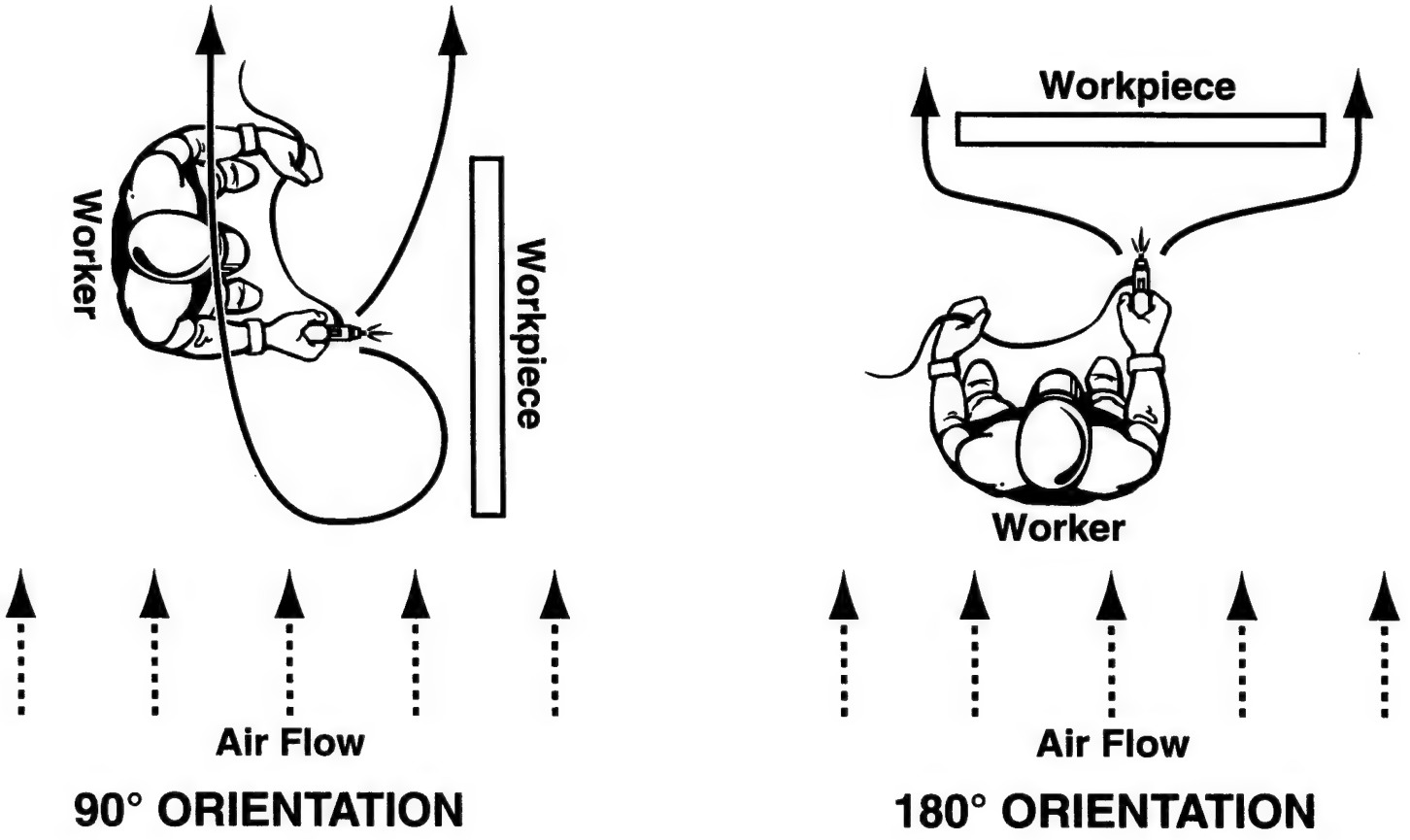

Figure 2.4: Path of the overspray for $p_n H/\mu_l U$ values greater than 5.0×10^6. In the 90° orientation the overspray passed directly through the mannequin's breathing zone, while in the 180° orientation the freestream captured the overspray before it could enter the breathing zone.

distance varies during the task and is not fixed as in this experiment, though it is poor practice to vary this distance much because it results in a poor-quality finish. A flat plate may not be representative of the workpiece. A non-volatile liquid simulated paint; in the field solvent evaporation may result in lower breathing zone concentrations than the model predicts. Most importantly, the available wind tunnel limited the laboratory set-up to a reduced scale mannequin and workpiece. Even though the spray nozzle air and liquid mass flows were less than an actual paint spray gun, scaling of the model may be a problem. Field studies are in progress to determine how well the model predicts worker exposures during actual spraying tasks and the importance of these limitations.

If validated in the field, the orientation effect may have important implications for conventional and HVLP spray painting. Conventional spraying typically operates at nozzle pressures and p_nH/μ_lU values to the right of the crossover point in Figure 2.3. Therefore, worker breathing zone concentrations may be higher when spraying in the 90° orientation and perhaps it is better to perform the task in the 180° orientation, at least from an exposure viewpoint. On the other hand, HVLP spray painting occurs at p_nH/μ_lU values to the left of the crossover point. As a result, the 90° orientation may result in lower breathing zone concentrations. Manufacturers claim HVLP spray guns reduce the mass generation rate of the overspray, but whether this leads to reduced worker exposures is questionable. The orientation effect could confound this assumption.

2.8. Conclusions

An empirical model based on dimensional analysis, which predicts breathing zone concentrations of paint mist during spray painting tasks, was developed in a laboratory wind tunnel using a mannequin, flat plate, and spray nozzle. The model indicates the nondimensional breathing zone concentration $CUHD/m_o$ is a strong function of the quantity p_nH/μ_lU and worker orientation to the freestream. A significant interaction occurs between p_nH/μ_lU and worker orientation. All other factors being equal, breathing zone concentrations are higher in the 90° orientation when p_nH/μ_lU exceeds 5.0×10^6 but

higher in the 180° orientation if $p_n H/\mu_l U$ is less than 5.0×10^6. The air-to-liquid mass flow ratio m_a/m_l does not significantly aid in predicting breathing zone concentrations in either orientation.

Field studies are in progress to determine whether the model can predict worker exposures during actual painting tasks. Differences between the laboratory set-up and field painting tasks could limit the model. This research, however, indicates the potential for an empirical-conceptual model to predict breathing zone concentrations and to identify improved control methods.

2.9. References

1. American Conference of Governmental Industrial Hygienists: Industrial Ventilation, A Manual of Recommended Practice. ACGIH, Cincinnati, OH (1995).

2. Kromhout, H.; Swuste, P.; Boleij, J.S.M: Empirical Modelling of Chemical Exposure in the Rubber-Manufacturing Industry. Ann. Occup. Hyg. 38(1):3-22 (1994).

3. Woskie, S.R.; Smith, T.J.; Hammond, S.K.; Hallock, M.H.: Factors Affecting Worker Exposures to Metal-Working Fluids During Automotive Component Manufacturing. Appl. Occup. Environ. Hyg. 9(9):612-621 (1994).

4. Taylor, E.S.: Dimensional Analysis for Engineers, pp. 1-47. Clarendon Press, Oxford, UK (1974).

5. Hund, J.P.: Spray Application Processes. Metal Finishing: Organic Finishing Guidebook and Directory Issue. 93(5A):97-111 (1993).

6. Bayvel, L.; Orzechowski, Z.: Liquid Atomization, pp. 194-199. Taylor and Francis, Washington D.C. (1993).

7. Lefebvre, A.H.: Atomization and Sprays, pp. 1-20, 238-261. Hemisphere Corp., New York, NY (1989).

8. Kim, K.Y.; Marshall, W.R.: Drop-Size Distributions from Pneumatic Atomizers. AIChE J. 17(3):575-584 (1971).

9. Kwok, K.C.: A Fundamental Study of Air Spray Painting. Ph.D. Thesis, University of Minnesota, MN (1991).

10. Hicks, P.G.; Senser, D.W.: Simulation of Paint Transfer in an Air Spray Process. In: Fluid Mechanics and Heat Transfer in Sprays, FED-Vol. 178/HTD-Vol 270, pp. 145-154. American Society of Mechanical Engineers, New York, NY (1993).

11. George, D.K.; Flynn, M.R.; Goodman, R.: The Impact of Boundary Layer Separation on Local Exhaust Design and Worker Exposure. Appl. Occup. Environ. Hyg. 5(8):501-509 (1990).

12. Kim, T.; Flynn, M.R.: Modeling a Worker's Exposure From a Hand-Held Source in a Uniform Freestream. Am. Ind. Hyg. Assoc. J. 52(11):456-463 (1991).

13. Flynn, M.R.; George, D.K.: Aerodynamics and Exposure Variability. Appl. Occup. Environ. Hyg. 6(1):36-39 (1991).

14. Flynn, M.R.; Shelton, W.K.: Factors Affecting the Design of Local Exhaust Ventilation for the Control of Contaminants from Hand-Held Sources. Appl. Occup. Environ. Hyg. 5(10):707-714 (1990).

15. O'Brien, D.M.; Hurley, D.E.: An Evaluation of Engineering Control Technology for Spray Painting. DHHS (NIOSH) Pub. No. 81-121. NIOSH, Cincinnati, OH (1981).

16. Cohen, B.S.; Brosseau, L.M.; Fang, C.P.; et al.: Measurement of Air Concentrations of Volatile Aerosols in Paint Spray Applications. Appl. Occup. Environ. Hyg. 7(8):514-521 (1992).

17. Whitehead, L.W.; Ball, G.L.; Fine, L.J.; Langolf, G.D.: Solvent Vapor Exposures in Booth Spray Painting and Spray Glueing, and Associated Operations. Am. Ind. Hyg. Assoc. J. 45(11):767-772 (1984).

18. Jayjock, M.A.; Levin, L.: Health Hazards in a Small Automotive Body Repair Shop. Ann. Occup. Hyg. 28(1):19-29 (1984).

19. Winder, C.; Turner, P.J.: Solvent Exposure and Related Work Practices Amongst Apprentice Spray Painter in Automotive Repair Workshops. Ann. Occup. Hyg. 36(4):385-394 (1992).

20. Garrett, J.W.; Kennedy, K.W.: A Collation of Anthropometry. Aerospace Medical Research Laboratory, Wright-Patterson AFB, OH (1971).

21. National Institute for Occupational Safety and Health: Particulates Not Otherwise Regulated, Total: Method 0500. In: NIOSH Manual of Analytical Methods, 4th Edition. P.M. Eller, Ed. NIOSH, Cincinnati, OH (1994).

22. Willeke, K.; Baron, P.A.: Sampling and Interpretation Errors in Aerosol Monitoring. Am. Ind. Hyg. Assoc. J. 51(3):160-168 (1990).

23. Raynor, G.S.: Variation in Entrance Efficiency of a Filter Sampler with Air Speed, Flow Rate, Angle and Particle Size. Am. Ind. Hyg. Assoc. J. 31(3):294-304 (1970).

24. Mark, D.; Vincent, J.H.: A New Personal Sampler for Airborne Total Dust in Workplaces. Ann. Occup. Hyg. 30(1):89-102 (1986).

25. Buchan, R.M.; Soderholm, S.C.; Tillery, M.I.: Aerosol Sampling Efficiency of 37 mm Filter Cassettes. Am. Ind. Hyg. Assoc. J. 47(12):825-831 (1986).

26. Chung, K.Y.K.; Ogden, T.L.; Vaughan, N.P.: Wind Effects on Personal Dust Samplers. J. Aerosol Sci. 18(2):159-174 (1987).

27. Vincent, J.H.; Mark, D.: Entry Characteristics of Practical Workplace Aerosol Samplers in Relation to the ISO Recommendations. Ann. Occup. Hyg. 34(3):249-262 (1990).

28. Mark, D.: The Use of Dust-Collecting Cassettes in Dust Samplers. Ann. Occup. Hyg. 34(3):281-291 (1990).

29. Demange, M.; Gendre, J.C.; Herve-Bazin, B.; et al.: Aerosol Evaluation Difficulties Due to Particle Deposition on Filter Holder Inner Walls. Ann. Occup. Hyg. 34(4):399-403 (1990).

30. Lee, K.W.; Ramamurthi, M.: Filter Collection. In: Aerosol Measurement: Principles, Techniques, and Applications, pp. 179-205. K. Willeke and P. Baron, Ed. Van Nostrand Reinhold, New York, NY (1993).

31. McAneny, J.J.; Leith, D.; Boundy, M.G.: Volatilization of Mineral Oil Mist Collected on Sampling Filters. Appl. Occup. Environ. Hyg. 10(9):783-787 (1995).

32. Beaulieu, H.J.; Fidino, M.S.; Arlington, K.L.B.; Buchan, R.M.: A Comparison of Aerosol Sampling Techniques: "Open" Versus "Closed-Face" Filter Cassettes. Am. Ind. Hyg. Assoc. J. 41(10):758-765 (1980).

33. American Society of Mechanical Engineers: Measurement Uncertainty, Part 1: Instruments and Apparatus. ANSI/ASME PTC 19.1-1985. ASME, New York, NY (1985).

34. Kim, T.; Flynn, M.R.: The Effect of Contaminant Source Momentum on a Worker's Breathing Zone Concentration in a Uniform Freestream. Am. Ind. Hyg. Assoc. J. 53(12):757-766 (1992).

Chapter 3: Variability in Spray Paint Mist Size Distributions[1]

3.1. Abstract

Published sampling data indicate large variability in overspray particle size distributions generated during compressed air spray painting. Several task parameters may influence this variability, including spray nozzle pressure, air-to-liquid mass flow ratio, and worker orientation to the spray booth freestream. This research investigated the importance of these parameters on the resulting breathing zone size distributions. To measure volatile paint mist distributions, droplets were collected on polycarbonate membrane filters treated with a spread retardant, then sized with a light microscope. Size distributions were measured first in a laboratory wind tunnel with a mannequin, flat plate, corn oil, and spray nozzle, then in an actual paint spray booth. The results indicate the worker's position to the freestream strongly influences breathing zone geometric mean diameters (GMD). Larger size distributions result when the worker stands with the freestream to the side (90° orientation) than to the back (180° orientation). This difference is attributed to overspray transport mechanisms that depend upon interaction of the spray gun air jet with the booth freestream. Both conventional and HVLP spraying exhibited this orientation effect, indicating that similar overspray transport mechanisms dominate both types of spraying. Nozzle pressure overall was not a significant factor. Neither the air-to-liquid mass flow ratio nor the spray mass median diameter (MMD) influenced the measured size distributions.

[1]Submitted to *Applied Occupational and Environmental Hygiene* under the title "The Influence of Spray Painting Parameters on Breathing Zone Particle Size Distributions".

3.2. Introduction

Manual spray application of paints and other types of coatings are widespread throughout industry. Spraying of paint is popular because it reduces application time and gives maintenance workers good control over the quality of the finish. Spraying, however, increases the potential for the worker to inhale contaminants in the form of droplets that fail to impact on the workpiece (the spray paint mist or overspray) and solvent vapors that evaporate from the droplets. Studies indicate vapor concentrations are generally low during spraying tasks as long as painting is done in an adequately ventilated spray booth.[1-5] Most of the worker's total mass exposure results from the overspray, consisting of paint solids and unevaporated solvent, which spray booths do a poorer job of controlling.

Several researchers have measured overspray size distributions. Bürkholz *et al.*[6] used a cascade impactor to size overspray generated by three different spray guns. The average mass median aerodynamic diameter (MMAD) varied from 5 to 7 μm. Ackley[7], also using an impactor, sprayed enamel and lacquer paints into a chamber and found MMADs around 6 μm. Chan *et al.*[8] measured the paint overspray in an automotive spray booth; MMADs ranged from 4.7 to 6.6 μm depending on the atomization pressure. D'Arcy and Chan[9] measured MMADs from 2.9 to 9.7 μm in a down-draft paint booth with a fixed target. Kwok[10] constructed a miniature spray booth and collected paint overspray exhausted from the booth. Although he did not calculate MMADs, Kwok's data indicate up to 36% of the overspray mass was greater than 17 μm, the cut-off for his first impactor stage.

These investigators dried their impactor substrates prior to gravimetric analysis. As a result, the reported MMADs represent the solids distribution in the overspray. If the solvent-to-solids ratio is not uniform across droplet sizes when collected, an unequal mass percentage volatilized from each impactor stage will bias the MMAD. Brosseau *et al.*[11], in a study of breathing zone droplet size distributions of automobile spray painters, wrapped the impactor in foil and iced it immediately after sampling completion to minimize solvent evaporation. Their results show MMADs ranging from 15.7 to 46 μm.

Even though the impactor handling method limited post-sampling evaporation, solvent may have evaporated from the substrates during sampling. This evaporation again may bias the MMAD.

Brosseau's findings, which are indicative of real worker exposures, suggest droplet size distributions are highly variable. Brosseau points out two possible sources of this variability, the type of paint used and operator technique (the workers may have sprayed toward each other as they walked around the automobiles). The key is identifying those parameters that can reduce exposure.

Compressed air spray painting is classified as either conventional or high-volume low-pressure (HVLP). Conventional spraying uses air pressures greater than 20 psig while HVLP spraying operates at 10 psig or less. Compressed air and liquid paint interact at a spray gun to form the paint spray. Adjusting the air atomization pressure of the gun (nozzle pressure p_n) changes the air feed rate (m_a). The liquid feed rate (m_l) is also adjustable. The important parameter is the air-to-liquid mass flow ratio (m_a/m_l), which influences the resulting spray size distribution.[12,13] The worker can vary the paint viscosity (μ_l) by either adding thinner or heating the paint. Spray gun-to-workpiece distances are variable, though guidelines recommend keeping this distance within six to eight inches.[14] If spraying takes place in a crossdraft paint spray booth, the worker generally orients the workpiece so the freestream flows either to the worker's side (90° orientation) or to the worker's back (180° orientation); see Figure 2.2.

The number of spray parameters within the worker's control is therefore limited. This research investigates the influence of nozzle pressure, air-to-liquid mass flow ratio, and worker orientation on the resulting breathing zone size distributions.

3.3. Sampling Method

To minimize bias from solvent evaporation, this research developed a new method for sizing volatile aerosols. Droplets were sized with an optical microscope and image processing system after collection on polycarbonate membrane filters. These filters have uniform pore sizes, possess a smooth, flat surface, and are transparent, making them

suitable for use with a light microscope.[15,16] The filter pore size used in this study was 0.2 μm. These filters collect essentially all droplets that contribute to the total mass exposure (diameters greater than 1μm).[17] The pore size is also less than the imaging limit of a light microscope, about 1 μm[18], preventing the image processing system from accidentally counting the pores. The filters were coated with Nyebar Type K® oil spread retardant to prevent droplet collapse on the filter surface. Nyebar is a 2% solution of a fluorocarbon surfactant. An even coating was applied to the collecting surface by dipping the filter in a petri dish containing the retardant solution and allowing the solvent to evaporate.

3.3.1. Calibration of Sampling Method

Even with the use of a spread retardant, droplets tend to flatten on the filter due to interfacial forces between the filter and liquid. Therefore, the droplet size observed on the filter (d_f) is larger than the true diameter prior to collection (d_p). A "spread factor" or "flattening coefficient" is necessary to relate the observed size to the true droplet diameter.

To measure the spread factor, monodisperse liquid aerosols were generated with a TSI® Model 3050 Vibrating Orifice Aerosol Generator (VOAG). This apparatus forces a solution through a small orifice. A piezoelectric crystal, which holds the orifice, vibrates and breaks the liquid jet into uniform droplets. The combination of orifice size, liquid flow, and breakup frequency produces primary droplets from 20 to 100 μm. Evaporation of a volatile solvent from the primary droplets produces smaller droplets.

The spread factor was measured with corn oil because paint solids would clog the VOAG orifice. Corn oil simulates paint enamel well because both have similar viscosities. Droplets from 2.9 to 16.7 μm were generated using a 20-μm orifice and a solution of corn oil in absolute ethanol. A trace quantity of methylene blue added to the solution improved droplet visibility under the microscope. Olan-Figueroa *et al.*[19] found adding a nonvolatile impurity had little effect on spread factor, especially at the low concentrations used here. Droplets passed through a charge neutralizer to reduce electrical charge before collection on the filters. The droplets were then sized with an optical microscope using a 20X

objective and 10X eyepiece equipped with a filar micrometer. Fifty droplets were sized at random on each filter. Droplets were also collected on Nyebar-treated microscope slides to compare with findings of previous investigators.

3.3.2. Determination of Spread Factor

The results of the VOAG calibration are shown in Figure 3.1. Error bars represent one standard deviation. The spread factor, the slope of the line of flattened diameter versus droplet diameter (d_f/d_p), equals 1.34 ($r^2 = 0.9998$). The same spread factor was found for droplets collected on microscope slides (results not shown). Olan-Figueroa measured a spread factor of 1.34 for oleic acid collected on Nyebar-treated slides. This agreement is not surprising considering oleic and linoleic acids usually constitute over 80% of the fatty acids in corn oil[20] and the surface tension of corn oil (32.5 dyne/cm, measured with a Fisher surface tensiomat) is similar to oleic acid (32.3 dyne/cm[21]).

Based on the geometry of a droplet spreading out on a flat surface, a spread factor of 1.34 corresponds to a contact angle between the liquid and filter surface of 83°. Liu *et al.*[21] found no apparent variation in spread factor for 2-50 μm oleic acid droplets collected on slides using a similar fluorocarbon surfactant. Therefore, the spread factor for corn oil droplets larger than those generated by the VOAG should be close to 1.34. To test this hypothesis, a 400 μm corn oil droplet on a Nyebar-treated microscope slide was viewed with a goniometer. The contact angle measured 81.5°, indicating a slight increase in spread factor to 1.35. For the droplets of interest to spray painting tasks (less than 100 μm), this increase is insignificant.

3.4. Experimental Methods

3.4.1. Laboratory Sampling

A laboratory model of a spray painting task was set-up in a wind tunnel to simulate a paint spray booth. The tunnel has a cross-sectional area of 25 square feet, is eight feet

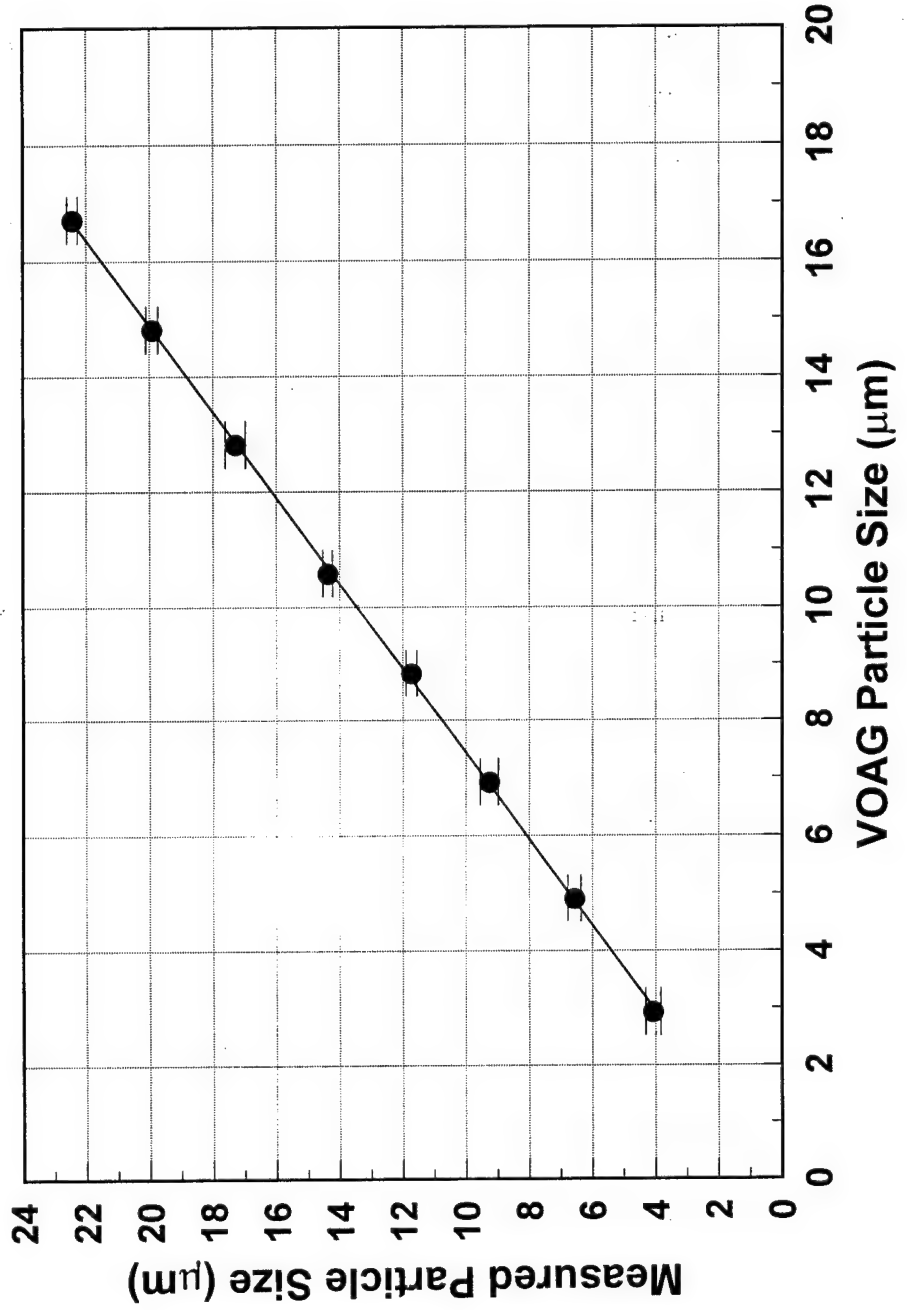

Figure 3.1: Relation between flattened diameter and true droplet diameter, corn oil collected on treated polycarbonate filters.

deep, and provides an average freestream velocity of 100 fpm with a longitudinal component of freestream turbulence intensity of 10%. A Spraying Systems 1/4J spray nozzle fitted with a 60100 fluid cap and 120 air cap (Spraying Systems Co., Wheaton, Illinois) represented the paint spray gun. This nozzle operates at pressures and air-to-liquid mass flow ratios similar to a conventional spray gun. Kim and Marshall[13] characterized its droplet size distribution. The liquid mass flow (m_l) varied by changing the gravity feed or siphon height of a liquid container. The nozzle pressure (p_n) and air mass flow (m_a) were set by regulating the compressed air fed to the nozzle. A mannequin and flat plate 41 inches in height represented the worker and workpiece, respectively. The spray nozzle was in the right hand position of the mannequin eight inches from the flat plate. Corn oil simulated paint.

The three experimental variables were nozzle pressure, air-to-liquid mass flow ratio, and worker orientation to the freestream. Nozzle pressures were 30, 40, and 50 psig. Air-to-liquid mass flow ratios were 0.70, 0.90, and 1.30. Worker orientations were 90° and 180° to the freestream. For each combination of p_n, m_a/m_l, and orientation, samples were collected in the breathing zone of the mannequin with 37 mm Nyebar-treated polycarbonate filters sampled at 2.0 liters per minute. Sampling was done in closed-face mode. Open-face sampling resulted in a nonuniform droplet pattern on the filter probably due to flow vortices within the sampler as described by Baron *et. al.*[22] A total of 18 experimental trials were done. Each trial had two replicates for a total of 36 experimental runs.

Samples were viewed with an optical microscope (200X) fitted with a digital camera. The camera fed pictures to a computer equipped with image processing software (NIH Image 1.57) which counted and sized the droplets. To increase droplet visibility, the filters were exposed to osmium tetraoxide vapors for three minutes prior to analysis. Osmium tetraoxide reacts with unsaturated lipids in the corn oil[23] and turns the droplets black. Twenty fields were examined on each filter using the equal area traverse method recommended by Leith and First.[24] The total number of droplets counted per filter averaged 2000.

3.4.2. Field Sampling

Field sampling took place in a paint spray booth measuring 46.5 square feet in cross-sectional area and 13.6 feet deep. The booth has an average freestream velocity of 100 fpm across the face with a 13% coefficient of variation. A worker 5 feet 11 inches in height painted a flat plate 3 feet wide and 6 feet tall with a high-solids enamel thinned to 23 seconds Zahn #2 Cup (45 centipoise). The worker applied the paint with a DeVilbiss conventional spray gun (model JGA-510-30EX) and a DeVilbiss HVLP spray gun (model MSV-533-4-FF). The conventional gun delivers paint through a siphon feed cup. A pressurized container provides paint to the HVLP gun. Air mass flows were calibrated with a primary standard spirometer. Weighing the paint containers before and after spraying determined liquid mass flows.

The experimental variables were nozzle pressure and worker orientation. Nozzle pressures were 10 psig (HVLP) and 30, 40, and 50 psig (conventional). These pressures corresponded to air-to-liquid mass flow ratios of 1.50 (HVLP) and 1.32, 1.51, and 1.46 (conventional). Worker orientation was 90° and 180° to the spray booth freestream. Sampling medium was 37 mm Nyebar-treated polycarbonate filters. The filter cassette was attached to the worker's lapel with a cassette holder designed to hold the face of the cassette parallel to the worker's body. Three replicates of the eight experimental trials were performed, for a total of 24 experimental runs. The filters were analyzed as before. An average of 2000 droplets were counted on each filter. A typical view of the collected droplets is shown in Figure 3.2.

Analysis of the data assumes a droplet spread factor of 1.34, although this was not measured directly. Kwok[10] measured the spread factor of paint droplets on untreated microscope slides. The spread factor averaged 1.31 for 10 to 60 μm droplets. The spread factor, however, tended to increase with increasing droplet size. Underestimating the spread factor will result in an overestimation of the true droplet diameter.

3.4.3. Statistical Analysis

Geometric mean diameters (GMD) and geometric standard deviations (GSD) were computed for each experimental run.[25] Analysis of variance (ANOVA) determined the significance of the task parameters (p_n, m_a/m_l, orientation) on the measured GMDs. If the ANOVA test for p_n or m_a/m_l was found statistically significant in a specific orientation, the Tukey method for multiple comparisons of the means[26] concluded which values were different.

3.5. Results

3.5.1. Laboratory Sampling

The breathing zone GMDs and GSDs of the mannequin averaged over spray nozzle pressure and orientation to the freestream are summarized in Table 3.1. The mean GMDs are graphed in Figure 3.3. Error bars represent standard error of the mean.

The overall average GMD is 13.5 μm in the 90° orientation and 10.9 μm in the

TABLE 3.1: Laboratory and Field GMDs (GSDs) Averaged Over Replicate Nozzle Pressure and Orientation Sampling Runs

	Laboratory		Field	
Pressure	**90°**	**180°**	**90°**	**180°**
30	13.4 (1.5)	11.2 (1.5)	8.6 (1.7)	7.3 (1.7)
40	13.8 (1.6)	11.0 (1.4)	8.3 (1.7)	7.3 (1.7)
50	13.2 (1.6)	10.6 (1.4)	9.0 (1.7)	7.8 (1.7)
10 (HVLP)	n/a	n/a	9.7 (1.6)	7.4 (1.7)

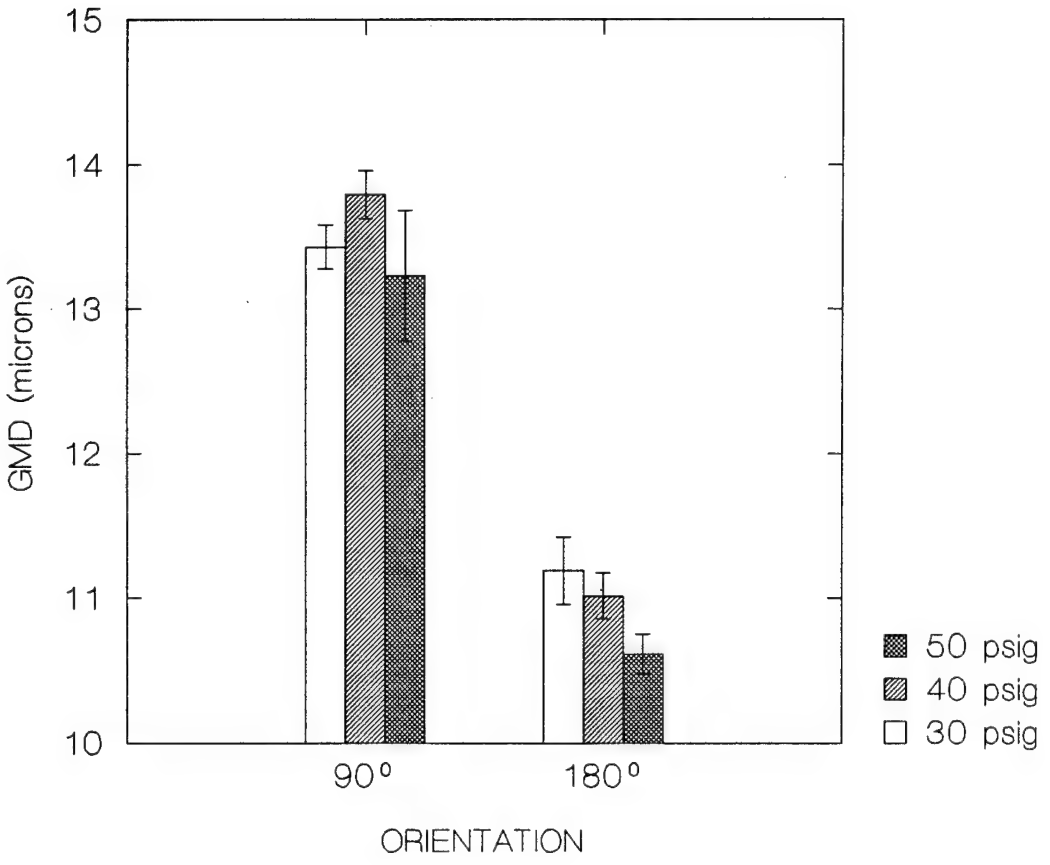

Figure 3.3: **Average mannequin "breathing zone" GMD versus worker orientation and spray nozzle pressure**

180° orientation. This difference is highly significant ($p = 0.0001$). Nozzle pressure was not a significant factor in the 90° orientation ($p = 0.40$). In the 180° orientation, however, average breathing zone GMDs decreased as nozzle pressures increased ($p = 0.049$). Statistical analysis using the Tukey method indicates the differences between the mean GMDs at 30 and 50 psig are significant at the 0.05 level of significance. The quantity m_s/m_l was not a significant experimental factor in either the 90° orientation ($p = 0.17$) or the 180° orientation ($p = 0.09$).

Another view of the orientation effect is in Figure 3.4, which shows the droplet size mass frequency distributions. The distributions shown are averages for each orientation. Error bars represent one standard deviation. Besides having a lower overall mass median diameter (MMD), the 180° orientation has a higher percentage of its mass in the smaller droplets, and less in the larger droplets, when compared to the 90° orientation.

The droplet MMD exiting the spray nozzle was calculated for each experimental run from the Kim and Marshall equation.[13] Spray MMDs ranged from 40 to 65 μm. Breathing zone MMDs were found from the measured size distributions. Linear regression was used to determine whether a correlation exists between spray and breathing zone MMDs. The null hypothesis of "no significant straight line relationship of breathing zone MMD to spray MMD" is not rejected ($p = 0.61$). The analysis indicates breathing zone MMD is not correlated to spray MMD.

3.5.2. Field Sampling

Measured breathing zone GMDs are summarized in Table 3.1 and graphed in Figure 3.5. For the conventional gun, average breathing zone GMDs were 8.6 and 7.5 μm in the 90° and 180° orientations, respectively. As in the laboratory, this difference is significant ($p = 0.04$). The HVLP gun produced average breathing zone GMDs of 9.7 μm in the 90° orientation and 7.4 μm in the 180° orientation ($p = 0.0001$). Nozzle pressure was not a significant factor in either the 90° orientation ($p = 0.73$) or the 180° orientation ($p = 0.80$).

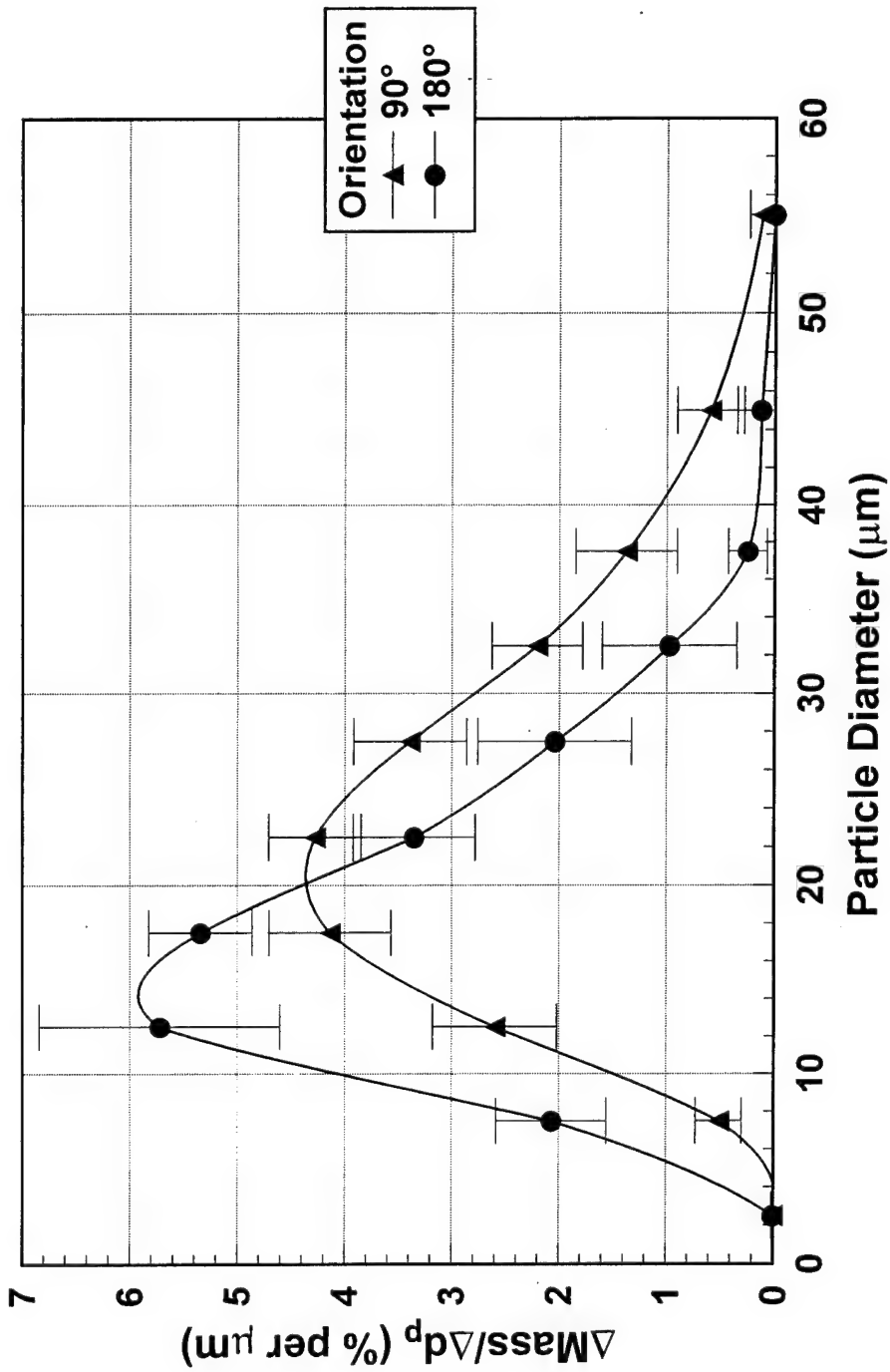

Figure 3.4: Breathing zone mass frequency distributions generated during laboratory sampling. The curves are averaged over all data in the 90° and 180° orientations.

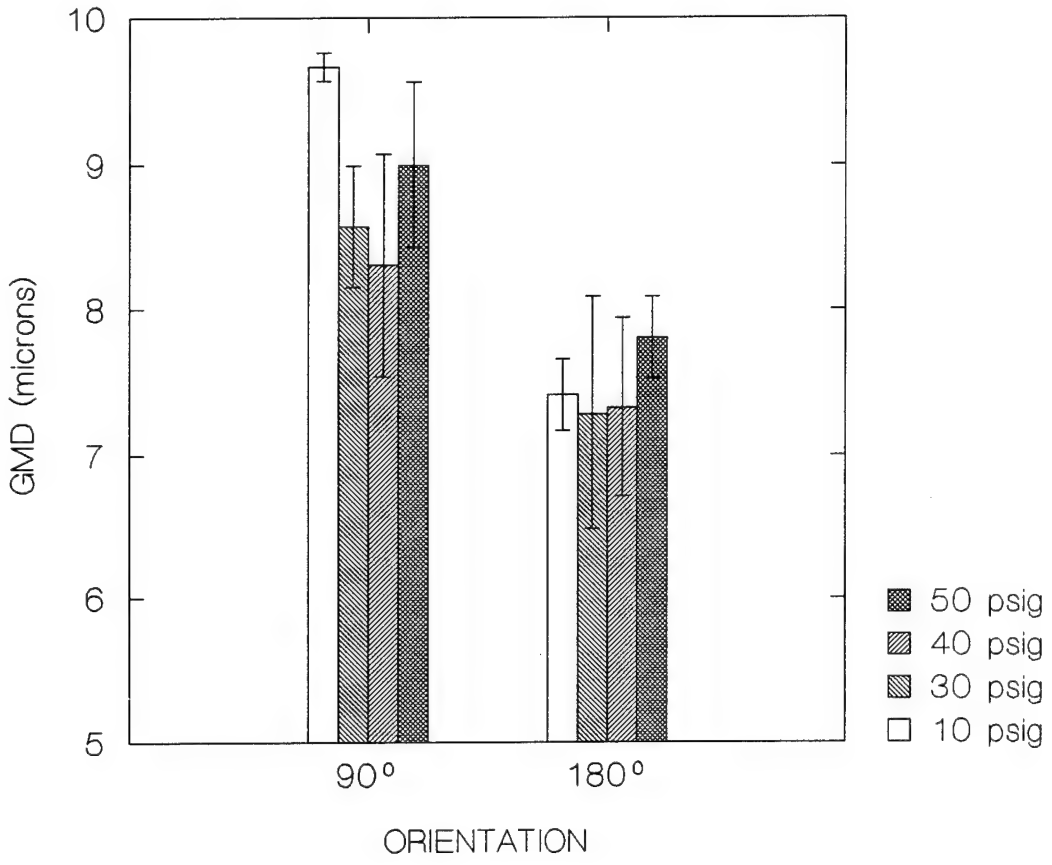

Figure 3.5: Average worker breathing zone GMD versus worker orientation and spray nozzle pressure, field sampling.

The count data were approximately log-normal for all runs. A typical cumulative distribution plot is in Figure 3.6. Generation of mass distributions from count data generally assumes constant particle density. If all paint droplets form with a uniform solvent-to-solids ratio, unequal evaporation rates across the size range could lead to varying particle densities and a biased frequency curve. The use of a high-solids enamel minimized these evaporative effects, although they were probably still present to some extent.

Keeping these reservations in mind, the droplet size mass distributions for the conventional and HVLP spray guns, averaged for each orientation, are shown in Figures 3.7 and 3.8. Average MMDs in the 90° and 180° orientations were 19.2 and 14.1 μm (conventional gun) and 18.9 and 14.8 μm (HVLP gun). As in the laboratory, the 180° orientation shows a higher mass percentage in the smaller sizes but less mass in the larger sizes versus the 90° orientation.

3.6. Discussion

Sampling an aerosol with filter cassettes can result in sizing bias due to sampling error.[27] Among the important errors with the sampling method developed here are the inlet sampling efficiency of the closed-face cassette (influenced by the droplet size distribution, freestream velocity in the booth, and the cassette orientation to the freestream[28-32]) and droplet deposition on the cassette walls prior to collection on the filter.[29,33-34] These sampling biases tend to discriminate against larger droplets and lower the measured GMD. Therefore, the true breathing zone GMDs probably were higher than indicated in Figures 3.3 and 3.5. Previous investigators found greater bias for a closed-face cassette sampling in the 90° orientation than the 180° orientation.[31] As a result, the differences in average GMDs between the two orientations is in all likelihood greater than found.

The most interesting finding is the influence of worker orientation on the droplet size distributions. Previous investigators who studied crossdraft flow booths found breathing zone concentrations varied in the two worker orientations.[35-38] This is the first

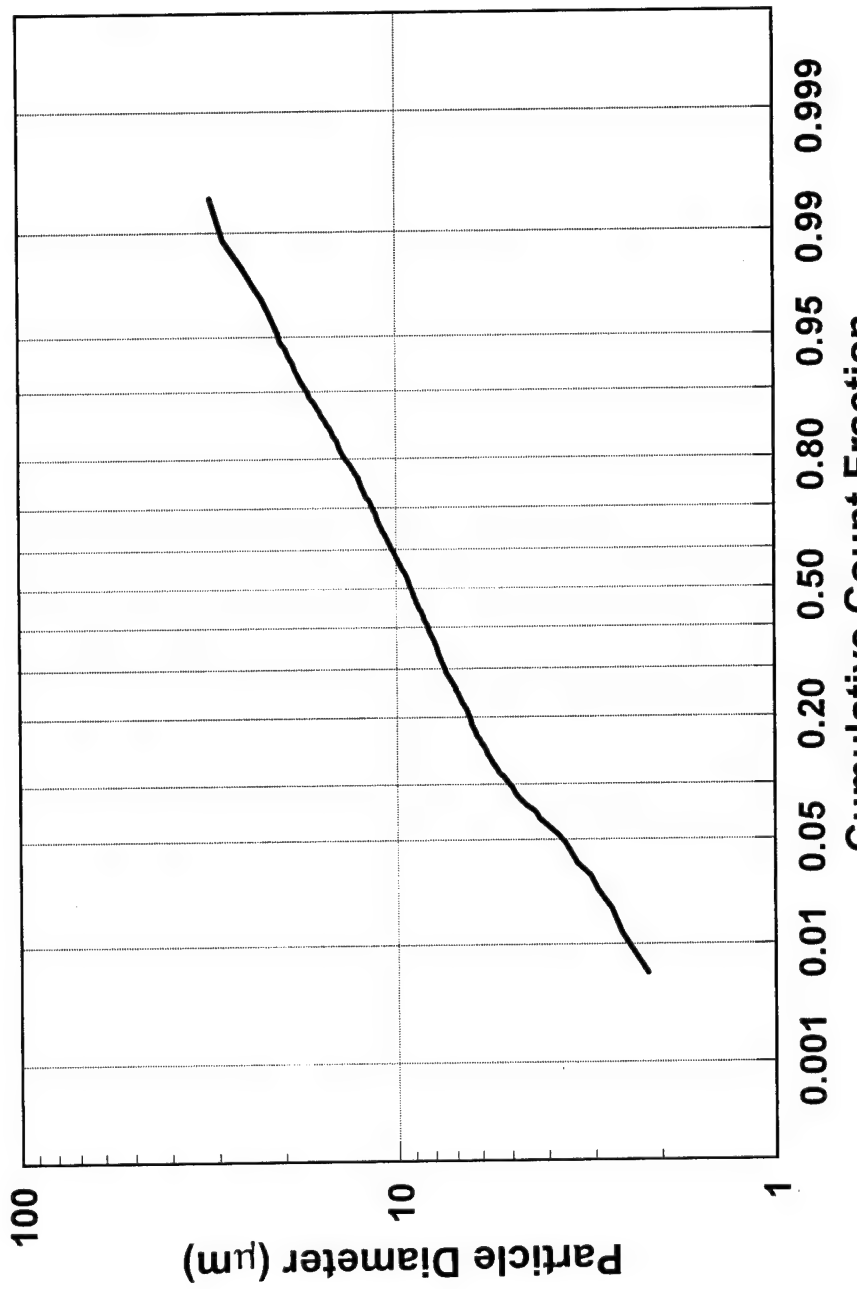

Figure 3.6: Cumulative count distribution, p_n = 30 psig, orientation = 90°. Plots for other field sampling runs are similar.

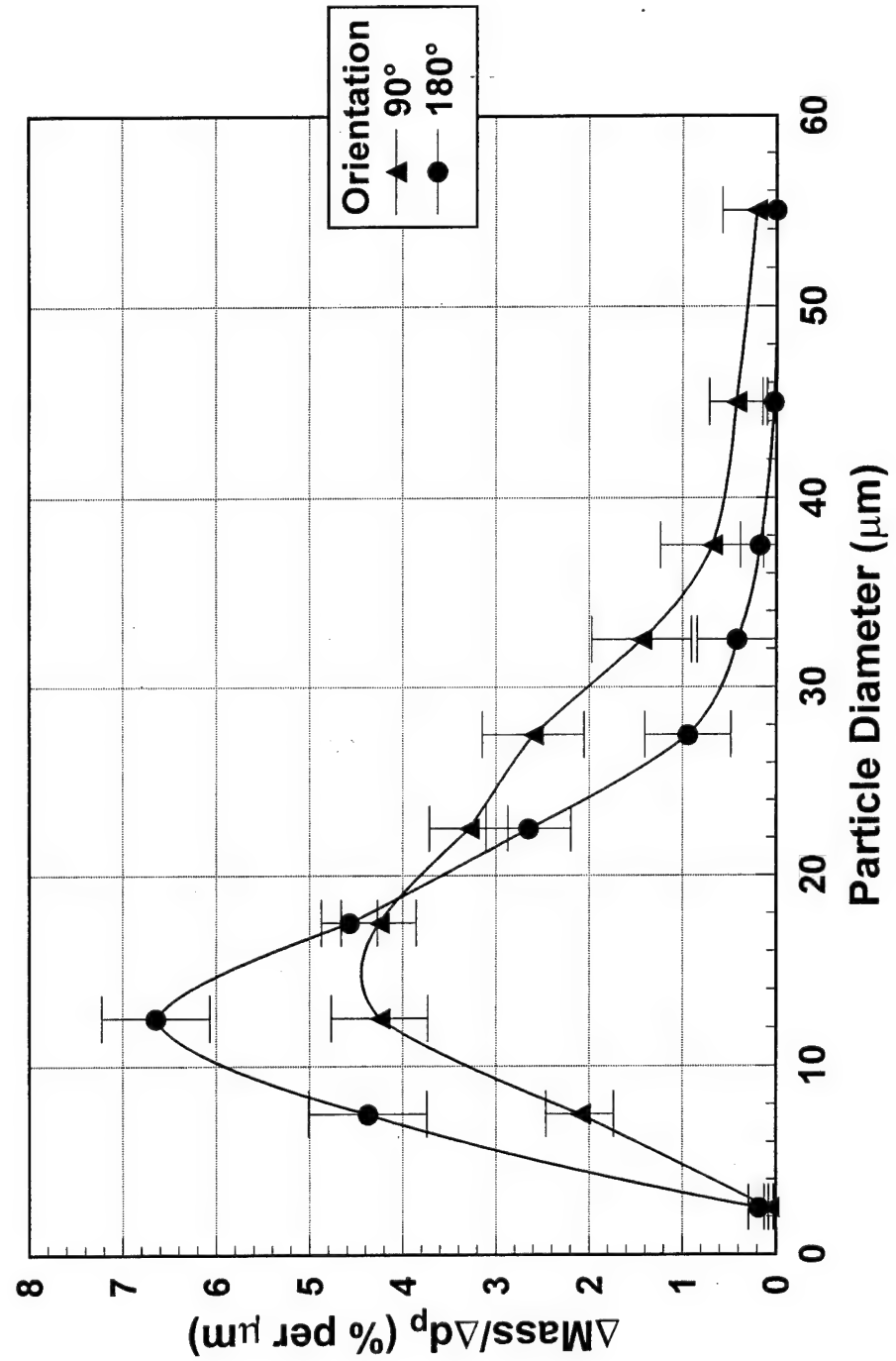

Figure 3.7: Breathing zone mass frequency distributions generated by conventional spray gun.

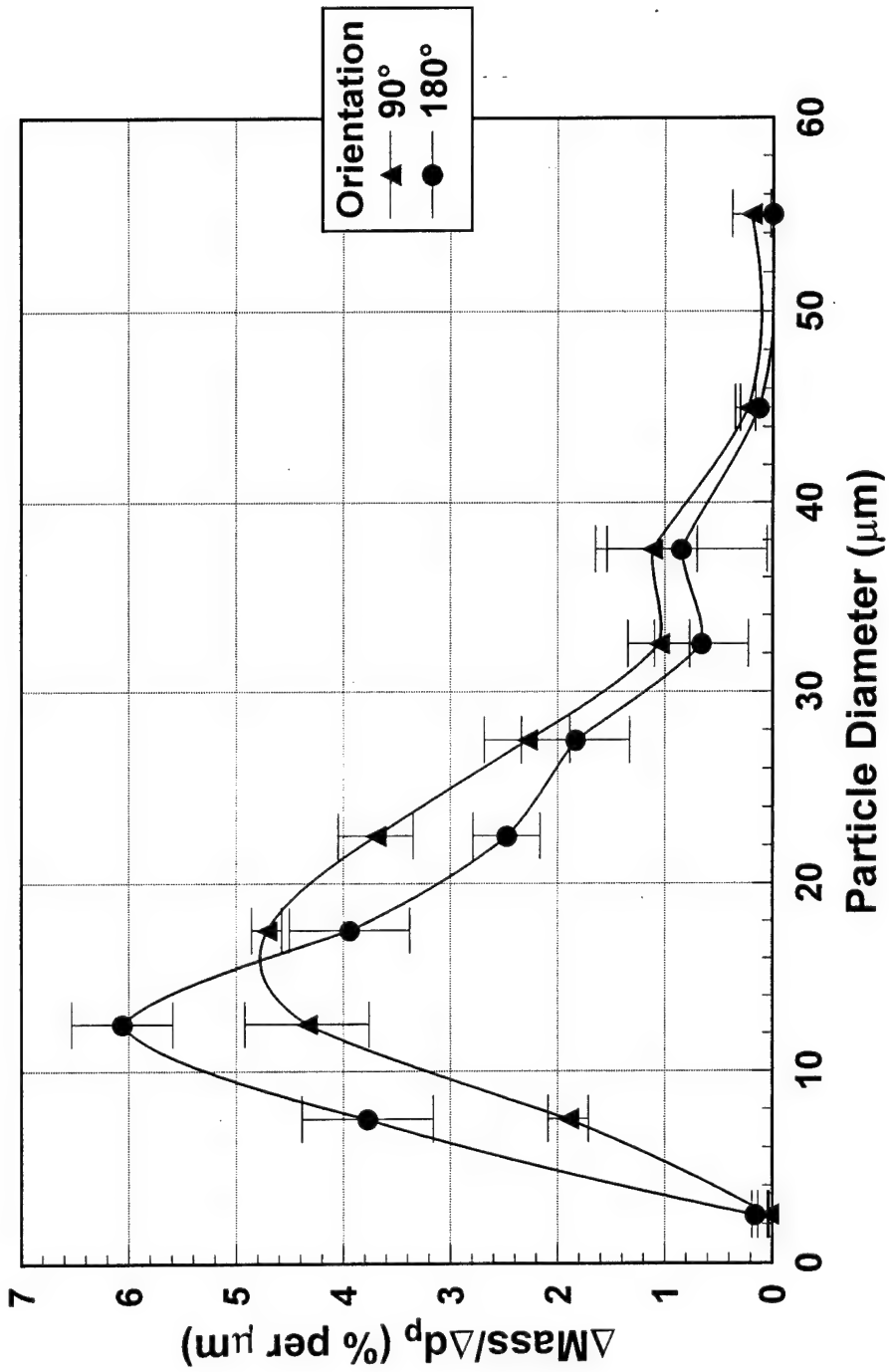

Figure 3.8: Breathing zone mass frequency distributions generated by HVLP spray gun.

study, however, to identify differences in particle size in the two orientations. It is also, as far as the author is aware, the first time an orientation effect has been seen in an actual field setting and is the major significance of this research. This difference in droplet size is suggestive of different transport mechanisms. In the 90° orientation the spray gun air jet propelled some of the overspray toward the booth inlet, where it mixed with the incoming air and subsequently passed through the worker's breathing zone. Heitbrink *et al.*[39] observed this transport mechanism in a study of spray painting in autobody repair shops. The mode of droplet transport in the 180° orientation is less clear. George *et al.*[36] performed flow visualizations with a passive source in a wind tunnel and attributed contaminant transport in this orientation to the formation of a boundary layer around the worker and a reverse flow region developed downstream of the worker. Whether this same transport mechanism is at work in a spray painting operation, which generates droplets with significant momentum, requires additional research. The orientation effect was present during both conventional and HVLP spraying, indicating the transport mechanisms in play during conventional spraying are the same ones dominating HVLP painting.

Kim and Marshall[13] found the air-to-liquid mass flow ratio affects the droplet size distribution exiting the spray nozzle. Given that this research discovered spray MMD did not influence the resulting breathing zone MMDs, it is not surprising that air-to-liquid mass flow ratio was not a significant experimental factor. Factors that solely affect the spray MMD apparently have minimal influence on the resulting breathing zone size distributions. Among these factors is paint viscosity. Changes in viscosity, like m_a/m_l, can change the spray MMD but beyond that do not influence the dynamics of the spraying task. Therefore, the influence of viscosity on breathing zone MMD is probably limited. The same can be said for other properties of the paint, such as density and surface tension, but these properties are relatively constant and do not show the large variability paint viscosity does. Note that changes in viscosity may affect total worker exposures by influencing the transfer efficiency of the spraying task.[40]

Nozzle pressure is another factor that influences the spray MMD. Its influence is, however, indirect. For a conventional spray gun operating at nozzle pressures greater

than about 20 psig, air flow through the nozzle is sonic[41] and exiting air jet velocities do not change with increasing pressures. The air mass flow will increase linearly with pressure, however.[42] Higher air flows result in smaller spray MMDs, all other factors being equal. Besides affecting the spray MMD, though, nozzle pressure can also influence the distribution of the resulting paint overspray in the spray booth. Higher nozzle pressures and the resulting higher air flows can lead to different fluid dynamic effects in a spray booth compared to lower nozzle pressures and air flows. This interaction of the air jet with the spray booth freestream influences transport of the overspray from the workpiece into the worker's breathing zone. It is not surprising, then, that nozzle pressure was found, in some cases, to influence the breathing zone size distributions.

3.7. Conclusions

This research measured the droplet size distributions of volatile paint mist in both laboratory and field settings. Droplets were collected in the breathing zone with treated polycarbonate filters and sized with a light microscope and image processing system. The results indicate a strong orientation effect, wherein the position of the worker relative to the spray booth freestream influences the breathing zone GMD. Smaller droplet sizes result when the worker stands with the freestream to the back versus standing with the freestream to the side. The only significant effect of nozzle pressure was in the 180° orientation of the laboratory model, where average breathing zone GMDs decreased as nozzle pressure increased. Spray MMD had no influence on the resulting breathing zone size distributions. Factors that influence the spray MMD but not the transport of overspray into the worker's breathing zone probably have minimal effect on the resulting size distribution. Among these factors are air-to-liquid mass flow ratio and paint viscosity. One factor not considered in this research was spray booth freestream velocity. Because droplet transport mechanisms in the two worker orientations probably are related to the freestream, changes in air velocity could influence the particulate nature of a worker's exposure.

3.8. References

1. O'Brien, D.M.; Hurley, D.E.: An Evaluation of Engineering Control Technology for Spray Painting. DHHS (NIOSH) Pub. No. 81-121. NIOSH, Cincinnati, OH (1981).

2. Cohen, B.S.; Brosseau, L.M.; Fang, C.P.; et al.: Measurement of Air Concentrations of Volatile Aerosols in Paint Spray Applications. Appl. Occup. Environ. Hyg. 7(8):514-521 (1992).

3. Whitehead, L.W.; Ball, G.L.; Fine, L.J.; Langolf, G.D.: Solvent Vapor Exposures in Booth Spray Painting and Spray Glueing, and Associated Operations. Am. Ind. Hyg. Assoc. J. 45(11):767-772 (1984).

4. Jayjock, M.A.; Levin, L.: Health Hazards in a Small Automotive Body Repair Shop. Ann. Occup. Hyg. 28(1):19-29 (1984).

5. Winder, C.; Turner, P.J.: Solvent Exposure and Related Work Practices Amongst Apprentice Spray Painter in Automotive Repair Workshops. Ann. Occup. Hyg. 36(4):385-394 (1992).

6. Bürkholz, A.; Widder, J.; Muller, W.; Dislich, M.: Particle Size Distribution of Overspray Generated During Spray Painting. Polymers Paint and Colour J. 167:285-290 (1977).

7. Ackley, M.W.: Paint Spray Tests for Respirators: Aerosol Characteristics. Am. Ind. Hyg. Assoc. J. 41(5):309-316 (1980).

8. Chan, T.L.; D'Arcy, J.B.; Schreck, R.M.: High Solids Paint Overspray Aerosols in a Spray Painting Booth: Particle Size Analysis and Scrubber Efficiency. Am. Ind. Hyg. Assoc. J. 47(7):411-417 (1986).

9. D'Arcy, J.B.; Chan, T.L.: Chemical Distribution in High Solids Paint Overspray Aerosols. Am. Ind. Hyg. Assoc. J. 51(3): 132-138 (1990).

10. Kwok, K.C.: A Fundamental Study of Air Spray Painting. Ph.D. Thesis, University of Minnesota, MN (1991).

11. Brosseau, L.M.; Fang, C.P.; Snyder, C.; Cohen, B.S.: Particle Size Distribution of Automobile Paint Sprays. Appl. Occup. Environ. Hyg. 7(9):607-612 (1992).

12. Lefebvre, A.H.: Atomization and Sprays, pp. 1-20, 238-261. Hemisphere Corp., New York, NY (1989).

13. Kim, K.Y.; Marshall, W.R.: Drop-Size Distributions from Pneumatic Atomizers. AIChE J. 17(3):575-584 (1971).

14. Hund, J.P.: Spray Application Processes. Metal Finishing: Organic Finishing Guidebook and Directory Issue. 93(5A):97-111 (1993).

15. Spurny, K.R.; Lodge, J.P.; Frank, E.R.; Sheesley, D.C.: Aerosol Filtration by Means of Nuclepore Filters: Aerosol Sampling and Measurement. Environ. Sci. Tech. 3(5): 464-468 (1969).

16. Lee, K.W.; Ramamurthi, M.: Filter Collection. In: Aerosol Measurement: Principles, Techniques, and Applications, pp. 179-205. K. Willeke and P. Baron, Ed. Van Nostrand Reinhold, New York, NY (1993).

17. Spurny, K.R.; Lodge, J.P.; Frank, E.R.; Sheesley, D.C.: Aerosol Filtration by Means of Nuclepore Filters: Structural and Filtration Properties. Environ. Sci. Tech. 3(5): 454-464 (1969).

18. Fletcher, R.A.; Small, J.A.: Analysis of Individual Collected Particles. In: Aerosol Measurement: Principles, Techniques and Applications, pp. 260-295. K. Willeke and P. Baron, Ed. Van Nostrand Reinhold, New York, NY (1993).

19. Olan-Figueroa, E.; McFarland, A.R.; Ortiz, C.A.: Flattening Coefficients for DOP and Oleic Acid Droplets Deposited on Treated Glass Slides. Am. Ind. Hyg. Assoc. J. 43(6):395-399 (1982).

20. Bailey, A.E.: Bailey's Industrial Oil and Fat Products, pp. 210-211. K.F. Mattil, Ed. Interscience Publishers, New York, NY (1964).

21. Liu, B.Y.H.; Pui, D.Y.H.: Drop Size Measurement of Liquid Aerosols. Atmos. Environ. 16(3):563-567 (1982).

22. Baron, P.A.; Chen, C.; Hemenway, D.R.; O'Shaughnessy, P.O.: Nonuniform Air Flow in Inlets: The Effect on Filter Deposits in the Fiber Sampling Cassette. Am. Ind. Hyg. Assoc. J. 55(8):722-732 (1994).

23. Hayat, M.A.: Basic Techniques for Transmission Electron Microscopy, pp. 3-4. Academic Press, Inc., Orlando, FL (1986).

24. Leith, D.; First, M.W.: Uncertainty in Particle Counting and Sizing Procedure. Am. Ind. Hyg. Assoc. J. 37(2):103-108 (1976).

25. Reist, P.C.: Aerosol Science and Technology, pp. 22-23. McGraw-Hill, Inc., New York, NY (1993).

26. Kleinbaum, D.G.; Kupper, L.L.; Muller, K.E.: Applied Regression Analysis and Other Multivariable Methods, pp. 365-368. Duxbury Press, Belmont, CA (1988).

27. Willeke, K.; Baron, P.A.: Sampling and Interpretation Errors in Aerosol Monitoring. Am. Ind. Hyg. Assoc. J. 51(3):160-168 (1990).

28. Raynor, G.S.: Variation in Entrance Efficiency of a Filter Sampler with Air Speed, Flow Rate, Angle and Particle Size. Am. Ind. Hyg. Assoc. J. (3):294-304 (1970).

29. Mark, D.; Vincent, J.H.: A New Personal Sampler for Airborne Total Dust in Workplaces. Ann. Occup. Hyg. 30(1):89-102 (1986).

30. Buchan, R.M.; Soderholm, S.C.; Tillery, M.I.: Aerosol Sampling Efficiency of 37 mm Filter Cassettes. Am. Ind. Hyg. Assoc. J. 47(12):825-831 (1986).

31. Chung, K.Y.K.; Ogden, T.L.; Vaughan, N.P.: Wind Effects on Personal Dust Samplers. J. Aerosol Sci. 18(2):159-174 (1987).

32. Vincent, J.H.; Mark, D.: Entry Characteristics of Practical Workplace Aerosol Samplers in Relation to the ISO Recommendations. Ann. Occup. Hyg. 34(3):249-262 (1990).

33. Mark, D.: The Use of Dust-Collecting Cassettes in Dust Samplers. Ann. Occup. Hyg. 34(3):281-291 (1990).

34. Demange, M.; Gendre, J.C.; Herve-Bazin, B.; et al.: Aerosol Evaluation Difficulties Due to Particle Deposition on Filter Holder Inner Walls. Ann. Occup. Hyg. 34(4):399-403 (1990).

35. Heriot, N.R.; Wilkinson, J.: Laminar Flow Booths for the Control of Dust. Filtration and Separation. 16(2):159-164 (1979).

36. George, D.K.; Flynn, M.R.; Goodman, R.: The Impact of Boundary Layer Separation on Local Exhaust Design and Worker Exposure. Appl. Occup. Environ. Hyg. 5(8):501-509 (1990).

37. Flynn, M.R.; Shelton, W.K.: Factors Affecting the Design of Local Exhaust Ventilation for the Control of Contaminants from Hand-Held Sources. Appl. Occup. Environ. Hyg. 5(10):707-714 (1990).

38. Kim, T.; Flynn, M.R.: Modeling a Worker's Exposure From a Hand-Held Source in a Uniform Freestream. Am. Ind. Hyg. Assoc. J. 52(11):456-463 (1991).

39. Heitbrink, W.A.; Wallace, M.E.; Bryant, C.J.; Ruch, W.E.: Control of Paint Overspray in Autobody Repair Shops. Am. Ind. Hyg. Assoc. J. 56(10):1023-1032 (1995).

40. Carlton, G.N.; Flynn, M.R.: A Model to Estimate Worker Exposure to Spray Paint Mists. Submitted for publication to Appl. Occup. Environ. Hyg.

41. Hicks, P.G.; Senser, D.W.: Simulation of Paint Transfer in an Air Spray Process. In: Fluid Mechanics and Heat Transfer in Sprays, FED-Vol. 178/HTD-Vol 270, pp. 145-154. American Society of Mechanical Engineers, New York, NY (1993).

42. White, F.M.: Fluid Mechanics, pp. 510-541. McGraw-Hill, Inc., New York, NY (1994).

Chapter 4: Field Evaluation of the Model[1]

4.1. Abstract

Empirical-conceptual models relate exposure to various process parameters responsible for the generation and transport of airborne contaminants. If the model includes all process parameters important to defining the exposure, it has the potential for *a priori* exposure prediction. This research tested the ability of an empirical-conceptual model of a spray painting task to predict worker exposures in the field. The model relates paint mist concentrations to spray booth ventilation rates and other process parameters, including spray gun nozzle pressure, paint viscosity, mist generation rates, and worker orientation to the booth freestream. Eight workers in a paint shop were sampled over a five week period. A total of 55 tasks were sampled; 40% of the measured task exposures are within the estimated experimental error of the model prediction and 71% are within a factor of three. Excluding tasks that either did not fit the model assumptions well, or where a sampling error may have occurred, increases the percentage to 84% within a factor of three. Four of the eight worker mean exposures are within one standard error of the model prediction. These positive results indicate empirical-conceptual models can predict exposure and also aid in the design and economic optimization of engineering controls.

4.2. Introduction

The importance of engineering controls is self-evident to an industrial hygienist. For inhalation hazards the benefits of a control measure such as ventilation include

[1]Submitted to *Applied Occupational and Environmental Hygiene* under the title "Field Evaluation of an Empirical-Conceptual Exposure Model".

capture of the contaminant and a reduction in the worker's exposure. Although exposure is related to ventilation, the form of this relationship is seldom known for a specific industrial operation due to variable process parameters. A successful exposure model would describe the relationship between these parameters, the ventilation rate and the exposure.

Previous attempts to model worker exposures were done either as part of retrospective exposure assessments for epidemiological purposes[1-4] or to identify factors that could influence exposure.[5-8] These studies associated the measured exposure to various process parameters statistically and therefore are known as "empirical-statistical" models. The ability of these *a posteriori* models to predict an exposure *a priori*, however, is unknown. In addition, the assumption of linearity implicit in statistical regression analysis can obscure the functional relationship among exposure, ventilation, and process parameters. As a result, application of these models to engineering control designs is difficult.

A different modeling technique which may have wider applicability than the statistical approach is the so-called "empirical-conceptual" model. These models relate the exposure to the ventilation and process parameters using a more deterministic approach. A conceptual model depicts contaminant generation and transport processes leading to the exposure. An examination of these processes identifies important parameters that characterize the industrial operation. Once these parameters are known, they are grouped into nondimensional ratios using the technique of dimensional analysis. Experiments are then performed to determine the functional relationship among these ratios. Empirical-conceptual models improve physical insight into a problem and, most important to an industrial hygienist, can potentially be generalized to new situations.[9] As long as a sound conceptual understanding of the industrial operation exists, the model should include all process parameters important to defining the exposure. These models raise the prospect for *a priori* application and economic optimization of control.

In a previous paper[10] the authors developed an empirical-conceptual model of a compressed air spray painting task. Such tasks take place in ventilated spray booths. The model related the breathing zone concentration of paint mist to the ventilation rate and

certain process parameters believed to influence the generation and transport of the paint mist into the breathing zone. The purpose of this paper is to test the model in the field and determine its ability to predict worker exposures *a priori*.

4.3. Description of the Model

4.3.1. Model Development

A short summary of the model development follows. A more complete description can be found in the original article.[10] A worker's exposure to paint mist results from three processes common to all compressed air painting tasks: droplet formation, droplet transfer, and droplet transport.

Droplet formation results when a spray gun causes compressed air to atomize paint and form droplets. Researchers have shown empirically the important factors influencing the resulting droplet size distributions are: air pressure at the spray gun nozzle (p_n); liquid paint viscosity (μ_l); and the ratio of air-to-liquid mass flows (m_a/m_l).[11-13]

Droplet transfer creates the paint mist or overspray (m_o) that fails to coat the workpiece. The transfer efficiency of the spray, i.e., the fraction of droplets that impact on the workpiece, primarily depends on droplet momentum and spray gun-to-workpiece distance. The model assumes this distance is constant at eight inches per industry recommendations.[14] Droplet momentum is a function of the droplet size and velocity, both of which are related to the nozzle pressure.

Droplet transport moves the overspray from the workpiece into the worker's breathing zone. This transport depends on the freestream velocity in the spray booth (U). In addition, empirical observations indicate both worker orientation to the freestream and the worker size (height H and breadth D) may influence droplet transport.[15-18] During spray painting tasks, the worker generally orients the workpiece so the freestream flows either to the worker's side (90° orientation) or to the back (180° orientation); see Figure 2.1.

The primary hypothesis is that the worker's average breathing zone concentration (C) is a function (ϕ) of the process factors identified in the conceptual model presented above. Representing the dependence as an equation,

$$C = \phi\left(m_o, p_n, \mu_l, \frac{m_a}{m_l}, U, H, D, \text{orientation}\right) \quad (1)$$

Dimensional analysis provides the following dimensionless representation of the model:

$$\frac{CUHD}{m_o} = \Phi\left(\frac{m_a}{m_l}, \frac{p_n H}{\mu_l U}, \text{orientation}\right) \quad (2)$$

The model indicates the concentration group $CUHD/m_o$ depends on worker orientation to the freestream and two other nondimensional groups: the air-to-liquid mass flow ratio, m_a/m_l, and the pressure group, p_nH/μ_lU.

A laboratory set-up of a mannequin, flat plate, and spray nozzle in a wind tunnel found the functional relationship among these quantities. The results are shown in Figure 2.3. The model indicates $CUHD/m_o$ is a strong function of the quantity p_nH/μ_lU and worker orientation. The air-to-liquid mass flow ratio was not a significant factor in either orientation.

4.3.2. Further Considerations

The original paper[10] discussed the importance of worker orientation and suggested several reasons for the orientation effect illustrated in Figure 2.3. It did not, however, address why the pressure group p_nH/μ_lU is an important factor in the resulting exposure. It is also unclear why m_a/m_l is not. Some further considerations help clarify these issues.

At first glance the significance of p_nH/μ_lU, a grouping of nozzle pressure, liquid viscosity, freestream velocity, and the scaling factor of worker height, appears obscure. The relationship among these quantities can be rewritten as

$$\frac{p_nH}{\mu_lU} = \frac{H/U}{\mu_l/p_n} \tag{3}$$

Both H/U and μ_l/p_n have units of time; therefore p_nH/μ_lU is actually the ratio of two time scales:

$$\frac{p_nH}{\mu_lU} = \frac{\tau_1}{\tau_2} \tag{4}$$

The ratio of the characteristic model length, i.e., worker height, to the average freestream velocity is τ_1. It represents a measure of the residence time of overspray droplets in the vicinity of the painting task. Higher residence times correspond to a greater chance for the droplets to enter and remain in the breathing zone. Therefore τ_1 is a measure of the potential for the overspray droplets, once formed, to result in exposure.

The ratio of paint viscosity to spray gun nozzle pressure is τ_2. While the atomization process is complicated (especially with a non-Newtonian fluid such as paint), p_n and μ_l influence the droplet size distribution created by the spray nozzle.[11-13] Therefore, τ_2 should influence droplet transfer to the workpiece and the resulting overspray generation rate. In fact, since the velocity of the exiting air jet is essentially sonic at all nozzle pressures greater than 20 psig[19], and the model assumes a constant spray gun-to-workpiece distance, droplet size is *the most important factor* influencing transfer efficiency. Therefore τ_2 is a measure of the transfer efficiency of the spraying task. The measured transfer efficiencies are graphed in Figure 4.1 as a function of τ_2 and m_s/m_l, for the 180 data points used to generate the model curves in Figure 2.3. A strong

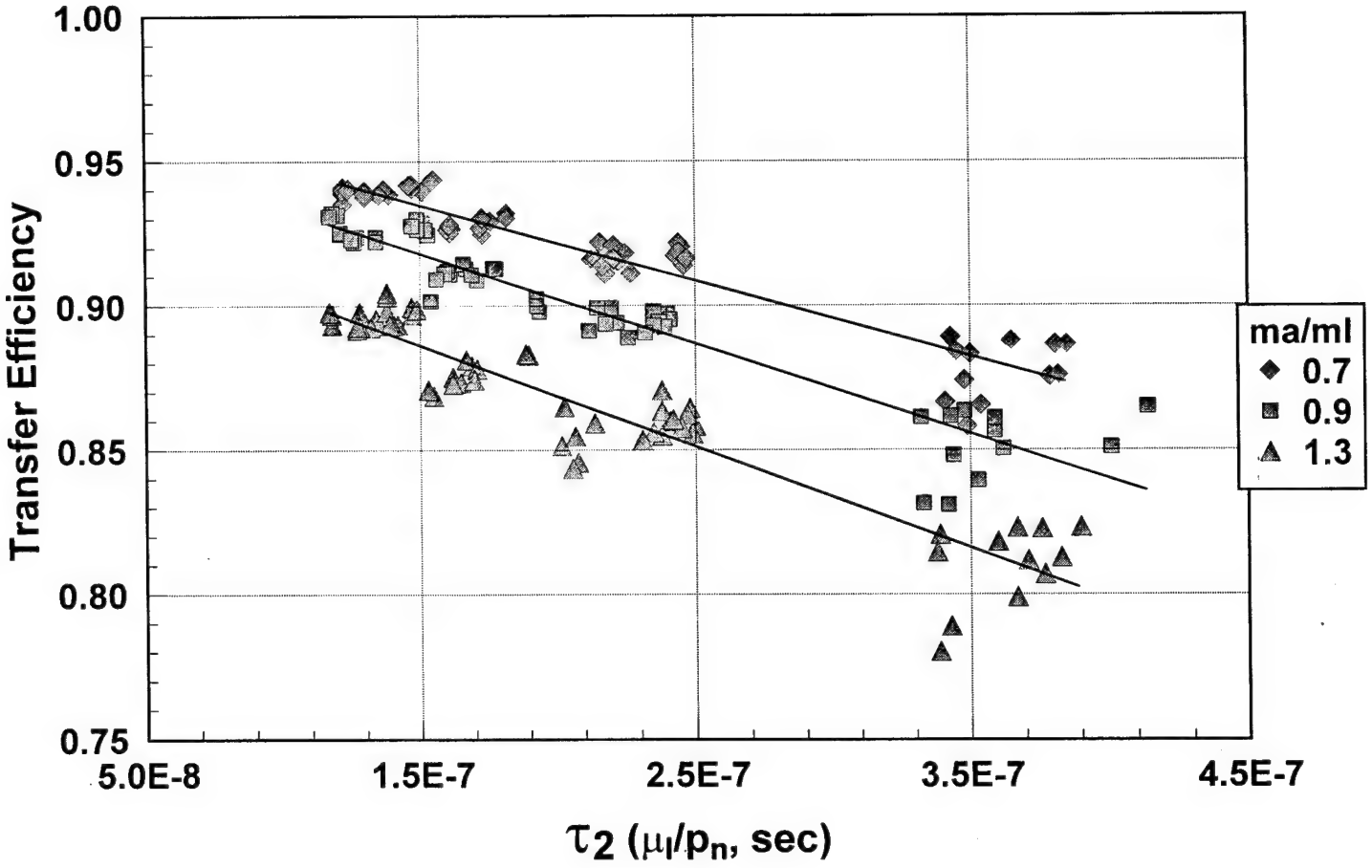

Figure 4.1: The relation between spray transfer efficiency and the spray nozzle parameters μ_l/p_n and m_a/m_l for the Spraying Systems 1/4J nozzle.

correlation between transfer efficiency and τ_2 is evident; r^2 equals 0.903, 0.901 and 0.872 for m_a/m_l values of 0.70, 0.90 and 1.30, respectively.[2]

. The quantity p_nH/μ_lU incorporates the relative contributions of the droplet transfer and transport processes in producing an exposure:

$$\frac{p_nH}{\mu_lU} = \frac{\text{droplet transport}}{\text{droplet transfer}} \qquad (5)$$

Therein lies its importance to spray painting. The quantity m_a/m_l, however, is also an important factor in the transfer efficiency of the task (in Figure 4.1 the three correlation lines are non-coincident per dummy variable regression[20], $p << 0.0001$). The factor m_a/m_l fails to enter the final model because the conceptual model related the breathing zone concentration to the overspray generation rate, not the task transfer efficiency. As a result, m_a/m_l, which influences the transfer process but not the transport process, did not appear in the analysis. Using m_o to normalize the concentration group $CUHD/m_o$ considerably simplifies the model and allows its application to spray nozzles which exhibit transfer efficiencies different than those indicated in Figure 4.1.

4.4. Methods

Field sampling took place at the Component Repair Paint Shop of Robins Air Force Base, Warner-Robins, Georgia. Robins AFB is a US Air Force logistics base performing depot level maintenance of C-141 and C-130 transport aircraft and F-15 fighter aircraft. Component parts are removed from the aircraft for necessary repairs. Prior to re-installation on the aircraft, the repaired components are primed and painted in the Paint Shop. Typical components painted include F-15 stabilizers and bomb racks, C-141 and C-130 wing flaps, and C-141 pylons.

The Paint Shop uses three spray booths of different sizes. The smallest measures

[2]Because m_a is a function of p_n, an increase in nozzle pressure does not necessarily lead to increased transfer efficiencies.

17.9 feet wide by 9.5 feet high by 29.8 feet deep. The largest measures 33.9 feet by 13.6 feet by 32.7 feet. Each booth has a water curtain to remove captured overspray in the exhaust. Workers prime with either an epoxy or a high-solids polyurethane primer, depending on the aircraft component. The paint used is a high-solids polyurethane enamel thinned with a solvent thinner. Workers use a DeVilbiss conventional spray gun, model MBC-510-30EX, in siphon feed cup configuration.

The field study followed eight workers over a five week period. A total of 55 spray painting tasks were sampled. Tasks were selected that best fit the assumptions of the model: the workpiece could be represented as a flat plate and its size was on the order of the worker's height. All tasks were video taped. The tapes were later viewed to determine the task time (t_{task}), spray time (t_{spray}), time spent spraying in the 90° orientation (t_{90}), and spraying time in the 180° orientation (t_{180}).

4.4.1. Task Exposure

Polyvinyl chloride membrane filters (5-μm pore size in 37-mm cassettes) were placed in the worker's breathing zone and sampled at 2.0 lpm to measure total aerosol mass.[21] To simulate the characteristics of the inhalable mass sampler[22] a 25-mm hole was drilled in the cap of the cassette. The filter cassette was attached to the worker's lapel with a holder designed to keep the face of the cassette parallel to the worker's body. To measure solvent that evaporated from the collected droplets during sampling, two large charcoal tubes in parallel backed-up the filter cassettes. The filters were weighed before and after sampling on a Cahn model 27 electrobalance with 0.001 mg sensitivity. An AIHA accredited lab analyzed the charcoal tubes using NIOSH Method 1550 for total hydrocarbons.[23] The task exposure was calculated from the sum of the collected solids and solvent, sampling rate, and task time.

4.4.2. Measurement of Task Parameters

A pressure tap was installed in a DeVilbiss model 30 air cap. After each spraying task, the air cap on the worker's gun was replaced with the modified air cap to measure the nozzle pressure. Paint viscosity was measured during each task with a Zahn #2 viscosity cup. Spray booth face velocities were measured with a calibrated Alnor® model 8565 thermoanemometer. Worker height and breadth were measured with a tape measure.

4.4.3. Overspray Generation Rate

The transfer efficiency of the DeVilbiss spray gun was measured directly. One siphon cup of high-solids enamel thinned to 17 seconds Zahn #2 Cup (15 centipoise, the average viscosity of the paint used) was sprayed onto a flat plate with the fan spray pattern and back-and-forth motion used by the painters. Paint that impacted on the plate drained into a trough located beneath it. The difference in trough weight before and after spraying was the mass of paint transferred to the plate. The transfer efficiency (TE) was the fraction of the sprayed mass that impacted the plate. This procedure was repeated for nozzle pressures from 50 to 90 psig, the range encountered during the field studies. Transfer efficiencies ranged from 0.78 at 50 psig (s.d. = 0.006) to 0.68 at 90 psig (s.d. = 0.009).

During each spraying task, the siphon cup was weighed before and after spraying. The difference was the amount sprayed from the cup. The total mass sprayed was the sum of these differences for all cups sprayed during the task. The overspray generation rate was estimated from the measured transfer efficiency at the nozzle pressure used:

$$m_o = (1 - TE) \times \left(\frac{\text{mass sprayed}}{t_{spray}} \right) \qquad (6)$$

4.4.4. Calculation of Predicted Exposure

The average breathing zone concentration predicted by the model (C_{model}) was weighted for the time the worker actually sprayed:

$$C_{model} = \frac{\left(C_{spray} t_{spray} + C_{off} t_{off}\right)}{t_{task}} \quad (7)$$

where total task time $t_{task} = t_{spray} + t_{off}$. Assuming the worker received an exposure only when spraying, $C_{off} = 0$. Similarly, C_{spray} was calculated as the concentration predicted by the model weighted for the times the worker spent in the two orientations:

$$C_{spray} = \frac{\left(C_{90} t_{90} + C_{180} t_{180}\right)}{t_{spray}} \quad (8)$$

where C_{90} and C_{180} were found from the measured task parameters, calculated overspray generation rate, and Figure 2.3. Combining equations 7 and 8,

$$C_{model} = \frac{\left(C_{90} t_{90} + C_{180} t_{180}\right)}{t_{task}} \quad (9)$$

For most of the spraying tasks, $p_n H/\mu_l U$ exceeded 2.0×10^7, placing the tasks in an area to the right of the model curves shown in Figure 2.3. To calculate C_{90} and C_{180} in these cases, it was assumed the curves had reached asymptotic values of 0.134 in the 90° orientation and 0.006 in the 180° orientation.

4.5. Results

The total worker exposure distribution is shown in Figure 4.2. Individual task exposures range from 7.7 to 568.6 mg/m^3. The group geometric mean exposure is 86.4 mg/m^3 with worker mean exposures varying from 40.4 to 235.2 mg/m^3. The individual task exposures are well characterized by a lognormal distribution as illustrated in Figure 4.3. A goodness-of-fit to the lognormal distribution using the Shapiro-Wilk test of normality on the log-transformed exposures indicates the hypothesis of lognormality is not rejected at the 0.05 level of significance ($p = 0.31$).

Calculated values of the dimensionless concentration group, $CUHD/m_o$, are graphed versus the pressure group, p_nH/μ_lU, in Figure 4.4. Forty-nine values (89% of the data) fall within the asymptotic limits of the model. Of the six values that fall outside the model limits, five are above the 90° orientation limit.

The predictive ability of the model is shown in Figure 4.5. Measured task exposures were on average less than that predicted by the model; 32 task exposures (58%) were less than the model prediction. Twenty-two tasks (40%) fall within the estimated experimental error of the model prediction[3], based on the measurement uncertainty of the task parameters and the overspray generation rate.[24] Thirty-nine task exposures (71%) are within a factor of three of the model prediction.

A Wilcoxon signed-rank test compared the differences between the measured exposures and the model predictions. This test was used instead of a paired t-test because the pairwise differences are not normally distributed. The signed-rank test indicates the hypothesis of no difference between measured and predicted exposures is not rejected at the 0.05 level of significance ($p = 0.91$). Regression of measured exposures on those predicted by the model gives a similar conclusion. Using either a linear regression (slope = 0.87, not significantly different from one; intercept not significantly different from zero) or a weighted regression with t_{task} as the weighting factor (slope = 0.96, not significantly

[3]The indicated experimental error represents a lower limit. Uncertainty in the measured exposure (from sampling and analysis error) is not included. In addition, additional between-worker variability not accounted for in the model may have increased the experimental error.

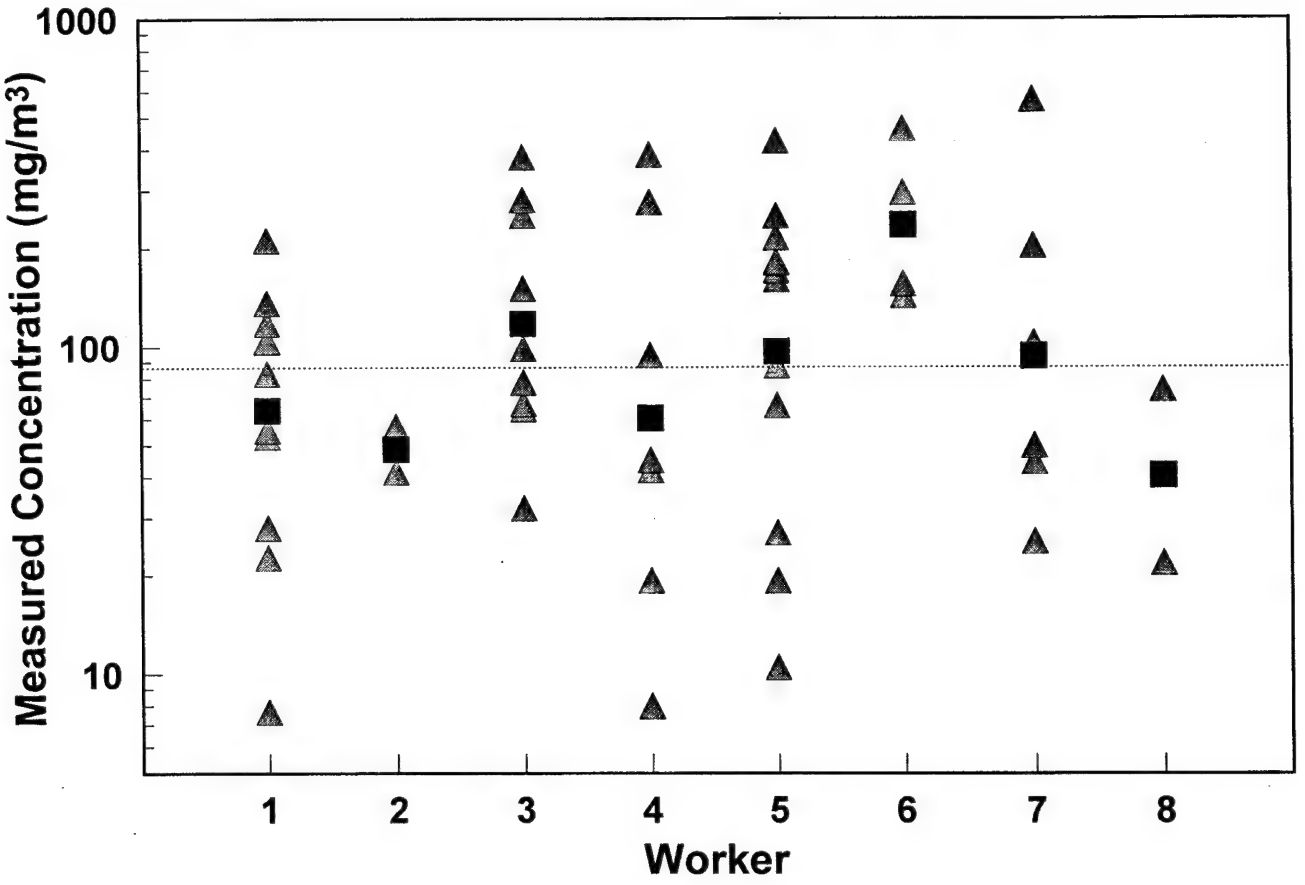

Figure 4.2: Total worker exposure distribution. Triangles represent individual tasks; squares the worker geometric mean exposure; dashed line the overall group mean exposure.

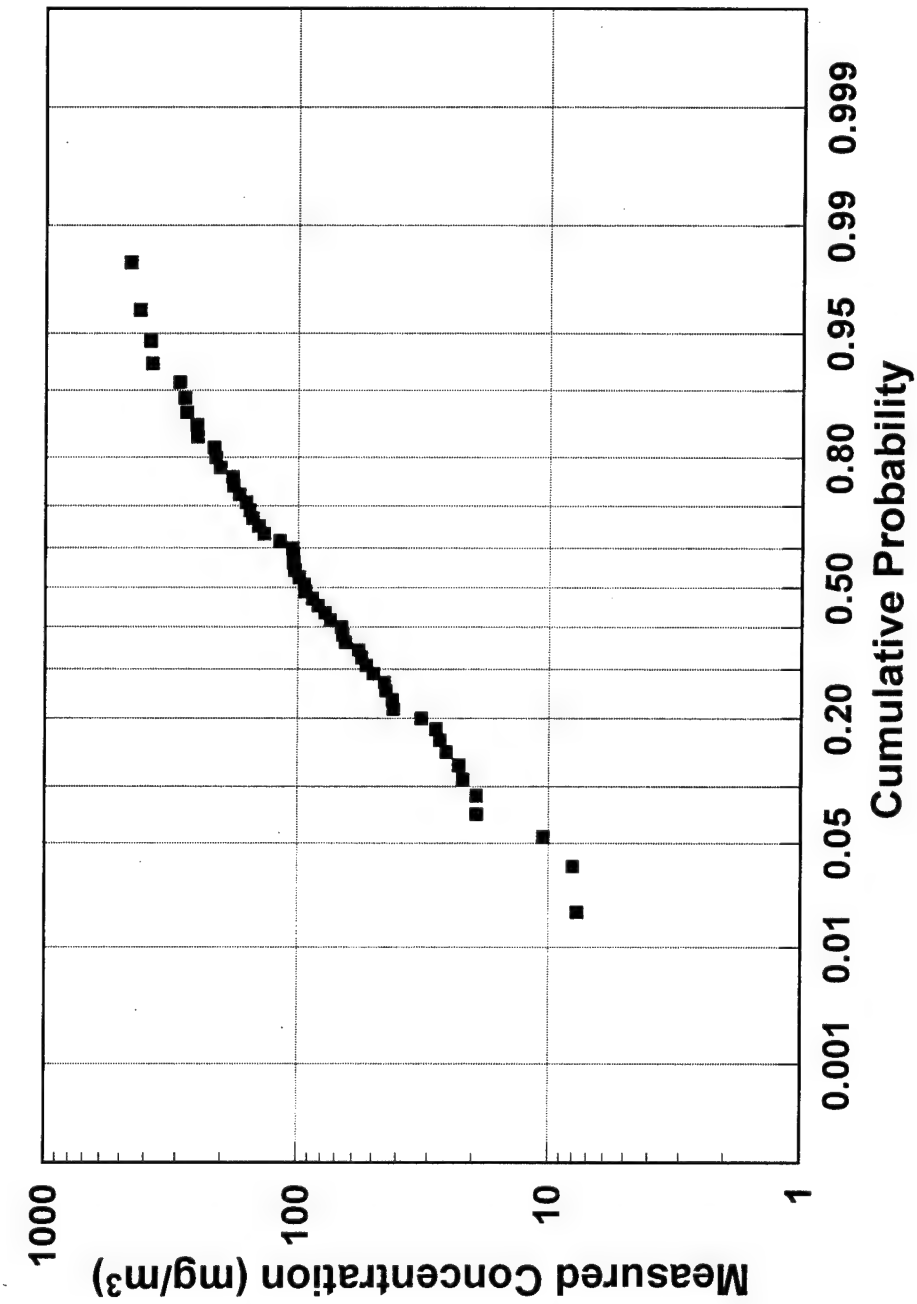

Figure 4.3: Graphic goodness-of-fit test of the worker task exposures to the lognormal distribution.

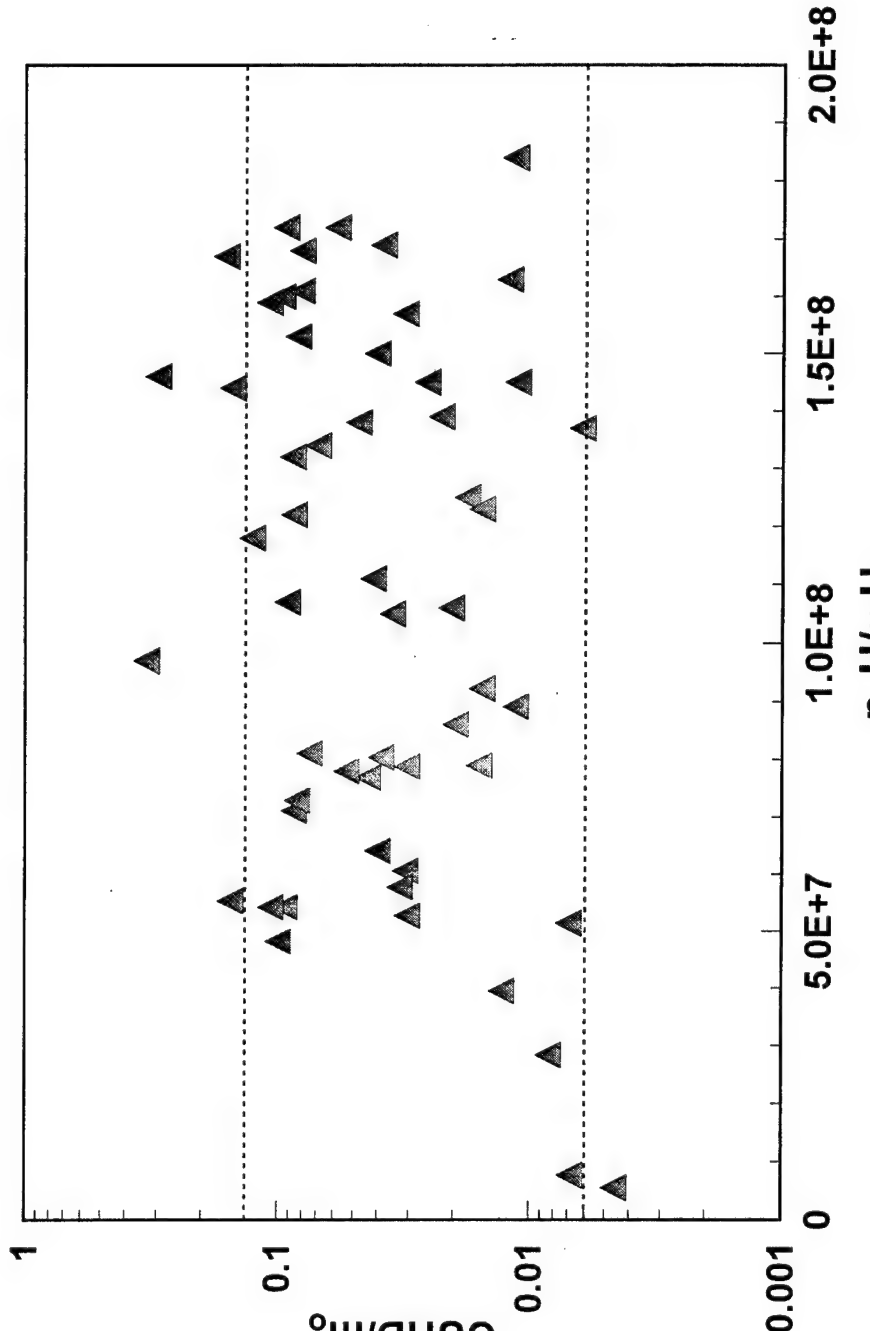

Figure 4.4: Individual CUHD/m_o values graphed as a function of the pressure group p_nH/μ_lU Dashed lines represent asymptotic values of the model in the 90° and 180° orientations.

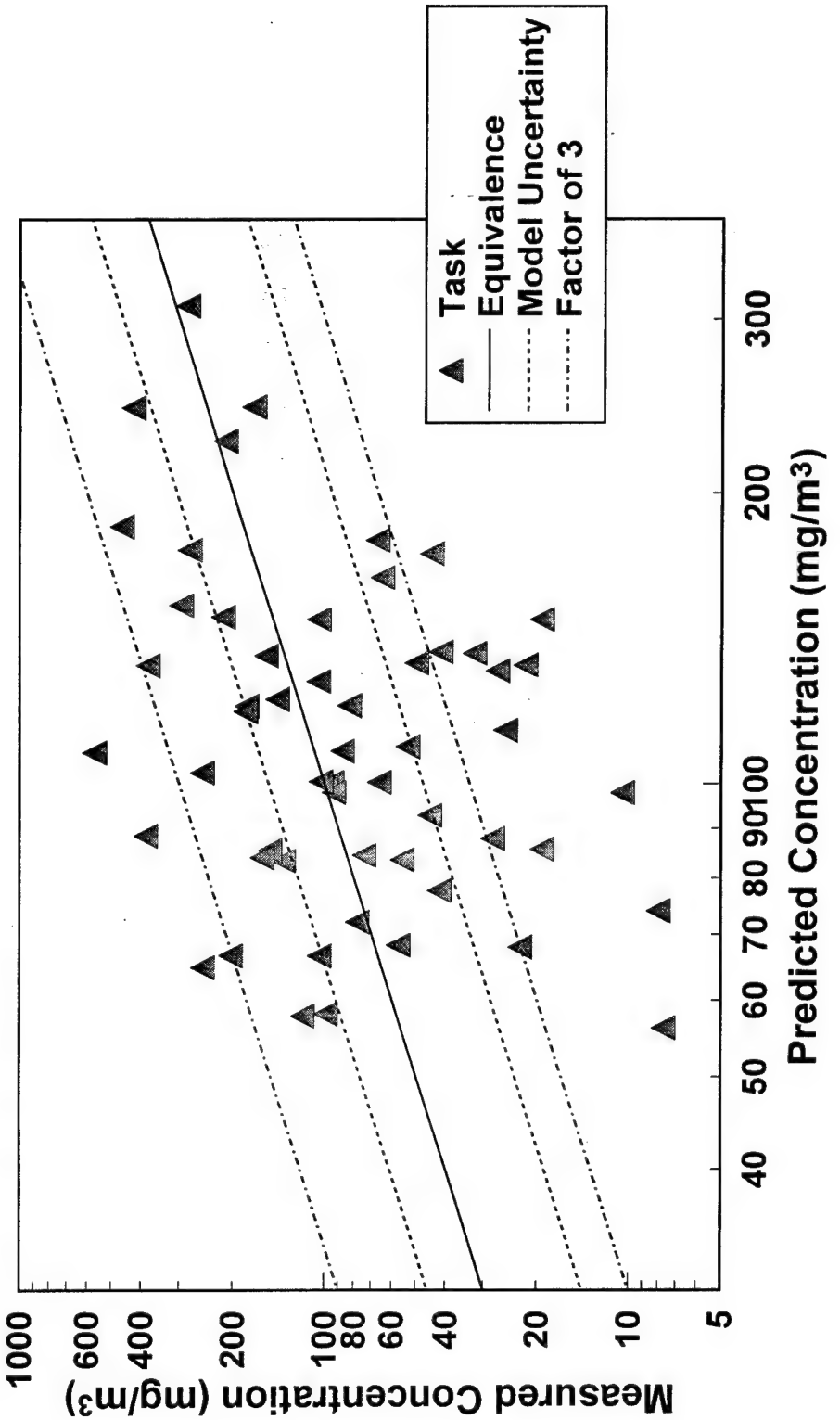

Figure 4.5: Scatter plot of measured worker exposures and model predictions. The majority of the data lie within a factor of three of the model prediction.

different from one; intercept not significantly different from zero) results in the conclusion that the regression line is not significantly different from the line of equivalence in Figure 4.5.[4]

The predicted and measured mean worker exposures, as well as the overall group exposure during the course of the field study, are shown in Figure 4.6. Error bars represent standard error of the mean. Four of the eight workers' mean exposures are within one standard error of the model prediction. Significantly, these four workers were among the five on whom the most samples were taken (workers 1, 3, 4, 5 and 7).

4.6. Discussion

Considering the simplicity of the model and mitigating factors present in actual field settings, the agreement between predicted and measured exposures is encouraging. The majority of individual task exposures are within a factor of three of the model prediction, persuasive in a model based solely on the dimensional relationship of the task parameters and not on any physical law. Although measured exposures tended to be less than those predicted by the model, statistical analysis indicates this trend was not significant. The ability of the model to predict worker mean exposures, illustrated in Figure 4.6, is good.

The extreme values in Figure 4.5, those that lie outside a factor of three from the model prediction, beg the question why the model did not do a better job for these tasks. To address this, task videos were viewed again and sampling results reviewed to identify other factors, not accounted for in the model, that may have affected the worker exposure.

All workers have a cart where they mix paint prior to starting the painting task. On occasion, the workers mixed additional paint during the task if they misjudged the amount required. Sometimes the workers would have to clean dried paint from the gun air cap by dipping the cap in a solvent tank located on the cart. This cleaning procedure

[4]Regression analysis assumes the measured task exposures are statistically independent of one another. Independence is violated if task exposures are related to the worker who performed the task. This does not appear to be the case; judging from Figure 4.2, the workers are uniformly exposed with similar within-worker variability.

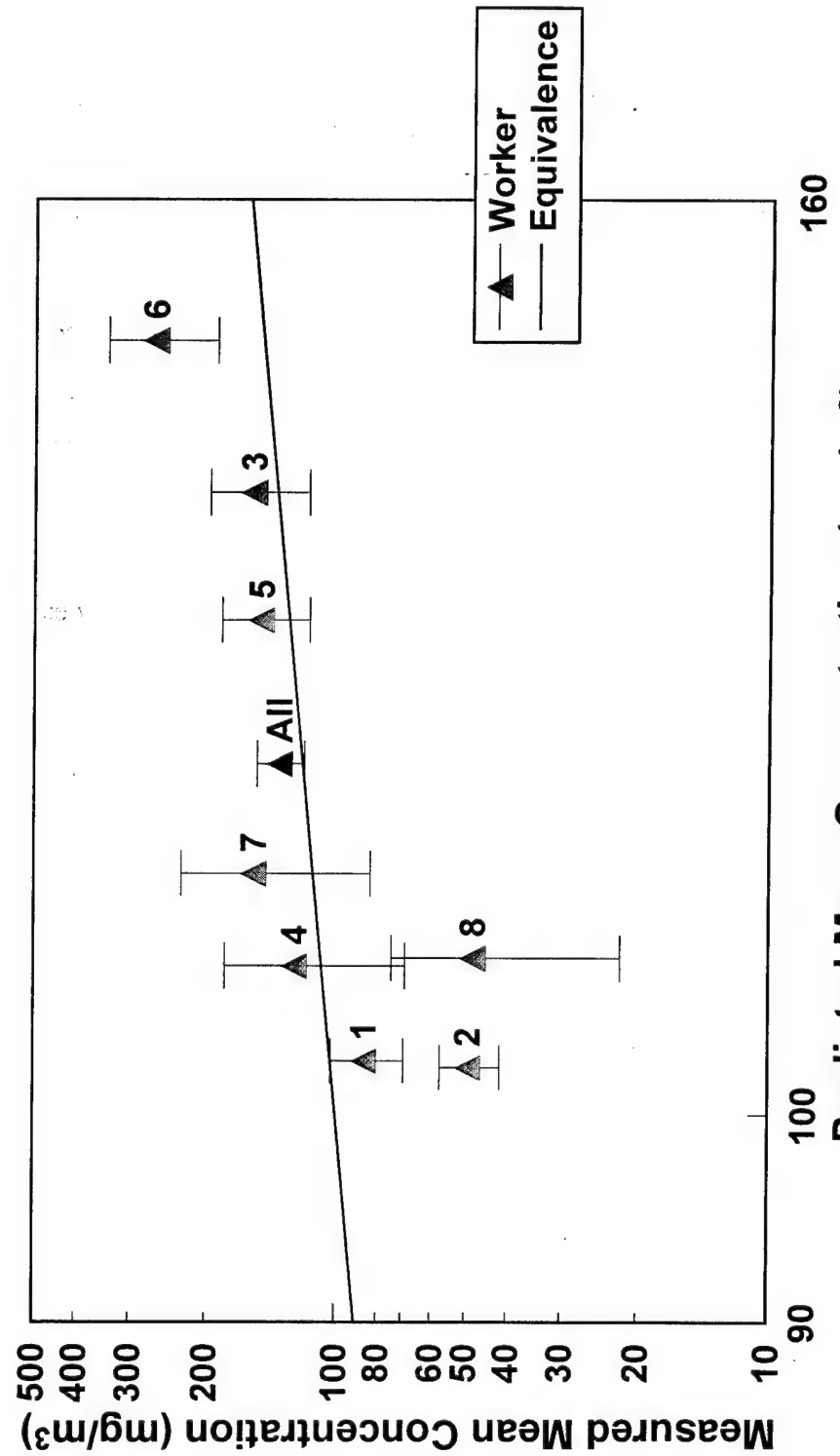

Figure 4.6: Measured mean worker exposures for the field study and their model predictions. Most of the predictions are within one standard error of the means.

could contribute additional solvent exposure above that predicted by the model. Of the 15 tasks identified where the worker either mixed or cleaned during the task, nine exposures are greater than the model prediction and of these nine, two are more than a factor of three different. However, six are below the model prediction. This possible additional exposure does not appear to explain the outliers, but it could have contributed to the overall tendency of these tasks to exceed the model predictions.

As mentioned earlier, painting tasks were sampled when a flat plate could represent the workpiece, ensuring the overspray generation and transport characteristics were similar to the laboratory set-up. Four of the tasks involved painting an air intake for the F-15 engine. This component has flat surfaces, but on one side has two end fins which form a 90° angle with the flat surface. Painting this surface requires the painter to stand between the two end fins. This positioning causes the overspray to channel directly toward the worker and not in the wrap-around pattern normally seen in the 90° orientation.[10,25] The measured exposures for three of these four tasks are more than a factor of three greater than the model prediction. The shape of the workpiece appears to have contributed to this difference.

Review of the charcoal tube analyses indicates no solvent exposure for six of the tasks. Considering that all other tasks had detectable solvent levels, this was unusual. These six tasks were sampled sequentially over a three-day period on different workers. The charcoal tubes were sent for analysis in a mailing separate from most of the other samples. These facts lead to a suspicion that a sampling, shipment, or analysis error occurred. All of these six tasks are more than a factor of three less than the model prediction. In addition, during one task the worker dripped some primer onto the cassette holder and filter. His task exposure is more than a factor of three greater than the model prediction.

Removing these 11 possibly anomalous observations from the sample results in the revised scatter plot in Figure 4.7. In the revised data set, 84% of the tasks fall within a factor of three of the model prediction and 95% of $CUHD/m_o$ values fall within the asymptotic model limits. A Wilcoxon signed-rank test on the revised data set leads to the previous conclusion, i.e., no statistical difference between the measured and predicted

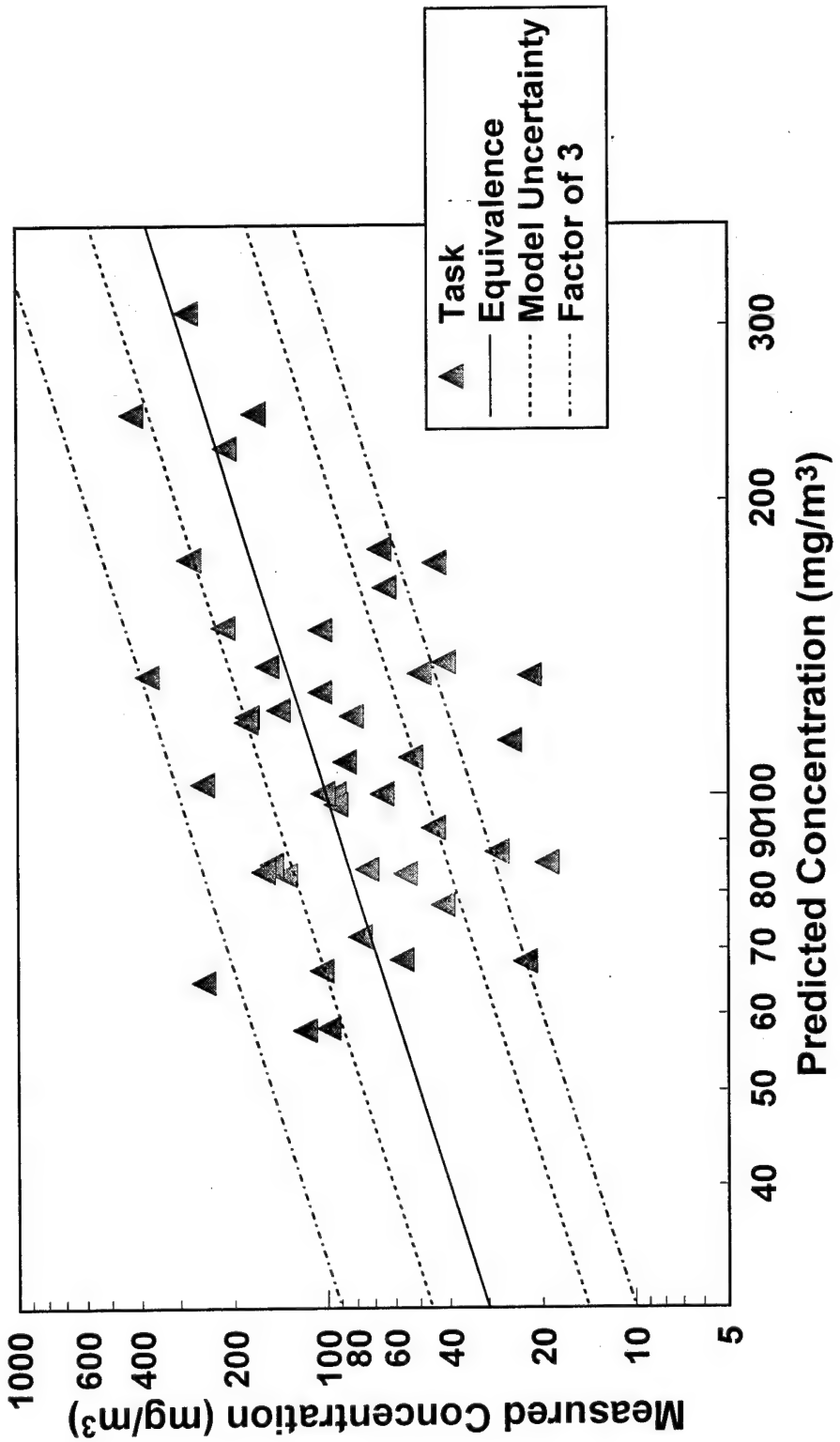

Figure 4.7: Revised scatter plot of Figure 4.5, with possible anomalous task exposures removed.

exposures ($p = 0.65$). Regression analysis also results in the same conclusion as before (regression line and line of equivalence are not significantly different). The predicted and measured mean exposures in Figure 4.6 shift slightly in the revised data set, most notably for workers 6 and 7 (points shifted down), but the overall predictive ability of the model is not changed appreciably.

The original article[10] identified several limitations that could affect the predictive ability of the model, and for the most part these limitations were borne out in the field. Movement of workers and their spray guns, plus the tendency for the spray pattern to miss the object when painting the edge of a workpiece, produced overspray generation rates that were probably higher than predicted by equation 6. The model assumes a fixed spray gun-to-workpiece distance of eight inches, but depending on the size of the workpiece this distance would increase if the worker could not reach far enough. This increase in distance tends to increase the overspray generation rate, although this effect was probably balanced by a decreased chance of overspray transport back to the worker due to the greater distance. The model assumes a workpiece parallel to the worker's body, but in actuality the workpiece could be at an angle, thereby diverting the overspray away from the worker. In these cases, actual overspray motion may have differed from that used to develop the model.

4.7. Conclusions

The author believes the positive results of this initial *a priori* application of an empirical-conceptual model are sufficiently encouraging to support additional work into the modeling technique. This research indicates empirical-conceptual models have the potential to predict individual worker task exposures within a factor of three and mean exposures within one standard error of the mean. Future models of spray painting tasks should address better the realities of field painting, some of which are highlighted above and are ultimately concerned with better estimates of spray transfer efficiencies and knowledge of overspray transport mechanisms. It is also important to account for other tasks that may occur coincident with spraying, most importantly additional solvent

exposure from mixing and cleaning. These improved models could have wider applicability than the current model and lead to improved exposure control methods.

4.8. References

1. Roach, S.A.: A Method of Relating the Incidence of Pneumoconiosis to Airborne Dust Exposure. Br. J. Ind. Med. 10:220-226 (1953).

2. Dement, J.M.; Harris, R.L.; Symons, M.J.; Shy, C.M.: Exposures and Mortality Among Chrysotile Asbestos Workers. Part 1: Exposure Estimates. Am. J. Ind. Med. 4:399-419 (1983).

3. Griefe, D.K.; Hornung, R.W.; Stayner, L.G.; Steenland, K.N.: Development of a Model for Use in Estimating Exposure to Ethylene Oxide in a Retrospective Cohort Mortality Study. Scand. J. Work Env. and Health. 14(supp 1):29-30 (1988).

4. Eisen, E.A.; Smith, T.J.; Wegman, M.D.; et. al.: Estimation of Long Term Dust Exposures in the Vermont Granite Sheds. Am. Ind. Hyg. Assoc. J. 45(2):89-94 (1984).

5. Woskie, S.R.; Smith, T.J.; Hammond, S.K.; Hallock, M.H.: Factors Affecting Worker Exposures to Metal-Working Fluids During Automotive Component Manufacturing. Appl. Occup. Environ. Hyg. 9(9):612-621 (1994).

6. Kromhout, H.; Swuste, P.; Boleij, J.S.M: Empirical Modelling of Chemical Exposure in the Rubber-Manufacturing Industry. Ann. Occup. Hyg. 38(1):3-22 (1994).

7. Kalliokoski, P.: Estimating Long-Term Exposure Levels in Process-Type Industries Using Production Rates. Am. Ind. Hyg. Assoc. J. 51(6):310-312 (1990).

8. Hansen, D.J.; Whitehead, L.W.: The Influence of Task and Location on Solvent Exposures in a Printing Plant. Am. Ind. Hyg. Assoc. J. 49(5):259-265 (1988).

9. Taylor, E.S.: Dimensional Analysis for Engineers, pp. 1-47. Clarendon Press, Oxford, UK (1974).

10. Carlton, G.N.; Flynn, M.R.: A Model to Estimate Worker Exposure to Spray Paint Mists. Submitted for publication to Appl. Occup. Environ. Hyg.

11. Lefebvre, A.H.: Atomization and Sprays, pp. 1-20, 238-261. Hemisphere Corp., New York, NY (1989).

12. Kim, K.Y.; Marshall, W.R.: Drop-Size Distributions from Pneumatic Atomizers. AIChE J. 17(3):575-584 (1971).

13. Kwok, K.C.: A Fundamental Study of Air Spray Painting. Ph.D. Thesis, University of Minnesota, MN (1991).

14. Hund, J.P.: Spray Application Processes. Metal Finishing: Organic Finishing Guidebook and Directory Issue. 93(5A):97-111 (1993).

15. George, D.K.; Flynn, M.R.; Goodman, R.: The Impact of Boundary Layer Separation on Local Exhaust Design and Worker Exposure. Appl. Occup. Environ. Hyg. 5(8):501-509 (1990).

16. Kim, T.; Flynn, M.R.: Modeling a Worker's Exposure From a Hand-Held Source in a Uniform Freestream. Am. Ind. Hyg. Assoc. J. 52(11):456-463 (1991).

17. Flynn, M.R.; George, D.K.: Aerodynamics and Exposure Variability. Appl. Occup. Environ. Hyg. 6(1):36-39 (1991).

18. Flynn, M.R.; Shelton, W.K.: Factors Affecting the Design of Local Exhaust Ventilation for the Control of Contaminants from Hand-Held Sources. Appl. Occup. Environ. Hyg. 5(10):707-714 (1990).

19. Hicks, P.G.; Senser, D.W.: Simulation of Paint Transfer in an Air Spray Process. In: Fluid Mechanics and Heat Transfer in Sprays, FED-Vol. 178/HTD-Vol 270, pp. 145-154. American Society of Mechanical Engineers, New York, NY (1993).

20. Kleinbaum, D.G.; Kupper, L.L.; Muller, K.E.: Applied Regression Analysis and Other Multivariable Methods, pp. 260-281. Duxbury Press, Belmont, CA (1988).

21. National Institute for Occupational Safety and Health: Particulates Not Otherwise Regulated, Total: Method 0500. In: NIOSH Manual of Analytical Methods, 4th Edition. P.M. Eller, Ed. NIOSH, Cincinnati, OH (1994).

22. Mark, D.; Vincent, J.H.: A New Personal Sampler for Airborne Total Dust in Workplaces. Ann. Occup. Hyg. 30(1):89-102 (1986).

23. National Institute for Occupational Safety and Health: Naphtha: Method 1550. In: NIOSH Manual of Analytical Methods, 4th Edition. P.M. Eller, Ed. NIOSH, Cincinnati, OH (1994).

24. American Society of Mechanical Engineers: Measurement Uncertainty, Part 1: Instruments and Apparatus. ANSI/ASME PTC 19.1-1985. ASME, New York, NY (1985).

25. Heitbrink, W.A.; Wallace, M.E.; Bryant, C.J.; Ruch, W.E.: Control of Paint Overspray in Autobody Repair Shops. Am. Ind. Hyg. Assoc. J. 56(10):1023-1032 (1995).

Appendix A: Chapter 2 Additional Materials

A.1. Thermoanemometer Calibration

Air velocity measurements were done with a TSI® model 1210-120 platinum hot film thermoanemometer probe and an IFA-100 flow analyzer. The anemometer consists of a cylindrical sensor suspended at the end of a rigid wire support. Calibration involves placing the sensor at right angles to a known velocity and recording the increase in bridge voltage necessary to maintain a constant sensor temperature. A low velocity wind tunnel specified in the ACGIH Ventilation Manual was used to calibrate the probe. The fan speed is adjustable with a frequency inverter. Changing the fan speed varies the wind tunnel velocity. This velocity was calibrated against the wind tunnel hood static pressure using a pitot tube traverse and micromanometer. The calibration curve is shown in Figure A.1, with the following best fit equation:

$$\text{Velocity (sfpm)} = -2.258 + 484.8(SP_{hood})^{1/2},\ r^2 = 0.9996 \qquad (1)$$

The anemometer probe was positioned in the calibration wind tunnel and the bridge voltage measured for 30 seconds at a sampling rate of 10 Hz. The results are in Figure A.2. A regression of the square root of velocity on the square of the voltage produced the following equation:

$$\text{Velocity (fpm)} = \left[-13.43 + 15.51(\text{Voltage})^2\right]^2,\ r^2 = 0.9998 \qquad (2)$$

A.2. Experimental Wind Tunnel Calibration

The experimental wind tunnel flow is adjustable by varying the speed of the fan drawing air through it. Air passing through the pegboard rear wall of the tunnel creates a measurable static pressure drop relative to atmospheric pressure. This static pressure drop was measured with a pitot tube located in the tunnel exhaust duct, downstream of the tunnel exit but upstream of the fan entrance. Sixteen equi-distant measurements of the normal velocity component were taken on each of four cross sectional planes located 18, 36, 54, and 72 inches from the wind tunnel entrance. The results are shown in Tables A.1-10. The average freestream velocity (U) was determined from the average of these 64 measurements and was proportional to the square root of the tunnel static pressure drop, as illustrated in Figure A.3 (errors bars represent one standard deviation). The calibration curve is:

$$\text{Velocity (sfpm)} = -11.64 + 411.5(SP_{hood})^{1/2}\ ,\ r^2 = 0.9998 \qquad (3)$$

A.3. Spray Nozzle Set-up

A schematic of the spraying system is in Figure A.4. Liquid was fed to the 1/4J nozzle from a 5-gallon container by raising or lowering the gravity head or siphon height. The liquid mass flow (m_l) was determined by comparing the weight of the container before and after spraying. Placing the container on a lab jack and adjusting the height during spraying maintained a constant liquid flow. A compressor provided air for the nozzle. The air passed through an air filter and dryer to remove condensables and deliver dry air at 70 psig. A pressure regulator was used to adjust the nozzle pressure (p_n) and air flow. The air mass flow (m_a) was calibrated with a primary standard spirometer and calculated air densities. The calibration curve is in Figure A.5, with the following best fit equation (error bars represent one standard deviation):

$$m_a\ (\text{lb/min}) = 5.973\text{x}10^{-2} + 4.072\text{x}10^{-3}(p_n)\ ,\ r^2 = 0.9997 \qquad (4)$$

The air-to-liquid mass flow ratio (m_a/m_l) was set prior to each experimental run by fixing the nozzle pressure and adjusting the height of the liquid container until the desired value of m_a/m_l was obtained.

A.4. Corn Oil Viscosity

Viscosity was measured with a Haake falling ball viscometer and constant temperature bath. The results are in Figure A.6 (error bars represent one standard deviation). The best fit regression equation is:

$$\log_{10}(\mu_l) = 2.491 - 1.012\text{x}10^{-2}(\text{Temp}) \text{ , } r^2 = 0.9986 \qquad (5)$$

A.5. Experimental Data

The measured data for the 180 experimental runs are in Tables A.11-16. Calculated data, including dimensionless quantities, are in Tables A.17-22.

A.6. Derivation of Empirical Model

A.6.1. Statement of the Pi Theorem of Buckingham

If the equation

$$\phi(q_1, q_2, \ldots q_n) = 0 \qquad (6)$$

is the only relationship among these quantities and if it holds for any arbitrary choice of the units in which $q_1, q_2, \ldots q_n$ are measured, then the solution has the form

$$\Phi(\Pi_1, \Pi_2, \ldots \Pi_m) = 0 \qquad (7)$$

where $\Pi_1, \Pi_2, \ldots \Pi_m$ are independent dimensionless products of the qs. If k is the minimum number of primary quantities necessary to express the dimensions of the qs, then

$$m = n - k. \tag{8}$$

A.6.2. Procedure for Finding Dimensionless Groups

Dimensional analysis involves the following three steps:

(1) Selection of initial variables (the qs). Determining these variables requires substituting a simplified conceptual model for the actual problem.

(2) Choice of primary quantities. A primary quantity has a unit of measurement assigned to it independent of units of measurement chosen for other primary quantities involved in the problem. For example, in the conventional MLT measuring system mass, length, and time are primary quantities, while force is a derived quantity from Newton's second law of motion:

$$[F] = MLT^{-2} \tag{9}$$

Therefore, the MLT system is an appropriate measuring system if the problem involves Newton's second law. It is unsuitable, however, in a problem that does not involve this law since dimensional analysis will result in an extra dimensionless group irrelevant to the problem (Taylor, 1974). The FMLT measuring system is the proper choice in this case because it treats force as a primary quantity and not derived from Newton's second law.

(3) Determination of final dimensionless groups (the Πs). Dimensional analysis does not provide a unique set of dimensionless groups; they are selected to most efficiently display the experimental data.

A.6.3. Dimensional Analysis for a Spray Painting Task

The conceptual model of a spray painting task was the basis for identifying the initial variables:

$$C = \phi\left(m_o, p_n, \mu_l, \frac{m_a}{m_l}, U, H, D, \text{orientation}\right), \quad n = 9 \tag{10}$$

Because Newton's second law is not relevant to the problem as defined, choosing the FMLT dimensional system designates four primary quantities ($k = 4$). Therefore, $m = 5$ and five nondimensional groups describe the functional relationship among the nine variables.

Two of the Pi groups are obvious because they are already dimensionless:

$$\Pi_1 = \frac{m_a}{m_l} \tag{11}$$

$$\Pi_2 = \text{orientation} \tag{12}$$

Finding the other three Pi groups requires selecting four of the variables as "repeating variables" which may appear in more than one of the groups. These repeating variables must have different dimensions, together contain all the dimensions F, M, L, and T, and not form by themselves a dimensionless group. In order to isolate C and p_n into separate groups, m_o, μ_l, U, and H are chosen. Therefore,

$$\Pi_3 = C\, m_o^{\,a}\, \mu_l^{\,b}\, U^c\, H^d \tag{13}$$

For this group to be dimensionless requires

$$(ML^{-3})\,(MT^{-1})^a\,(FTL^{-2})^b\,(LT^{-1})^c\,(L)^d = F^0\,M^0\,L^0\,T^0 \tag{14}$$

Equating indices, a = -1, b = 0, c = 1, and d = 2, so that

$$\Pi_3 = C\,m_o^{-1}\,\mu_l^{\,0}\,U^1\,H^2 = \frac{CUH^2}{m_o} \tag{15}$$

Similarly,

$$\Pi_4 = p_n\,m_o^{\,a}\,\mu_l^{\,b}\,U^c\,H^d = \frac{p_n H}{\mu_l U} \tag{16}$$

$$\Pi_5 = D\,m_o^{\,a}\,\mu_l^{\,b}\,U^c\,H^d = \frac{H}{D} \tag{17}$$

The nondimensional representation has the form

$$\frac{CUH^2}{m_o} = \Phi\left(\frac{m_a}{m_l}, \frac{p_n H}{\mu_l U}, \frac{H}{D}, \text{orientation}\right) \tag{18}$$

Assuming H/D is constant eliminates this group from the functional relationship. Dividing CUH^2/m_o by this constant results in the final model:

$$\frac{CUHD}{m_o} = \Phi\left(\frac{m_a}{m_l}, \frac{p_n H}{\mu_l U}, \text{orientation}\right) \tag{19}$$

A.7. Uncertainty Analysis

A.7.1 Bias, Precision and Uncertainty

The bias and precision errors of the nondimensional quantities, and their calculated uncertainties, were found according to the ANSI/ASME standard on measurement uncertainty. A summary of the analysis follows.

Measurement equipment is subject to two types of error: bias and precision. Bias (or fixed error) is the systematic error constant for the duration of the experiment. Calibration reduces bias, but never totally eliminates it. The bias limit (B), the upper limit of the bias error, is difficult to estimate, especially if special test data which provide bias information are unavailable. Estimates of B are usually based on instrument reports from manufacturers and other references.

Precision error (also called random error) is the closeness of agreement among repeated measurements of the same quantity. It is measured by the precision index (S_x), which is an estimate of the standard deviation in repeated measurements. Several ways to estimate S_x are outlined in the ANSI standard.

The estimated relative bias and precision errors in the measured experimental quantities are listed in Table A.23.

The 95% uncertainty in the measurement (assuming the error is symmetrical about the measurement mean) is defined as:

$$U(95\%) = \left[B^2 + \left(t S_x\right)^2\right]^{1/2} \qquad (20)$$

where t is the 97.5th percentile of the two-tailed t-distribution and is a function of the number of degrees of freedom used to calculate S_x. For large samples t approaches 1.96 and is approximated as 2.0 for simplicity.

A.7.2. Propagation of Error

Measurement errors are propagated through the functional relationship between a quantity and its parameters. The propagation formula is approximated by a Taylor series expansion. Sensitivity is the error propagated due to errors in the parameters. For a quantity F, if

$$F = f(x_1, x_2, \ldots, x_j) \tag{21}$$

then the relative sensitivity coefficient is

$$\Theta_i = \frac{\partial F/\partial x_i}{F/x_i} \tag{22}$$

The bias and precision errors are propagated separately until combined into an uncertainty.

$$S_F = \left[\sum_{i=1}^{j}\left(\Theta_i S_{x_i}\right)^2\right]^{1/2} \tag{23}$$

$$B_F = \left[\sum_{i=1}^{j}\left(\Theta_i B_{x_i}\right)^2\right]^{1/2} \tag{24}$$

A.7.3. Sample Calculation

For the dimensionless quantity

$$\tilde{C} = \frac{CUHD}{m_o} \tag{25}$$

$$B_{\tilde{C}} = \left[\left(\frac{\partial \tilde{C} / \partial C}{\tilde{C} / C} B_C \right)^2 + \left(\frac{\partial \tilde{C} / \partial U}{\tilde{C} / U} B_U \right)^2 + \left(\frac{\partial \tilde{C} / \partial H}{\tilde{C} / H} B_H \right)^2 + \left(\frac{\partial \tilde{C} / \partial D}{\tilde{C} / D} B_D \right)^2 + \left(\frac{\partial \tilde{C} / \partial m_o}{\tilde{C} / m_o} B_{m_o} \right)^2 \right]^{1/2} \quad (26)$$

$$= \left[(1 \times 0.001)^2 + (1 \times 0.045)^2 + (1 \times 0.001)^2 + (1 \times 0.004)^2 + (1 \times 0.001)^2 \right]^{1/2}$$

$$= 0.045 = 4.5\%$$

Similarly,

$$S_{\tilde{C}} = \left[\left(\frac{\partial \tilde{C} / \partial C}{\tilde{C} / C} S_C \right)^2 + \left(\frac{\partial \tilde{C} / \partial U}{\tilde{C} / U} S_U \right)^2 + \left(\frac{\partial \tilde{C} / \partial H}{\tilde{C} / H} S_H \right)^2 + \left(\frac{\partial \tilde{C} / \partial D}{\tilde{C} / D} S_D \right)^2 + \left(\frac{\partial \tilde{C} / \partial m_o}{\tilde{C} / m_o} S_{m_o} \right)^2 \right]^{1/2} \quad (27)$$

$$= \left[(1 \times 0.056)^2 + (1 \times 0.021)^2 + (1 \times 0.002)^2 + (1 \times 0.008)^2 + (1 \times 0.008)^2 \right]^{1/2}$$

$$= 0.061 = 6.1\%$$

The 95% uncertainty in the measured quantity $\tilde{C}$ is

$$U_{\tilde{C}}(95\%) = \left[(0.045)^2 + (2 \times 0.061)^2 \right]^{1/2}$$

$$= 0.130 = 13.0\%$$

A.8. Sample Calculations, Dimensionless Numbers (Run Number 1)

A.8.1. m_a/m_l

The measured value of m_a at p_n = 30 psig was 0.183 lb/min.

$$m_l = \frac{\text{mass container (before)} - \text{mass container (after)}}{\text{sampling time}}$$

$$= \frac{(8305 - 8027)\ \text{g}}{180.07\ \text{sec}} \times \left(\frac{60\ \text{sec}}{\text{min}}\right)$$

$$= 92.63\ \text{g/min} = 0.204\ \text{lb/min}$$

$$\frac{m_a}{m_l} = \frac{0.183\ \text{lb/min}}{0.204\ \text{lb/min}} = 0.90$$

A.8.2 p_nH/μ_lU

p_n, H and U were set in the experiment. From equation (A-5),

$$\log_{10}(\mu_l) = 2.491 - (1.012\times10^{-2}) \times (\text{Temp, °F})$$

$$= 2.491 - (1.012\times10^{-2}) \times (82.3)$$

$$\mu_l = 45.51\ \text{cp}$$

$$\frac{p_n H}{\mu_l U} = \frac{(30\ \text{psi})(41\ \text{in})}{(45.51\ \text{cp})(112.5\ \text{fpm})} \times \left(\frac{\text{atm}}{14.7\ \text{psi}}\right) \times \left(\frac{1.01325\times10^6\ \text{dyne/cm}^2}{\text{atm}}\right) \times \left(\frac{\text{ft}}{12\ \text{in}}\right) \times \left(\frac{\text{cp}}{0.01\ \text{dyne-s/cm}^2}\right) \times \left(\frac{60\ \text{sec}}{\text{min}}\right)$$

$$= 8.28 \times 10^6$$

A.8.3. CUHD/m_o

U, H and D were fixed in the experiment.

$$C = \frac{\text{mass filter (after)} - \text{mass filter (before)}}{\text{flow x sampling time}}$$

$$= \frac{(13.895 - 13.537)\ \text{mg}}{(2.05\ \text{lpm})(180.07\ \text{sec})} \times \left(\frac{10^3\ \text{lit}}{\text{m}^3}\right) \times \left(\frac{60\ \text{sec}}{\text{min}}\right)$$

$$= 58.19\ \text{mg/m}^3$$

$$m_o = m_1 - \frac{\text{mass trough (after)} - \text{mass trough (before)}}{\text{sampling time}}$$

$$= (92.63\ \text{g/min}) - \frac{(833.2 - 583.2)\ \text{g}}{180.07\ \text{sec}} \times \left(\frac{60\ \text{sec}}{\text{min}}\right)$$

$$= 9.33\ \text{g/min}$$

$$\frac{\text{CUHD}}{m_o} = \frac{(58.19\ \text{mg/m}^3)(112.5\ \text{fpm})(41\ \text{in})(8\ \text{in})}{(9.33\ \text{g/min})} \times \left(\frac{\text{g}}{10^3\ \text{mg}}\right) \times \left(\frac{\text{ft}^2}{144\ \text{in}^2}\right) \times \left(\frac{\text{m}}{3.281\ \text{ft}}\right)^3$$

$$= 0.0452$$

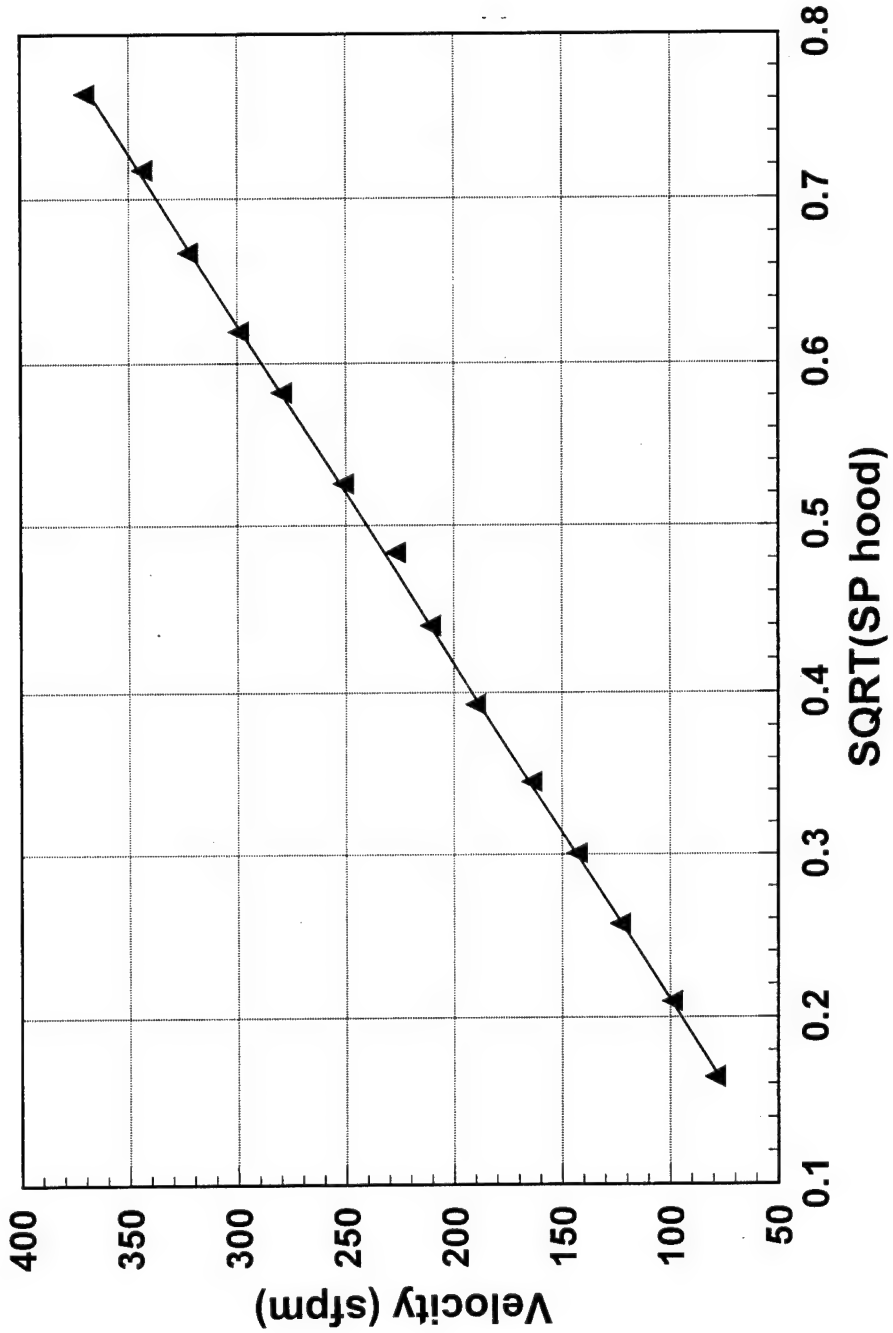

Figure A.1: Calibration wind tunnel data.

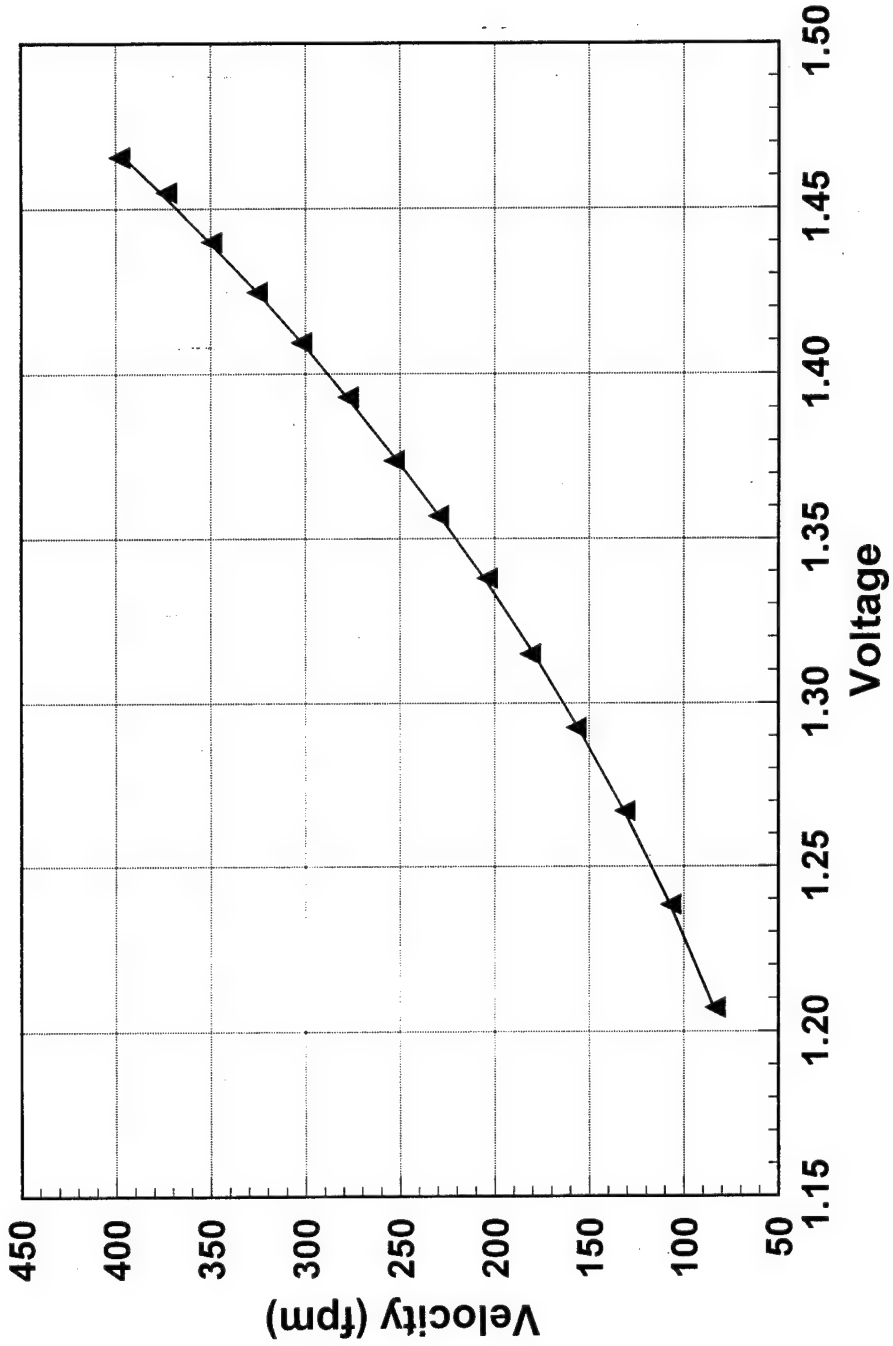

Figure A.2. Thermoanemometer calibration.

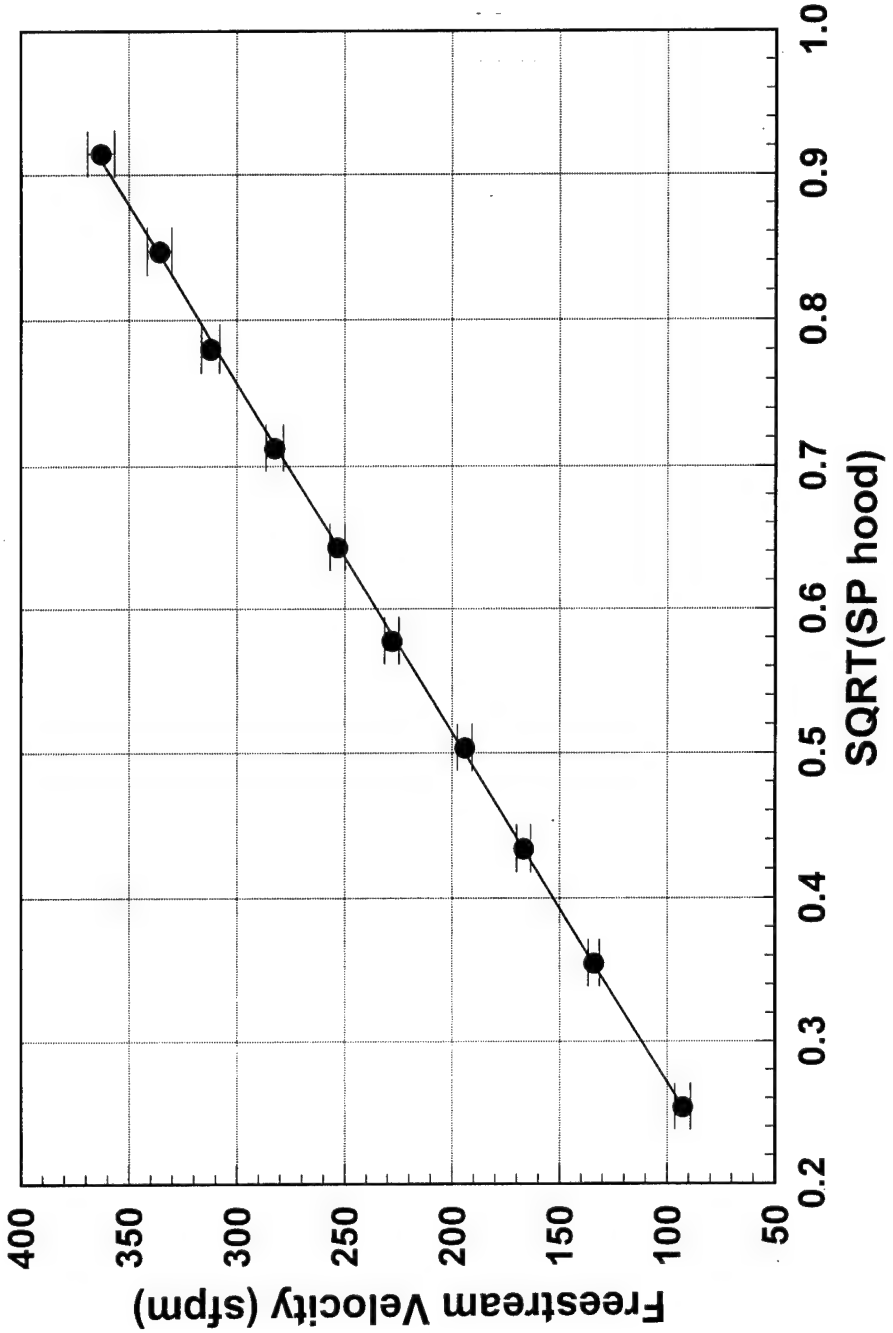

Figure A.3: Experimental wind tunnel calibration.

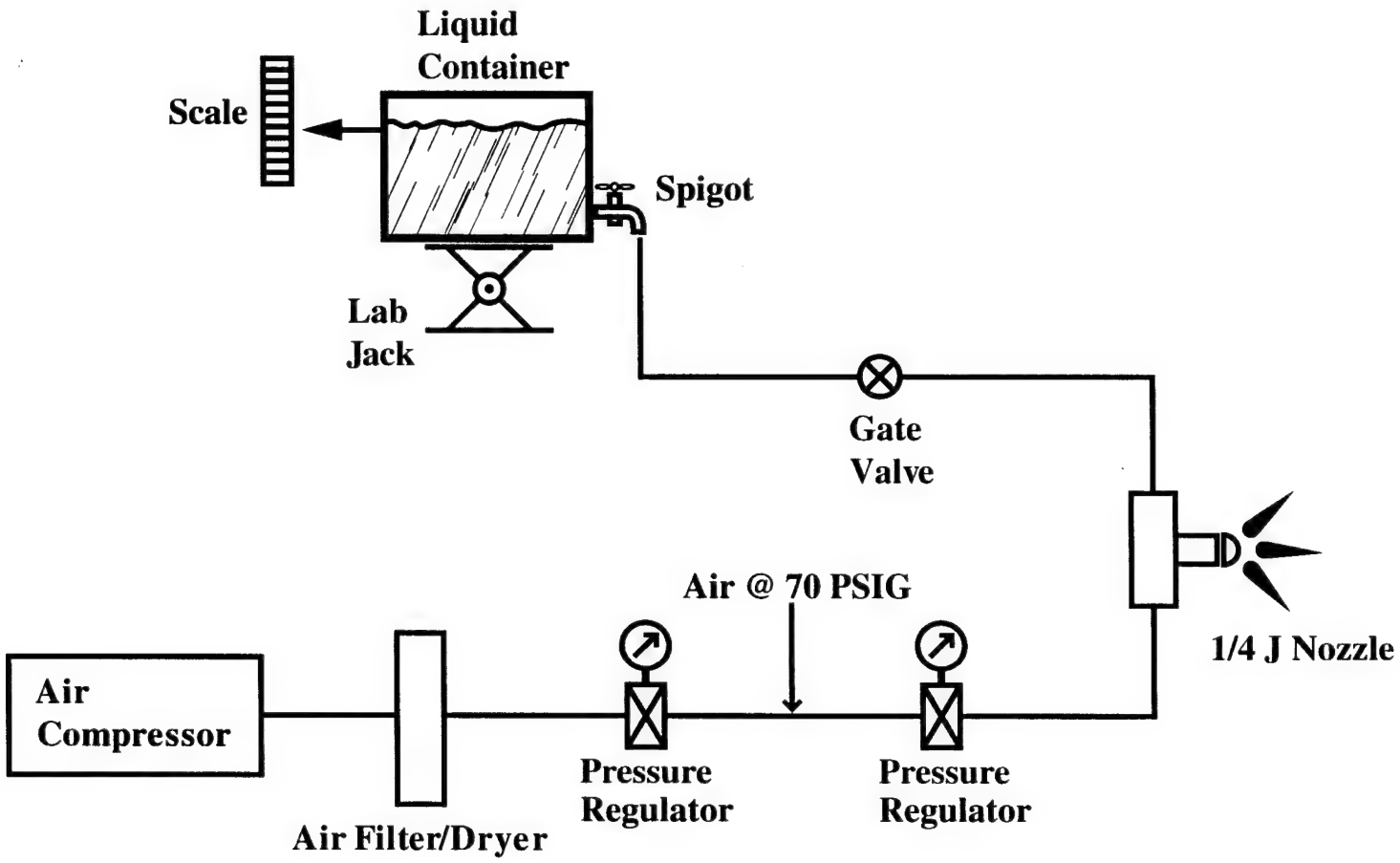

Figure A.4: Schematic of laboratory spraying system

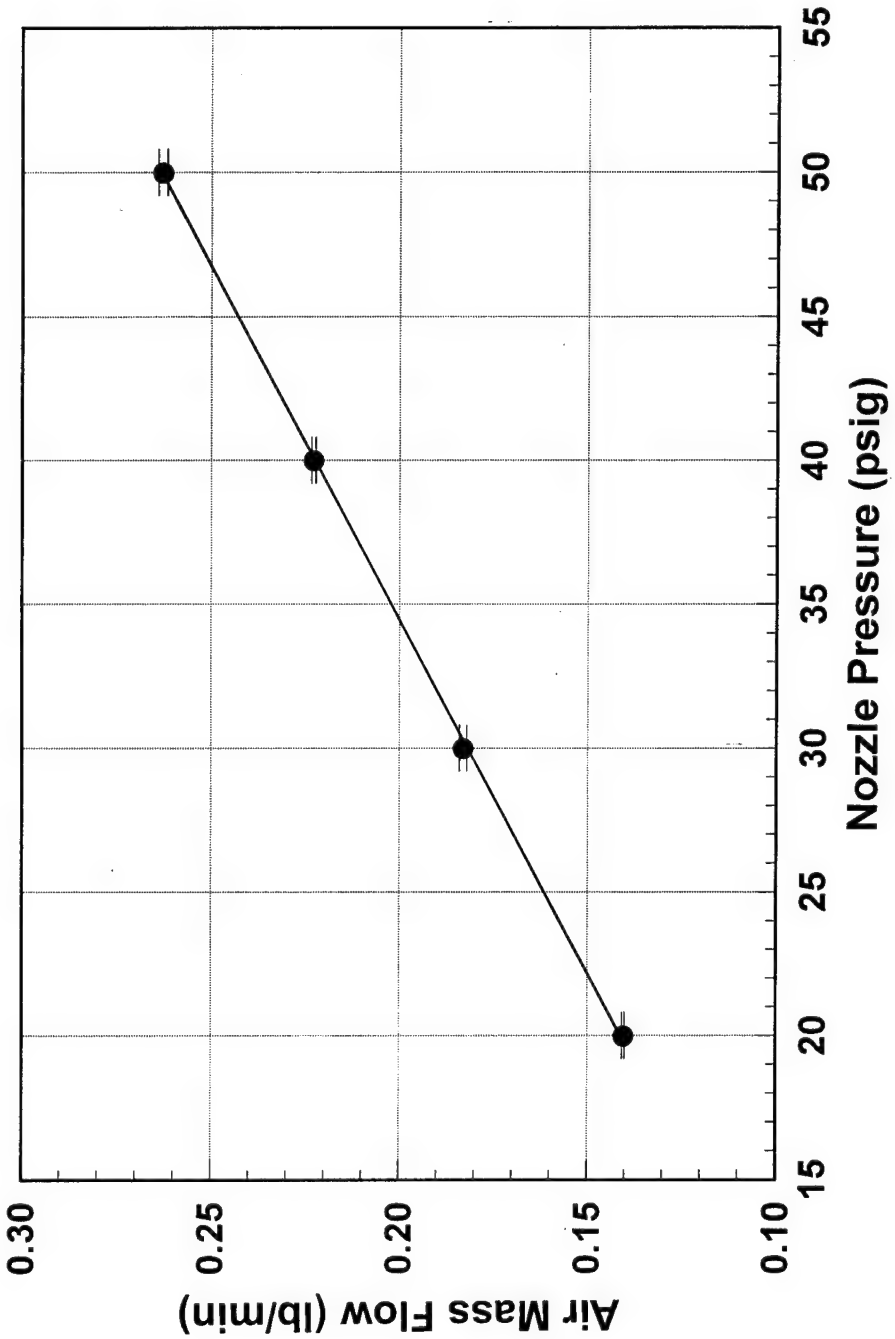

Figure A.5: 1/4J spray nozzle calibration.

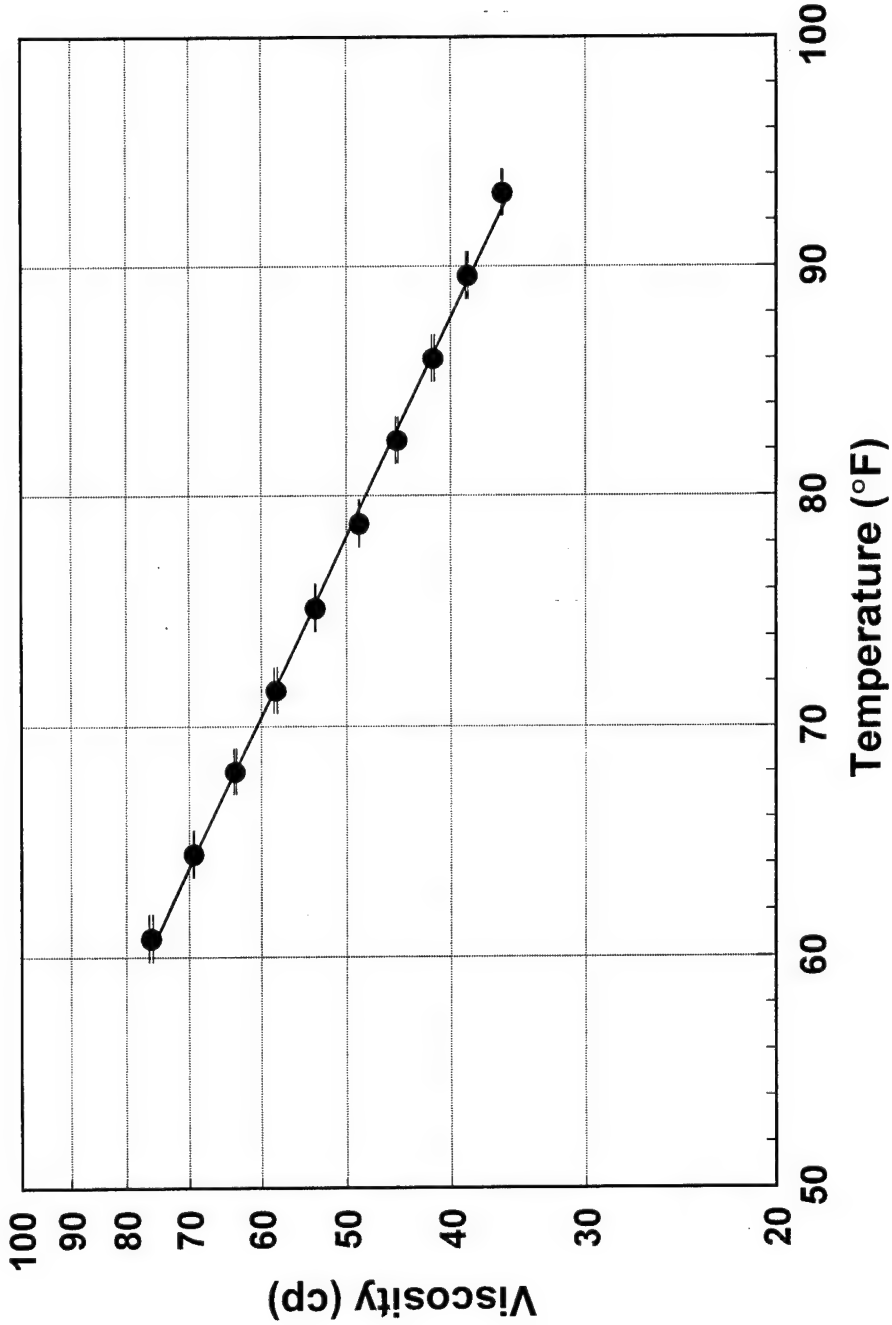

Figure A.6: Corn oil viscosity measurements.

Table A.1: Wind Tunnel Freestream Velocity Profiles (sfpm), $SP_h = 0.065"\ H_2O$

94.8	90.9	93.1	96.0
92.8	93.9	94.8	97.6
98.4	90.0	92.4	95.0
93.2	90.6	94.9	94.2

Cross Section 1 - 18" from face

92.7	88.2	92.9	92.5
94.3	98.6	90.0	90.2
97.0	97.4	97.0	88.4
92.5	94.2	93.8	90.4

Cross Section 2 - 36" from face

88.7	86.6	95.9	90.5
93.7	98.5	96.8	93.5
93.9	93.3	95.7	82.0
96.0	91.9	89.1	91.3

Cross Section 3 - 54" from face

85.5	85.7	92.6	96.1
93.9	93.2	95.0	91.7
98.6	92.6	91.7	88.5
94.9	92.4	85.8	84.9

Cross Section 4 - 72" from face

Cross Section	Avg Velocity	Standard Deviation	CV (%)
1	93.9	2.34	2.49
2	93.1	3.20	3.44
3	92.3	4.24	4.59
4	91.5	4.16	4.55
Total	92.7	3.60	3.89

Table A.2: Wind Tunnel Freestream Velocity Profiles (sfpm), $SP_h = 0.126"\ H_2O$

130.8	131.0	129.7	137.0
131.6	133.4	132.0	132.3
136.3	130.9	132.6	134.9
136.9	134.5	135.2	136.8

Cross Section 1 - 18" from face

130.1	133.2	130.3	134.1
131.6	132.9	136.5	135.4
136.7	135.4	132.3	134.7
137.0	134.9	134.9	137.1

Cross Section 2 - 36" from face

129.4	132.9	133.9	131.5
135.6	136.1	132.1	136.7
138.5	134.5	132.0	133.9
138.7	137.5	135.4	134.9

Cross Section 3 - 54" from face

128.3	125.9	132.0	134.3
136.9	135.6	134.9	132.6
136.8	134.4	132.0	132.5
139.4	135.2	135.8	134.2

Cross Section 4 - 72" from face

Cross Section	Avg Velocity	Standard Deviation	CV (%)
1	133.5	2.47	1.85
2	134.2	2.26	1.68
3	134.6	2.60	1.94
4	133.8	3.30	2.47
Total	134.0	2.66	1.98

Table A.3: Wind Tunnel Freestream Velocity Profiles (sfpm), $SP_h = 0.188"\ H_2O$

167.2	160.9	160.0	167.8
168.0	162.0	164.5	164.1
167.0	163.3	164.5	166.5
168.3	166.2	168.3	171.2

Cross Section 1 - 18" from face

167.5	164.2	158.9	164.2
167.7	166.9	164.1	168.9
168.4	169.1	166.2	167.4
167.9	170.1	166.0	170.0

Cross Section 2 - 36" from face

168.7	166.8	156.2	163.4
168.6	168.8	171.1	169.2
168.4	167.7	165.0	167.6
168.7	169.1	170.2	170.7

Cross Section 3 - 54" from face

171.3	165.0	157.9	162.2
169.5	166.1	164.3	171.0
167.4	166.0	170.3	169.4
167.8	167.3	165.8	166.1

Cross Section 4 - 72" from face

Cross Section	Avg Velocity	Standard Deviation	CV (%)
1	165.6	3.05	1.84
2	166.7	2.83	1.70
3	167.5	3.59	2.15
4	166.7	3.47	2.08
Total	166.6	3.24	1.95

Table A.4: Wind Tunnel Freestream Velocity Profiles (sfpm), $SP_h = 0.254"\ H_2O$

189.0	187.9	190.8	192.0
198.5	192.3	189.3	192.3
194.7	194.2	191.1	193.2
201.9	197.1	193.4	194.5

Cross Section 1 - 18" from face

191.2	189.5	188.3	189.7
194.5	195.0	197.3	196.0
194.4	197.8	193.6	195.6
202.2	196.6	196.2	191.8

Cross Section 2 - 36" from face

189.1	186.9	187.7	190.8
198.0	198.0	196.0	194.6
197.6	196.6	197.9	193.4
199.2	194.9	193.3	192.6

Cross Section 3 - 54" from face

194.0	191.9	193.7	196.1
197.5	195.3	194.9	197.4
198.0	196.4	192.0	192.2
199.4	193.3	191.5	192.0

Cross Section 4 - 72" from face

Cross Section	Avg Velocity	Standard Deviation	CV (%)
1	193.3	3.63	1.88
2	194.3	3.59	1.85
3	194.2	3.88	2.00
4	194.7	2.53	1.30
Total	194.1	3.41	1.76

Table A.5: Wind Tunnel Freestream Velocity Profiles (sfpm), SP_h = 0.334" H_2O

229.0	226.1	225.7	227.1
227.9	222.8	224.3	227.2
227.6	221.3	222.7	225.6
232.6	227.2	231.4	235.5

Cross Section 1 - 18" from face

228.8	224.2	229.5	231.7
227.5	231.4	226.6	219.8
229.8	228.2	226.4	220.5
230.6	227.4	229.4	232.3

Cross Section 2 - 36" from face

225.3	223.5	226.7	228.2
232.8	231.2	226.0	227.8
230.9	229.9	226.1	222.8
229.3	229.4	227.5	235.4

Cross Section 3 - 54" from face

227.0	230.8	228.9	235.6
230.3	229.7	229.4	226.3
230.7	229.6	225.8	227.3
232.3	228.4	227.1	228.0

Cross Section 4 - 72" from face

Cross Section	Avg Velocity	Standard Deviation	CV (%)
1	227.1	3.73	1.64
2	227.8	3.65	1.60
3	228.3	3.34	1.46
4	229.2	2.47	1.08
Total	228.1	3.34	1.47

Table A.6: Wind Tunnel Freestream Velocity Profiles (sfpm), SP_h = 0.413" H_2O

245.7	244.4	247.7	253.1
254.4	249.0	250.7	250.0
254.1	249.8	250.7	249.8
260.8	252.8	253.9	254.0

Cross Section 1 - 18" from face

245.1	250.5	252.0	247.1
255.3	253.4	254.1	253.7
256.9	254.8	254.2	252.3
252.7	255.1	256.8	254.8

Cross Section 2 - 36" from face

249.8	250.4	249.2	251.9
253.9	257.2	256.4	252.3
259.1	257.2	254.5	253.5
258.1	256.8	255.1	255.4

Cross Section 3 - 54" from face

248.0	253.2	254.8	255.2
256.4	257.4	258.7	253.6
255.5	252.9	252.1	253.9
259.7	253.2	250.6	250.1

Cross Section 4 - 72" from face

Cross Section	Avg Velocity	Standard Deviation	CV (%)
1	251.3	3.93	1.56
2	253.0	3.20	1.26
3	254.4	3.04	1.20
4	254.1	3.12	1.23
Total	253.2	3.48	1.38

Table A.7: Wind Tunnel Freestream Velocity Profiles (sfpm), SP_h = 0.508" H_2O

283.7	275.4	277.6	281.3
284.3	275.2	276.5	276.1
280.0	279.6	277.9	281.7
291.2	287.6	282.8	286.1

Cross Section 1 - 18" from face

278.7	282.1	276.4	280.7
284.8	282.7	276.2	279.3
285.3	288.9	285.3	278.6
286.7	288.2	285.2	278.3

Cross Section 2 - 36" from face

284.0	284.9	279.6	281.2
284.8	285.3	282.0	280.1
287.0	288.7	283.1	279.3
288.9	290.1	278.3	276.6

Cross Section 3 - 54" from face

282.7	284.5	281.9	287.5
284.5	283.8	282.7	281.6
286.8	279.6	279.6	282.1
288.6	282.1	278.8	276.9

Cross Section 4 - 72" from face

Cross Section	Avg Velocity	Standard Deviation	CV (%)
1	281.1	4.69	1.67
2	282.3	4.13	1.46
3	283.4	4.04	1.43
4	282.7	3.19	1.13
Total	282.4	4.04	1.43

Table A.8: Wind Tunnel Freestream Velocity Profiles (sfpm), SP_h = 0.610" H_2O

312.4	309.1	310.6	313.8
317.2	306.5	309.5	310.2
315.0	306.3	308.5	309.5
316.0	307.1	310.3	312.3

Cross Section 1 - 18" from face

308.8	310.8	317.4	316.8
315.3	315.2	312.4	314.0
315.2	315.0	313.6	311.8
310.8	305.7	313.0	311.6

Cross Section 2 - 36" from face

307.4	311.6	316.0	315.0
316.8	312.8	313.6	316.2
311.8	319.1	311.5	315.1
311.9	310.4	308.6	308.1

Cross Section 3 - 54" from face

310.1	311.7	318.7	319.9
324.2	313.7	314.0	317.2
310.5	313.6	308.2	312.9
304.2	303.3	304.5	302.4

Cross Section 4 - 72" from face

Cross Section	Avg Velocity	Standard Deviation	CV (%)
1	310.9	3.31	1.06
2	313.0	3.04	0.97
3	312.9	3.34	1.07
4	311.8	6.32	2.03
Total	312.1	4.21	1.35

Table A.9: Wind Tunnel Freestream Velocity Profiles (sfpm), $SP_h = 0.717"\ H_2O$

331.7	336.0	340.6	343.1
333.0	328.8	338.0	332.1
331.2	329.5	330.1	335.6
338.1	332.2	330.9	337.3

Cross Section 1 - 18" from face

325.0	336.4	334.6	349.3
340.1	330.8	339.3	329.9
336.2	338.8	333.8	334.7
330.8	334.9	335.5	338.3

Cross Section 2 - 36" from face

330.2	326.3	337.3	340.0
344.1	336.6	347.4	336.0
336.9	339.4	335.1	333.4
337.0	331.2	333.9	336.7

Cross Section 3 - 54" from face

336.7	337.0	337.3	349.2
347.6	341.0	345.8	350.5
336.3	332.0	331.9	332.1
331.7	331.0	327.1	327.1

Cross Section 4 - 72" from face

Cross Section	Avg Velocity	Standard Deviation	CV (%)
1	334.3	4.23	1.26
2	335.5	5.40	1.61
3	336.4	5.08	1.51
4	337.1	7.62	2.26
Total	335.8	5.69	1.69

Table A.10: Wind Tunnel Freestream Velocity Profiles (sfpm), $SP_h = 0.837"\ H_2O$

358.9	349.8	348.7	358.0
365.3	356.5	354.4	360.4
362.2	355.5	357.8	362.3
373.3	364.4	364.7	368.7

Cross Section 1 - 18" from face

354.0	354.5	352.0	357.0
365.5	365.4	360.6	361.5
364.6	366.0	367.1	362.9
371.6	362.0	366.7	362.0

Cross Section 2 - 36" from face

351.0	357.0	350.7	362.1
372.7	366.5	369.7	365.2
366.0	363.6	364.9	365.0
370.0	369.4	363.1	368.7

Cross Section 3 - 54" from face

354.4	362.0	356.2	368.6
372.9	364.9	364.4	370.8
366.7	367.1	365.3	365.8
376.2	367.9	356.2	362.9

Cross Section 4 - 72" from face

Cross Section	Avg Velocity	Standard Deviation	CV (%)
1	360.1	6.54	1.82
2	362.1	5.38	1.49
3	364.1	6.36	1.75
4	365.1	5.95	1.63
Total	362.8	6.25	1.72

Table A.11: 90° Orientation Raw Data, Experimental Replicate 1

Run Number	p_n (psig)	m_s/m_l (predicted)	U (fpm)	Temp (F)	BZC Flow (lpm)	Mass Filter (mg)		Mass Container (g)		Mass Trough (g)		Sampling Time (sec)
						Before	After	Before	After	Before	After	
1	30	0.90	112.5	82.3	2.05	13.537	13.895	8305	8027	583.2	833.2	180.07
2	30	0.90	131.8	83.3	2.05	13.355	13.576	8300	8016	583.6	839.0	180.03
3	30	0.90	150.0	84.0	2.05	13.705	13.898	8301	8011	585.1	843.6	180.17
4	50	0.90	112.5	86.0	2.02	13.597	14.383	8304	7905	583.6	952.7	180.19
5	50	0.90	93.8	86.2	2.02	13.608	14.959	8300	7902	584.0	952.1	180.12
6	50	0.90	75.0	86.1	2.02	13.684	15.179	8302	7905	585.6	953.0	180.24
7	50	1.30	93.8	81.7	2.04	14.148	15.623	8300	8022	583.8	832.8	180.08
8	50	1.30	112.5	82.4	2.04	15.043	16.060	8301	8019	584.7	836.4	180.27
9	50	1.30	75.0	83.5	2.04	14.967	16.697	8301	8016	584.3	840.2	180.08
10	30	1.30	112.5	84.7	2.04	14.599	14.958	8300	8110	584.4	745.1	180.08
11	30	1.30	150.0	85.2	2.04	12.696	12.879	8304	8114	584.0	744.3	180.09
12	30	1.30	131.8	86.0	2.04	17.269	17.624	8301	8111	584.2	746.0	180.15
13	30	0.70	150.0	82.4	2.05	15.922	16.043	8300	7940	584.1	914.0	180.05
14	30	0.70	112.5	83.2	2.05	15.641	16.143	8301	7937	583.6	919.2	180.16
15	30	0.70	131.8	83.7	2.05	15.619	15.902	8302	7936	583.3	918.6	180.12
16	50	0.70	112.5	85.6	2.03	15.617	16.613	8301	7791	582.7	1059.7	180.02
17	50	0.70	93.8	85.8	2.03	15.326	16.749	8301	7792	584.5	1063.4	180.22
18	50	0.70	75.0	85.8	2.03	14.943	16.486	8307	7798	583.7	1061.6	180.11
55	40	0.90	105.0	83.3	2.02	14.165	15.834	8303	7737	581.4	1097.0	300.15
56	40	0.90	125.0	83.6	2.02	14.347	15.220	8301	7733	583.0	1101.0	300.11
57	40	1.30	105.0	85.1	2.02	16.987	18.684	8301	7916	581.5	916.0	300.05
58	40	1.30	125.0	85.6	2.02	17.707	18.627	8301	7916	582.3	917.6	300.17
59	40	0.70	125.0	86.2	2.02	17.933	18.740	8302	7869	582.3	983.0	180.11
60	40	0.70	105.0	86.4	2.02	17.946	19.190	8301	7870	583.5	984.0	180.13
163	20	1.30	150.0	76.7	2.03	14.387	14.429	8302	7810	580.4	985.3	600.12
164	20	1.30	200.0	77.7	2.03	14.505	14.511	8303	7560	582.7	1176.5	900.02
165	20	0.90	200.0	79.4	2.03	14.598	14.608	8302	7249	581.6	1465.6	900.08
166	20	0.90	150.0	80.1	2.03	14.873	14.998	8302	7243	581.7	1496.1	900.28
167	20	0.70	150.0	80.7	2.03	15.088	15.246	8302	6950	582.4	1784.4	900.06
168	20	0.70	200.0	80.9	2.03	15.091	15.116	8302	6947	583.2	1757.5	900.15

Table A.12: 90° Orientation Raw Data, Experimental Replicate 2

Run Number	p_n (psig)	m_e/m_l (predicted)	U (fpm)	Temp (F)	BZC Flow (lpm)	Mass Filter (mg)		Mass Container (g)		Mass Trough (g)		Sampling Time (sec)
						Before	After	Before	After	Before	After	
19	30	1.30	131.8	78.4	2.01	14.367	14.642	8301	8111	582.4	745.8	180.14
20	30	1.30	150.0	79.0	2.01	14.508	14.565	8302	8115	584.1	745.6	180.05
21	30	1.30	112.5	79.0	2.01	12.906	13.405	8301	8113	583.8	747.5	180.18
22	50	1.30	93.8	80.3	2.02	13.734	15.140	8301	8025	582.5	830.4	180.14
23	50	1.30	112.5	80.3	2.02	14.209	15.273	8304	8031	583.0	829.6	180.09
24	50	1.30	75.0	80.3	2.02	14.377	16.013	8303	8028	582.8	831.6	180.01
25	50	0.70	75.0	75.4	2.02	14.874	16.386	8303	7786	585.1	1073.0	180.08
26	50	0.70	112.5	75.7	2.02	15.255	16.320	8300	7780	584.6	1074.8	180.12
27	50	0.70	93.8	76.5	2.02	15.693	17.064	8302	7772	586.6	1084.6	180.12
28	30	0.70	112.5	77.7	2.03	16.191	16.767	8302	7947	585.5	912.3	180.13
29	30	0.70	131.8	77.8	2.03	15.238	15.559	8300	7947	584.4	909.8	180.09
30	30	0.70	150.0	77.5	2.03	15.105	15.204	8300	7947	584.1	906.7	180.11
31	50	0.90	112.5	76.1	2.02	15.121	16.286	8301	7895	583.5	958.9	180.11
32	50	0.90	75.0	76.6	2.02	14.963	16.516	8301	7893	584.8	963.8	180.13
33	50	0.90	93.8	77.1	2.02	15.090	16.387	8302	7892	585.2	966.5	180.15
34	30	0.90	112.5	78.6	2.02	14.329	14.764	8305	8027	582.2	831.6	180.12
35	30	0.90	150.0	79.2	2.02	14.121	14.289	8303	8023	583.3	834.5	180.18
36	30	0.90	131.8	79.5	2.02	14.058	14.381	8302	8021	583.0	835.4	180.16
61	40	1.30	125.0	82.8	2.02	18.178	19.222	8302	7909	581.3	924.5	300.18
62	40	1.30	105.0	83.0	2.02	17.851	19.782	8301	7907	582.5	927.4	300.14
63	40	0.70	105.0	83.4	2.02	17.547	18.683	8303	7873	581.0	978.9	180.25
64	40	0.70	125.0	83.6	2.02	17.219	17.816	8302	7872	583.0	981.4	180.14
65	40	0.90	105.0	83.8	2.02	17.314	19.509	8302	7736	583.2	1098.8	300.22
66	40	0.90	125.0	83.9	2.02	16.862	18.088	8306	7742	582.3	1096.3	300.10
169	20	0.70	150.0	78.0	2.02	15.137	15.332	8305	6952	581.7	1783.0	899.97
170	20	0.70	200.0	79.3	2.02	15.208	15.236	8301	6933	581.8	1766.0	900.16
171	20	1.30	200.0	80.6	2.02	15.380	15.388	8300	7559	585.8	1170.5	900.03
172	20	1.30	150.0	81.2	2.02	15.672	15.893	8303	7563	583.4	1190.8	900.02
173	20	0.90	200.0	81.9	2.02	15.740	15.768	8303	7257	583.2	1453.1	900.07
174	20	0.90	150.0	82.1	2.02	15.775	15.943	8303	7259	581.7	1480.9	900.05

Table A.13: 90° Orientation Raw Data, Experimental Replicate 3

Run Number	p_n (psig)	m_e/m_l (predicted)	U (fpm)	Temp (F)	BZC Flow (lpm)	Mass Filter (mg)		Mass Container (g)		Mass Trough (g)		Sampling Time (sec)
						Before	After	Before	After	Before	After	
37	30	0.70	131.8	81.4	2.02	15.828	16.029	8304	7935	580.9	919.7	180.19
38	30	0.70	112.5	82.1	2.02	16.344	16.704	8302	7936	581.8	918.9	180.04
39	30	0.70	150.0	83.4	2.02	16.543	16.687	8301	7938	582.6	915.1	180.33
40	50	0.70	75.0	84.9	2.01	16.796	18.291	8305	7786	583.0	1071.1	180.12
41	50	0.70	112.5	85.7	2.01	16.964	17.859	8302	7781	582.6	1072.3	180.25
42	50	0.70	93.8	85.1	2.01	17.406	18.705	8304	7789	584.4	1068.6	180.18
43	30	1.30	131.8	83.6	2.02	16.991	17.440	8300	7978	581.5	858.2	300.02
44	30	1.30	150.0	85.0	2.02	17.260	17.478	8302	7977	582.3	860.1	300.09
45	30	1.30	112.5	85.7	2.02	17.152	17.926	8302	7976	581.6	863.6	300.10
46	50	1.30	75.0	87.0	2.02	17.110	19.700	8301	7854	582.5	981.9	300.22
47	50	1.30	112.5	87.2	2.02	17.121	18.740	8302	7848	582.4	989.7	300.14
48	50	1.30	93.8	87.5	2.02	16.710	18.905	8306	7839	584.3	1003.6	300.10
49	50	0.90	112.5	86.5	2.02	17.838	19.720	8301	7639	581.1	1197.7	300.19
50	50	0.90	93.8	87.0	2.02	18.050	19.898	8301	7770	581.6	1076.6	240.06
51	50	0.90	75.0	87.6	2.02	18.001	19.545	8304	7901	583.0	958.2	180.15
52	30	0.90	150.0	87.8	2.02	17.354	17.612	8303	7842	581.3	995.3	299.26
53	30	0.90	112.5	88.0	2.02	17.293	18.328	8303	7839	582.8	1001.5	300.02
54	30	0.90	131.8	87.9	2.02	14.285	14.960	8303	7840	582.7	999.4	300.08
67	40	0.70	125.0	80.2	2.02	17.256	17.825	8303	7876	582.1	976.9	180.11
68	40	0.70	105.0	80.6	2.02	16.864	17.888	8303	7873	582.4	981.0	180.17
69	40	1.30	125.0	81.2	2.02	16.911	17.868	8300	7908	583.0	927.7	300.18
70	40	1.30	105.0	81.7	2.02	16.269	18.049	8302	7909	582.3	928.7	300.07
71	40	0.90	125.0	81.9	2.02	15.947	16.902	8301	7741	581.6	1092.8	300.18
72	40	0.90	105.0	82.0	2.02	15.829	17.565	8305	7744	583.4	1096.5	300.23
175	20	0.90	200.0	80.8	2.03	15.983	16.005	8303	7230	582.9	1474.7	900.05
176	20	0.90	150.0	78.7	2.03	15.977	16.066	8302	7253	583.6	1482.4	900.16
177	20	0.70	200.0	79.9	2.03	13.868	13.879	8300	6926	581.7	1761.0	900.02
178	20	0.70	150.0	80.4	2.03	14.612	14.828	8302	6957	583.5	1772.9	900.18
179	20	1.30	150.0	81.3	2.03	15.944	16.083	8304	7562	582.0	1186.6	900.14
180	20	1.30	200.0	81.2	2.03	15.112	15.131	8304	7562	584.0	1163.0	900.09

Table A.14: 180° Orientation Raw Data, Experimental Replicate 1

Run Number	p_n (psig)	m_e/m_l (predicted)	U (fpm)	Temp (F)	BZC Flow (lpm)	Mass Filter (mg)		Mass Container (g)		Mass Trough (g)		Sampling Time (sec)
						Before	After	Before	After	Before	After	
73	30	0.90	150.0	81.2	2.02	15.586	15.815	8303	7380	581.3	1401.8	599.99
74	30	0.90	112.5	82.0	2.02	15.562	15.746	8302	7371	582.5	1414.9	600.13
75	30	0.90	131.8	82.8	2.02	15.491	15.723	8303	7368	583.1	1418.7	600.13
76	50	0.90	75.0	84.0	2.02	15.450	15.714	8304	6980	585.2	1808.5	600.08
77	50	0.90	112.5	84.2	2.02	15.140	15.300	8302	6971	583.7	1810.9	600.06
78	50	0.90	93.8	84.6	2.02	15.080	15.322	8303	6971	583.5	1812.9	600.17
79	40	0.90	125.0	85.2	2.02	14.975	15.142	8301	7194	582.9	1581.1	600.20
80	40	0.90	105.0	84.8	2.02	14.761	14.927	8305	7203	583.7	1585.8	600.24
81	50	0.70	93.8	80.1	2.03	14.602	14.718	8302	7103	581.9	1707.1	420.02
82	50	0.70	75.0	80.8	2.03	14.260	14.494	8302	7092	582.7	1720.3	420.08
83	50	0.70	112.5	81.4	2.03	14.310	14.467	8304	6915	583.7	1887.2	480.11
84	30	0.70	131.8	82.5	2.03	14.178	14.406	8302	7118	582.9	1663.2	600.11
85	30	0.70	150.0	82.7	2.03	14.108	14.371	8303	7119	584.1	1662.6	600.12
86	30	0.70	112.5	83.0	2.03	17.115	17.331	8304	7119	583.7	1666.5	600.24
87	40	0.70	125.0	83.1	2.03	17.162	17.281	8301	7171	583.1	1630.2	480.02
88	40	0.70	105.0	83.5	2.03	17.094	17.257	8302	7173	583.3	1631.1	480.09
89	30	1.30	131.8	79.0	2.03	17.111	17.307	8300	7658	581.4	1130.4	600.24
90	30	1.30	112.5	79.4	2.03	14.058	14.271	8305	7664	583.1	1131.9	600.08
91	30	1.30	150.0	80.2	2.03	13.966	14.221	8303	7655	583.2	1136.3	600.06
92	40	1.30	105.0	82.2	2.03	13.808	14.004	8304	7529	581.2	1258.2	600.13
93	40	1.30	125.0	83.0	2.03	13.863	14.012	8303	7524	583.7	1263.8	600.14
94	50	1.30	75.0	83.7	2.03	14.139	14.474	8302	7386	581.8	1399.7	600.17
95	50	1.30	112.5	83.9	2.03	14.828	15.074	8304	7387	584.2	1402.1	600.19
96	50	1.30	93.8	84.1	2.03	15.473	15.742	8302	7387	583.4	1400.4	600.03
145	20	1.30	200.0	76.6	2.01	14.670	14.986	8302	7805	580.5	981.7	600.02
146	20	1.30	150.0	78.6	2.01	13.805	14.082	8306	7800	582.4	996.5	600.05
147	20	0.70	150.0	79.8	2.01	13.676	13.900	8306	7410	585.6	1377.0	599.95
148	20	0.70	200.0	80.1	2.01	13.762	14.023	8302	7399	583.2	1372.5	600.14
149	20	0.90	200.0	80.5	2.01	17.106	17.471	8306	7609	582.5	1173.7	600.09
150	20	0.90	150.0	80.6	2.01	17.110	17.435	8303	7608	583.2	1182.1	600.07

Table A.15: 180° Orientation Raw Data, Experimental Replicate 2

Run Number	p_n (psig)	m_e/m_l (predicted)	U (fpm)	Temp (F)	BZC Flow (lpm)	Mass Filter (mg)		Mass Container (g)		Mass Trough (g)		Sampling Time (sec)
						Before	After	Before	After	Before	After	
97	50	0.70	93.8	77.8	2.01	16.367	16.516	8304	6958	583.4	1849.5	480.08
98	50	0.70	75.0	77.7	2.01	16.773	16.914	8303	6942	583.5	1865.5	479.99
99	50	0.70	112.5	78.1	2.01	16.585	16.685	8304	6859	583.1	1944.0	509.97
100	40	0.70	105.0	78.2	2.02	15.671	15.774	8309	6905	584.8	1893.5	600.02
101	40	0.70	125.0	78.2	2.02	15.467	15.581	8301	6901	584.1	1886.8	600.12
102	30	0.70	150.0	78.0	2.02	15.358	15.525	8309	7143	582.8	1652.3	600.20
103	30	0.70	112.5	77.9	2.02	15.318	15.427	8302	7139	585.0	1653.5	600.11
104	30	0.70	131.8	77.4	2.02	15.244	15.417	8301	7142	584.5	1646.6	600.06
105	40	1.30	105.0	76.3	2.02	15.011	15.193	8301	7532	582.2	1261.2	600.05
106	40	1.30	125.0	76.5	2.02	14.520	14.659	8306	7537	583.4	1262.7	600.13
107	30	1.30	150.0	76.8	2.02	14.684	14.856	8300	7663	583.5	1130.3	600.08
108	30	1.30	112.5	77.2	2.02	14.613	14.781	8303	7668	582.6	1131.6	600.08
109	30	1.30	131.8	77.4	2.02	14.439	14.629	8307	7671	583.2	1131.7	600.13
110	50	1.30	75.0	77.7	2.02	14.724	14.970	8300	7395	583.2	1395.1	600.14
111	50	1.30	93.8	77.7	2.02	15.720	15.880	8302	7390	584.1	1404.6	600.11
112	50	1.30	112.5	77.0	2.02	16.359	16.459	8302	7397	583.8	1397.2	600.09
113	50	0.90	75.0	76.3	2.02	16.966	17.242	8303	6977	582.4	1810.8	600.08
114	50	0.90	112.5	77.1	2.02	17.263	17.444	8302	6969	583.5	1818.5	600.09
115	50	0.90	93.8	77.7	2.02	16.875	17.081	8303	6965	583.9	1825.3	600.24
116	30	0.90	112.5	78.4	2.02	16.983	17.163	8304	7395	583.3	1397.1	600.10
117	30	0.90	150.0	78.7	2.02	16.899	17.136	8301	7387	584.0	1399.7	600.02
118	30	0.90	131.8	79.1	2.02	16.956	17.227	8303	7385	582.9	1404.0	600.16
119	40	0.90	105.0	79.3	2.02	17.133	17.304	8303	7188	583.2	1601.3	600.04
120	40	0.90	125.0	79.1	2.02	13.911	14.007	8302	7190	583.2	1598.3	600.29
151	20	0.70	150.0	76.1	2.02	17.103	17.355	8303	7402	582.4	1381.3	600.12
152	20	0.70	200.0	76.4	2.02	17.185	17.519	8302	7396	582.7	1376.0	600.04
153	20	1.30	200.0	77.3	2.02	17.057	17.391	8301	7806	582.5	984.4	600.04
154	20	1.30	150.0	77.7	2.02	17.326	17.627	8305	7809	582.8	991.1	599.99
155	20	0.90	200.0	78.3	2.02	17.353	17.750	8302	7600	582.5	1179.6	600.00
156	20	0.90	150.0	78.7	2.02	16.813	17.066	8300	7599	583.1	1186.7	600.08

Table A.16: 180° Orientation Raw Data, Experimental Replicate 3

Run Number	p_n (psig)	m_e/m_i (predicted)	U (fpm)	Temp (F)	BZC Flow (lpm)	Mass Filter (mg)		Mass Container (g)		Mass Trough (g)		Sampling Time (sec)
						Before	After	Before	After	Before	After	
121	30	1.30	131.8	77.0	2.03	13.895	14.097	8301	7657	581.8	1132.9	600.12
122	30	1.30	150.0	77.7	2.03	14.124	14.349	8305	7660	582.1	1135.3	600.10
123	30	1.30	112.5	78.3	2.03	13.865	14.069	8303	7654	582.5	1141.0	600.02
124	50	1.30	75.0	79.3	2.03	13.910	14.171	8301	7393	582.6	1394.0	600.21
125	50	1.30	93.8	79.8	2.03	14.450	14.613	8308	7397	582.7	1396.5	600.04
126	50	1.30	112.5	80.2	2.03	15.744	15.918	8302	7389	583.6	1399.3	600.00
127	40	1.30	105.0	80.8	2.03	16.369	16.551	8302	7509	582.1	1278.4	600.12
128	40	1.30	125.0	81.1	2.03	16.199	16.328	8301	7508	583.4	1276.7	599.98
129	30	0.90	112.5	78.7	2.02	16.022	16.195	8305	7373	582.2	1414.2	600.09
130	30	0.90	131.8	79.5	2.02	14.192	14.383	8308	7370	584.4	1422.1	599.96
131	30	0.90	150.0	80.1	2.02	14.424	14.612	8306	7362	583.7	1424.4	600.10
132	40	0.90	125.0	80.9	2.02	14.475	14.625	8303	7192	582.8	1592.6	600.13
133	40	0.90	105.0	81.2	2.02	14.609	14.742	8303	7190	583.6	1597.4	600.21
134	50	0.90	75.0	81.8	2.02	14.587	14.865	8303	6992	583.1	1794.0	600.05
135	50	0.90	93.8	81.7	2.02	14.823	14.995	8301	6993	584.4	1792.8	600.11
136	50	0.90	112.5	81.8	2.02	14.837	14.951	8306	6995	583.7	1792.9	600.13
137	40	0.70	125.0	79.5	2.03	14.870	14.984	8307	6874	582.7	1914.5	600.16
138	40	0.70	105.0	80.3	2.03	14.946	15.078	8304	6860	584.2	1927.8	600.14
139	30	0.70	150.0	80.9	2.03	14.933	15.128	8305	7130	583.8	1654.5	600.09
140	30	0.70	112.5	81.7	2.03	15.998	16.149	8304	7109	583.4	1677.3	600.14
141	30	0.70	131.8	82.2	2.03	16.353	16.540	8301	7101	583.9	1683.5	600.10
142	50	0.70	112.5	82.9	2.03	16.740	16.836	8302	6946	583.8	1855.3	480.08
143	50	0.70	75.0	83.0	2.03	16.000	16.219	8302	6610	584.1	2174.4	600.15
144	50	0.70	93.8	83.0	2.03	15.734	15.878	8302	6615	584.3	2168.1	600.03
157	20	0.90	150.0	72.6	2.02	16.555	16.819	8301	7589	582.3	1198.2	600.02
158	20	0.90	200.0	74.0	2.02	15.883	16.305	8304	7596	583.6	1186.2	600.12
159	20	1.30	150.0	75.2	2.02	15.299	15.540	8305	7808	581.9	991.2	599.98
160	20	1.30	200.0	75.9	2.02	15.013	15.346	8302	7802	583.1	989.6	600.15
161	20	0.70	200.0	76.0	2.02	14.047	14.518	8303	7412	582.2	1362.8	600.15
162	20	0.70	150.0	75.7	2.02	14.273	14.519	8302	7413	582.6	1370.8	600.10

Table A.17: 90° Orientation Calculated Data, Experimental Replicate 1

Run Number	p_n (psig)	m_e/m_l (predicted)	U (fpm)	m_l (g/min)	m_o (g/min)	C (mg/m^3)	p_nH/μ_lU	m_e/m_l (actual)	$CUHD/m_o$
1	30	0.90	112.5	92.63	9.33	58.19	8.28E+06	0.90	0.0452
2	30	0.90	131.8	94.65	9.53	35.93	7.24E+06	0.88	0.0320
3	30	0.90	150.0	96.58	10.49	31.35	6.46E+06	0.86	0.0289
4	50	0.90	112.5	132.86	9.96	129.89	1.50E+07	0.90	0.0947
5	50	0.90	93.8	132.58	9.96	223.34	1.81E+07	0.90	0.1356
6	50	0.90	75.0	132.16	9.85	246.98	2.26E+07	0.90	0.1212
7	50	1.30	93.8	92.63	9.66	240.91	1.63E+07	1.29	0.1507
8	50	1.30	112.5	93.86	10.08	165.93	1.38E+07	1.27	0.1194
9	50	1.30	75.0	94.96	9.70	282.55	2.13E+07	1.26	0.1410
10	30	1.30	112.5	63.31	9.76	58.78	8.76E+06	1.31	0.0437
11	30	1.30	150.0	63.30	9.90	29.96	6.64E+06	1.31	0.0293
12	30	1.30	131.8	63.28	9.39	58.10	7.71E+06	1.31	0.0526
13	30	0.70	150.0	119.97	10.03	19.72	6.22E+06	0.69	0.0190
14	30	0.70	112.5	121.23	9.46	81.75	8.45E+06	0.69	0.0627
15	30	0.70	131.8	121.92	10.23	46.10	7.30E+06	0.68	0.0383
16	50	0.70	112.5	169.98	11.00	163.53	1.49E+07	0.70	0.1079
17	50	0.70	93.8	169.46	10.02	233.38	1.80E+07	0.70	0.1408
18	50	0.70	75.0	169.56	10.36	253.21	2.25E+07	0.70	0.1182
55	40	0.90	105.0	113.14	10.07	165.57	1.21E+07	0.89	0.1113
56	40	0.90	125.0	113.56	10.00	86.62	1.02E+07	0.89	0.0699
57	40	1.30	105.0	76.99	10.10	167.99	1.26E+07	1.32	0.1126
58	40	1.30	125.0	76.96	9.93	91.04	1.07E+07	1.32	0.0739
59	40	0.70	125.0	144.25	10.76	133.09	1.09E+07	0.70	0.0997
60	40	0.70	105.0	143.56	10.16	205.13	1.30E+07	0.71	0.1367
163	20	1.30	150.0	49.19	8.71	2.07	3.63E+06	1.29	0.0023
164	20	1.30	200.0	49.53	9.95	0.20	2.79E+06	1.28	0.0003
165	20	0.90	200.0	70.19	11.27	0.33	2.90E+06	0.91	0.0004
166	20	0.90	150.0	70.58	9.64	4.10	3.93E+06	0.90	0.0041
167	20	0.70	150.0	90.13	10.00	5.19	3.99E+06	0.71	0.0050
168	20	0.70	200.0	90.32	12.04	0.82	3.01E+06	0.70	0.0009

Table A.18: 90° Orientation Calculated Data, Experimental Replicate 2

Run Number	p_n (psig)	m_e/m_l (predicted)	U (fpm)	m_l (g/min)	m_o (lpm)	C (mg/m^3)	p_nH/μ_lU	m_e/m_l (actual)	$CUHD/m_o$
19	30	1.30	131.8	63.28	8.86	45.57	6.46E+06	1.31	0.0437
20	30	1.30	150.0	62.32	8.50	9.45	5.75E+06	1.33	0.0108
21	30	1.30	112.5	62.60	8.09	82.67	7.67E+06	1.33	0.0741
22	50	1.30	93.8	91.93	9.36	231.83	1.58E+07	1.30	0.1498
23	50	1.30	112.5	90.95	8.80	175.49	1.32E+07	1.31	0.1448
24	50	1.30	75.0	91.66	8.73	269.95	1.98E+07	1.30	0.1495
25	50	0.70	75.0	172.26	9.70	250.01	1.76E+07	0.69	0.1247
26	50	0.70	112.5	173.22	9.93	176.06	1.18E+07	0.69	0.1287
27	50	0.70	93.8	176.55	10.66	226.65	1.45E+07	0.68	0.1286
28	30	0.70	112.5	118.25	9.39	94.75	7.44E+06	0.70	0.0732
29	30	0.70	131.8	117.61	9.20	52.81	6.37E+06	0.71	0.0488
30	30	0.70	150.0	117.59	10.13	16.29	5.55E+06	0.71	0.0156
31	50	0.90	112.5	135.25	10.19	192.13	1.19E+07	0.88	0.1367
32	50	0.90	75.0	135.90	9.66	256.09	1.81E+07	0.88	0.1282
33	50	0.90	93.8	136.55	9.56	213.85	1.47E+07	0.87	0.1353
34	30	0.90	112.5	92.60	9.53	71.91	7.60E+06	0.90	0.0548
35	30	0.90	150.0	93.24	9.59	27.76	5.78E+06	0.89	0.0280
36	30	0.90	131.8	93.58	9.52	53.39	6.62E+06	0.89	0.0476
61	40	1.30	125.0	78.55	9.95	103.56	1.01E+07	1.29	0.0839
62	40	1.30	105.0	78.76	9.82	191.57	1.20E+07	1.29	0.1322
63	40	0.70	105.0	143.13	10.69	187.66	1.21E+07	0.71	0.1189
64	40	0.70	125.0	143.22	10.53	98.68	1.02E+07	0.71	0.0756
65	40	0.90	105.0	113.12	10.07	217.71	1.22E+07	0.90	0.1464
66	40	0.90	125.0	112.76	10.00	121.65	1.03E+07	0.90	0.0981
169	20	0.70	150.0	90.20	10.11	6.45	3.75E+06	0.70	0.0062
170	20	0.70	200.0	91.18	12.25	0.93	2.90E+06	0.70	0.0010
171	20	1.30	200.0	49.40	10.42	0.26	2.98E+06	1.29	0.0003
172	20	1.30	150.0	49.33	8.84	7.31	4.03E+06	1.29	0.0080
173	20	0.90	200.0	69.73	11.74	0.93	3.08E+06	0.91	0.0010
174	20	0.90	150.0	69.60	9.65	5.56	4.12E+06	0.91	0.0056

Table A.19: 90° Orientation Calculated Data, Experimental Replicate 3

Run Number	p_n (psig)	m_a/m_l (predicted)	U (fpm)	m_l (g/min)	m_o (lpm)	C (mg/m^3)	p_nH/μ_lU	m_a/m_l (actual)	$CUHD/m_o$
37	30	0.70	131.8	122.87	10.06	33.22	6.92E+06	0.68	0.0281
38	30	0.70	112.5	121.97	9.63	59.54	8.24E+06	0.68	0.0449
39	30	0.70	150.0	120.78	10.15	23.78	6.37E+06	0.69	0.0227
40	50	0.70	75.0	172.88	10.29	248.38	2.20E+07	0.69	0.1167
41	50	0.70	112.5	173.43	10.42	148.59	1.49E+07	0.69	0.1035
42	50	0.70	93.8	171.50	10.26	215.74	1.77E+07	0.70	0.1272
43	30	1.30	131.8	64.40	9.06	44.56	7.29E+06	1.29	0.0418
44	30	1.30	150.0	64.98	9.44	21.63	6.61E+06	1.28	0.0222
45	30	1.30	112.5	65.18	8.80	76.80	8.96E+06	1.27	0.0633
46	50	1.30	75.0	89.33	9.51	256.88	2.31E+07	1.34	0.1306
47	50	1.30	112.5	90.76	9.34	160.62	1.55E+07	1.32	0.1248
48	50	1.30	93.8	93.37	9.54	217.79	1.87E+07	1.28	0.1381
49	50	0.90	112.5	132.32	9.07	186.68	1.52E+07	0.90	0.1493
50	50	0.90	93.8	132.72	9.00	229.22	1.85E+07	0.90	0.1540
51	50	0.90	75.0	134.22	9.26	255.21	2.34E+07	0.89	0.1333
52	30	0.90	150.0	92.43	9.42	25.67	7.06E+06	0.90	0.0264
53	30	0.90	112.5	92.79	9.06	102.72	9.46E+06	0.90	0.0823
54	30	0.90	131.8	92.58	9.26	66.98	8.06E+06	0.90	0.0615
67	40	0.70	125.0	142.25	10.73	94.07	9.46E+06	0.71	0.0707
68	40	0.70	105.0	143.20	10.46	169.24	1.14E+07	0.71	0.1096
69	40	1.30	125.0	78.35	9.45	94.93	9.68E+06	1.29	0.0809
70	40	1.30	105.0	78.58	9.32	176.63	1.17E+07	1.29	0.1284
71	40	0.90	125.0	111.93	9.75	94.73	9.84E+06	0.90	0.0783
72	40	0.90	105.0	112.11	9.57	172.18	1.17E+07	0.90	0.1218
175	20	0.90	200.0	71.53	12.08	0.72	3.00E+06	0.89	0.0008
176	20	0.90	150.0	69.92	10.01	2.93	3.81E+06	0.91	0.0028
177	20	0.70	200.0	91.60	12.98	0.36	2.94E+06	0.69	0.0004
178	20	0.70	150.0	89.65	10.37	7.11	3.96E+06	0.71	0.0066
179	20	1.30	150.0	49.46	9.16	4.58	4.04E+06	1.29	0.0048
180	20	1.30	200.0	49.46	10.87	0.63	3.03E+06	1.29	0.0007

Table A.20: 180° Orientation Calculated Data, Experimental Replicate 1

Run Number	p_n (psig)	m_e/m_l (predicted)	U (fpm)	m_l (g/min)	m_o (lpm)	C (mg/m^3)	p_nH/μ_lU	m_e/m_l (actual)	$CUHD/m_o$
73	30	0.90	150.0	92.30	10.25	11.36	6.05E+06	0.90	0.0107
74	30	0.90	112.5	93.08	9.86	9.13	8.22E+06	0.89	0.0067
75	30	0.90	131.8	93.48	9.94	11.51	7.15E+06	0.89	0.0098
76	50	0.90	75.0	132.38	10.07	13.10	2.15E+07	0.90	0.0063
77	50	0.90	112.5	133.09	10.38	7.94	1.44E+07	0.90	0.0055
78	50	0.90	93.8	133.16	10.26	12.01	1.75E+07	0.90	0.0071
79	40	0.90	125.0	110.66	10.88	8.29	1.06E+07	0.91	0.0061
80	40	0.90	105.0	110.16	9.99	8.23	1.25E+07	0.92	0.0056
81	50	0.70	93.8	171.28	10.54	8.18	1.57E+07	0.70	0.0047
82	50	0.70	75.0	172.82	10.34	16.50	2.00E+07	0.69	0.0077
83	50	0.70	112.5	173.59	10.69	9.69	1.35E+07	0.69	0.0066
84	30	0.70	131.8	118.38	10.37	11.26	7.10E+06	0.70	0.0092
85	30	0.70	150.0	118.38	10.55	12.99	6.27E+06	0.70	0.0119
86	30	0.70	112.5	118.45	10.22	10.66	8.42E+06	0.70	0.0076
87	40	0.70	125.0	141.24	10.36	7.35	1.01E+07	0.72	0.0057
88	40	0.70	105.0	141.10	10.15	10.06	1.22E+07	0.72	0.0067
89	30	1.30	131.8	64.17	9.30	9.68	6.55E+06	1.29	0.0088
90	30	1.30	112.5	64.09	9.22	10.52	7.74E+06	1.30	0.0083
91	30	1.30	150.0	64.79	9.49	12.59	5.91E+06	1.28	0.0128
92	40	1.30	105.0	77.48	9.80	9.68	1.18E+07	1.31	0.0067
93	40	1.30	125.0	77.88	9.89	7.36	1.01E+07	1.30	0.0060
94	50	1.30	75.0	91.57	9.81	16.54	2.14E+07	1.30	0.0082
95	50	1.30	112.5	91.67	9.91	12.14	1.43E+07	1.30	0.0089
96	50	1.30	93.8	91.50	9.80	13.28	1.73E+07	1.31	0.0082
145	20	1.30	200.0	49.70	9.58	15.72	2.72E+06	1.28	0.0212
146	20	1.30	150.0	50.60	9.19	13.78	3.80E+06	1.26	0.0145
147	20	0.70	150.0	89.61	10.46	11.15	3.91E+06	0.71	0.0103
148	20	0.70	200.0	90.28	11.37	12.98	2.95E+06	0.70	0.0147
149	20	0.90	200.0	69.69	10.58	18.16	2.98E+06	0.91	0.0221
150	20	0.90	150.0	69.49	9.61	16.17	3.98E+06	0.91	0.0163

Table A.21: 180° Orientation Calculated Data, Experimental Replicate 2

Run Number	p_n (psig)	m_e/m_l (predicted)	U (fpm)	m_l (g/min)	m_o (lpm)	C (mg/m^3)	p_nH/μ_lU	m_e/m_l (actual)	$CUHD/m_o$
97	50	0.70	93.8	168.22	9.99	9.26	1.49E+07	0.71	0.0056
98	50	0.70	75.0	170.13	9.88	8.77	1.86E+07	0.70	0.0043
99	50	0.70	112.5	170.01	9.89	5.85	1.25E+07	0.70	0.0043
100	40	0.70	105.0	140.40	9.53	5.11	1.07E+07	0.72	0.0036
101	40	0.70	125.0	139.97	9.73	5.66	9.03E+06	0.72	0.0047
102	30	0.70	150.0	116.56	9.65	8.26	5.62E+06	0.71	0.0083
103	30	0.70	112.5	116.28	9.45	5.40	7.47E+06	0.71	0.0041
104	30	0.70	131.8	115.89	9.69	8.56	6.31E+06	0.72	0.0075
105	40	1.30	105.0	76.89	9.00	9.01	1.03E+07	1.32	0.0068
106	40	1.30	125.0	76.88	8.97	6.88	8.68E+06	1.32	0.0062
107	30	1.30	150.0	63.69	9.02	8.51	5.46E+06	1.30	0.0091
108	30	1.30	112.5	63.49	8.60	8.32	7.35E+06	1.31	0.0070
109	30	1.30	131.8	63.59	8.75	9.40	6.31E+06	1.31	0.0091
110	50	1.30	75.0	90.48	9.31	12.18	1.86E+07	1.32	0.0063
111	50	1.30	93.8	91.18	9.15	7.92	1.49E+07	1.31	0.0052
112	50	1.30	112.5	90.49	9.16	4.95	1.22E+07	1.32	0.0039
113	50	0.90	75.0	132.58	9.76	13.66	1.80E+07	0.90	0.0068
114	50	0.90	112.5	133.28	9.80	8.96	1.22E+07	0.90	0.0066
115	50	0.90	93.8	133.75	9.66	10.19	1.49E+07	0.89	0.0064
116	30	0.90	112.5	90.88	9.52	8.91	7.56E+06	0.91	0.0068
117	30	0.90	150.0	91.40	9.83	11.73	5.71E+06	0.91	0.0115
118	30	0.90	131.8	91.78	9.69	13.41	6.56E+06	0.91	0.0118
119	40	0.90	105.0	111.49	9.69	8.46	1.10E+07	0.91	0.0059
120	40	0.90	125.0	111.15	9.69	4.75	9.22E+06	0.91	0.0040
151	20	0.70	150.0	90.08	10.21	12.47	3.58E+06	0.71	0.0118
152	20	0.70	200.0	90.59	11.27	16.53	2.71E+06	0.70	0.0189
153	20	1.30	200.0	49.50	9.31	16.53	2.76E+06	1.28	0.0229
154	20	1.30	150.0	49.60	8.77	14.90	3.72E+06	1.28	0.0164
155	20	0.90	200.0	70.20	10.49	19.65	2.83E+06	0.91	0.0242
156	20	0.90	150.0	70.09	9.74	12.52	3.81E+06	0.91	0.0124

Table A.22: 180° Orientation Calculated Data, Experimental Replicate 3

Run Number	p_n (psig)	m_e/m_l (predicted)	U (fpm)	m_l (g/min)	m_o (lpm)	C (mg/m^3)	p_nH/μ_lU	m_e/m_l (actual)	$CUHD/m_o$
121	30	1.30	131.8	64.39	9.29	9.95	6.25E+06	1.29	0.0091
122	30	1.30	150.0	64.49	9.18	11.08	5.58E+06	1.29	0.0117
123	30	1.30	112.5	64.90	9.05	10.05	7.54E+06	1.28	0.0081
124	50	1.30	75.0	90.77	9.66	12.85	1.93E+07	1.32	0.0064
125	50	1.30	93.8	91.09	9.72	8.03	1.56E+07	1.31	0.0050
126	50	1.30	112.5	91.30	9.73	8.57	1.31E+07	1.31	0.0064
127	40	1.30	105.0	79.28	9.67	8.96	1.14E+07	1.28	0.0063
128	40	1.30	125.0	79.30	9.97	6.35	9.66E+06	1.28	0.0051
129	30	0.90	112.5	93.19	10.00	8.56	7.61E+06	0.89	0.0062
130	30	0.90	131.8	93.81	10.03	9.46	6.62E+06	0.89	0.0080
131	30	0.90	150.0	94.38	10.33	9.31	5.90E+06	0.88	0.0087
132	40	0.90	125.0	111.08	10.12	7.42	9.62E+06	0.91	0.0059
133	40	0.90	105.0	111.26	9.92	6.58	1.15E+07	0.91	0.0045
134	50	0.90	75.0	131.09	10.01	13.76	2.05E+07	0.91	0.0066
135	50	0.90	93.8	130.78	9.96	8.51	1.63E+07	0.91	0.0052
136	50	0.90	112.5	131.07	10.18	5.64	1.36E+07	0.91	0.0040
137	40	0.70	125.0	143.26	10.12	5.63	9.31E+06	0.71	0.0045
138	40	0.70	105.0	144.37	10.04	6.52	1.13E+07	0.70	0.0044
139	30	0.70	150.0	117.48	10.43	9.63	6.01E+06	0.71	0.0089
140	30	0.70	112.5	119.47	10.11	7.46	8.16E+06	0.70	0.0054
141	30	0.70	131.8	119.98	10.04	9.23	7.05E+06	0.69	0.0078
142	50	0.70	112.5	169.47	10.56	5.92	1.40E+07	0.70	0.0041
143	50	0.70	75.0	169.16	10.17	10.81	2.10E+07	0.71	0.0051
144	50	0.70	93.8	168.69	10.32	7.11	1.68E+07	0.71	0.0042
157	20	0.90	150.0	71.20	9.61	13.07	3.30E+06	0.89	0.0132
158	20	0.90	200.0	70.79	10.54	20.89	2.56E+06	0.90	0.0256
159	20	1.30	150.0	49.70	8.77	11.93	3.51E+06	1.28	0.0132
160	20	1.30	200.0	49.99	9.35	16.48	2.67E+06	1.27	0.0227
161	20	0.70	200.0	89.08	11.04	23.31	2.68E+06	0.71	0.0272
162	20	0.70	150.0	88.89	10.08	12.18	3.55E+06	0.72	0.0117

Table A.23: Estimated Bias and Precision Error in Measured Experimental Parameters (percent)

Measured Parameter	Bias Error	Precision Error
C[1]	< 0.1	5.6
U[3]	4.5	2.1
H[3]	< 0.1	0.2
D[3]	0.4	0.8
m_o[2]	< 0.1	0.8
p_n[2]	5.0	2.9
μ_l[2]	1.0	0.5
m_a[3]	2.4	0.7
m_l[2]	< 0.1	0.6

[1]NIOSH Sampling Method
[2]Manufacturer's Literature
[3]Estimate

Appendix B: Chapter 3 Additional Materials

B.1. VOAG Particle Size Generation

A schematic of the Vibrating Orifice Aerosol Generator (VOAG) set-up is in Figure B.1. A corn oil and ethanol solution was pumped through a 20 μm orifice with an HPLC pump, forming a thin filament of liquid. The piezoelectric crystal causes the orifice to oscillate along the axis of the filament. Each oscillation breaks the filament and forms a droplet. A constant liquid flow (Q_l, cm^3/sec) and oscillating frequency (*f*, hertz) produces monodisperse droplets of diameter d_p, calculated from the following equation (Hinds, 1982):

$$d_p\,(\text{cm}) = \left[\frac{6Q_l}{\pi f}\right]^{1/3} \qquad (1)$$

The droplets are close together when initially formed and can coagulate. Therefore, a jet of air is fed to the exit area to disperse the droplet stream. Dilution air carries the droplets through a neutralization chamber which contains a Kr-85 source to reduce droplet charge created during the formation process. The droplets pass through a drying chamber where the ethanol evaporates from the droplets, leaving monodisperse droplets of corn oil of the desired size. The corn oil droplets are then collected and sized.

Corn oil and methylene blue were added to a 250 ml class A volumetric flask, the masses determined by a scale with 0.1 mg sensitivity. Absolute ethanol was added to the flask to produce 250 ml of solution. The HPLC pump was calibrated with a standard class A pipet. The solution compositions and resulting droplet sizes are summarized in Table B.1.

The calibration curve for corn oil droplets collected on Nyebar-treated glass

microscope slides is in Figure B.2 (error bars represent one standard deviation). The spread factor is 1.34 ($r^2 = 0.9999$).

B.2. Relationship Between Spread Factor and Contact Angle

Consider a spherical droplet of size d_p landing on a flat surface, resulting in a flattened droplet of size d_f (see Figure B.3). The volumes of the original and flattened droplets are (McLenaghan and Levy, 1996):

$$V_p = \left(\frac{\pi}{6}\right) d_p^3 \tag{2}$$

$$V_f = \left(\frac{\pi}{6}\right) h \left(\frac{3}{4} d_f^2 + h^2\right) \tag{3}$$

where h is the height of the flattened droplet. From Figure B.3, rewriting h in terms of the contact angle,

$$h = \frac{d_f}{2 \tan\left[(180 - \theta)/2\right]} \tag{4}$$

Substituting for h in equation (3),

$$V_f = \left(\frac{\pi}{6}\right)\left[\frac{d_f}{2 \tan\left[(180 - \theta)/2\right]}\right]\left[\frac{3}{4} d_f^2 + \frac{d_f^2}{4 \tan^2\left[(180 - \theta)/2\right]}\right] \tag{5}$$

Since the volumes of the original and flattened droplets are the same, equating equations (2) and (5) and solving for the spread factor d_f/d_p provides the following relationship between spread factor and contact angle:

$$\frac{d_f}{d_p} = \left[\frac{2\tan[(180-\theta)/2]}{\frac{3}{4} + \left(\frac{1}{4\tan^2[(180-\theta)/2]} \right)} \right]^{1/3} \quad (6)$$

B.3. Corn Oil and Paint Properties

The corn oil density was measured with a 5 ml standard class A pipet and a 0.1 mg sensitivity scale. The average density is 0.908 g/ml (s.d. = 0.003). The corn oil surface tension was found with a Fisher surface tensiomat-21 and averages 32.50 dynes/cm (s.d. = 0.11). The liquid paint density was measured with a volumetric flask and the 0.1 mg sensitivity scale. The average density is 0.808 g/ml (s.d. = 0.006). The paint surface tension, measured on the tensiomat, averages 24.85 dynes/cm (s.d. = 0.10).

B.4. Prediction of Spray MMD with Kim and Marshall Equation

The Kim and Marshall equation for the 1/4J nozzle is:

$$\text{MMD}\ (\mu\text{m}) = 249\left[\frac{\sigma_l^{0.41}\mu_l^{0.32}}{\left(v_{rel}^2\rho_a\right)^{0.57} A_a^{0.36}\rho_l^{0.16}} \right] + 1260\left[\left(\frac{\mu_l^{\,2}}{\rho_l\sigma_l} \right)^{0.17} \left(\frac{1}{v_{rel}^{0.54}} \right) \left(\frac{m_a}{m_l} \right)^{-1} \right] \quad (7)$$

where

σ_l = liquid surface tension, dynes/cm

μ_l = liquid viscosity, centipoise

ρ_l = liquid density, lb/ft^3

ρ_a = air density, lb/ft^3

= m_a/v_aA_a

v_{rel} = v_a - v_l, ft/sec

v_a = air jet velocity, ft/sec

= $(\gamma RT)^{1/2}$ = $49.02[T(°R)]^{1/2}$ for air at choked flow (White, 1994)

v_l = liquid velocity, ft/sec

= $m_l/\rho_l A_l$

A_a = air nozzle area, in^2 (= 0.00346 in^2 for 1/4J nozzle)

A_l = liquid nozzle area, in^2 (= 0.00283 in^2 for 1/4J nozzle)

m_a = air mass flow, lb/min

m_l = liquid mass flow, lb/min

The calculated MMDs for each wind tunnel run are in Tables B.2-3.

B.5. Wind Tunnel Sampling Results

Parameters of the droplet size distributions for the 36 sampling runs in the wind tunnel are summarized in Tables B.4-5.[1] The calculated parameters are the geometric mean diameter (GMD), geometric standard deviation (GSD), count median diameter (CMD), mass median diameter (MMD), and mass median aerodynamic diameter (MMAD). Droplet size mass frequency distributions for the runs are graphed in Figures B.4-12. Each curve represents the average for the two experimental replicates. Error bars represent high and low values.

B.6. Thermoanemometer Calibration

Air velocity measurements were done in the paint spray booth with an Alnor® model 8565 thermoanemometer. This device is a hand-held, battery operated instrument capable of measuring velocities from 20 to 3000 fpm. The velocity sensor is a fine nickel wire located in the probe tip and heated with a constant current flow. Air passing over the

[1]To obtain the raw data, contact Dr. Michael Flynn, Department of Environmental Sciences and Engineering, University of North Carolina, Chapel Hill, NC 27599.

sensor cools it and changes its resistance. The thermoanemometer was calibrated according to manufacturer's instructions in the calibration wind tunnel described in Section A.1. The results are shown in Figure B.13. A regression of the wind tunnel freestream velocity to the instrument reading found the following best-fit equation:

$$\text{Velocity (fpm)} = -10.43 + 1.069(\text{Reading}_{\text{instrument}}),\ r^2 = 0.9991 \qquad (8)$$

B.7. Paint Spray Booth Velocity Profiles

The paint spray booth is located in the basement of Rosenau Hall, University of North Carolina at Chapel Hill. The entrance was modified with a sheet metal flange to reduce flow separation as air entered the booth. The air velocity is adjustable by varying the speed of the fan. The spray booth freestream velocity was measured with the calibrated thermoanemometer prior to each sampling run. Sixteen equi-distant measurements of the normal velocity component were taken on a cross-sectional plane located 80 inches from the spray booth entrance. The results are shown in Table B.6. The average freestream velocity was calculated as the average of the 16 measurements.

B.8. Paint Spray Gun Calibrations

A compressor provided air for the spray guns. The air passed through an air filter and dryer to remove condensables. A pressure regulator was used to adjust the gun inlet pressure and nozzle pressure (p_n). The spray gun air mass flow (m_a) was calibrated with a primary standard spirometer and calculated air densities. The calibration curve for the conventional spray gun is in Figure B.14, with the following best-fit equation (error bars represent one standard deviation):

$$m_a\ (\text{lb/min}) = 0.210 + 0.013(p_n),\ r^2 = 0.9999 \qquad (9)$$

The HVLP gun delivered an average m_a of 1.453 lb/min (s.d. = 0.009).

The air-to-liquid mass flow ratios (m_a/m_l), overspray generation rates (m_o), and transfer efficiencies measured for the two spray guns are summarized in Table B.7. A flat plate was sprayed for approximately two minutes. Weighing the paint container before and after spraying with a 1g sensitivity scale determined the paint mass flow (m_l). Paint that transferred to the plate drained into a trough which was also weighed before and after spraying. The overspray generation rate is the difference between m_l and the paint transfer rate to the plate.

B.9. Paint Spray Booth Sampling Results

Parameters for the droplet size distributions measured in the paint spray booth are summarized in Table B.8.[2] Calculated mass median diameters (MMD) assume constant droplet density across the size range; actual droplet densities probably varied due to evaporation, smaller droplets most likely having a higher solids percentage than larger droplets. The droplet count distributions on a log-probability scale are graphed in Figures B.15-22. Each curve represents one of the three experimental replicates.

[2]Contact Dr. Flynn for the raw data.

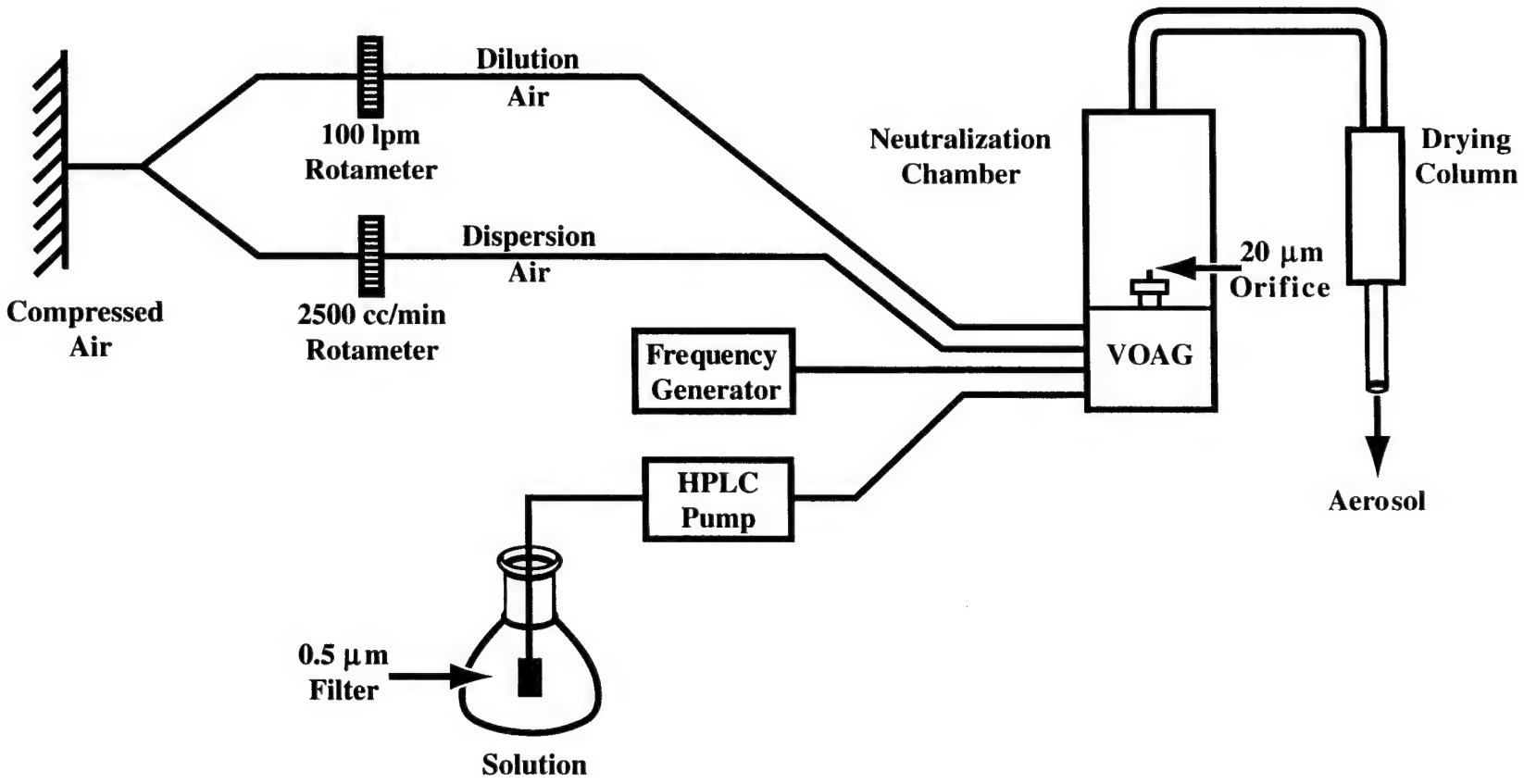

Figure B.1: Schematic of Vibrating Orifice Aerosol Generator (VOAG)

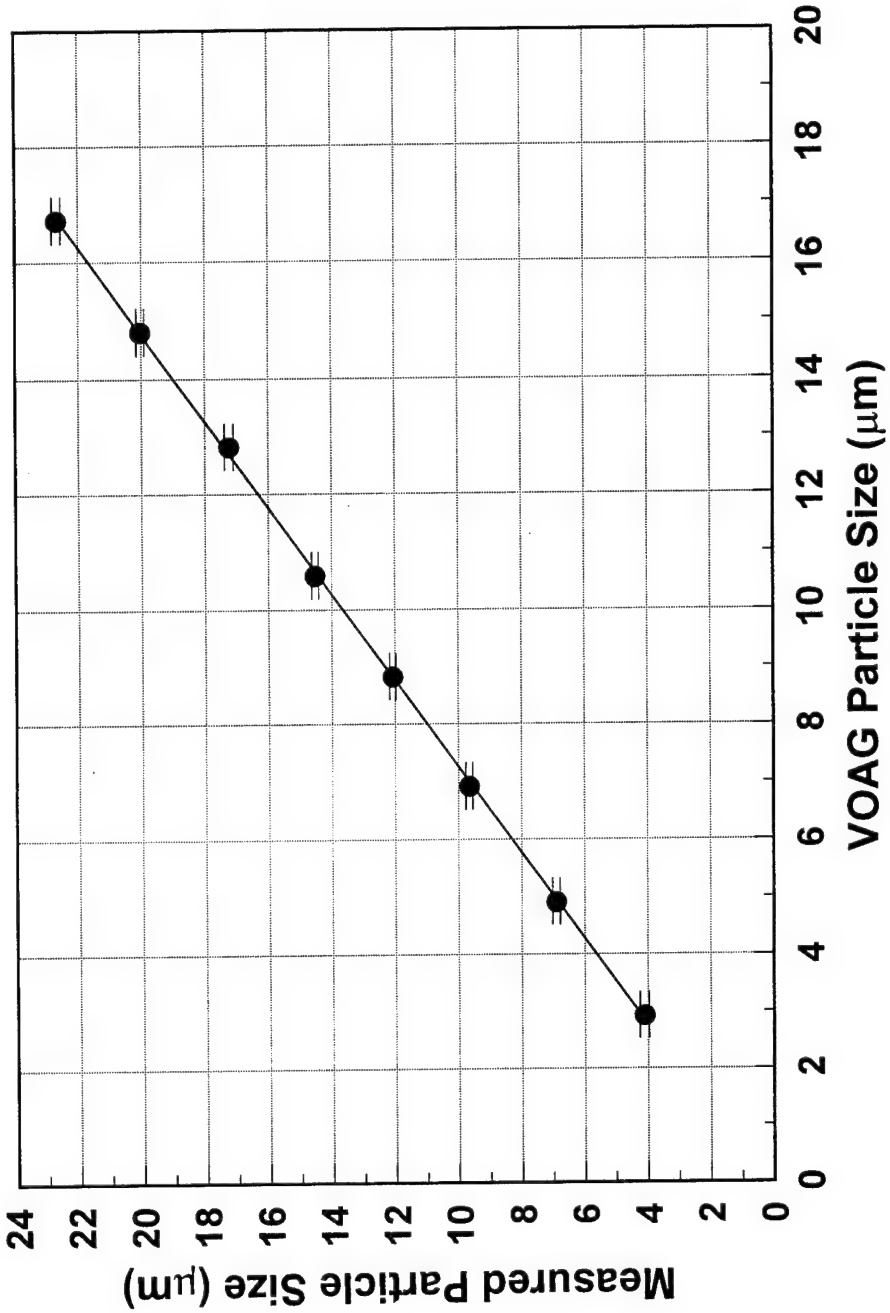

Figure B.2: Relation between flattened diameter and true droplet diameter, corn oil collected on treated microscope slides.

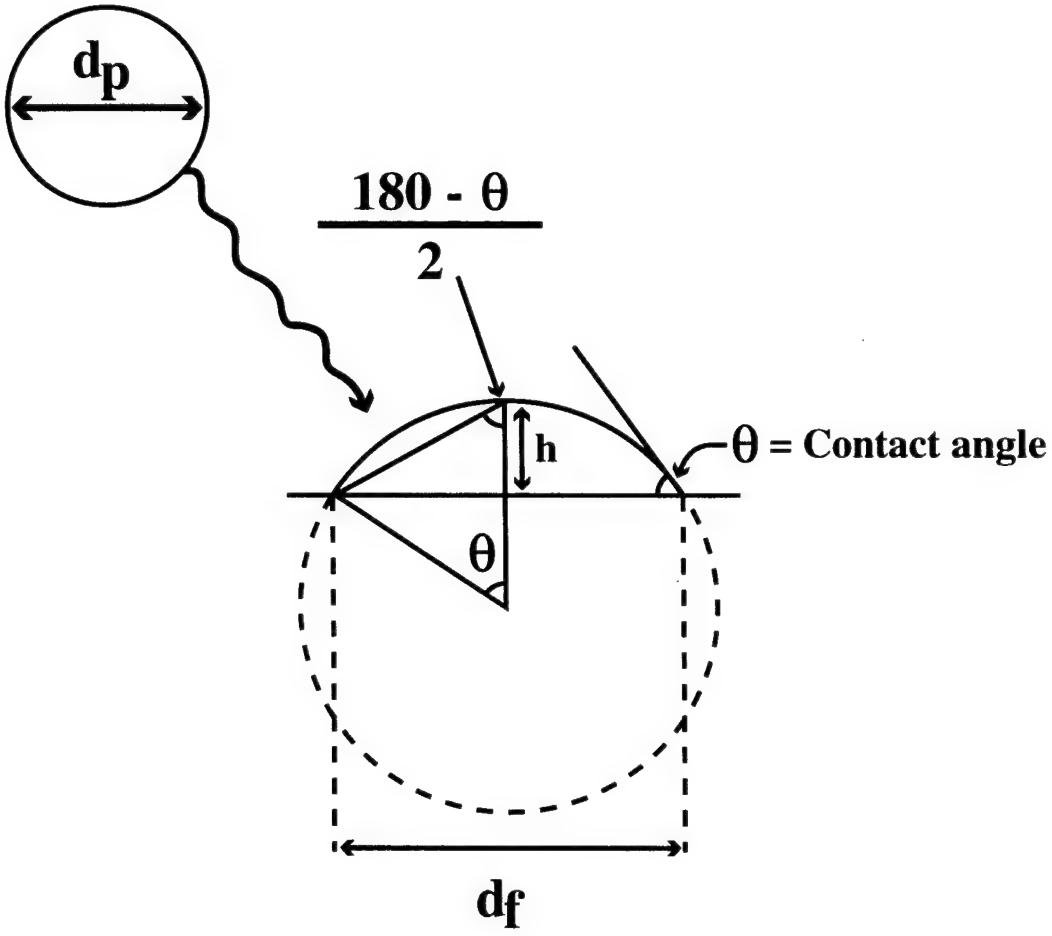

Figure B.3: Geometry of a liquid droplet landing on a flat surface

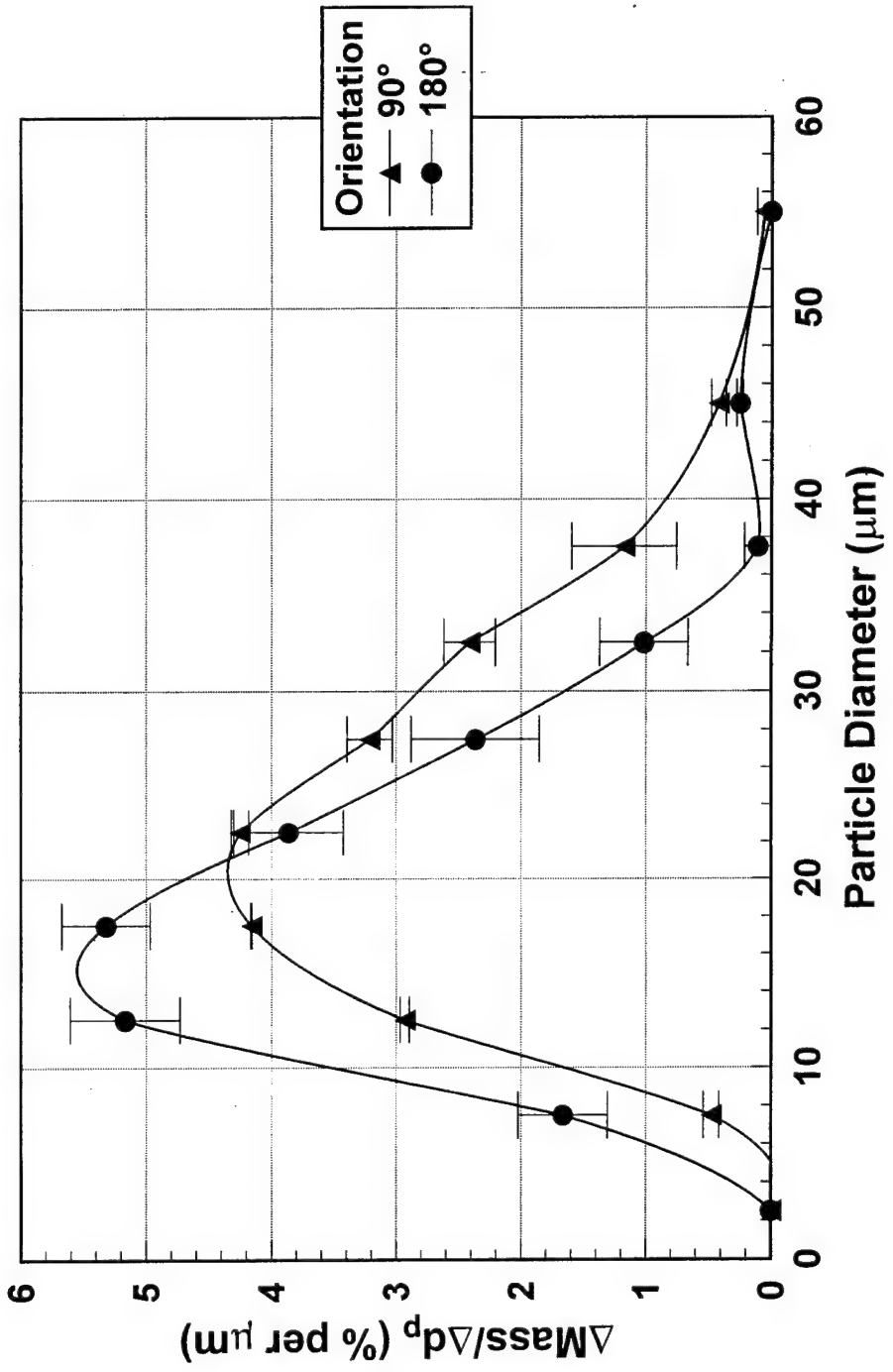

Figure B.4: Wind tunnel droplet sizing data, p_n = 30 psig, m_a/m_l = 0.70.

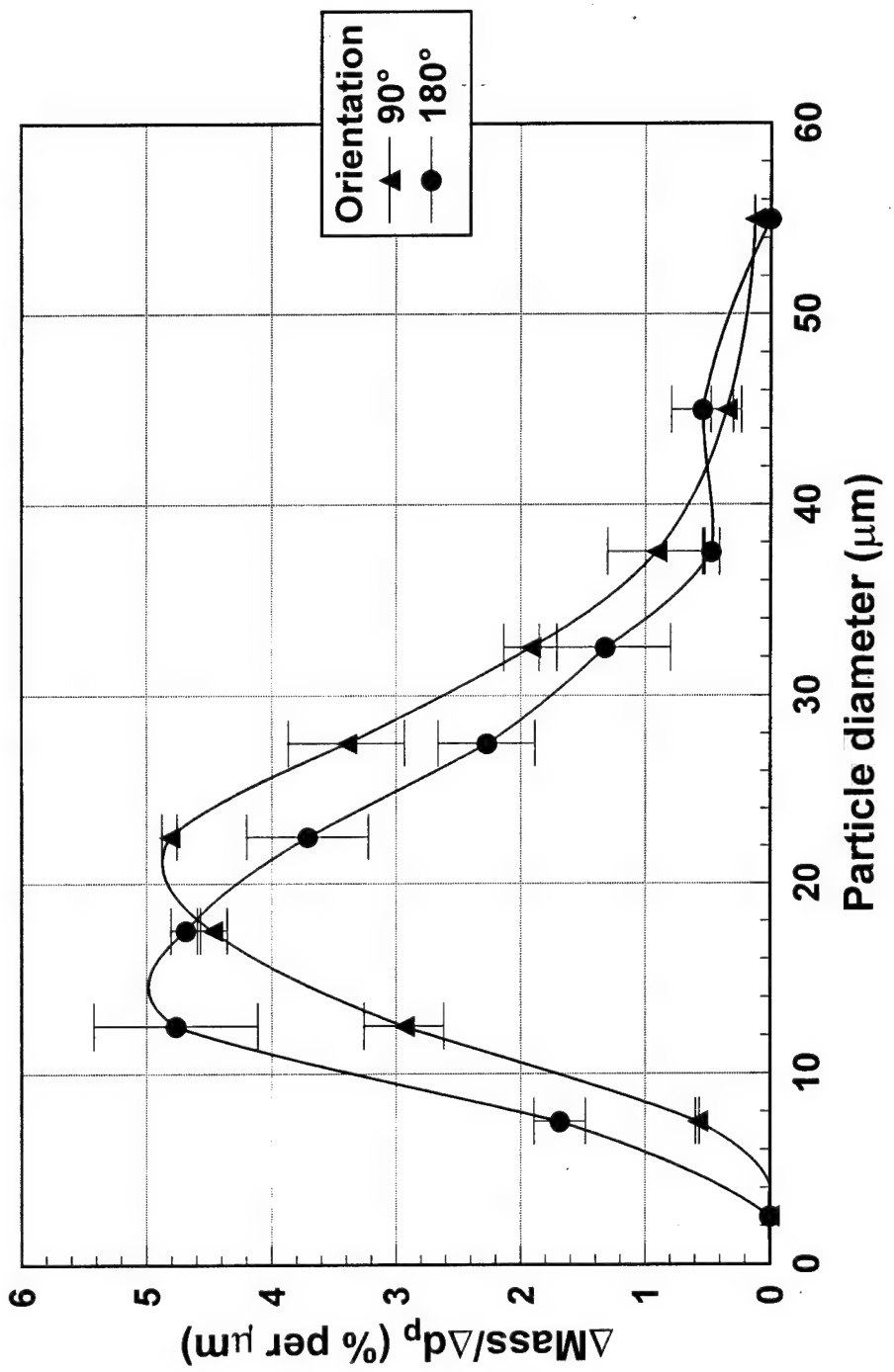

Figure B.5: Wind tunnel droplet sizing data, p_n = 30 psig, m_a/m_l = 0.90.

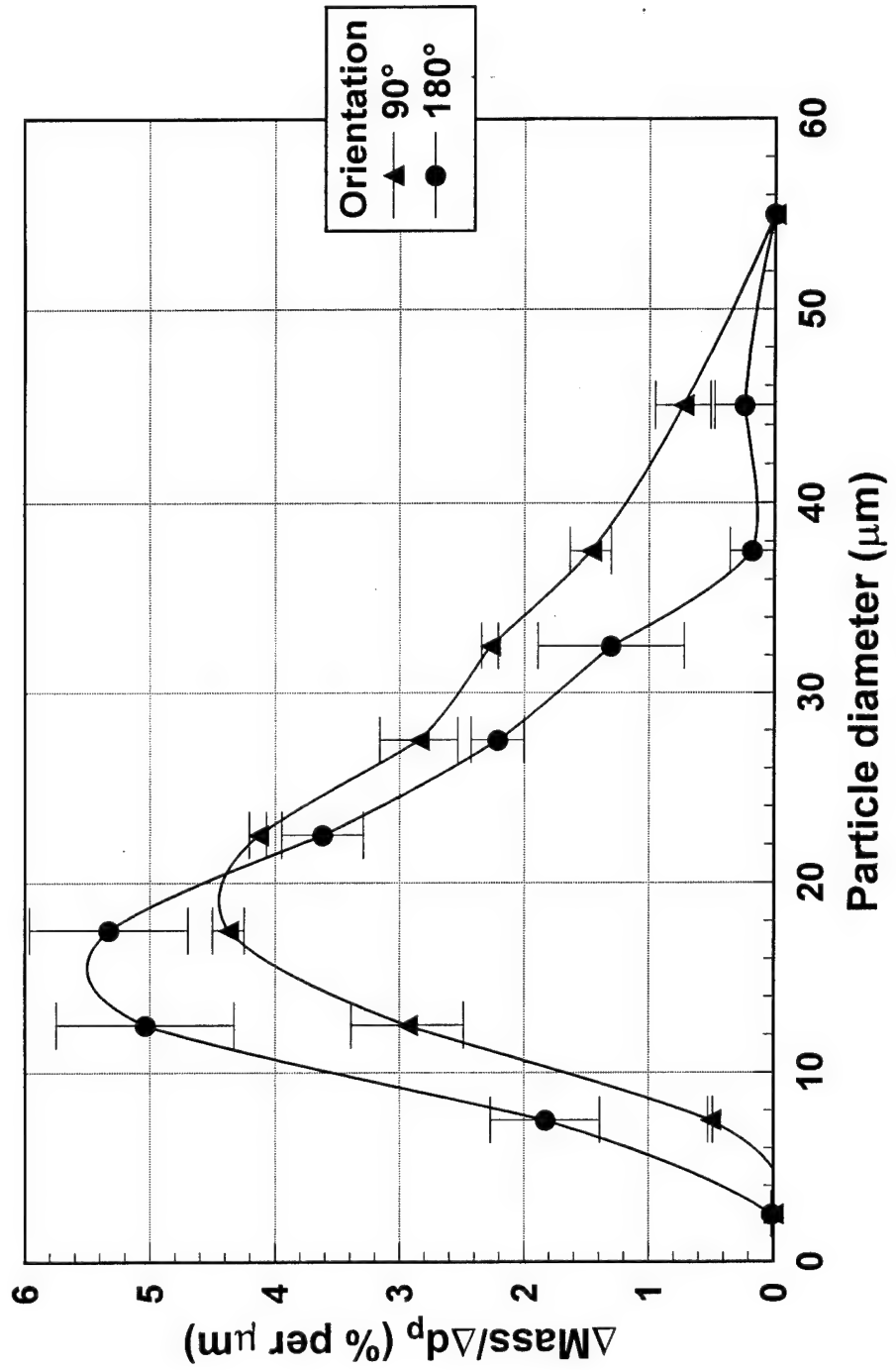

Figure B.6: Wind tunnel droplet sizing data, p_n = 30 psig, m_a/m_l = 1.30.

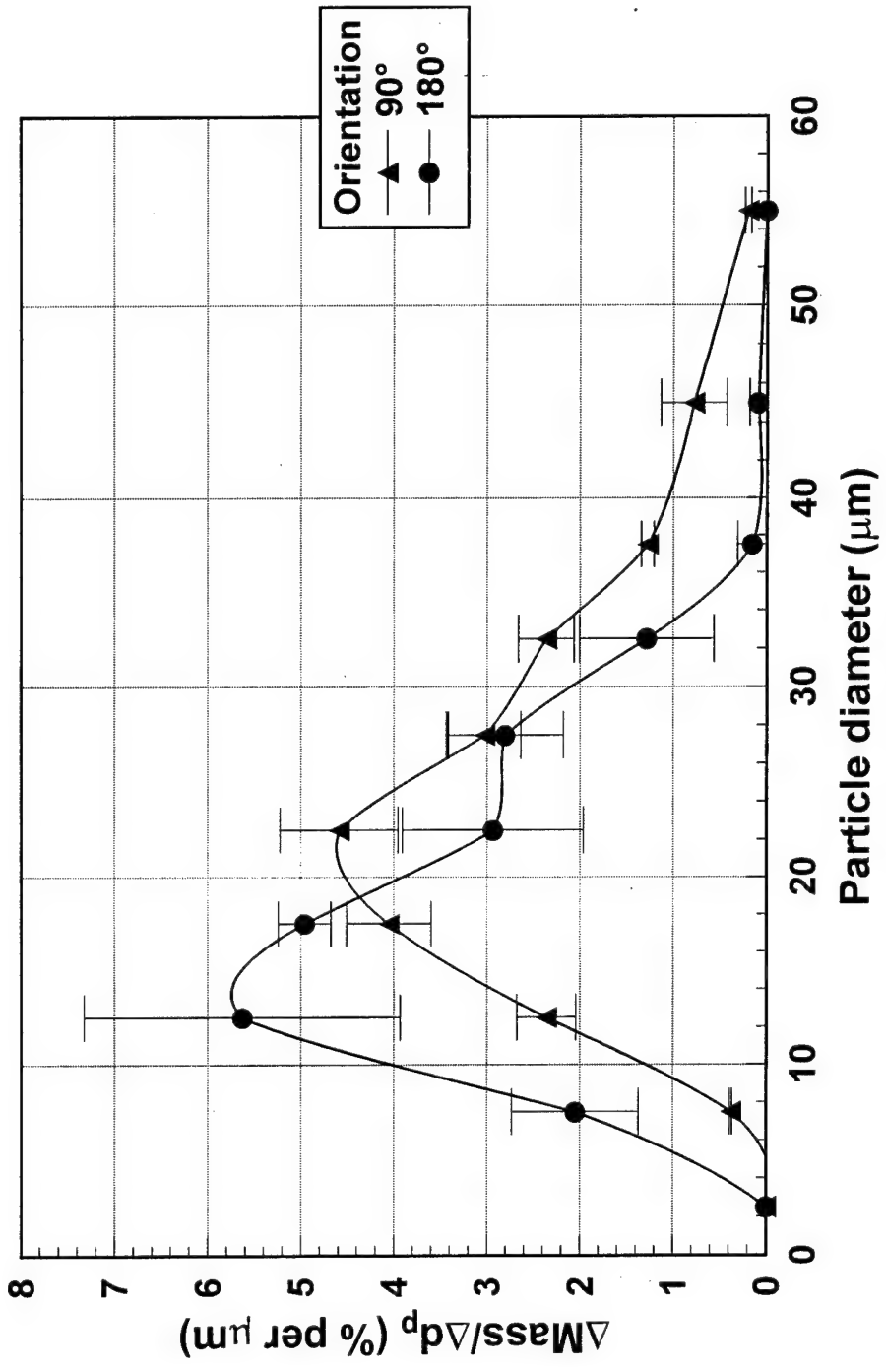

Figure B.7: Wind tunnel droplet sizing data, p_n = 40 psig, m_a/m_l = 0.70.

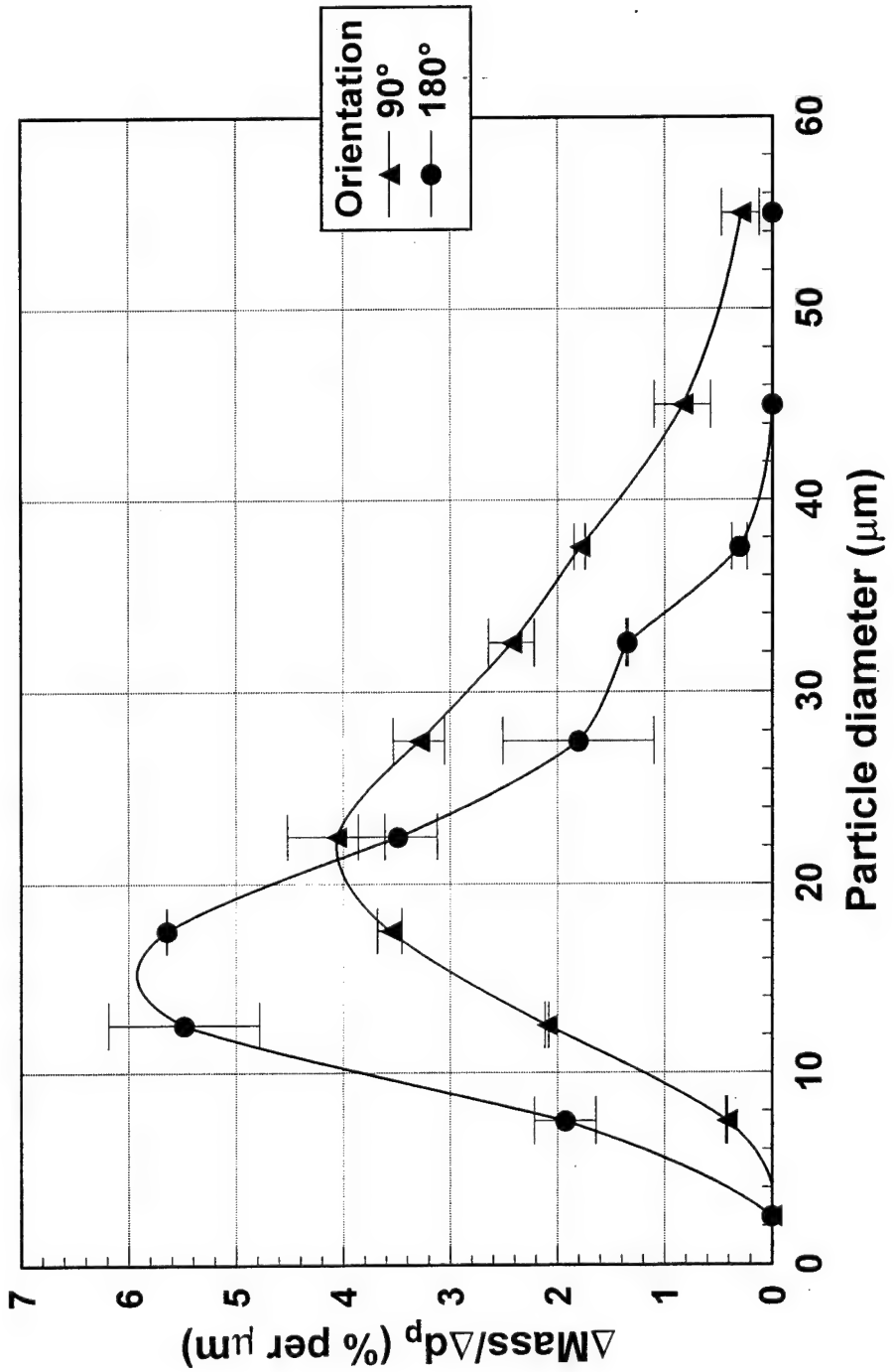

Figure B.8: Wind tunnel droplet sizing data, p_n = 40 psig, m_a/m_l = 0.90.

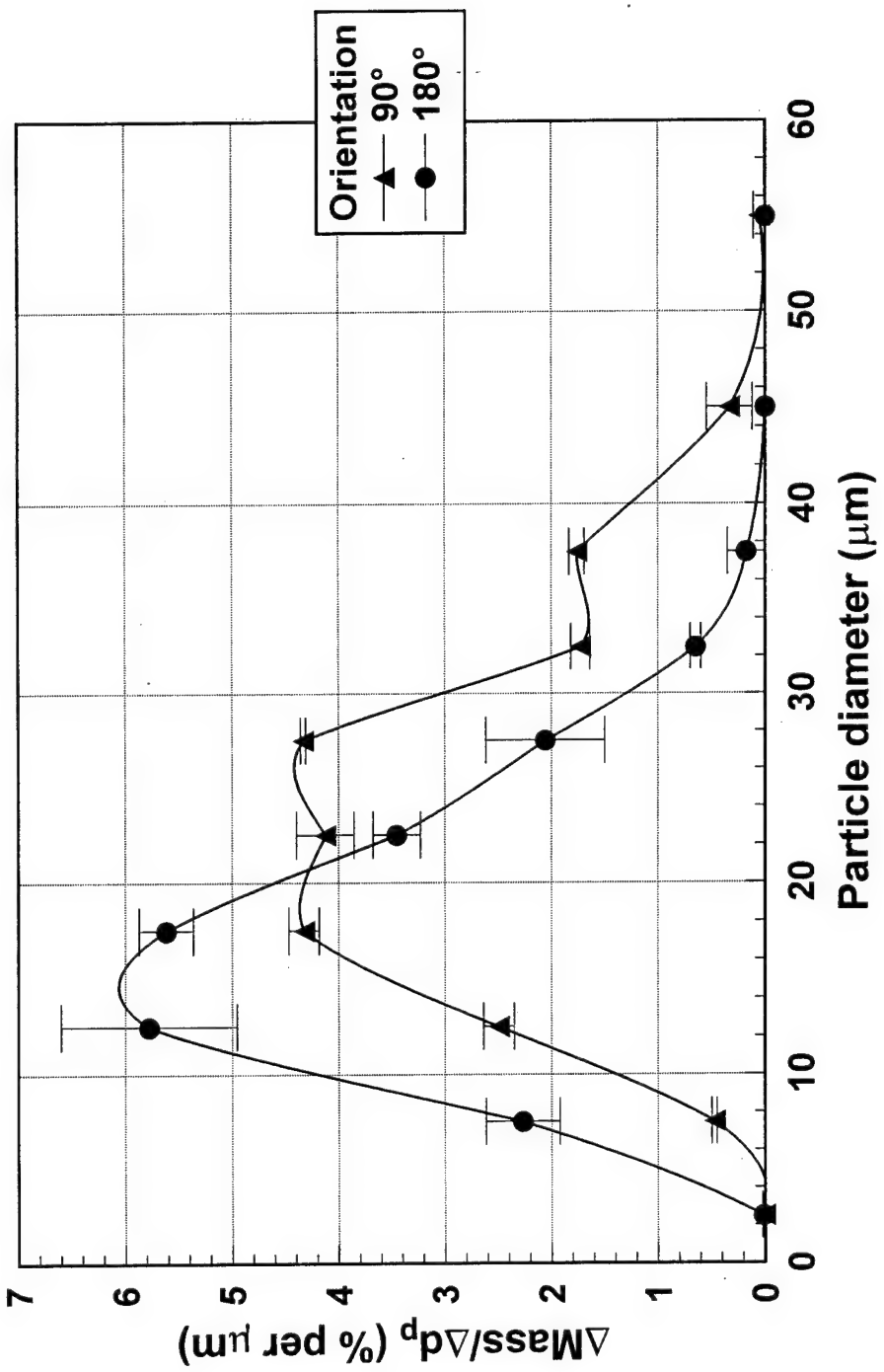

Figure B.9: Wind tunnel droplet sizing data, p_n = 40 psig, m_a/m_l = 1.30.

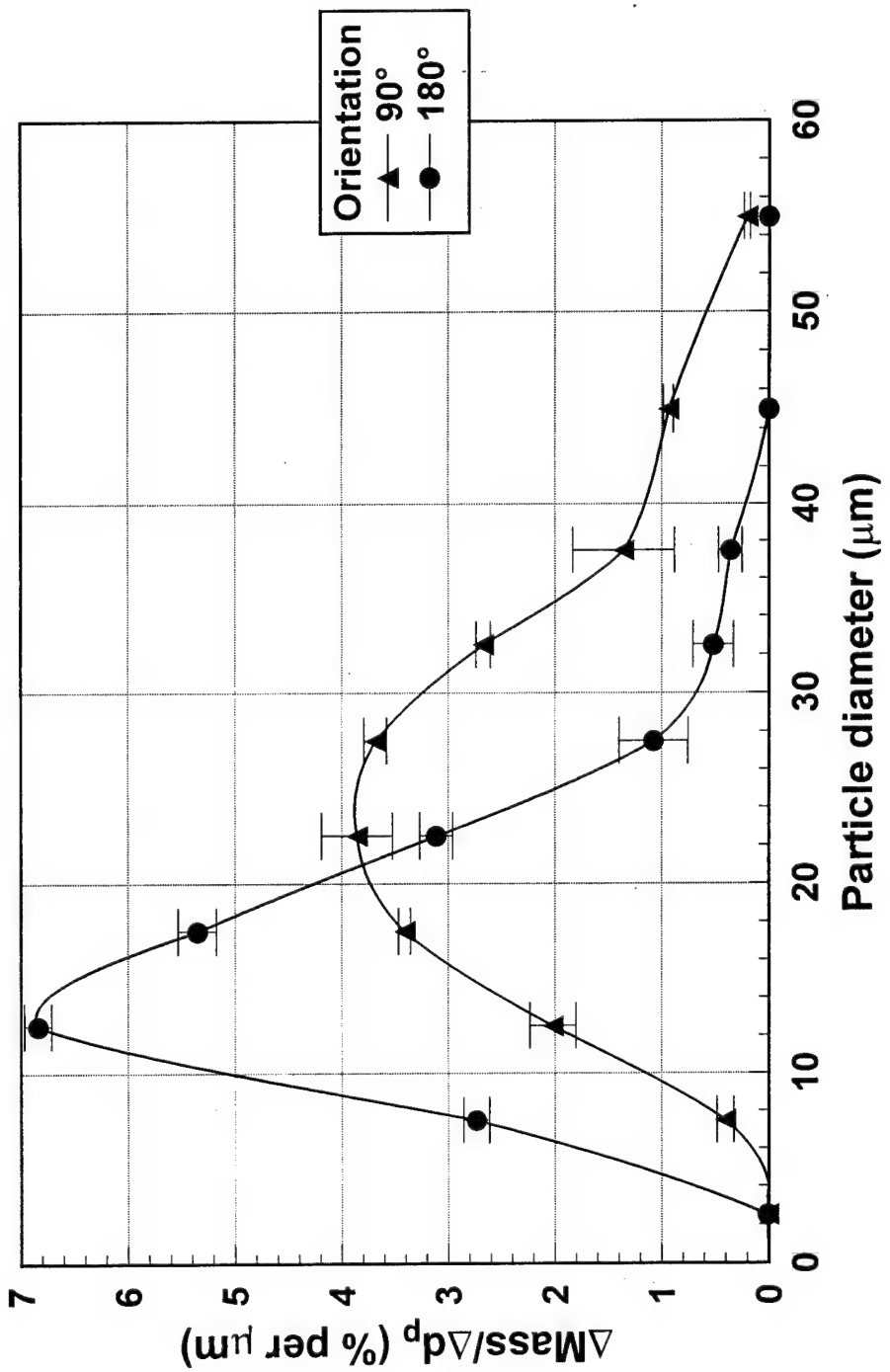

Figure B.10: Wind tunnel droplet sizing data, p_n = 50 psig, m_a/m_l = 0.70.

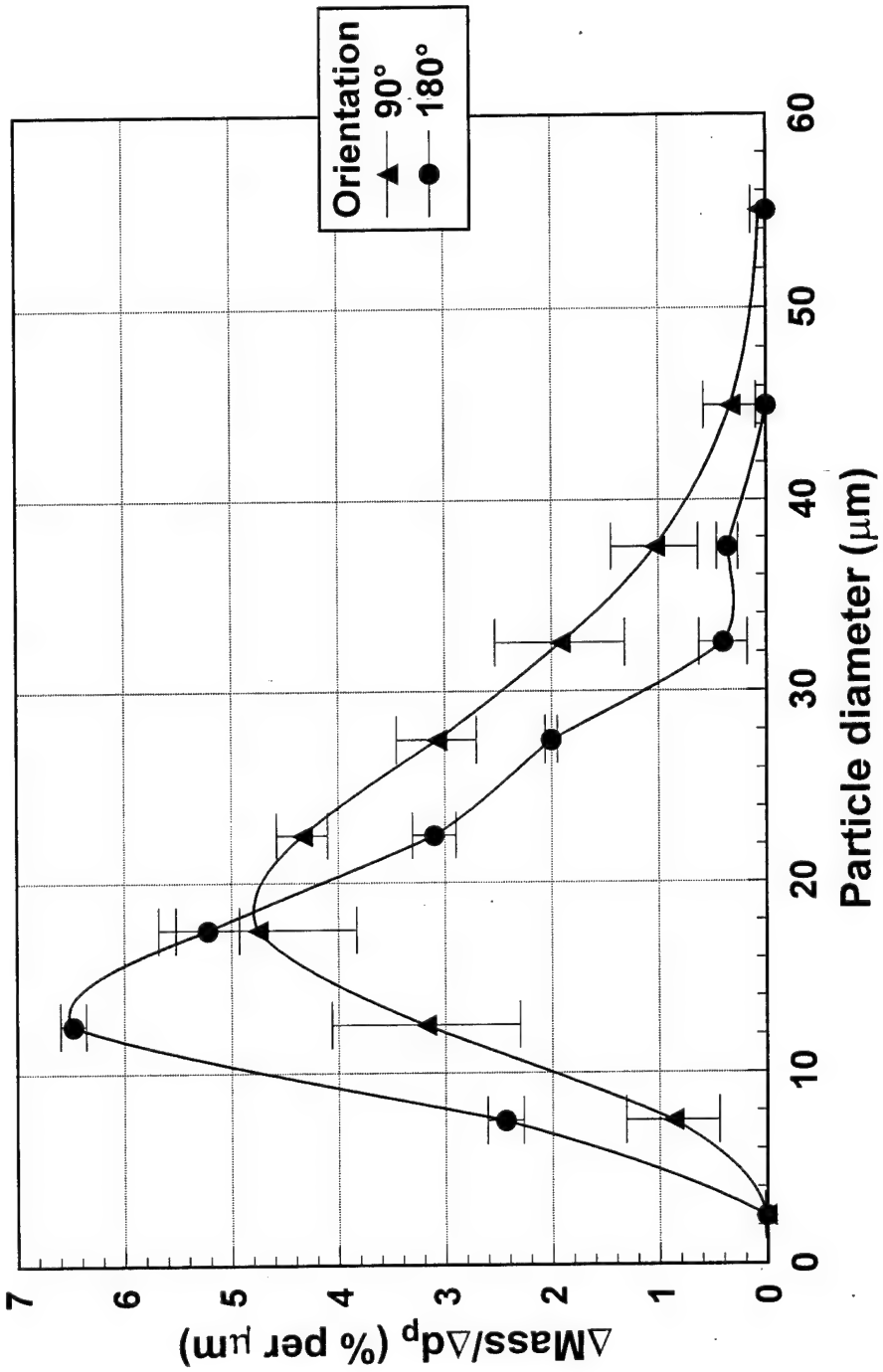

Figure B.11: Wind tunnel droplet sizing data, p_n = 50 psig, m_a/m_l = 0.90.

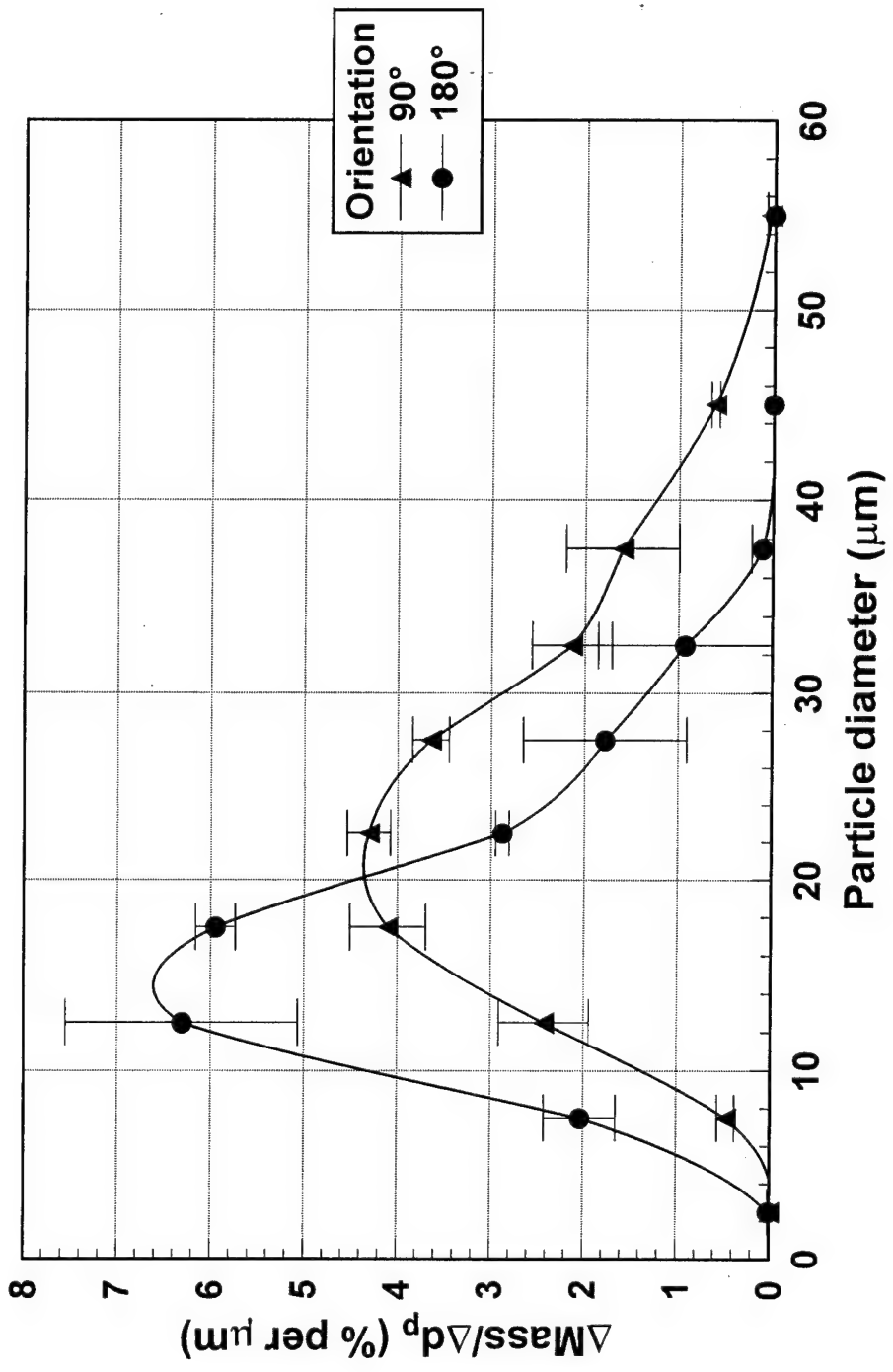

Figure B.12: Wind tunnel droplet sizing data, p_n = 50 psig, m_a/m_l = 1.30.

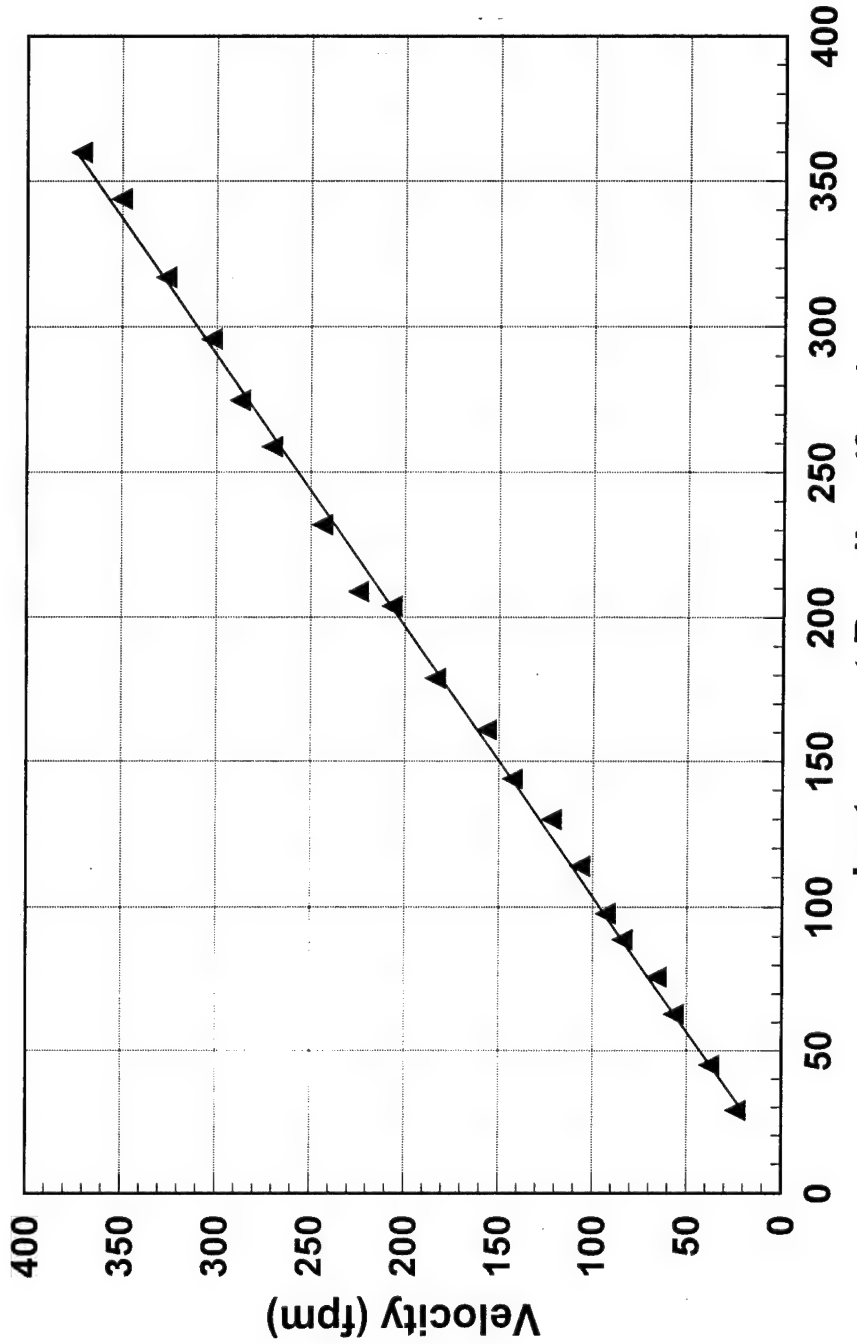

Figure B.13: Thermoanemometer calibration.

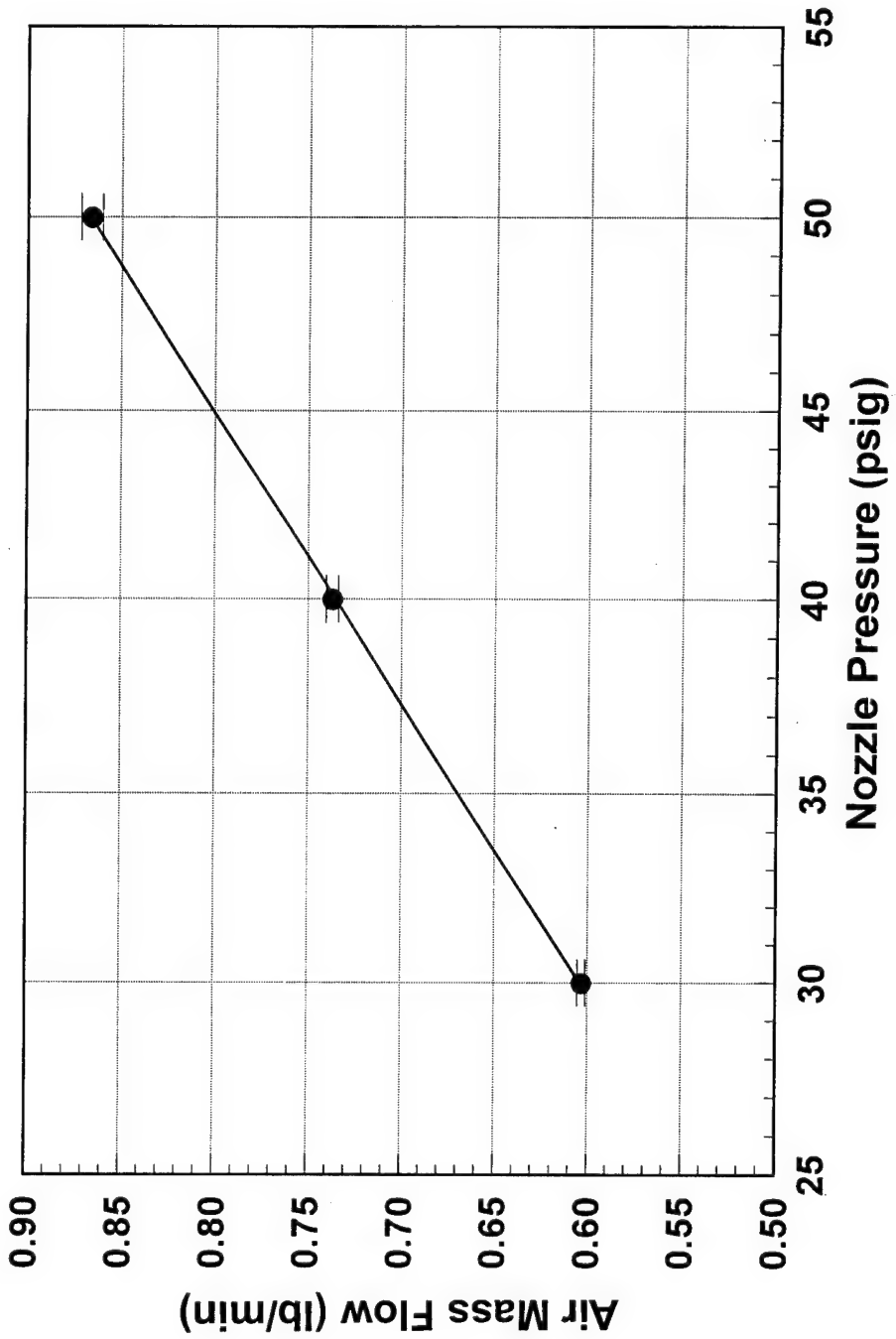

Figure B.14: Conventional spray gun air flow calibration.

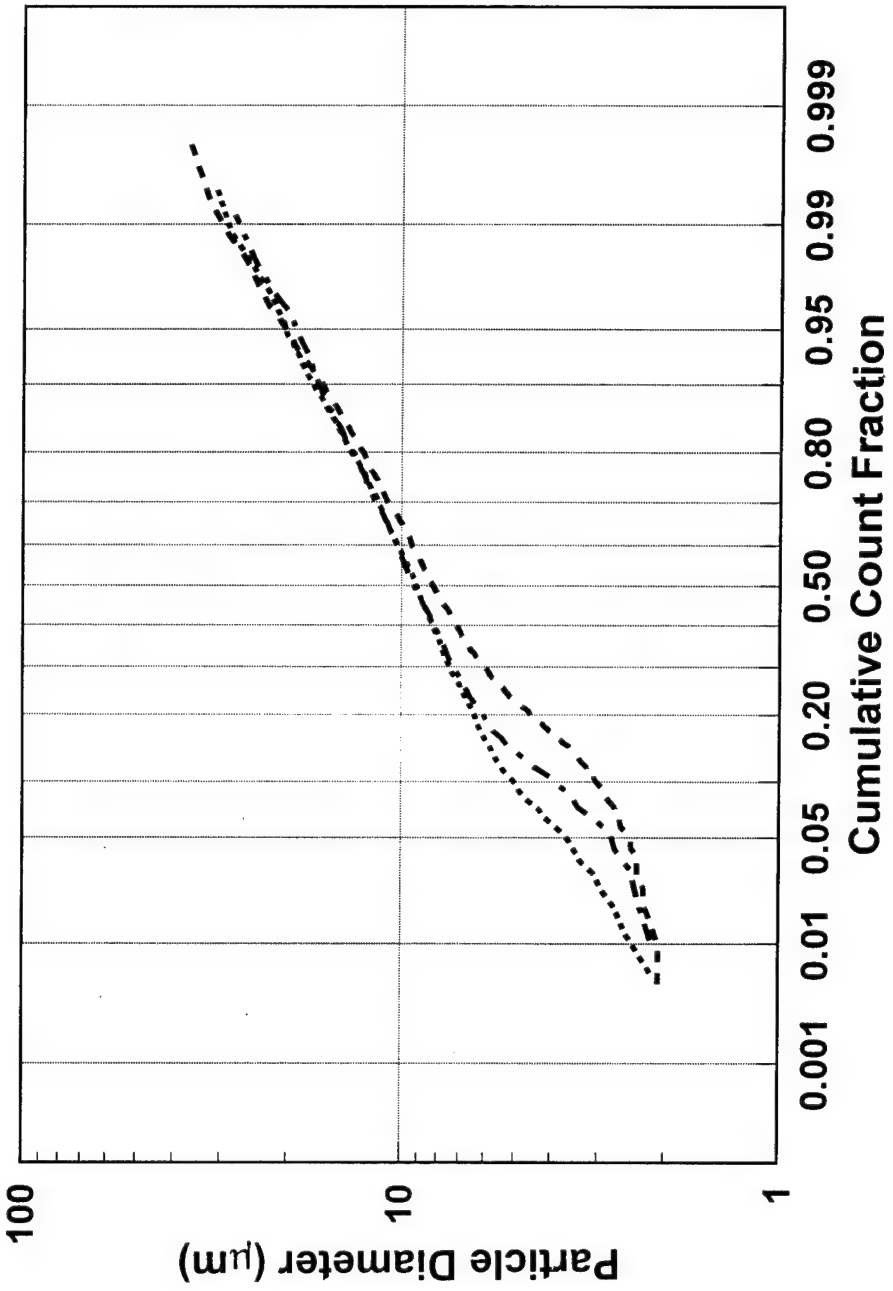

Figure B.15: Spray booth droplet sizing data, p_n = 30 psig, orientation = 90°.

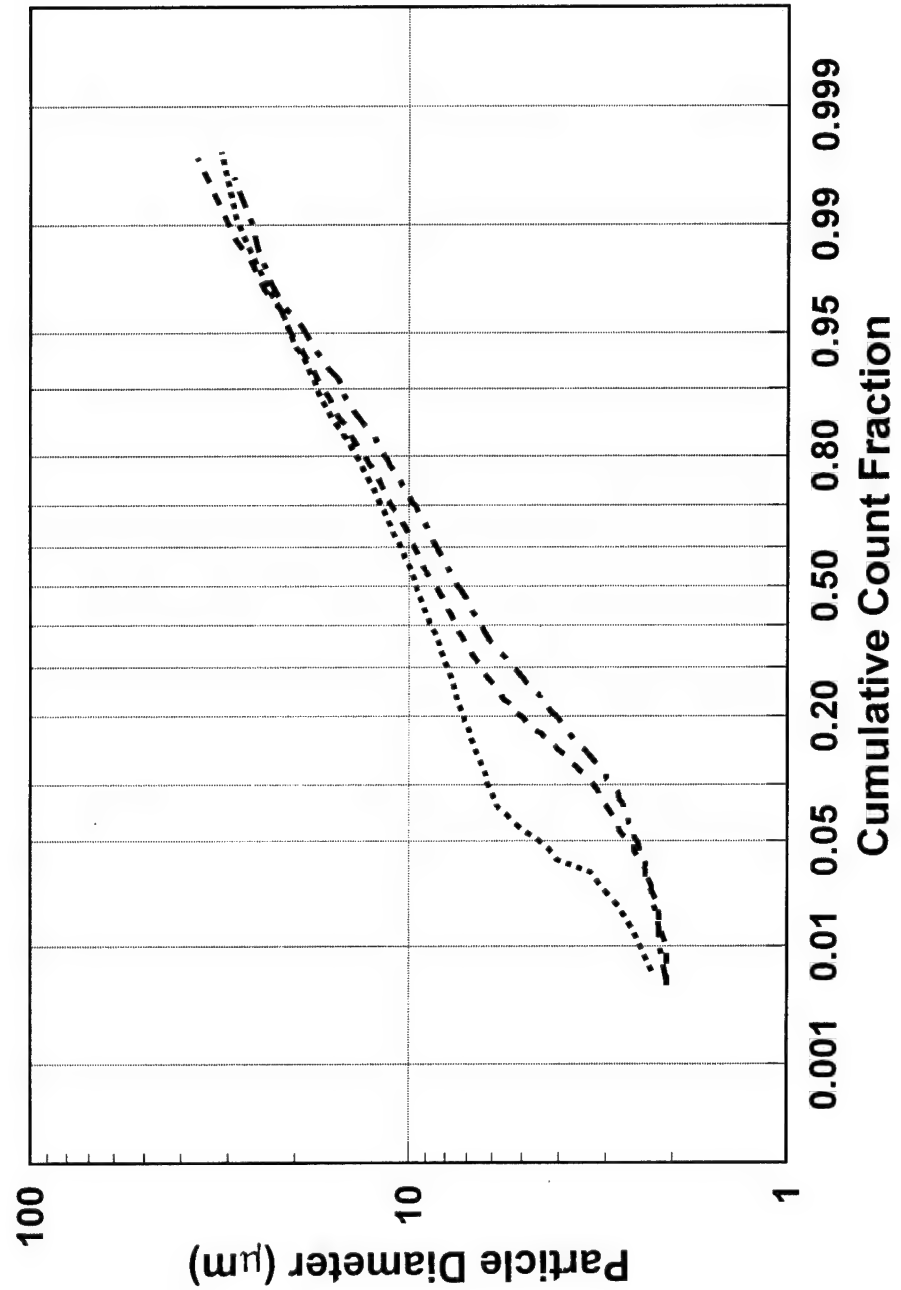

Figure B.16: Spray booth droplet sizing data, p_n = 40 psig, orientation = 90°.

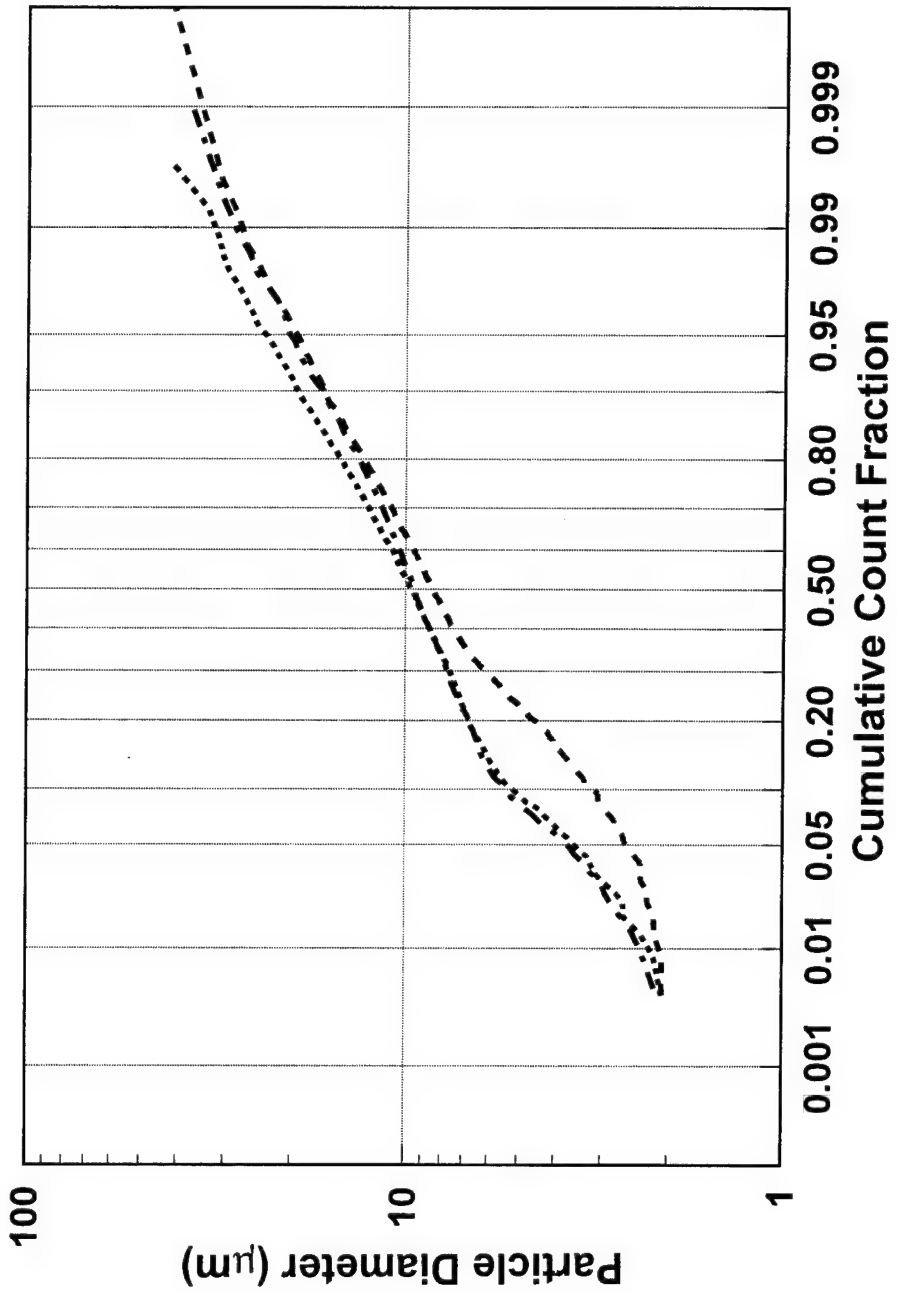

Figure B.17: Spray booth droplet sizing data, p_n = 50 psig, orientation = 90°.

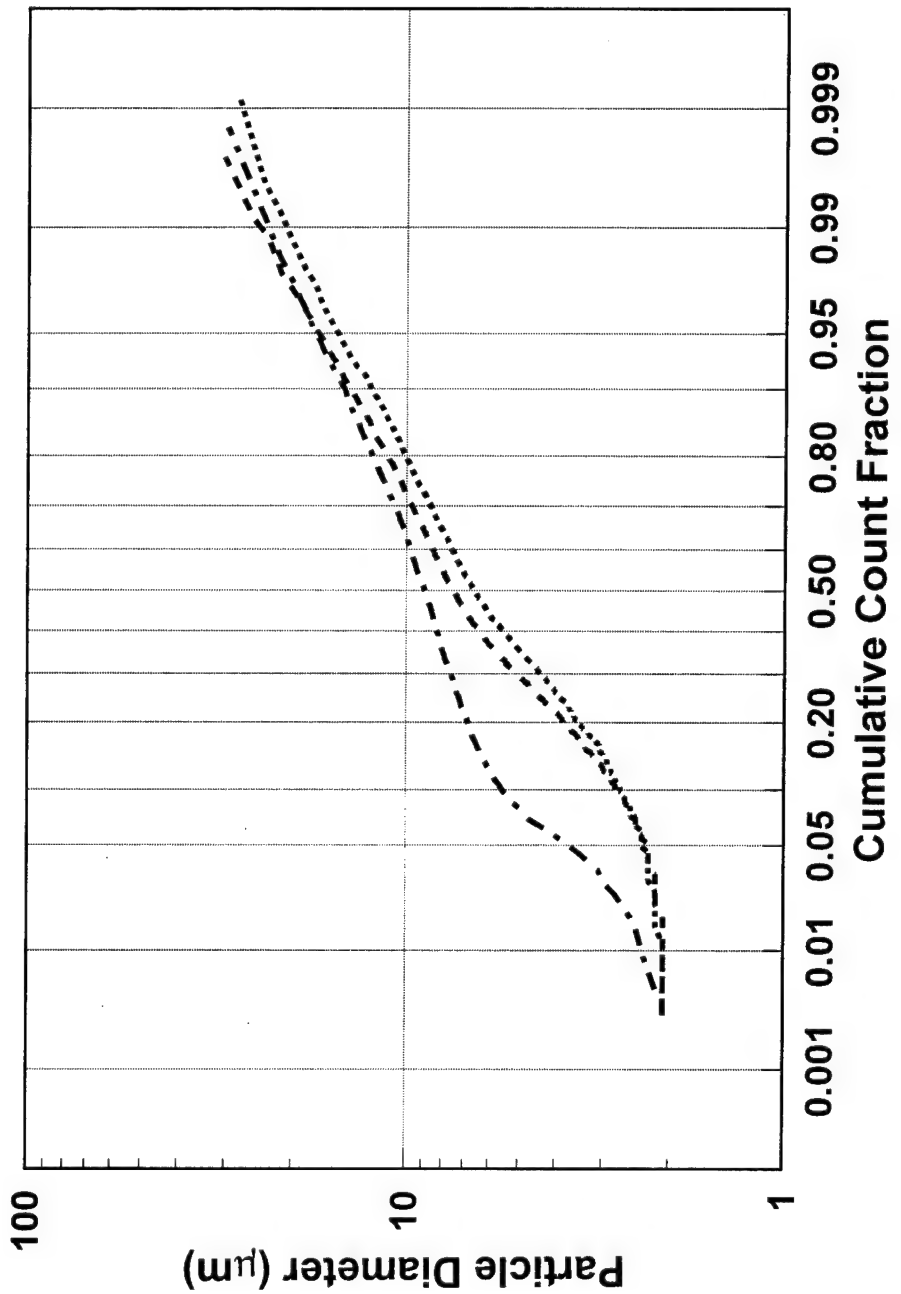

Figure B.18: Spray booth droplet sizing data, p_n = 30 psig, orientation = 180°.

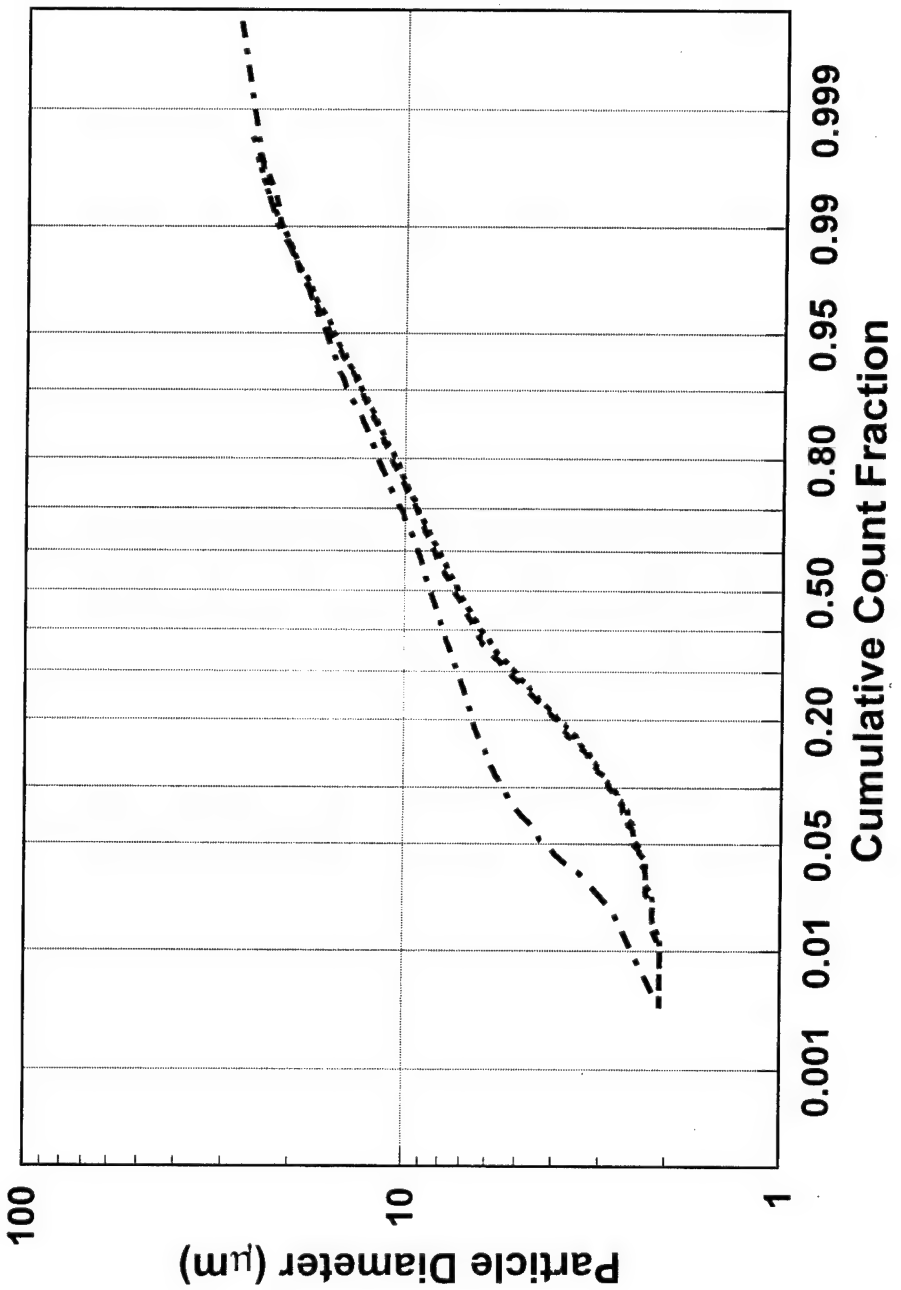

Figure B.19: Spray booth droplet sizing data, p_n = 40 psig, orientation = 180°.

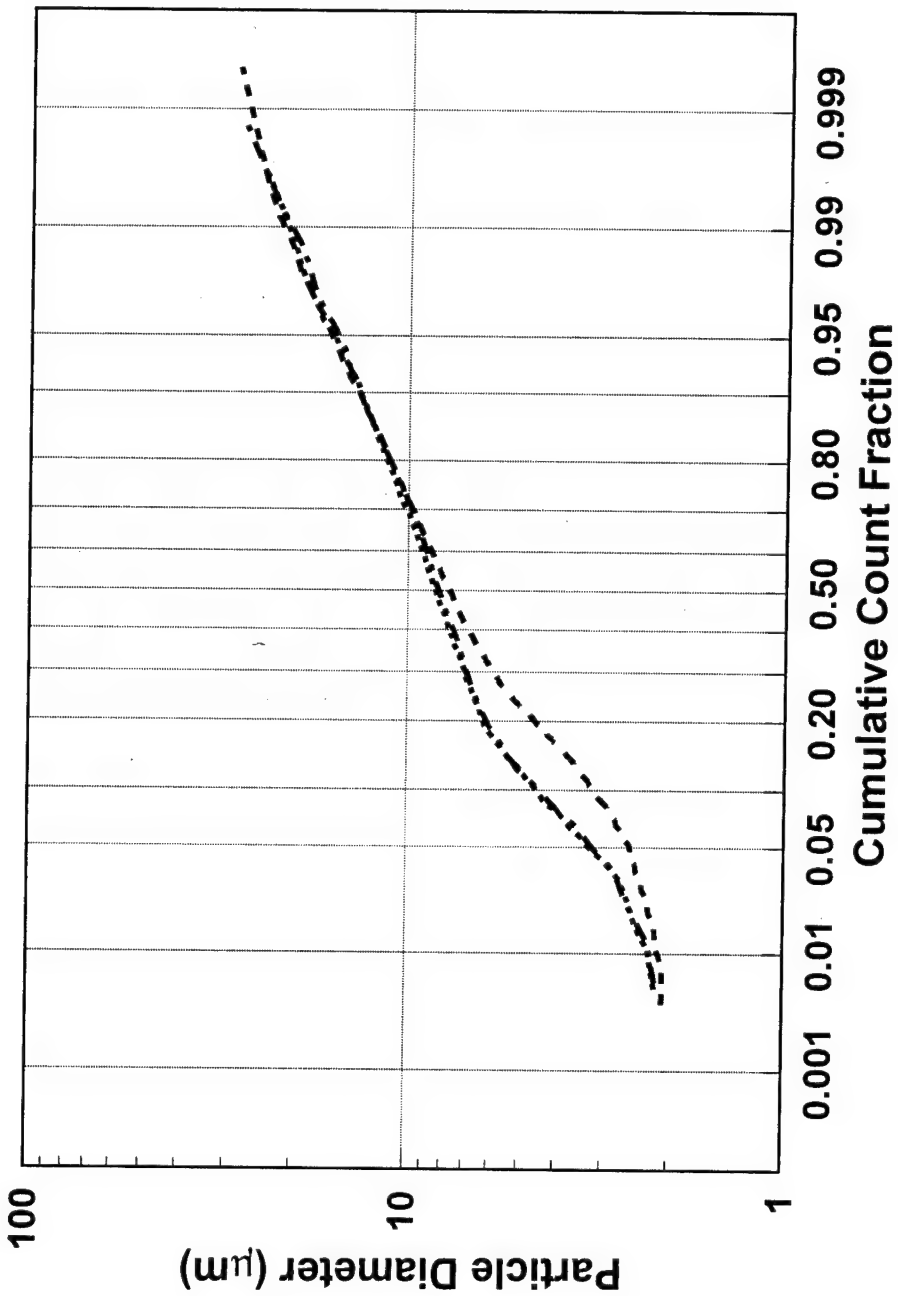

Figure B.20: Spray booth droplet sizing data, p_n = 50 psig, orientation = 180°.

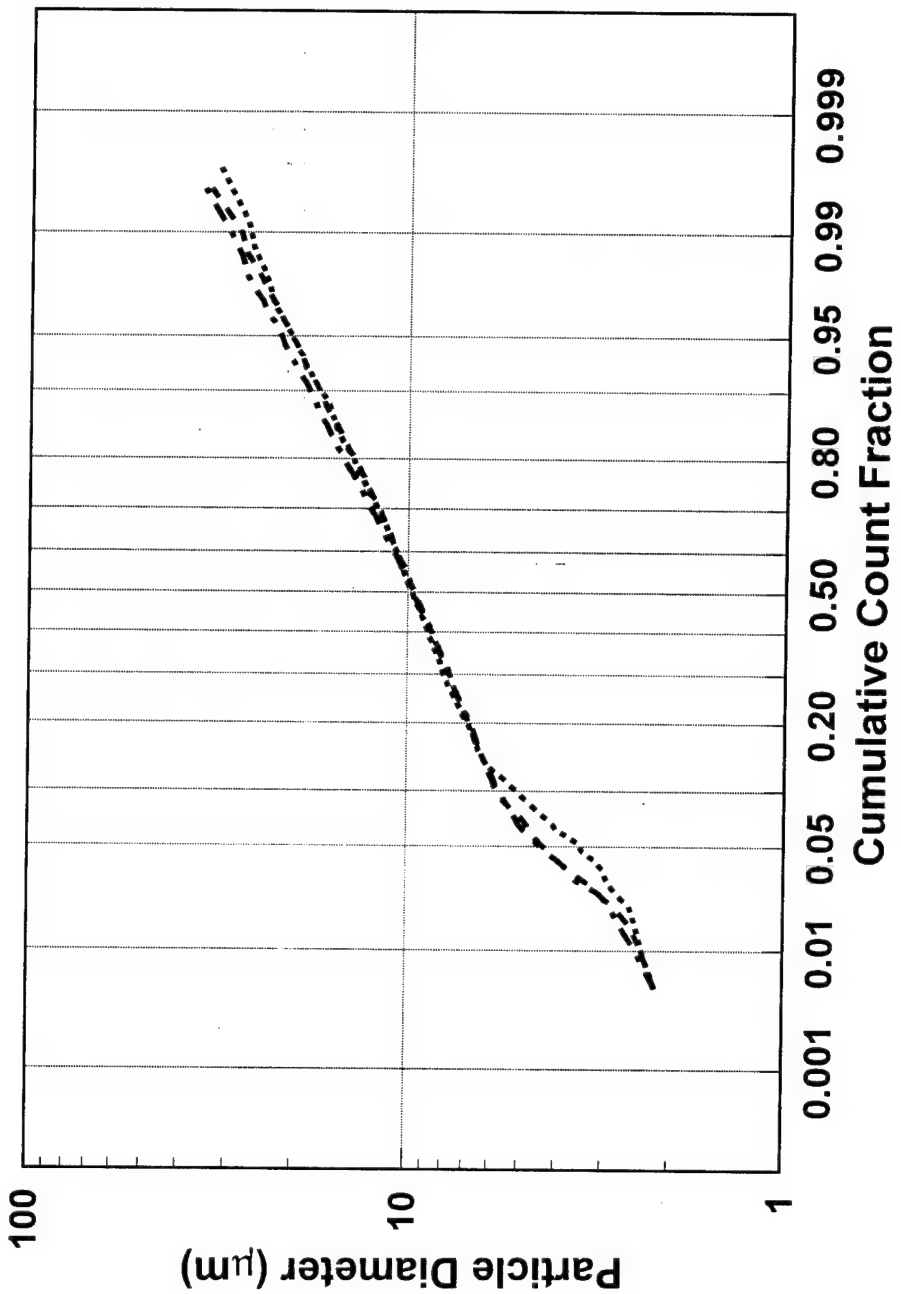

Figure B.21: Spray booth droplet sizing data, p_n = 10 psig, orientation = 90°.

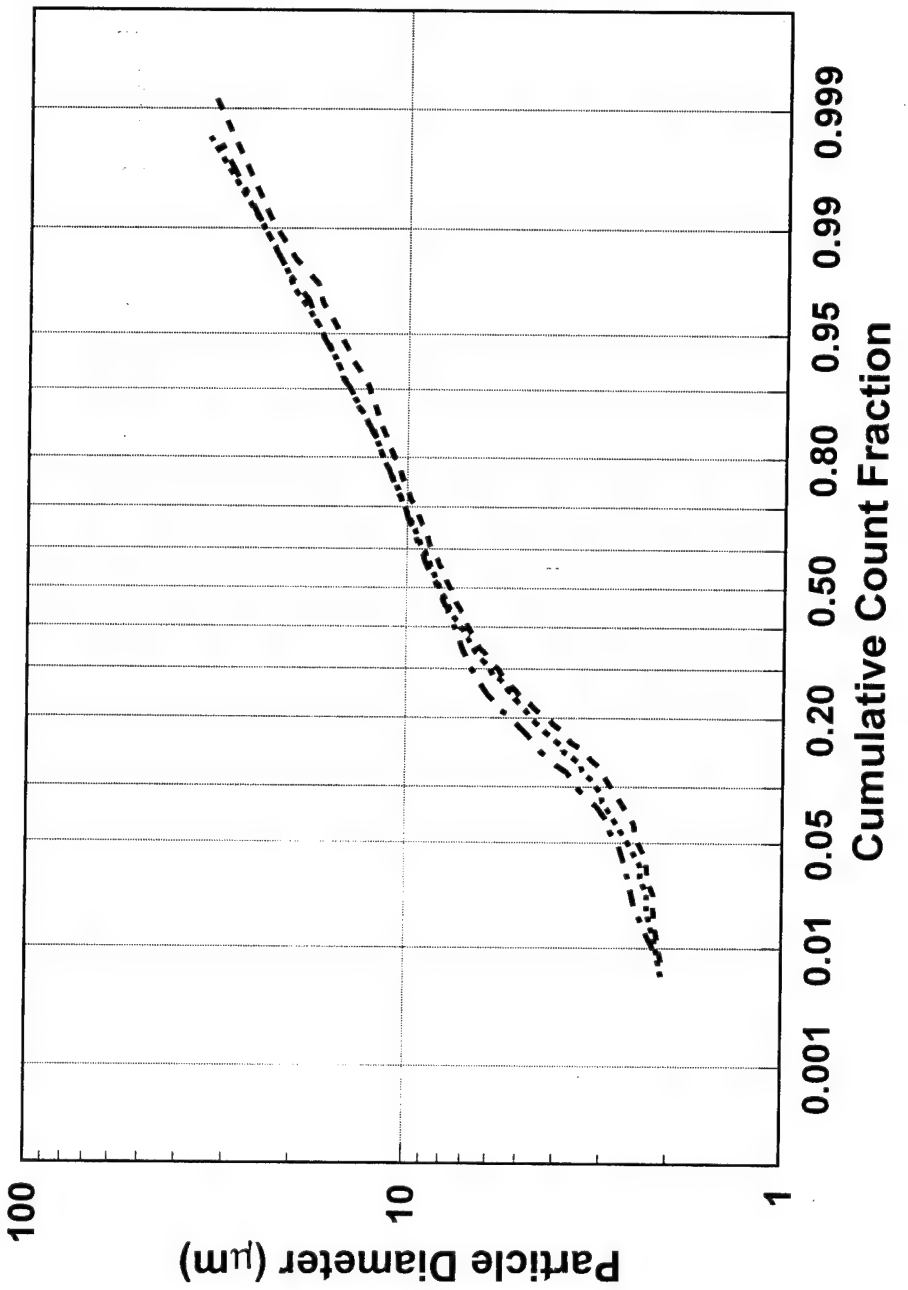

Figure B.22: Spray booth droplet sizing data, p_n = 10 psig, orientation = 180°.

Table B.1: Droplet Sizes Generated by VOAG

Desired droplet size (μm)	3.0	5.0	7.0	9.0	11.0	13.0	15.0	17.0
Amount solution (ml)	250	250	250	250	250	250	250	250
Density corn oil (g/ml)	0.908	0.908	0.908	0.908	0.908	0.908	0.908	0.908
Density methylene blue (g/ml)	1.26	1.26	1.26	1.26	1.26	1.26	1.26	1.26
Mass corn oil (g)	0.0437	0.2054	0.5730	1.2181	2.0218	3.6534	5.6253	8.1756
Mass methylene blue (g)	0.0010	0.0013	0.0015	0.0015	0.0012	0.0010	0.0013	0.0011
Volume corn oil (ml)	0.048	0.226	0.631	1.342	2.227	4.024	6.195	9.004
Meth blue/corn oil ratio (g/ml)	0.021	0.006	0.002	0.001	0.001	0.000	0.000	0.000
Mass average density (g/ml)	0.914	0.910	0.909	0.908	0.908	0.908	0.908	0.908
Concentration corn oil (vol frac)	0.0002	0.0009	0.0025	0.0054	0.0089	0.0161	0.0248	0.0360
Generator frequency (Hz)	72375	72259	72018	73779	71084	72349	72282	72926
Feed flow (ml/sec)	0.005	0.005	0.005	0.005	0.005	0.005	0.005	0.005
Primary droplet size (μm)	50.77	50.80	50.86	50.45	51.08	50.78	50.80	50.65
Actual droplet size (μm)	2.93	4.91	6.92	8.83	10.59	12.82	14.81	16.72

Table B.2: Calculation of Spray MMD (Wind Tunnel), 90° Orientation

Run Number	p_n (psig)	μ_l (cp)	m_a (lb/min)	m_l (g/min)	m_a/m_l	ρ_a (lb/ft^3)	v_a (ft/sec)	v_l (ft/sec)	v_{rel} (ft/sec)	Spray MMD
1	30	62.45	0.180	119.78	0.68	0.111	1126.79	3.95	1122.84	65.61
2	30	59.05	0.180	92.64	0.88	0.111	1129.34	3.06	1126.29	53.79
3	30	61.15	0.180	65.95	1.24	0.111	1127.75	2.18	1125.57	43.98
4	40	57.16	0.218	149.70	0.66	0.134	1130.83	4.94	1125.90	63.23
5	40	57.29	0.218	111.70	0.89	0.134	1130.73	3.68	1127.04	51.24
6	40	62.30	0.218	78.95	1.25	0.134	1126.90	2.60	1124.29	42.09
7	50	57.83	0.257	172.71	0.68	0.158	1130.30	5.70	1124.61	61.08
8	50	58.92	0.257	137.72	0.85	0.158	1129.45	4.54	1124.91	51.97
9	50	62.59	0.257	90.92	1.28	0.158	1126.68	3.00	1123.68	40.11
19	30	56.36	0.180	125.70	0.65	0.110	1131.47	4.15	1127.32	65.52
20	30	59.47	0.180	93.38	0.88	0.111	1129.03	3.08	1125.95	54.21
21	30	59.33	0.180	65.88	1.24	0.111	1129.13	2.17	1126.96	43.48
22	40	58.92	0.218	148.50	0.67	0.134	1129.45	4.90	1124.55	63.54
23	40	59.74	0.218	114.74	0.86	0.134	1128.81	3.78	1125.03	52.98
24	40	59.05	0.218	77.60	1.28	0.134	1129.34	2.56	1126.79	40.87
25	50	56.49	0.257	174.54	0.67	0.158	1131.36	5.76	1125.61	61.06
26	50	60.16	0.257	123.40	0.95	0.158	1128.49	4.07	1124.42	48.44
27	50	60.30	0.257	94.59	1.23	0.158	1128.39	3.12	1125.27	40.59

Table B.3: Calculation of Spray MMD (Wind Tunnel), 180° Orientation

Run Number	p_n (psig)	μ_l (cp)	m_a (lb/min)	m_l (g/min)	m_a/m_l	ρ_a (lb/ft^3)	v_a (ft/sec)	v_l (ft/sec)	v_{rel} (ft/sec)	Spray MMD
10	30	59.61	0.180	119.53	0.68	0.111	1128.92	3.94	1124.98	64.43
11	30	58.64	0.180	94.64	0.86	0.111	1129.66	3.12	1126.54	54.43
12	30	63.33	0.180	66.39	1.23	0.111	1126.15	2.19	1123.96	44.70
13	40	58.64	0.218	145.05	0.68	0.134	1129.66	4.78	1124.88	62.33
14	40	52.03	0.218	112.17	0.88	0.134	1129.13	3.70	1125.43	52.03
15	40	64.37	0.218	78.18	1.27	0.135	1125.40	2.58	1122.82	42.33
16	50	58.64	0.257	168.60	0.69	0.158	1129.66	5.56	1124.10	60.27
17	50	58.23	0.257	128.85	0.91	0.158	1129.98	4.25	1125.73	49.35
18	50	67.13	0.257	89.49	1.30	0.159	1123.48	2.95	1120.53	40.71
28	30	57.96	0.180	118.40	0.69	0.111	1130.20	3.91	1126.29	63.36
29	30	66.50	0.180	90.82	0.90	0.111	1123.91	3.00	1120.91	55.37
30	30	59.74	0.180	63.28	1.29	0.111	1128.81	2.09	11.26.73	42.58
31	40	65.12	0.218	140.16	0.71	0.135	1124.87	4.62	1120.24	63.08
32	40	63.48	0.218	111.23	0.89	0.134	1126.04	3.67	1122.37	52.99
33	40	58.50	0.218	76.65	1.29	0.134	1129.77	2.53	1127.24	40.43
34	50	59.88	0.257	166.86	0.70	0.158	1128.71	5.50	1123.20	60.24
35	50	59.47	0.257	131.31	0.89	0.158	1129.03	4.33	1124.69	50.39
36	50	64.07	0.257	91.03	1.28	0.159	1125.61	3.00	1122.61	40.47

Table B.4: Wind Tunnel Droplet Size Distribution Parameters, 90° Orientation

Run Number	p_n (psig)	m_a/m_l	Spray MMD	Breathing Zone				
				GMD	GSD	CMD	MMD	MMAD
1	30	0.70	65.61	14.04	1.46	13.76	22.81	21.74
2	30	0.90	53.79	13.17	1.50	12.96	21.50	20.49
3	30	1.30	43.98	13.45	1.54	13.32	23.55	22.44
4	40	0.70	63.23	13.75	1.59	13.57	25.01	23.83
5	40	0.90	51.24	13.60	1.58	13.52	25.43	24.23
6	40	1.30	42.09	14.12	1.48	13.91	22.44	21.38
7	50	0.70	61.08	13.43	1.58	13.13	24.51	23.36
8	50	0.90	51.97	13.51	1.58	13.58	23.89	22.76
9	50	1.30	40.11	13.41	1.50	13.26	22.01	20.97
19	30	0.70	65.52	13.33	1.51	13.10	22.72	21.65
20	30	0.90	54.21	12.98	1.58	13.10	22.25	21.20
21	30	1.30	43.48	13.61	1.45	13.23	21.60	20.58
22	40	0.70	63.54	14.35	1.46	14.14	22.50	21.44
23	40	0.90	52.98	13.78	1.58	13.74	24.01	22.88
24	40	1.30	40.87	13.16	1.59	13.26	23.87	22.75
25	50	0.70	61.06	14.00	1.62	14.17	26.35	25.11
26	50	0.90	48.44	11.03	1.56	11.03	19.27	18.36
27	50	1.30	40.59	14.00	1.58	14.06	24.88	23.71

GMD = Geometric Mean Diameter
GSD = Geometric Standard Deviation
CMD = Count Median Diameter
MMD = Mass Median Diameter
MMAD = Mass Median Aerodynamic Diameter

Table B.5: Wind Tunnel Droplet Size Distribution Parameters, 180° Orientation

Run Number	p_n (psig)	m_a/m_l	Spray MMD	Breathing Zone				
				GMD	GSD	CMD	MMD	MMAD
10	30	0.70	64.43	12.03	1.42	11.60	18.80	17.91
11	30	0.90	54.43	11.32	1.39	10.79	17.67	16.84
12	30	1.30	44.70	10.77	1.56	10.69	19.39	18.48
13	40	0.70	62.33	10.81	1.34	10.32	14.97	14.26
14	40	0.90	52.03	11.04	1.38	10.53	16.17	15.41
15	40	1.30	42.33	10.56	1.50	10.28	17.78	16.94
16	50	0.70	60.27	10.60	1.38	10.30	15.30	14.58
17	50	0.90	49.35	10.99	1.38	10.53	16.15	15.39
18	50	1.30	40.71	10.45	1.41	10.40	15.00	14.29
28	30	0.70	63.36	11.26	1.39	10.81	17.02	16.22
29	30	0.90	55.37	11.37	1.48	10.85	19.67	18.74
30	30	1.30	42.58	10.38	1.45	10.13	16.37	15.60
31	40	0.70	63.08	11.57	1.48	11.09	20.00	19.06
32	40	0.90	52.99	11.36	1.44	10.87	18.25	17.39
33	40	1.30	40.43	10.75	1.38	10.34	15.73	14.99
34	50	0.70	60.24	10.11	1.42	9.81	15.31	14.59
35	50	0.90	50.39	10.57	1.40	10.30	15.67	14.93
36	50	1.30	40.47	10.98	1.47	10.79	17.80	16.96

GMD = Geometric Mean Diameter
GSD = Geometric Standard Deviation
CMD = Count Median Diameter
MMD = Mass Median Diameter
MMAD = Mass Median Aerodynamic Diameter

Table B.6: Paint Spray Booth Velocity Profiles

77.5	84.0	110.1	122.0
84.0	109.0	106.8	112.3
90.5	109.0	93.8	102.5
87.2	100.3	87.2	104.6

Measurement 1

70.6	90.4	90.4	116.8
84.9	101.4	104.7	113.5
89.3	116.8	102.5	111.3
88.2	94.8	100.3	110.2

Measurement 2

64.0	83.8	95.9	131.1
95.9	103.6	103.6	117.9
101.4	112.4	99.2	108.0
94.8	101.4	88.2	104.7

Measurement 3

80.8	91.7	99.3	114.6
85.2	101.5	107.0	114.6
87.4	105.9	97.2	114.6
97.2	98.2	102.6	103.7

Measurement 4

Measurement	Avg Velocity (fpm)	Standard Deviation	CV (%)
1	98.8	12.72	12.87
2	99.2	13.05	13.16
3	100.4	14.86	14.80
4	100.1	10.26	10.25
Total	99.6	12.72	12.77

Table B.7: Spray Gun Air-to-Liquid Mass Flow Ratios and Transfer Efficiencies

p_n[1] (psig)	Mass Cup (g)		Mass Trough (g)		Spray Time (sec)	m_l (g/min)	m_o (g/min)	m_a/m_l	TE
	Before	After	Before	After					
10	2595	1663	614	1354	120.06	465.77	95.95	1.42	0.794
10	2587	1752	624	1263	120.05	417.33	97.96	1.58	0.765
10	2339	1491	613	1264	120.16	423.44	98.37	1.56	0.768
10	2790	1871	618	1316	120.08	459.19	110.43	1.44	0.760
30	1210	801	611	859	120.13	204.28	80.41	1.34	0.606
30	1217	804	615	857	120.05	206.41	85.46	1.33	0.586
30	1247	831	623	856	120.07	207.88	91.45	1.32	0.560
30	1193	774	626	889	120.04	209.43	77.97	1.31	0.628
30	1229	808	624	880	120.14	210.25	82.40	1.30	0.608
40	1204	766	598	859	120.06	218.89	88.46	1.53	0.596
40	1225	779	614	886	120.07	222.87	86.95	1.50	0.610
40	1221	779	624	900	120.23	220.58	82.84	1.52	0.624
40	1214	771	628	865	120.10	221.32	102.91	1.51	0.535
40	1238	787	626	879	120.00	225.50	99.00	1.48	0.561
50	1218	675	611	939	120.06	271.36	107.45	1.45	0.604
50	1219	681	615	958	120.16	268.64	97.37	1.46	0.638
50	1202	671	621	939	120.05	265.39	106.46	1.48	0.599
50	1246	711	622	940	120.07	267.34	108.44	1.47	0.594
50	1227	688	624	936	119.98	269.54	113.52	1.46	0.579

[1] 10 psig = HVLP spray gun; 30, 40, 50 psig = conventional spray gun

Table B.8: Spray Booth Breathing Zone Droplet Size Parameters

Run Number	Orientation	p_n (psig)	Breathing Zone			
			GMD	GSD	CMD	MMD
37	90°	30	7.76	1.85	8.25	20.13
38	90°	30	9.17	1.64	9.12	19.27
39	90°	30	8.78	1.73	9.26	18.32
40	90°	40	8.12	1.82	8.49	20.15
41	90°	40	9.72	1.58	9.56	18.09
42	90°	40	7.08	1.82	7.43	18.24
43	90°	50	7.88	1.82	8.46	18.19
44	90°	50	9.74	1.71	9.67	22.39
45	90°	50	9.37	1.61	9.51	18.34
46	180°	30	6.86	1.83	7.49	16.42
47	180°	30	6.16	1.77	6.63	13.93
48	180°	30	8.88	1.54	8.93	14.49
49	180°	40	6.79	1.75	7.40	13.74
50	180°	40	6.64	1.76	7.16	13.94
51	180°	40	8.55	1.50	8.56	13.57
52	180°	50	7.25	1.71	7.77	14.02
53	180°	50	8.15	1.56	8.43	13.05
54	180°	50	8.01	1.56	8.30	13.25
55	90°	10	9.60	1.61	9.58	18.53
56	90°	10	9.54	1.64	9.76	18.19
57	90°	10	9.86	1.64	9.74	20.04
58	180°	10	6.97	1.74	7.68	13.67
59	180°	10	7.46	1.75	8.20	15.62
60	180°	10	7.81	1.68	8.28	15.22

GMD = Geometric Mean Diameter
GSD = Geometric Standard Deviation
CMD = Count Median Diameter
MMD = Mass Median Diameter

Appendix C: Chapter 4 Additional Materials

C.1. Laboratory Transfer Efficiency

The transfer efficiency data of the 1/4J nozzle measured during the laboratory studies are summarized in Tables C.1-6. From dummy variable regression (Kleinbaum *et al.*, 1988) the transfer efficiency curves in Figure 4.1 are judged to be non-parallel ($p = 0.0001$) with unequal intercepts ($p < 0.0001$). The best-fit equations are:

$$\frac{m_a}{m_l} = 0.70: \quad TE = 0.974 - 2.61 \times 10^{5} \left[\frac{\mu_l}{p_n}, \sec \right], \; r^2 = 0.903 \qquad (1)$$

$$\frac{m_a}{m_l} = 0.90: \quad TE = 0.965 - 3.11 \times 10^{5} \left[\frac{\mu_l}{p_n}, \sec \right], \; r^2 = 0.901 \qquad (2)$$

$$\frac{m_a}{m_l} = 1.30: \quad TE = 0.939 - 3.50 \times 10^{5} \left[\frac{\mu_l}{p_n}, \sec \right], \; r^2 = 0.872 \qquad (3)$$

C.2. Field Transfer Efficiency

The measured transfer efficiencies of the DeVilbiss MBC-510-30EX spray gun are in Table C.7.

C.3. Spray Painting Task Summary

The worker who performed each task, the type of workpiece painted, and the type of primer or paint used is shown in Table C.8.

C.4. Measured Task Parameters

Parameters directly measured for each task are listed in Table C.9, including spray gun nozzle pressure, paint viscosity, and average booth freestream velocity; worker height and breadth; mass of paint sprayed; and task, spray, and 90° and 180° orientation times.

C.5. Measurement of Worker Task Exposures

The results of the charcoal tube analyses are shown in Table C.10. The calculation of individual worker task exposures (C_{task}) is summarized in Table C.11.

C.6. Calculated Task Parameters

The task calculated parameters are listed in Table C.12, including overspray generation rates; the dimensionless groups p_nH/μ_lU and $CUHD/m_o$; and exposures predicted by the model. Paint viscosities were determined from a Zahn #2 Cup calibration chart (Hund, 1993b). Transfer efficiencies were estimated from Table C.7. For nozzle pressure less than 50 psig, it was assumed transfer efficiency had reached an asymptotic value of 0.78.

C.7. Estimated Experimental Error

The estimated experimental error indicated in Figures 4.5 and 4.7 was calculated as the 95% measurement uncertainty in the predicted exposure. The uncertainty was found from the estimated bias and precision of the task parameters (Table C.13) using the measurement uncertainty analysis outlined in the ANSI/ASME standard on measurement uncertainty. A summary of the calculation follows. From equation (4-9),

$$C_{model} = \frac{C_{90}t_{90} + C_{180}t_{180}}{t_{task}} \qquad (4)$$

$$= \frac{m_o}{UHD}\left[\frac{\tilde{C}_{90}t_{90} + \tilde{C}_{180}t_{180}}{t_{task}}\right] \qquad (5)$$

where $\tilde{C} = CUHD/m_o$.

$$B_{C_{model}} = \left[\begin{array}{l}\left(\frac{\partial C_{model}/\partial m_o}{C_{model}/m_o}B_{m_o}\right)^2 + \left(\frac{\partial C_{model}/\partial U}{C_{model}/U}B_U\right)^2 + \left(\frac{\partial C_{model}/\partial H}{C_{model}/H}B_H\right)^2 \\ + \left(\frac{\partial C_{model}/\partial D}{C_{model}/D}B_D\right)^2 + \left(\frac{\partial C_{model}/\partial t_{task}}{C_{model}/t_{task}}B_{t_{task}}\right)^2 \\ + \left(\frac{\partial C_{model}/\partial t_{90}}{C_{model}/t_{90}}B_{t_{90}}\right)^2 + \left(\frac{\partial C_{model}/\partial t_{180}}{C_{model}/t_{180}}B_{t_{180}}\right)^2\end{array}\right]^{1/2}$$

$$= \left[\begin{array}{c}(1 \times 0.029)^2 + (-1 \times 0.040)^2 + (-1 \times 0.004)^2 + (-1 \times 0.017)^2 \\ + (-1 \times 0.001)^2 + (0.94 \times 0.001)^2 + (0.06 \times 0.001)^2\end{array}\right]^{1/2}$$

$$= 0.052 = 5.2\%$$

$$S_{C_{model}} = \left[\begin{array}{l}\left(\frac{\partial C_{model}/\partial m_o}{C_{model}/m_o}S_{m_o}\right)^2 + \left(\frac{\partial C_{model}/\partial U}{C_{model}/U}S_U\right)^2 + \left(\frac{\partial C_{model}/\partial H}{C_{model}/H}S_H\right)^2 \\ + \left(\frac{\partial C_{model}/\partial D}{C_{model}/D}S_D\right)^2 + \left(\frac{\partial C_{model}/\partial t_{task}}{C_{model}/t_{task}}S_{t_{task}}\right)^2 \\ + \left(\frac{\partial C_{model}/\partial t_{90}}{C_{model}/t_{90}}S_{t_{90}}\right)^2 + \left(\frac{\partial C_{model}/\partial t_{180}}{C_{model}/t_{180}}S_{t_{180}}\right)^2\end{array}\right]^{1/2}$$

$$= \left[\begin{array}{c}(1 \times 0.053)^2 + (-1 \times 0.083)^2 + (-1 \times 0.007)^2 + (-1 \times 0.050)^2 \\ + (-1 \times 0.006)^2 + (0.94 \times 0.250)^2 + (0.06 \times 0.167)^2\end{array}\right]^{1/2}$$

$$= 0.259 = 25.9\%$$

$$U_{C(model)}(95\%) = \left[(0.052)^2 + (2 \times 0.259)^2\right]^{1/2}$$

$$= 0.521 = 52.1\%$$

C.8. Sample Calculations (Task Number 1)

C.8.1. Transfer Efficiency

As calculated in Section A.8,

$\mu_l = 45.41$ cp

$m_l = 92.63$ g/min

$m_o = 9.33$ g/min

$$\frac{\mu_l}{p_n} = \frac{45.51\ \text{cp}}{30\ \text{psi}} \times \left(\frac{14.7\ \text{psi}}{\text{atm}}\right) \times \left(\frac{\text{atm}}{1.01325 \times 10^6\ \text{dyne/cm}^2}\right) \times \left(\frac{0.01\ \text{dyne} - \text{s/cm}^2}{\text{cp}}\right)$$

$$= 2.20 \times 10^{-7}\ \text{sec}$$

$$TE = 1 - \frac{m_o}{m_l}$$

$$= 1 - \frac{9.33\ \text{g/min}}{92.63\ \text{g/min}}$$

$$= 0.900$$

C.8.2. Task Exposure

$$C_{task} = \frac{\text{mass solids} + \text{mass solvent}}{\text{flow x task time}}$$

$$= \frac{[\text{mass filter (after)} - \text{mass filter (before)}] + [\text{mass charcoal tubes}]}{\text{flow x task time}}$$

$$= \frac{(15.341 - 14.799 + 0.017^{[1]})\ \text{mg} + (0.5838 + 0.7581)\ \text{mg}}{(2.00\ \text{lpm}) \times (996\ \text{sec})} \times \left(\frac{10^3\ \text{lit}}{\text{m}^3}\right) \times \left(\frac{60\ \text{sec}}{\text{min}}\right)$$

$$= 57.3\ \text{mg/m}^3$$

[1]Blank filter correction

C.8.3. Predicted Exposure

$$C_{model} = \frac{C_{90}t_{90} + C_{180}t_{180}}{t_{task}}$$

$$= \frac{m_o}{UHD}\left[\frac{\tilde{C}_{90}t_{90} + \tilde{C}_{180}t_{180}}{t_{task}}\right]$$

where $\tilde{C} = CUHD/m_o$.

$$m_o = (1 - TE) \times \frac{\text{mass sprayed}}{t_{spray}}$$

$$= (1 - 0.78) \times \frac{3539\ g}{460.4\ sec}$$

$$= 1.69\ g/sec$$

$$C_{model} = \frac{1.69\ g/sec}{(131.2\ fpm)(75\ in)(13\ in)}\left[\frac{0.134(110.2\ sec) + 0.006(350.2\ sec)}{996\ sec}\right] \times \left(\frac{10^3\ mg}{g}\right) \times \left(\frac{144\ in^2}{ft^2}\right) \times \left(\frac{3.281\ ft}{m}\right)^3 \times \left(\frac{60\ sec}{min}\right)$$

$$= 68.3\ mg/m^3$$

C.8.4. Dimensionless Numbers

$$\frac{p_n H}{\mu_1 U} = \frac{(50\ psi)(75\ in)}{(12.5\ cp)(131.2\ fpm)} \times \left(\frac{atm}{14.7\ psi}\right) \times \left(\frac{1.01325 \times 10^6\ dyne/cm^2}{atm}\right) \times \left(\frac{ft}{12\ in}\right) \times \left(\frac{cp}{0.01\ dyne - s/cm^2}\right) \times \left(\frac{60\ sec}{min}\right)$$

$$= 7.88 \times 10^7$$

$$\frac{CUHD}{m_o} = \frac{C_{task}\,(t_{task}/t_{spray})\,UHD}{m_o}$$

where C_{task} is the measured task exposure, not that predicted by the model.

$$= \frac{(57.26\ mg/m^3)(131.2\ fpm)(75\ in)(13\ in)}{(1.69\ g/sec)} \times \left(\frac{996\ sec}{460.4\ sec}\right) \times \left(\frac{g}{10^3\ mg}\right) \times \left(\frac{ft^2}{144\ in^2}\right) \times \left(\frac{m}{3.281\ ft}\right)^3 \times \left(\frac{min}{60\ sec}\right)$$

$$= 0.0307$$

Table C.1: 1/4J Nozzle Transfer Efficiency (90° Orientation, $m_a/m_l = 0.70$)

Run Number	m_a/m_l	p_n (psig)	μ_l (cp)	m_l (g/min)	m_o (g/min)	μ_l/p_n (sec)	TE
13	0.69	30	45.41	119.97	10.03	2.20E-07	0.916
14	0.69	30	44.57	121.23	9.46	2.16E-07	0.922
15	0.68	30	44.05	121.92	10.23	2.13E-07	0.916
16	0.70	50	42.14	169.98	11.00	1.22E-07	0.935
17	0.70	50	41.95	169.46	10.02	1.22E-07	0.941
18	0.70	50	41.95	169.56	10.36	1.22E-07	0.939
25	0.69	50	53.45	172.26	9.70	1.55E-07	0.944
26	0.69	50	53.08	173.22	9.93	1.54E-07	0.943
27	0.68	50	52.10	176.55	10.66	1.51E-07	0.940
28	0.70	30	50.66	118.25	9.39	2.45E-07	0.921
29	0.71	30	50.54	117.61	9.20	2.44E-07	0.922
30	0.71	30	50.90	117.59	10.13	2.46E-07	0.914
37	0.68	30	46.48	122.87	10.06	2.25E-07	0.918
38	0.68	30	45.72	121.97	9.63	2.21E-07	0.921
39	0.69	30	44.36	120.78	10.15	2.15E-07	0.916
40	0.69	50	42.84	172.88	10.29	1.24E-07	0.940
41	0.69	50	42.05	173.43	10.42	1.22E-07	0.940
42	0.70	50	42.64	171.50	10.26	1.24E-07	0.940
59	0.70	40	41.56	144.25	10.76	1.51E-07	0.925
60	0.71	40	41.36	143.56	10.16	1.50E-07	0.929
63	0.71	40	44.36	143.13	10.69	1.61E-07	0.925
64	0.71	40	44.15	143.22	10.53	1.60E-07	0.927
67	0.71	40	47.79	142.25	10.73	1.73E-07	0.925
68	0.71	40	47.35	143.20	10.46	1.72E-07	0.927
167	0.71	20	47.24	90.13	10.00	3.43E-07	0.889
168	0.70	20	47.02	90.32	12.04	3.41E-07	0.867
169	0.70	20	50.31	90.20	10.11	3.65E-07	0.888
170	0.70	20	48.81	91.18	12.25	3.54E-07	0.866
177	0.69	20	48.13	91.60	12.98	3.49E-07	0.858
178	0.71	20	47.57	89.65	10.37	3.45E-07	0.884

Table C.2: 1/4J Nozzle Transfer Efficiency (90° Orientation, $m_a/m_l = 0.90$)

Run Number	m_a/m_l	p_n (psig)	μ_l (cp)	m_l (g/min)	m_o (g/min)	μ_l/p_n (sec)	TE
1	0.90	30	45.51	92.63	9.33	2.20E-07	0.899
2	0.88	30	44.46	94.65	9.53	2.15E-07	0.899
3	0.86	30	43.74	96.58	10.49	2.12E-07	0.891
4	0.90	50	41.75	132.86	9.96	1.21E-07	0.925
5	0.90	50	41.56	132.58	9.96	1.21E-07	0.925
6	0.90	50	41.66	132.16	9.85	1.21E-07	0.925
31	0.88	50	52.59	135.25	10.19	1.53E-07	0.925
32	0.88	50	51.98	135.90	9.66	1.51E-07	0.929
33	0.87	50	51.37	136.55	9.56	1.49E-07	0.930
34	0.90	30	49.61	92.60	9.53	2.40E-07	0.897
35	0.89	30	48.92	93.24	9.59	2.37E-07	0.897
36	0.89	30	48.58	93.58	9.52	2.35E-07	0.898
49	0.90	50	41.27	132.32	9.07	1.20E-07	0.931
50	0.90	50	40.79	132.72	9.00	1.18E-07	0.932
51	0.89	50	40.22	134.22	9.26	1.17E-07	0.931
52	0.90	30	40.04	92.43	9.42	1.94E-07	0.898
53	0.90	30	39.85	92.79	9.06	1.93E-07	0.902
54	0.90	30	39.94	92.58	9.26	1.93E-07	0.900
55	0.89	40	44.46	113.14	10.07	1.61E-07	0.911
56	0.89	40	44.15	113.56	10.00	1.60E-07	0.912
65	0.90	40	43.95	113.12	10.07	1.59E-07	0.911
66	0.90	40	43.85	112.76	10.00	1.59E-07	0.911
71	0.90	40	45.94	111.93	9.75	1.67E-07	0.913
72	0.90	40	45.83	112.11	9.57	1.66E-07	0.915
165	0.91	20	48.69	70.19	11.27	3.53E-07	0.840
166	0.90	20	47.91	70.58	9.64	3.48E-07	0.863
173	0.91	20	45.94	69.73	11.74	3.33E-07	0.832
174	0.91	20	45.72	69.60	9.65	3.32E-07	0.861
175	0.89	20	47.13	71.53	12.08	3.42E-07	0.831
176	0.91	20	49.49	69.92	10.01	3.59E-07	0.857

Table C.3: 1/4J Nozzle Transfer Efficiency (90° Orientation, $m_a/m_l = 1.30$)

Run Number	m_a/m_l	p_n (psig)	μ_l (cp)	m_l (g/min)	m_o (g/min)	μ_l/p_n (sec)	TE
7	1.29	50	46.15	92.63	9.66	1.34E-07	0.896
8	1.27	50	45.41	93.86	10.08	1.32E-07	0.893
9	1.26	50	44.26	94.96	9.70	1.28E-07	0.898
10	1.31	30	43.04	63.31	9.76	2.08E-07	0.846
11	1.31	30	42.54	63.30	9.90	2.06E-07	0.844
12	1.31	30	41.75	63.28	9.39	2.02E-07	0.852
19	1.31	30	49.84	63.28	8.86	2.41E-07	0.860
20	1.33	30	49.15	62.32	8.50	2.38E-07	0.864
21	1.33	30	49.15	62.60	8.09	2.38E-07	0.871
22	1.30	50	47.68	91.93	9.36	1.38E-07	0.898
23	1.31	50	47.68	90.95	8.80	1.38E-07	0.903
24	1.30	50	47.68	91.66	8.73	1.38E-07	0.905
43	1.29	30	44.15	64.40	9.06	2.14E-07	0.859
44	1.28	30	42.74	64.98	9.44	2.07E-07	0.855
45	1.27	30	42.05	65.18	8.80	2.03E-07	0.865
46	1.34	50	40.79	89.33	9.51	1.18E-07	0.894
47	1.32	50	40.60	90.76	9.34	1.18E-07	0.897
48	1.28	50	40.32	93.37	9.54	1.17E-07	0.898
57	1.32	40	42.64	76.99	10.10	1.55E-07	0.869
58	1.32	40	42.14	76.96	9.93	1.53E-07	0.871
61	1.29	40	44.98	78.55	9.95	1.63E-07	0.873
62	1.29	40	44.78	78.76	9.82	1.62E-07	0.875
69	1.29	40	46.69	78.35	9.45	1.69E-07	0.879
70	1.29	40	46.15	78.58	9.32	1.67E-07	0.881
163	1.29	20	51.86	49.19	8.71	3.76E-07	0.823
164	1.28	20	50.66	49.53	9.95	3.67E-07	0.799
171	1.29	20	47.35	49.40	10.42	3.43E-07	0.789
172	1.29	20	46.69	49.33	8.84	3.39E-07	0.821
179	1.29	20	46.58	49.46	9.16	3.38E-07	0.815
180	1.29	20	46.69	49.46	10.87	3.39E-07	0.780

Table C.4: 1/4J Nozzle Transfer Efficiency (180° Orientation, $m_a/m_l = 0.70$)

Run Number	m_a/m_l	p_n (psig)	μ_l (cp)	m_l (g/min)	m_o (g/min)	μ_l/p_n (sec)	TE
81	0.70	50	47.91	171.28	10.54	1.39E-07	0.938
82	0.69	50	47.13	172.82	10.34	1.37E-07	0.940
83	0.69	50	46.48	173.59	10.69	1.35E-07	0.938
84	0.70	30	45.30	118.38	10.37	2.19E-07	0.912
85	0.70	30	45.09	118.38	10.55	2.18E-07	0.911
86	0.70	30	44.78	118.45	10.22	2.17E-07	0.914
87	0.72	40	44.67	141.24	10.36	1.62E-07	0.927
88	0.72	40	44.26	141.10	10.15	1.61E-07	0.928
97	0.71	50	50.54	168.22	9.99	1.47E-07	0.941
98	0.70	50	50.66	170.13	9.88	1.47E-07	0.942
99	0.70	50	50.19	170.01	9.89	1.46E-07	0.942
100	0.72	40	50.07	140.40	9.53	1.82E-07	0.932
101	0.72	40	50.07	139.97	9.73	1.82E-07	0.931
102	0.71	30	50.31	116.56	9.65	2.43E-07	0.917
103	0.71	30	50.43	116.28	9.45	2.44E-07	0.919
104	0.72	30	51.02	115.89	9.69	2.47E-07	0.916
137	0.71	40	48.58	143.26	10.12	1.76E-07	0.929
138	0.70	40	47.68	144.37	10.04	1.73E-07	0.930
139	0.71	30	47.02	117.48	10.43	2.27E-07	0.911
140	0.70	30	46.15	119.47	10.11	2.23E-07	0.915
141	0.69	30	45.62	119.98	10.04	2.21E-07	0.916
142	0.70	50	44.88	169.47	10.56	1.30E-07	0.938
143	0.71	50	44.78	169.16	10.17	1.30E-07	0.940
144	0.71	50	44.78	168.69	10.32	1.30E-07	0.939
147	0.71	20	48.24	89.61	10.46	3.50E-07	0.883
148	0.70	20	47.91	90.28	11.37	3.48E-07	0.874
151	0.71	20	52.59	90.08	10.21	3.81E-07	0.887
152	0.70	20	52.22	90.59	11.27	3.79E-07	0.876
161	0.71	20	52.71	89.08	11.04	3.82E-07	0.876
162	0.72	20	53.08	88.89	10.08	3.85E-07	0.887

Table C.5: 1/4J Nozzle Transfer Efficiency (180° Orientation, $m_a/m_l = 0.90$)

Run Number	m_a/m_l	p_n (psig)	μ_l (cp)	m_l (g/min)	m_o (g/min)	μ_l/p_n (sec)	TE
73	0.90	30	46.69	92.30	10.25	2.26E-07	0.889
74	0.89	30	45.83	93.08	9.86	2.22E-07	0.894
75	0.89	30	44.98	93.48	9.94	2.18E-07	0.894
76	0.90	50	43.74	132.38	10.07	1.27E-07	0.924
77	0.90	50	43.54	133.09	10.38	1.26E-07	0.922
78	0.90	50	43.14	133.16	10.26	1.25E-07	0.923
79	0.91	40	42.54	110.66	10.88	1.54E-07	0.902
80	0.92	40	42.94	110.16	9.99	1.56E-07	0.909
113	0.90	50	52.34	132.58	9.76	1.52E-07	0.926
114	0.90	50	51.37	133.28	9.80	1.49E-07	0.926
115	0.89	50	50.66	133.75	9.66	1.47E-07	0.928
116	0.91	30	49.84	90.88	9.52	2.41E-07	0.895
117	0.91	30	49.49	91.40	9.83	2.39E-07	0.892
118	0.91	30	49.04	91.78	9.69	2.37E-07	0.894
119	0.91	40	48.81	111.49	9.69	1.77E-07	0.913
120	0.91	40	49.04	111.15	9.69	1.78E-07	0.913
129	0.89	30	49.49	93.19	10.00	2.39E-07	0.893
130	0.89	30	48.58	93.81	10.03	2.35E-07	0.893
131	0.88	30	47.91	94.38	10.33	2.32E-07	0.891
132	0.91	40	47.02	111.08	10.12	1.71E-07	0.909
133	0.91	40	46.69	111.26	9.92	1.69E-07	0.911
134	0.91	50	46.05	131.09	10.01	1.34E-07	0.924
135	0.91	50	46.15	130.78	9.96	1.34E-07	0.924
136	0.91	50	46.05	131.07	10.18	1.34E-07	0.922
149	0.91	20	47.46	69.69	10.58	3.44E-07	0.848
150	0.91	20	47.35	69.49	9.61	3.43E-07	0.862
155	0.91	20	49.96	70.20	10.49	3.62E-07	0.851
156	0.91	20	49.49	70.09	9.74	3.59E-07	0.861
157	0.89	20	57.05	71.20	9.61	4.14E-07	0.865
158	0.90	20	55.22	70.79	10.54	4.01E-07	0.851

Table C.6: 1/4J Nozzle Transfer Efficiency (180° Orientation, $m_a/m_l = 1.30$)

Run Number	m_a/m_l	p_n (psig)	μ_l (cp)	m_l (g/min)	m_o (g/min)	μ_l/p_n (sec)	TE
89	1.29	30	49.15	64.17	9.30	2.38E-07	0.855
90	1.30	30	48.69	64.09	9.22	2.35E-07	0.856
91	1.28	30	47.79	64.79	9.49	2.31E-07	0.854
92	1.31	40	45.62	77.48	9.80	1.65E-07	0.874
93	1.30	40	44.78	77.88	9.89	1.62E-07	0.873
94	1.30	50	44.05	91.57	9.81	1.28E-07	0.893
95	1.30	50	43.85	91.67	9.91	1.27E-07	0.892
96	1.31	50	43.64	91.50	9.80	1.27E-07	0.893
105	1.32	40	52.34	76.89	9.00	1.90E-07	0.883
106	1.32	40	52.10	76.88	8.97	1.89E-07	0.883
107	1.30	30	51.73	63.69	9.02	2.50E-07	0.858
108	1.31	30	51.25	63.49	8.60	2.48E-07	0.865
109	1.31	30	51.02	63.59	8.75	2.47E-07	0.862
110	1.32	50	50.66	90.48	9.31	1.47E-07	0.897
111	1.31	50	50.66	91.18	9.15	1.47E-07	0.900
112	1.32	50	51.49	90.49	9.16	1.49E-07	0.899
121	1.29	30	51.49	64.39	9.29	2.49E-07	0.856
122	1.29	30	50.66	64.49	9.18	2.45E-07	0.858
123	1.28	30	49.96	64.90	9.05	2.42E-07	0.861
124	1.32	50	48.81	90.77	9.66	1.42E-07	0.894
125	1.31	50	48.24	91.09	9.72	1.40E-07	0.893
126	1.31	50	47.79	91.30	9.73	1.39E-07	0.893
127	1.28	40	47.13	79.28	9.67	1.71E-07	0.878
128	1.28	40	46.80	79.30	9.97	1.70E-07	0.874
145	1.28	20	51.98	49.70	9.58	3.77E-07	0.807
146	1.26	20	49.61	50.60	9.19	3.60E-07	0.818
153	1.28	20	51.14	49.50	9.31	3.71E-07	0.812
154	1.28	20	50.66	49.60	8.77	3.67E-07	0.823
159	1.28	20	53.70	49.70	8.77	3.90E-07	0.824
160	1.27	20	52.83	49.99	9.35	3.83E-07	0.813

Table C.7: DeVilbiss MBC Spray Gun Transfer Efficiency

Nozzle Pressure	Mass Cup (g)		Mass Trough (g)		Time (sec)	TE
	Before	After	Before	After		
50	1229	576	703	1212	120.22	0.779
50	1210	560	704	1206	120.16	0.772
50	1232	576	705	1220	120.22	0.785
60	1205	461	715	1236	120.20	0.700
60	1234	492	716	1261	120.07	0.735
60	1240	496	716	1246	119.99	0.712
70	1208	401	706	1311	120.27	0.750
70	1233	429	709	1326	120.28	0.767
70	1253	447	713	1329	120.08	0.764
80	1253	424	712	1311	120.21	0.723
80	1217	392	714	1301	120.14	0.712
80	1219	391	712	1305	120.18	0.716
90	1265	452	717	1259	120.02	0.667
90	1258	444	721	1275	120.29	0.681
90	1246	434	722	1278	120.08	0.685

Table C.8: Spray Painting Task Summary

Task #	Date	Worker #	Workpiece Description	Paint Type
1	14-Mar-96	2	F-15 wing	High-solids polyurethane enamel
2	14-Mar-96	4	F-15 wing	High-solids polyurethane enamel
3	14-Mar-96	5	C-130 wing flap	High-solids polyurethane enamel
4	15-Mar-96	2	F-15 stabilizers	High-solids polyurethane enamel
5	15-Mar-96	3	C-141 wing flap	High-solids polyurethane enamel
6	19-Mar-96	4	F-15 stabilizers	High-solids polyurethane enamel
7	19-Mar-96	1	F-15 stabilizers	High-solids polyurethane enamel
8	19-Mar-96	5	C-141 pylons	High-solids polyurethane enamel
9	20-Mar-96	1	F-15 stabilizers	Epoxy resin primer
10	20-Mar-96	7	F-15 stabilizers	High-solids polyurethane enamel
11	20-Mar-96	3	C-130 ailerons	High-solids polyurethane enamel
12	21-Mar-96	5	C-141 engine cowls	High-solids polyurethane primer
13	21-Mar-96	1	F-15 stabilizers	High-solids polyurethane enamel
14	21-Mar-96	5	C-141 engine cowls	High-solids polyurethane enamel
15	22-Mar-96	3	C-130 ailerons	High-solids polyurethane enamel
16	27-Mar-96	1	Shelter van	Epoxy resin primer
17	27-Mar-96	4	Shelter van	Epoxy resin primer
18	27-Mar-96		Field filter blank	
19	27-Mar-96		Field filter blank	
20	27-Mar-96	4	Shelter van	Chemical agent resistant polyurethane
21	27-Mar-96	1	Shelter van	Chemical agent resistant polyurethane
22	28-Mar-96	5	Miscellaneous parts	High-solids polyurethane primer
23	28-Mar-96	4	F-15 stabilizers	High-solids polyurethane enamel
24	28-Mar-96	3	Miscellaneous parts	High-solids polyurethane enamel
25	29-Mar-96	5	C-141 ailerons	High-solids polyurethane primer
26	29-Mar-96	1	C-141 ailerons	High-solids polyurethane enamel
27	29-Mar-96	8	F-15 stabilizers	High-solids polyurethane enamel
28	1-Apr-96	6	C-141 wing flaps	High-solids polyurethane enamel
29	1-Apr-96	6	C-141 wing flaps	High-solids polyurethane enamel
30	2-Apr-96	3	C-141 engine cowls/wing flap	High-solids polyurethane primer

Table C.8: Spray Painting Task Summary (continued)

Task #	Date	Worker #	Workpiece Description	Paint Type
31	2-Apr-96	1	F-15 bombracks	Epoxy resin primer
32	2-Apr-96	7	F-15 bombracks	High-solids polyurethane enamel
33	2-Apr-96	5	C-141 enginer cowls	High-solids polyurethane enamel
34	3-Apr-96	4	F-15 stabilizers	Epoxy resin primer
35	3-Apr-96	1	F-15 stabilizers	High-solids polyurethane enamel
36	3-Apr-96	3	C-141 engine cowl/aircraft door	High-solids polyurethane enamel
37	4-Apr-96	7	F-15 vari-ramps/stabilizer	Epoxy resin primer
38	4-Apr-96	7	F-15 vari-ramps/stabilizer	High-solids polyurethane enamel
39	4-Apr-96		Field filter blank	
40	4-Apr-96	5	C-141 wing flap	High-solids polyurethane enamel
41	4-Apr-96	3	C-141 engine cowls	High-solids polyurethane enamel
42	5-Apr-96	3	C-141 pylons	High-solids polyurethane primer
43	5-Apr-96	5	C-141 pylons	High-solids polyurethane enamel
44	5-Apr-96	1	F-15 bombracks	Epoxy resin primer
45	5-Apr-96	1	F-15 bombracks	High-solids polyurethane enamel
46	9-Apr-96	5	C-141 pylon/wing flap	High-solids polyurethane primer
47	9-Apr-96	7	F-15 bombracks	Epoxy resin primer
48	9-Apr-96	1	F-15 bombracks	High-solids polyurethane enamel
49	9-Apr-96	8	C-141 pylon/wing flap	High-solids polyurethane enamel
50	9-Apr-96		Field filter blank	
51	10-Apr-96	5	C-130 ailerons/C-141 wing flap	High-solids polyurethane primer
52	10-Apr-96	4	F-15 bombracks/stabilizers	Epoxy resin primer
53	10-Apr-96	1	F-15 bombracks/stabilizers	High-solids polyurethane enamel
54	10-Apr-96	6	F-15 vari-ramps	Epoxy resin primer
55	10-Apr-96	6	F-15 vari-ramps	High-solids polyurethane enamel
56	11-Apr-96		Field filter blank	
57	11-Apr-96	5	C-141 wing flaps/engine cowl	High-solids polyurethane primer
58	11-Apr-96	3	C-141 wing flaps/engine cowl	High-solids polyurethane enamel
59	12-Apr-96	7	F-15 bombracks	Epoxy resin primer
60	12-Apr-96	7	F-15 bombracks	High-solids polyurethane enamel

Table C.9: Measured Spray Painting Task Parameters

Task Number	p_n (psig)	μ_l (sec)	U (fpm)	H (in)	D (in)	m_l (g)	Time (sec)			
							Task	Spray	90°	180°
1	50	16.5	131.2	75.0	13	3539	996	460.4	110.2	350.2
2	30	16.7	132.7	68.5	15	2959	415	265.2	42.4	222.8
3	68	14.0	115.3	71.5	15	3440	1180	430.9	146.9	284.0
4	55	16.0	134.2	75.0	13	4313	1092	564.7	271.1	293.6
5	62	18.0	116.3	66.0	15	5314	1292	584.3	104.0	480.3
6	36	16.0	132.5	68.5	15	4260	891	468.6	134.0	334.6
7	84	16.8	132.5	67.0	15	3641	1057	491.1	172.0	319.1
8	80	14.8	114.6	71.5	15	5055	1197	529.3	319.9	209.4
9	84	14.4	128.9	67.0	15	1480	405	188.3	75.5	112.9
10	84	26.0	129.7	72.0	15	4013	859	336.9	82.1	254.9
11	72	15.0	112.7	66.0	15	5058	1317	574.8	279.5	295.4
12	76	15.6	111.8	71.5	15	1756	513	232.7	84.4	148.3
13	84	16.2	128.0	67.0	15	4929	1600	660.1	268.8	391.3
14	74	16.9	113.1	71.5	15	5086	1595	543.4	194.7	348.7
15	78	16.5	113.9	66.0	15	3971	795	377.3	114.6	262.7
16	45	14.6	131.6	67.0	15	2859	1015	476.5	154.6	321.8
17	48	12.0	131.6	68.5	15	4002	930	443.7	105.3	338.4
20	30	41.0	128.3	68.5	15	5848	1695	615.2	270.9	344.3
21	32	32.0	128.3	67.0	15	5076	2355	830.3	336.9	493.4
22	83	15.1	111.3	71.5	15	1867	589	290.2	112.5	177.7
23	28	15.8	128.7	68.5	15	4264	779	431.8	159.3	272.5
24	80	14.6	111.6	66.0	15	4987	1452	661.5	234.0	427.5
25	70	13.1	126.1	71.5	15	4427	1410	557.5	224.7	332.9
26	70	15.2	131.1	67.0	15	7109	2185	1211.2	403.4	807.9
27	62	16.6	130.8	71.0	18	7273	1579	588.7	287.6	301.1
28	75	18.0	112.6	67.0	13	5727	1417	690.1	169.1	521.0
29	75	18.0	111.1	67.0	13	5879	1659	764.9	242.8	522.1
30	50	17.7	113.3	66.0	15	2697	1528	591.3	226.4	364.8

Table C.9: Measured Spray Painting Task Parameters (continued)

Task Number	p_n (psig)	μ_l (sec)	U (fpm)	H (in)	D (in)	m_l (g)	Time (sec)			
							Task	Spray	90°	180°
31	67	13.9	131.4	67.0	15	2259	1341	435.7	190.3	245.4
32	77	17.6	132.0	72.0	15	6763	1625	739.8	200.9	538.8
33	74	14.7	114.7	71.5	15	4724	2052	675.3	267.0	408.3
34	60	15.8	132.7	68.5	15	4714	802	385.7	156.2	229.5
35	63	17.8	132.7	67.0	15	9080	2816	1420.6	480.2	940.5
36	62	16.0	115.4	66.0	15	2047	717	249.3	83.2	166.1
37	78	15.3	132.9	72.0	15	2760	835	474.3	188.0	286.3
38	80	18.2	132.9	72.0	15	7578	1910	771.1	133.9	637.3
40	75	13.4	115.9	71.5	15	3199	787	308.3	45.7	262.6
41	69	18.9	115.9	66.0	15	3433	889	374.6	139.5	235.1
42	66	13.6	113.5	66.0	15	1386	280	121.0	85.2	35.9
43	79	14.2	116.2	71.5	15	4523	1172	482.7	325.6	157.1
44	78	15.4	134.0	67.0	15	3096	1262	616.7	185.0	431.7
45	74	17.5	134.0	67.0	15	4310	1004	720.7	469.1	251.6
46	79	12.5	113.4	71.5	15	2150	653	258.9	118.0	140.9
47	84	16.3	130.6	72.0	15	1876	547	217.1	91.3	125.8
48	82	19.5	130.6	67.0	15	3592	1388	893.8	395.4	498.4
49	78	15.5	113.1	71.0	18	7915	1895	891.4	261.6	629.8
51	70	14.6	109.6	71.5	15	2561	754	300.0	97.2	202.8
52	53	12.8	128.9	68.5	15	3430	1489	465.4	253.6	211.8
53	77	17.4	128.9	67.0	15	6175	2153	1206.4	374.5	831.8
54	92	16.6	113.5	67.0	13	3452	1113	552.9	235.1	317.8
55	90	20.8	112.9	67.0	13	5532	1983	889.3	342.1	547.2
57	74	13.8	113.6	71.5	15	2359	689	261.9	98.0	163.9
58	63	19.2	114.5	66.0	15	4187	1022	436.3	117.5	318.8
59	82	15.2	132.8	72.0	15	1542	772	377.4	223.0	154.4
60	84	17.4	132.8	72.0	15	4716	1049	445.8	189.6	256.2

Table C.10: Charcoal Tube Sampling Results

Charcoal Tube Sample #	Task Number	Mass as n-Hexane (μg)
SZ-96-0001	1	583.8
SZ-96-0002	1	758.1
SZ-96-0003	2	304.2
SZ-96-0004	2	230.1
SZ-96-0005	3	82.6
SZ-96-0006	3	ND
BK-96-0007	Blank	ND
SZ-96-0008	4	539.8
SZ-96-0009	4	619.2
SZ-96-0010	5	73.0
SZ-96-0011	5	2674
BK-96-0012	Blank	ND
SZ-96-0013	6	456.5
SZ-96-0014	6	1647
SZ-96-0015	7	1131.6
SZ-96-0016	7	1100
SZ-96-0017	8	2447
SZ-96-0018	8	2768
BK-96-0019	Blank	ND
SZ-96-0020	9	728.9
SZ-96-0021	9	599.1
SZ-96-0022	10	ND
SZ-96-0023	10	575.2
SZ-96-0024	11	162.8
SZ-96-0025	11	1920
BK-96-0026	Blank	ND
SZ-96-0027	12	1920
SZ-96-0028	12	845.2
SZ-96-0029	13	1709
SZ-96-0030	13	2504
SZ-96-0031	14	583.5
SZ-96-0032	14	3321

Charcoal Tube Sample #	Task Number	Mass as n-Hexane (μg)
BK-96-0033	Blank	ND
SZ-96-0034	15	49.94
SZ-96-0035	15	1371.2
BK-96-0036	Blank	ND
SZ-96-0037	16	ND
SZ-96-0038	16	366
SZ-96-0039	17	1026
SZ-96-0040	17	4.59
SZ-96-0041	20	ND
SZ-96-0042	20	ND
SZ-96-0043	21	15.7
SZ-96-0044	21	19.0
BK-96-0045	Blank	ND
SZ-96-0046	22	ND
SZ-96-0047	22	ND
SZ-96-0048	23	ND
SZ-96-0049	23	ND
SZ-96-0050	24	10.3
SZ-96-0051	24	20.9
BK-96-0052	Blank	ND
SZ-96-0053	25	5.30
SZ-96-0054	25	ND
SZ-96-0055	26	158
SZ-96-0056	26	19.5
SZ-96-0057	27	824
SZ-96-0058	27	ND
BK-96-0059	Blank	ND
SZ-96-0060	28	5274
SZ-96-0061	28	168
SZ-96-0062	29	2750
SZ-96-0063	29	4741
BK-96-0064	Blank	ND

Table C.10: Charcoal Tube Sampling Results (continued)

Charcoal Tube Sample #	Task Number	Mass as n-Hexane (μg)
SZ-96-0065	30	3631
SZ-96-0066	30	664
SZ-96-0067	31	2616
SZ-96-0068	31	2386
SZ-96-0069	32	2314
SZ-96-0070	32	2116
SZ-96-0071	33	5493
SZ-96-0072	33	4425
BK-96-0073	Blank	ND
SZ-96-0074	34	3323
SZ-96-0075	34	3225
SZ-96-0076	35	3408
SZ-96-0077	35	268
SZ-96-0078	36	1683
SZ-96-0079	36	1522
BK-96-0080	Blank	ND
SZ-96-0081	37	7109
SZ-96-0082	37	7436
SZ-96-0083	38	6098
SZ-96-0084	38	5800
SZ-96-0085	40	3518
SZ-96-0086	40	2458
SZ-96-0087	41	4997
SZ-96-0088	41	5412
BK-96-0089	Blank	ND
SZ-96-0090	42	1370
SZ-96-0091	42	687
SZ-96-0092	43	7695
SZ-96-0093	43	6670
SZ-96-0094	44	2206
SZ-96-0095	44	1877
SZ-96-0096	45	2864
SZ-96-0097	45	3267
BK-96-0098	Blank	ND
SZ-96-0099	46	2136
SZ-96-0100	46	2182
SZ-96-0101	47	412
SZ-96-0102	47	472
SZ-96-0103	48	1033
SZ-96-0104	48	1115
SZ-96-0105	49	2170
SZ-96-0106	49	1710
BK-96-0107	Blank	ND
SZ-96-0108	51	836
SZ-96-0109	51	553
SZ-96-0110	52	9409
SZ-96-0111	52	8123
SZ-96-0112	53	4553
SZ-96-0113	53	3887
SZ-96-0114	54	7625
SZ-96-0115	54	8119
SZ-96-0116	55	8590
SZ-96-0117	55	8251
BK-96-0118	Blank	ND
SZ-96-0119	57	1764
SZ-96-0120	57	2043
SZ-96-0121	58	4687
SZ-96-0122	58	3345
BK-96-0123	Blank	ND
SZ-96-0124	59	1306
SZ-96-0125	59	1292
SZ-96-0126	60	684
SZ-96-0127	60	560
BK-96-0128	Blank	ND

Table C.11: Measured Worker Exposures (Individual Tasks)

Task Number	BZC Flow Rate (lpm)		Mass Filter (mg)		Mass Solids (mg)	Mass Solvent (mg)[1]	C_{task} (mg/m^3)
	Before	After	Before	After			
1	2.01	1.99	14.799	15.341	0.559	1.342	57.3
2	2.01	1.99	13.894	13.968	0.091	0.534	45.2
3	2.01	1.99	13.719	14.381	0.679	0.083	19.4
4	2.01	2.06	13.930	14.295	0.382	1.159	41.6
5	2.01	2.06	13.759	14.423	0.681	2.747	78.2
6	2.01	1.98	14.035	14.719	0.701	2.104	94.7
7	2.01	2.02	14.145	14.849	0.721	2.232	83.2
8	2.01	1.98	13.776	15.358	1.599	5.215	171.2
9	2.01	1.96	14.111	14.168	0.074	1.328	104.6
10	2.01	1.96	13.906	14.039	0.150	0.575	25.5
11	2.01	2.04	16.442	17.325	0.900	2.083	67.1
12	2.01	2.02	16.360	16.719	0.376	2.765	182.3
13	2.01	2.02	16.607	18.024	1.434	4.213	105.1
14	2.01	2.02	15.694	16.462	0.785	3.905	87.5
15	2.01	2.02	15.404	15.692	0.305	1.421	64.7
16	2.01	2.02	16.122	16.516	0.411	0.366	22.8
17	2.01	1.99	15.034	15.290	0.273	1.031	42.1
20	2.01	2.02	14.009	14.449	0.457	0.000	8.0
21	2.01	1.99	14.465	15.018	0.570	0.035	7.7
22	2.01	2.02	14.869	15.388	0.536	0.000	27.1
23	2.01	2.02	14.246	14.736	0.507	0.000	19.4
24	2.01	2.02	15.187	16.712	1.542	0.031	32.3
25	2.01	2.02	14.884	15.360	0.493	0.005	10.5
26	2.01	2.02	14.985	16.853	1.885	0.178	28.1
27	2.01	2.02	14.610	14.933	0.340	0.824	22.0
28	2.01	1.97	13.681	14.960	1.296	5.442	143.4
29	2.01	1.95	14.396	15.412	1.033	7.491	155.7
30	2.01	1.97	15.717	16.423	0.723	4.295	99.0

[1]Sum of solvent masses collected on the two charcoal tubes used per task

Table C.11: Measured Worker Exposures (Individual Tasks, continued)

Task Number	BZC Flow Rate (lpm)		Mass Filter (mg)		Mass Solids (mg)	Mass Solvent (mg)[1]	C_{task} (mg/m^3)
	Before	After	Before	After			
31	2.01	1.97	15.780	16.017	0.254	5.002	118.2
32	2.01	1.97	16.060	16.651	0.608	4.430	93.5
33	2.01	1.95	15.100	16.059	0.976	9.918	160.9
34	2.01	1.96	14.819	15.616	0.814	6.548	277.5
35	2.02	1.91	15.196	16.641	1.462	3.676	55.7
36	2.01	1.96	13.282	13.654	0.389	3.205	151.5
37	2.01	1.95	13.265	14.371	1.123	14.545	568.6
38	2.01	1.95	13.198	14.126	0.945	11.898	203.8
40	2.01	1.95	12.896	13.439	0.560	5.976	251.7
41	2.02	2.00	14.981	15.880	0.916	10.409	380.3
42	2.01	2.03	15.159	15.745	0.603	2.057	282.2
43	2.01	2.03	14.750	17.156	2.423	14.365	425.5
44	2.02	2.05	15.592	15.954	0.379	4.083	104.2
45	2.01	2.03	15.223	16.246	1.040	6.131	212.2
46	2.01	2.04	15.863	16.287	0.441	4.318	215.9
47	2.01	1.99	16.673	16.684	0.028	0.884	50.0
48	2.01	1.99	16.331	16.638	0.324	2.148	53.4
49	2.01	1.99	15.873	16.669	0.813	3.880	74.3
51	2.01	1.98	15.580	15.834	0.271	1.389	66.2
52	2.01	1.98	13.819	15.434	1.632	17.532	387.1
53	1.99	1.99	13.701	15.002	1.318	8.440	136.7
54	2.01	1.98	13.613	14.980	1.384	15.744	462.8
55	1.99	1.99	15.490	18.096	2.623	16.841	295.9
57	2.01	1.98	14.816	15.131	0.332	3.807	180.7
58	1.99	2.02	15.578	16.166	0.605	8.032	252.9
59	2.02	2.01	15.661	15.718	0.074	2.598	103.1
60	2.02	2.00	15.598	15.902	0.321	1.244	44.5

[1]Sum of solvent masses collected on the two charcoal tubes used per task

Table C.12: Calculated Spray Painting Task Parameters

Run Number	μ_l (cp)	TE	m_o (g/sec)	p_nH/μ_lU	CUHD/m_o	C_{model} (mg/m^3)
1	12.5	0.78	1.69	7.88E+07	0.0307	68.3
2	13.5	0.78	2.45	3.95E+07	0.0129	92.9
3	10.0	0.76	1.92	1.45E+08	0.0112	85.7
4	10.0	0.78	1.68	1.06E+08	0.0205	136.7
5	20.0	0.77	2.09	6.06E+07	0.0312	72.2
6	10.0	0.78	2.00	6.41E+07	0.0402	100.4
7	14.0	0.70	2.22	1.05E+08	0.0351	120.4
8	10.0	0.72	2.67	1.72E+08	0.0583	244.7
9	10.0	0.70	2.36	1.50E+08	0.0405	147.9
10	56.7	0.70	3.57	2.84E+07	0.0084	113.6
11	10.0	0.75	2.20	1.45E+08	0.0256	179.2
12	10.0	0.74	1.96	1.68E+08	0.0805	118.7
13	11.0	0.70	2.24	1.38E+08	0.0479	127.4
14	14.5	0.74	2.43	1.11E+08	0.0420	108.2
15	12.5	0.73	2.84	1.25E+08	0.0177	163.7
16	10.0	0.78	1.32	7.90E+07	0.0159	68.0
17	10.0	0.78	1.98	8.61E+07	0.0197	77.7
20	100.0	0.78	2.09	5.52E+06	0.0046	74.1
21	75.0	0.78	1.35	7.68E+06	0.0069	56.2
22	10.0	0.71	1.87	1.84E+08	0.0115	130.7
23	10.0	0.78	2.17	5.14E+07	0.0070	147.9
24	10.0	0.72	2.11	1.63E+08	0.0121	136.2
25	10.0	0.76	1.91	1.37E+08	0.0062	97.9
26	10.0	0.76	1.41	1.23E+08	0.0155	87.9
27	13.0	0.77	2.84	8.92E+07	0.0114	132.5
28	20.0	0.74	2.16	7.69E+07	0.0439	122.1
29	20.0	0.74	2.00	7.80E+07	0.0536	135.5
30	18.5	0.78	1.00	5.42E+07	0.0938	58.1

Table C12: Calculated Spray Painting Task Parameters (continued)

Run Number	μ_l (cp)	TE	m_o (g/sec)	p_nH/μ_lU	CUHD/m_o	C_{model} (mg/m^3)
31	10.0	0.76	1.24	1.18E+08	0.1265	57.8
32	18.0	0.73	2.47	8.04E+07	0.0389	98.0
33	10.0	0.74	1.82	1.59E+08	0.1084	84.0
34	10.0	0.77	2.81	1.07E+08	0.0917	175.0
35	19.0	0.77	1.47	5.77E+07	0.0328	83.6
36	10.0	0.77	1.89	1.22E+08	0.0864	85.4
37	10.0	0.73	1.57	1.46E+08	0.2996	107.7
38	21.0	0.72	2.75	7.11E+07	0.0863	66.7
40	10.0	0.74	2.70	1.60E+08	0.0970	64.8
41	24.5	0.76	2.20	5.53E+07	0.1542	132.3
42	10.0	0.76	2.75	1.32E+08	0.0875	310.0
43	10.0	0.72	2.62	1.67E+08	0.1609	244.2
44	10.0	0.73	1.36	1.34E+08	0.0695	66.6
45	17.5	0.74	1.55	7.29E+07	0.0839	225.9
46	10.0	0.72	2.33	1.72E+08	0.0933	148.8
47	11.5	0.70	2.59	1.39E+08	0.0225	133.2
48	27.5	0.71	1.17	5.27E+07	0.0306	109.2
49	10.0	0.78	1.95	1.69E+08	0.0383	84.5
51	10.0	0.76	2.05	1.57E+08	0.0313	100.4
52	10.0	0.78	1.62	9.70E+07	0.3316	88.4
53	17.0	0.73	1.38	8.11E+07	0.0749	83.4
54	13.0	0.68	2.00	1.44E+08	0.1511	185.1
55	34.0	0.68	1.99	5.42E+07	0.1068	153.1
57	10.0	0.74	2.34	1.61E+08	0.0810	120.2
58	26.0	0.77	2.21	4.82E+07	0.0997	102.7
59	10.0	0.71	1.18	1.53E+08	0.0836	100.6
60	17.0	0.70	3.17	9.23E+07	0.0155	173.4

Table C.13: Estimated Bias and Precision Error in Measured Task Parameters (percent)

Task Parameter	Bias Error	Precision Error
m_o[1]	2.9	4.7
U[2]	4.0	8.3
H[2]	0.4	0.7
D[2]	1.7	6.7
t_{task}[2]	< 0.1	0.6
t_{90}[2]	< 0.1	25.0
t_{180}[2]	< 0.1	16.7

[1]Manufacturer's Literature
[2]Estimate

REFERENCES

Ackley, M.W.: Paint Spray Tests for Respirators: Aerosol Characteristics. Am. Ind. Hyg. Assoc. J. 41(5):309-316 (1980).

American Conference of Governmental Industrial Hygienists: Industrial Ventilation, A Manual of Recommended Practice. ACGIH, Cincinnati, OH (1995).

American Society of Mechanical Engineers: Measurement Uncertainty, Part 1: Instruments and Apparatus. ANSI/ASME PTC 19.1-1985. ASME, New York, NY (1985).

Bailey, A.E.: Bailey's Industrial Oil and Fat Products, pp. 210-211. K.F. Mattil, Ed. Interscience Publishers, New York, NY (1964).

Baron, P.A.; Chen, C.; Hemenway, D.R.; O'Shaughnessy, P.O.: Nonuniform Air Flow in Inlets: The Effect on Filter Deposits in the Fiber Sampling Cassette. Am. Ind. Hyg. Assoc. J. 55(8):722-732 (1994).

Bayvel, L.; Orzechowski, Z.: Liquid Atomization, pp. 194-199. Taylor and Francis, Washington D.C. (1993).

Beaulieu, H.J.; Fidino, M.S.; Arlington, K.L.B.; Buchan, R.M.: A Comparison of Aerosol Sampling Techniques: "Open" Versus "Closed-Face" Filter Cassettes. Am. Ind. Hyg. Assoc. J. 41(10):758-765 (1980).

Brosseau, L.M.; Fang, C.P.; Snyder, C.; Cohen, B.S.: Particle Size Distribution of Automobile Paint Sprays. Appl. Occup. Environ. Hyg. 7(9):607-612 (1992).

Buchan, R.M.; Soderholm, S.C.; Tillery, M.I.: Aerosol Sampling Efficiency of 37 mm Filter Cassettes. Am. Ind. Hyg. Assoc. J. 47(12):825-831 (1986).

Bürkholz, A.; Widder, J.; Muller, W.; Dislich, M.: Particle Size Distribution of Overspray Generated During Spray Painting. Polymers Paint and Colour J. 167:285-290 (1977).

Chan, T.L.; D'Arcy, J.B.; Schreck, R.M.: High Solids Paint Overspray Aerosols in a Spray Painting Booth: Particle Size Analysis and Scrubber Efficiency. Am. Ind. Hyg. Assoc. J. 47(7):411-417 (1986).

Chung, K.Y.K.; Ogden, T.L.; Vaughan, N.P.: Wind Effects on Personal Dust Samplers. J. Aerosol Sci. 18(2):159-174 (1987).

Cohen, B.S.; Brosseau, L.M.; Fang, C.P.; et al.: Measurement of Air Concentrations of Volatile Aerosols in Paint Spray Applications. Appl. Occup. Environ. Hyg. 7(8):514-521 (1992).

D'Arcy, J.B.; Chan, T.L.: Chemical Distribution in High Solids Paint Overspray Aerosols. Am. Ind. Hyg. Assoc. J. 51(3): 132-138 (1990).

Demange, M.; Gendre, J.C.; Herve-Bazin, B.; et al.: Aerosol Evaluation Difficulties Due to Particle Deposition on Filter Holder Inner Walls. Ann. Occup. Hyg. 34(4):399-403 (1990).

Dement, J.M.; Harris, R.L.; Symons, M.J.; Shy, C.M.: Exposures and Mortality Among Chrysotile Asbestos Workers. Part 1: Exposure Estimates. Am. J. Ind. Med. 4:399-419 (1983).

Eisen, E.A.; Smith, T.J.; Wegman, M.D.; et. al.: Estimation of Long Term Dust Exposures in the Vermont Granite Sheds. Am. Ind. Hyg. Assoc. J. 45(2):89-94 (1984).

Fletcher, R.A.; Small, J.A.: Analysis of Individual Collected Particles. In: Aerosol Measurement: Principles, Techniques and Applications, pp. 260-295. K. Willeke and P. Baron, Ed. Van Nostrand Reinhold, New York, NY (1993).

Flynn, M.R.; Chen, M.; Kim, T.; Muthedath, P.: Computational Simulation of Worker Exposure Using a Particle Trajectory Method. Ann. Occup. Hyg. 39(3):277-289 (1995).

Flynn, M.R.; George, D.K.: Aerodynamics and Exposure Variability. Appl. Occup. Environ. Hyg. 6(1):36-39 (1991).

Flynn, M.R.; Lackey, B.D.; Muthedath, P.: Experimental and Numerical Studies on the Impact of Work Practices Used to Control Exposures Occurring in Booth-Type Hoods. Am. Ind. Hyg. Assoc. J. 57(5):469-475 (1996).

Flynn, M.R.; Shelton, W.K.: Factors Affecting the Design of Local Exhaust Ventilation for the Control of Contaminants from Hand-Held Sources. Appl. Occup.Environ. Hyg. 5(10):707-714 (1990).

Garrett, J.W.; Kennedy, K.W.: A Collation of Anthropometry. Aerospace Medical Research Laboratory, Wright-Patterson AFB, OH (1971).

George, D.K.; Flynn, M.R.; Goodman, R.: The Impact of Boundary Layer Separation on Local Exhaust Design and Worker Exposure. Appl. Occup. Environ. Hyg. 5(8):501-509 (1990).

Griefe, D.K.; Hornung, R.W.; Stayner, L.G.; Steenland, K.N.: Development of a Model for Use in Estimating Exposure to Ethylene Oxide in a Retrospective Cohort Mortality Study. Scand. J. Work Env. and Health. 14(supp 1):29-30 (1988).

Hansen, D.J.; Whitehead, L.W.: the Influence of Task and Location on Solvent Exposures in a Printing Plant. Am. Ind. Hyg. Assoc. J. 49(5):259-265 (1988).

Hayat, M.A.: Basic Techniques for Transmission Electron Microscopy, pp. 3-4. Academic Press, Inc., Orlando, FL (1986).

Heitbrink, W.A.; Wallace, M.E.; Bryant, C.J.; Ruch, W.E.: Control of Paint Overspray in Autobody Repair Shops. Am. Ind. Hyg. Assoc. J. 56(10):1023-1032 (1995).

Heriot, N.R.; Wilkinson, J.: Laminar Flow Booths for the Control of Dust. Filtration and Separation. 16(2):159-164 (1979).

Hicks, P.G.; Senser, D.W.: Simulation of Paint Transfer in an Air Spray Process. In: Fluid Mechanics and Heat Transfer in Sprays, FED-Vol. 178/HTD-Vol 270, pp. 145-154. American Society of Mechanical Engineers, New York, NY (1993).

Hinds, W.G.: Aerosol Technology: Properties, Behavior, and Measurement of Airborne Particles, p. 382. J. Wiley and Sons, New York, NY (1982).

Hund, J.P.: Spray Application Processes. Metal Finishing: Organic Finishing Guidebook and Directory Issue. 93(5A):97-111 (1993a).

Hund, J.P.: Determination of Viscosity. Metal Finishing: Organic Finishing Guidebook and Directory Issue. 93(5A):97-111 (1993b).

Jayjock, M.A.; Levin, L.: Health Hazards in a Small Automotive Body Repair Shop. Ann. Occup. Hyg. 28(1):19-29 (1984).

Kalliokoski, P.: Estimating Long-Term Exposure Levels in Process-Type Industries Using Production Rates. Am. Ind. Hyg. Assoc. J. 51(6):310-312 (1990).

Kim, K.Y.; Marshall, W.R.: Drop-Size Distributions from Pneumatic Atomizers. AIChE J. 17(3):575-584 (1971).

Kim, T.; Flynn, M.R.: Modeling a Worker's Exposure From a Hand-Held Source in a Uniform Freestream. Am. Ind. Hyg. Assoc. J. 52(11):456-463 (1991).

Kim, T.; Flynn, M.R.: The Effect of Contaminant Source Momentum on a Worker's Breathing Zone Concentration in a Uniform Freestream. Am. Ind. Hyg. Assoc. J. 53(12):757-766 (1992).

Kleinbaum, D.G.; Kupper, L.L.; Muller, K.E.: Applied Regression Analysis and Other Multivariable Methods, pp. 260-281, 365-368. Duxbury Press, Belmont, CA (1988).

Kromhout, H.; Swuste, P.; Boleij, J.S.M: Empirical Modelling of Chemical Exposure in the Rubber-Manufacturing Industry. Ann. Occup. Hyg. 38(1):3-22 (1994).

Kromhout, H.; Symanski, E.; Rappaport, S.M.: A Comprehensive Evaluation of Within- and Between-Worker Components of Occupational Exposure to Chemical Agents. Ann. Occup. Hyg. 37(3):253-270 (1993).

Kwok, K.C.: A Fundamental Study of Air Spray Painting. Ph.D. Thesis, University of Minnesota, MN (1991).

Lee, K.W.; Ramamurthi, M.: Filter Collection. In: Aerosol Measurement: Principles, Techniques, and Applications, pp. 179-205. K. Willeke and P. Baron, Ed. Van Nostrand Reinhold, New York, NY (1993).

Lefebvre, A.H.: Atomization and Sprays, pp. 1-20, 238-261. Hemisphere Corp., New York, NY (1989).

Leith, D.; First, M.W.: Uncertainty in Particle Counting and Sizing Procedure. Am. Ind. Hyg. Assoc. J. 37(2):103-108 (1976).

Liu, B.Y.H.; Pui, D.Y.H.: Drop Size Measurement of Liquid Aerosols. Atmos. Environ. 16(3):563-567 (1982).

Mark, D.: The Use of Dust-Collecting Cassettes in Dust Samplers. Ann. Occup. Hyg. 34(3):281-291 (1990).

Mark, D.; Vincent, J.H.: A New Personal Sampler for Airborne Total Dust in Workplaces. Ann. Occup. Hyg. 30(1):89-102 (1986).

McAneny, J.J.; Leith, D.; Boundy, M.G.: Volatilization of Mineral Oil Mist Collected on Sampling Filters. Appl. Occup. Environ. Hyg. 10(9):783-787 (1995).

McLenaghan, R.; Levy, S.: Geometry. In: Standard Mathematical Tables and Formulae, p. 134. D. Zwillinger, Ed. CRC Press, Boca Raton, FL (1996).

National Institute for Occupational Safety and Health: Naphtha: Method 1550. In: NIOSH Manual of Analytical Methods, 4th Edition. P.M. Eller, Ed. NIOSH, Cincinnati, OH (1994).

National Institute for Occupational Safety and Health: Particulates Not Otherwise Regulated, Total: Method 0500. In: NIOSH Manual of Analytical Methods, 4th Edition. P.M. Eller, Ed. NIOSH, Cincinnati, OH (1994).

O'Brien, D.M.; Hurley, D.E.: An Evaluation of Engineering Control Technology for Spray Painting. DHHS (NIOSH) Pub. No. 81-121. NIOSH, Cincinnati, OH (1981).

Olan-Figueroa, E.; McFarland, A.R.; Ortiz, C.A.: Flattening Coefficients for DOP and Oleic Acid Droplets Deposited on Treated Glass Slides. Am. Ind. Hyg. Assoc. J. 43(6):395-399 (1982).

Rappaport, S.M.; Kromhout, H.E.; Symanski, E.: Variation of Exposure Between Workers in Homogeneous Exposure Groups. Am. Ind. Hyg. Assoc. J. 54(11):654-662 (1993).

Raynor, G.S.: Variation in Entrance Efficiency of a Filter Sampler with Air Speed, Flow Rate, Angle and Particle Size. Am. Ind. Hyg. Assoc. J. 31(3):294-304 (1970).

Reist, P.C.: Aerosol Science and Technology, pp. 22-23. McGraw-Hill, Inc., New York, NY (1993).

Roach, S.A.: A Method of Relating the Incidence of Pneumoconiosis to Airborne Dust Exposure. Br. J. Ind. Med. 10:220-226 (1953).

Spurny, K.R.; Lodge, J.P.; Frank, E.R.; Sheesley, D.C.: Aerosol Filtration by Means of Nuclepore Filters: Aerosol Sampling and Measurement. Environ. Sci. Tech. 3(5): 464-468 (1969).

Taylor, E.S.: Dimensional Analysis for Engineers, pp. 1-47. Clarendon Press, Oxford, UK (1974).

Vincent, J.H.; Mark, D.: Entry Characteristics of Practical Workplace Aerosol Samplers in Relation to the ISO Recommendations. Ann. Occup. Hyg. 34(3):249-262 (1990).

White, F.M.: Fluid Mechanics, pp. 510-541. McGraw-Hill, Inc., New York, NY (1994).

Whitehead, L.W.; Ball, G.L.; Fine, L.J.; Langolf, G.D.: Solvent Vapor Exposures in Booth Spray Painting and Spray Glueing, and Associated Operations. Am. Ind. Hyg. Assoc. J. 45(11):767-772 (1984).

Willeke, K.; Baron, P.A.: Sampling and Interpretation Errors in Aerosol Monitoring. Am. Ind. Hyg. Assoc. J. 51(3):160-168 (1990).

Winder, C.; Turner, P.J.: Solvent Exposure and Related Work Practices Amongst Apprentice Spray Painter in Automotive Repair Workshops. Ann. Occup. Hyg. 36(4):385-394 (1992).

Woskie, S.R.; Smith, T.J.; Hammond, S.K.; Hallock, M.H.: Factors Affecting Worker Exposures to Metal-Working Fluids During Automotive Component Manufacturing. Appl. Occup. Environ. Hyg. 9(9):612-621 (1994).